MAOXIAO PENG

Regulatory mechanism of bivalve shell biomineralization and its response to global climate change

UNIVERSIDADE DO ALGARVE
Faculdade de Ciências e Tecnologia

Faro, 2023

MAOXIAO PENG

Regulatory mechanism of bivalve shell biomineralization and its response to global climate change

Doutoramento em Ciências Biológicas
Especialidade em Biologia de Desenvolvimento,
Funcional e Integrativa

Trabalho efetuado sob a orientação de:
Prof. Doutora Deborah M. Power
Prof. Doutor João Carlos dos Reis Cardoso

UNIVERSIDADE DO ALGARVE
Faculdade de Ciências e Tecnologia

Faro, 2023

MAOXIAO PENG

Regulatory mechanism of bivalve shell biomineralization and its response to global climate change

Doctoral Programme in Biological Sciences
Specialty in Developmental,
Functional and Integrative Biology

Supervisors:
Prof. Doctor Deborah M. Power
Prof. Doctor João Carlos dos Reis Cardoso

UNIVERSIDADE DO ALGARVE
Faculdade de Ciências e Tecnologia

Faro, 2023

Título | Thesis title

Regulatory mechanism of bivalve shell biomineralization and its response to global climate change

Declaração de autoria de trabalho:

Declaro ser a autora deste trabalho que é original e inédito. Autores e trabalhos consultados estão devidamente citados no texto e constam da listagem de referências incluída.

Declaration of authorship:

This work has not previously been submitted for a degree in any university. To the best of my knowledge and belief, the thesis contains no material previously published or written by another person except where due reference is made in the thesis itself.

Maoxiao Peng

Support

This study received Portuguese national funds from FCT - Foundation for Science and Technology through projects UIDB/04326/2020, 2021, 2022 and 2023 UIDP/04326/2020 and LA/P/0101/2020 and from the operational programs CRESC Algarve 2020 and COMPETE 2020 through the project EMBRC.PT ALG-01-0145-FEDER-022121.

Acknowledgments

In early autumn of 2018, a young individual set foot on unfamiliar European soil, brimming with enthusiasm for scientific research. Time has swiftly passed, and in the span of five years as the seasons changed, Portugal's warmth became my second home. Now, the moment to complete this PhD work has arrived. Today, I take up my pen to depict these marvelous, unforgettable, and unparalleled five years. This thesis was completed under the meticulous guidance of Professor Deborah Mary Power, my supervisor. I am grateful for every enlightening moment my supervisor has provided over the past five years, for their selfless nurturing and care in life, and for imparting invaluable research skills bit by bit. Over these five years, my research abilities have gradually become proficient, my research skills have grown increasingly adept, and my scientific perspectives have expanded. My supervisor's profound and rigorous academic achievements, tireless dedication to educating, and enthusiastic work spirit radiate a unique charisma. I express my most heartfelt gratitude and endless admiration to my supervisor.

I want to express my gratitude to my second supervisor, professor João Carlos dos Reis Cardoso. Over the past five years, it's been his guidance that facilitated my rapid growth. His meticulous explanations helped me comprehend the mysteries of research, his dedication resulted in tangible achievements, and his selfless care ensured I had no worries living in a foreign land. The completion of this thesis was also achieved under the guidance of professor João Cardoso. I extend my thanks and deep gratitude to professor João Cardoso for his selfless assistance and mentorship.

The successful passage of five years, the publication of research papers, and the high-quality completion of my thesis wouldn't have been possible without the help of the laboratory members. I especially want to express my gratitude to Professor Adelino Vicente Mendonça Canário, Pol Sorigué, Rute Felix, Cármen Sousa, Soraia Santos, Alexandra Alves, Elsa Couto, and others for their assistance and care in both experiments and daily life. I am thankful to Shanghai Ocean University for providing me with a full scholarship for the first three years of my studies.

I want to extend special thanks to Zhi Li, my fiancée, who came to Portugal in 2020 to pursue her PhD degree. Her arrival improved my life in Portugal, bringing more joy into my daily experiences. Her companionship helped me navigate through many difficult moments smoothly, including the challenging times we faced together during the pandemic (COVID-19) in Portugal. Her assistance in the experiments contributed significantly to the successful completion of my doctoral thesis. Her presence has added vibrant colors to my otherwise solitary life. As I reach the completion of my graduation thesis, a thousand words wouldn't suffice to express my gratitude and love for her. I hope that in the near future, she will also successfully complete her PhD thesis, and our joint efforts will lead us to a joyful life.

Abstract

Bivalves are one of the most diverse animal groups in the ocean and are found everywhere on Earth. They provide important ecosystem services in the marine environment as they filter environmental waters but also contribute to the nutrient and carbon cycle and are a rich source of nutrients for humans and other animals. Aquaculture of marine bivalve is an economically important industry worldwide that is currently expanding and because bivalve production is environmental-friendly they can provide an alternative protein source to meet the growing demand for food by the growing world population. Bivalves are characterized by possessing two valves that form the shell that is secreted by the mantle which is essential for their survival since it protects them from the environment and predators but also serves as a store of minerals. How bivalves produce and maintain their shells has been the topic of many studies especially because this structure is considered to be highly sensitive to changes in the ocean environment as a consequence of climate change and environmental pollution compromising their existence and survival. However, the large biodiversity of bivalves, the limited number of species studied and the diversity of exuberant shells with different mineralized structures suggests that the mechanisms of shell formation and growth and their susceptibility to environmental stressors might be species-specific. The main objective of this thesis is to increase knowledge about bivalve shell biomineralization by exploring and comparing the molecular factors that regulate shell growth and maintenance and composition in two commercially important aquaculture species that occupy the same ecological niche but possess different shell morphologies the Pacific oyster (*Magallana gigas*) and the Mediterranean mussel (*Mytilus galloprovincialis*) using animal experimentation, and multi-omics analysis using available bivalve genomes and transcriptomes, biochemical and gene knock down approaches. The results of this thesis revealed that: 1) long non-coding RNAs (lncRNA) and non-matrix protein encoding genes are important factors in the regulation of shell matrix protein (SMP) and non-SMP genes that modify shell structure (Chapter 2), 2) shell growth in *M. gigas* and *M. galloprovincialis* is hampered by OA but the two animals respond differently and *M. galloprovincialis* employs a larger number of biomineralization genes and most likely invests more energy to maintain the shell (Chapter 3) and 3) there is a large diversity of CHS (Chitin-synthase) isoforms with a complex evolutionary history and that *M. gigas* and *M. galloprovincialis* (Chapter 4). The tissue distribution of CHS indicates a far more complex suite of actions than the production of part of the organic scaffold for calcium carbonate crystal deposition in the shell. Furthermore, CHS respond differently to OA implying plasticity in the response of chitin production and an involvement in modulating the production of the shell.

Keywords: bivalve, shell biomineralization toolbox, lncRNA, ocean acidification, chitin synthase

Resumo

Os bivalves são um dos grupos de animais mais diversos existentes nos oceanos. Eles têm uma função importante em vários serviços no ecossistema marinho pois são importantes filtradores das águas ambientais, mas também têm um papel importante no ciclo de nutrientes e de carbono no ambiente marinho e são uma fonte importante de nutrientes na alimentação dos humanos e outros animais. A aquicultura de bivalves marinhos é uma das indústrias economicamente mais importantes no mundo e a produção de bivalves marinhos encontra-se em larga expansão. Como tem um baixo impacto ambiental, quando comparada com outros sistemas de produção animal, o consumo de bivalves representa uma fonte alternativa de proteína saudável para satisfazer as necessidades no aumento da procura de alimentos associado ao crescimento da população mundial. Os bivalves caracterizam-se por possuir duas válvulas que formam a sua concha calcificada produzida devido à atividade secretora do manto. Esta estrutura é essencial para a sua sobrevivência, pois os protege das agressões do meio ambiente e de predadores, mas também serve como uma importante reserva de minerais que são utilizados em caso de necessidade. A forma como os bivalves produzem e mantêm a sua concha calcificada tem sido tema de vários estudos de investigação, principalmente porque esta estrutura é sensível às alterações no ambiente marinho como consequência do impacto das alterações climáticas e da poluição ambiental causada pelo homem que comprometem a sua existência e sobrevivência. Considerando a grande biodiversidade de bivalves (~ 3000 espécies), os estudos existentes concentram-se especificamente em um número limitado de espécies. No entanto a diversidade de formas de conchas existentes com diferentes estruturas mineralizadas, sugerem que os mecanismos de formação e crescimento da concha e consequentemente as suas suscetibilidades aos fatores de stress ambiental poderão ser diferentes entre espécies. O objetivo principal desta tese é contribuir para uma melhor compreensão dos mecanismos que regulam a formação da concha em bivalves e sobre o impacto da Acidificação dos Oceanos (AO) na homeostase da manutenção da concha, tendo em consideração a diversidade de formas, estruturas e composição existentes. Nesta tese, pretende-se aumentar o conhecimento sobre o processo de biomineralização explorando e comparando os fatores moleculares que regulam o crescimento, manutenção e composição da concha comparando duas espécies de bivalves importantes em aquicultura que ocupam o mesmo nicho ecológico, mas possuem diferentes morfologias de conchas: a ostra do Pacífico (*Magallana gigas*, com conchas de válvulas moles e assimétricas) e o mexilhão mediterrâneo (*Mytilus galloprovincialis*, com conhas de válvulas duras e simétricas) através do uso da experimentação animal e de análises de multi-ómica (consulta de genomas e transcritomas de bivalves disponíveis em bases de dados públicas), abordagens bioquímicas e genéticas. Especificamente, esta tese foca-se em três objetivos principais: 1) Caracterizar os fatores envolvidos no crescimento e biomineralização da concha - através da análise multi-ómica e

experimentação animal para identificar os fatores centrais envolvidos na formação da concha e caracterizar as vias regulatórias associados ao crescimento da concha em bivalves com válvulas assimétricas; 2) Determinar o impacto das alterações climáticas na concha- através da caracterização e comparação do efeito da AO no crescimento e na estrutura da concha por análises de transcritomas do manto, ensaios bioquímicos e analise fenotípica entre a ostra *M. gigas* e o mexilhão *M. galloprovincialis*; 3) Caracterizar a evolução e papel funcional das enzimas quitina sintases (CHS, envolvidas na formação da quitina presente na concha) em bivalves- através de análises comparativas e evolutivas dos diferentes membros desta família e da caracterização do impacto da AO na regulação da sua expressão no manto. Os resultados desta tese sugerem que: 1) Os RNAs não codificantes longos (lncRNA) têm um papel importante na regulação da expressão das proteínas da matriz da concha (SMP) e dos genes não-SMP que estão envolvidos no crescimento e na formação da estrutura da concha calcária (Capítulo 2); 2) A AO afeta o crescimento da concha tanto na ostra *M. gigas* como no mexilhão *M. galloprovincialis*, mas os dois bivalves desenvolvem mecanismos de resposta diferentes, sendo que o mexilhão *M. galloprovincialis* utiliza um número maior de genes envolvidos no processo de biomineralização e provavelmente investe mais energia para manter a estrutura da concha calcária quando comparado com a ostra *M. gigas* (Capítulo 3) e 3) Existe uma grande diversidade de isoformas de enzimas CHS em bivalves e a sua evolução é bastante complexa. Distribuição tecidular dos transcritos sugere que estas poderão estar envolvidas em um conjunto de ações diversas para além da produção da estrutura orgânica da concha e a resposta das CHS ao efeito da AO é especifica de cada espécie. Em resumo, os resultados descritos nesta tese contribuem para o aumento do conhecimento sobre os mecanismos de regulação da concha em bivalves marinhos e especula que a resposta fisiológica associada ao efeito da AO é diferente entre espécies e pode estar relacionada com os custos energéticos associados à construção e manutenção das microestruturas das suas conchas.

Palavras-Chave: Bivalves, fatores de biomineralização da concha, lncRNA, Acidificação dos oceanos, quitina sintase.

Contents

List of Tables

Chapter 1

Chapter 4

List of Figures

Chapter 1

Chapter 2

Chapter 3

Chapter 4

CHAPTER 1

General Introduction and main goals

1.1 General introduction

The Mollusca is an animal phylum that has attracted much attention (its species diversity ranks second in the biological world) (Gaston, 2000). They are major parts of benthic and planktonic (larval) ecosystems worldwide and account for approximately 23% of marine species biodiversity and some species are among the most economically and commercially important aquaculture species for human consumption (Gaston, 2000; Gosling, 2008; Gutiérrez et al., 2003; Pompa et al., 2011). Molluscs are not only widely studied because of their importance as a marine food resource for aquaculture expansion (Khan and Liu, 2019), but also because of their production of biomineralized products such as calcified pearls coated in lustrous nacre found inside their bodies, that have a very high economic market value worldwide (Zenger et al., 2019; Zieritz et al., 2022). Most molluscs produce a biomineralized shell that is secreted by the mantle (a specialized tissue that involves the animal soft body). The shell consists of calcium carbonate crystals attached to an organic scaffold composed of proteins, lipids and polysaccharides and pearl production arises from a similar process to that described for the shells. The shell in mollusc is highly variable in shape, structure and composition and serves as an exoskeleton that provides support for the soft body and plays an important role in the maintenance of internal ion homeostasis and it also provides protection against predators and the

environment and is an essential structure for their survival. The study of the hard calcified shell of the mollusc has been favored in materials science (Meyers et al., 2008) and military technology research due to its unique properties (Arif et al., 2017; Muzzarelli, 2011; Vecchio, 2005). The heavily calcified shell of the mollusc also has an important role in the Earth's carbon cycle as dissolved carbon dioxide is captured and used for the formation of calcium carbonate crystals the main inorganic material of the shell (Peijnenburg et al., 2020; Smith et al., 2016).

Recently a lot of interest has been devoted to understanding shell composition and the mechanisms involved in shell formation not only from a biological perspective but also to understand how global climate change (especially seawater pH value and seawater CO_2 partial pressure-ocean acidification, OA) will affect shell production, species biodiversity and survival. This will help establish the impact of OA on aquatic ecosystems and aquaculture productivity for human consumption especially bivalves. A consensus “biomineralization toolbox” has been described but despite considerable efforts the mechanisms of shell formation and regulation are only barely understood. In addition, the mechanism on how the global impact of climate change in the oceans will negatively impact on the diverse Mollusca/bivalve taxa is far from being understood (Baag and Mandal, 2022; Pörtner and Peck, 2010; Waldbusser and Salisbury, 2014). Therefore, this thesis aims to contribute to the state-

of-art knowledge on bivalve shell biomineralization and the impact of environmental stressors (OA) on the dynamics of shell homeostasis by looking at mantle response and shell composition in two commercially important aquaculture bivalve species that occupying a similar ecological niche but possess different shell morphologies: the Pacific oyster (*Magallana gigas*) and the Mediterranean mussel (*Mytilus galloprovincialis*).

1.2 The Mollusca phylum and the bivalvia class

1.2.1 The Mollusca phylum

The Mollusca phylum is the second most diverse and widespread animal groups on Earth, comprising over 100,000 extant species and an even larger number of extinct species (Caron and Jackson, 2008; Runnegar and Pojeta Jr, 1974; Simon, 1985; Zhang, 2011). Their success is linked to their adaptation to a wide variety of habitats, and they are found almost everywhere on Earth, from the deep sea to freshwater rivers, to the tropics and poles and from the abysses of the sea to mud flats and even as parasites dwelling in other animals. They exhibit a wide range of shell morphologies, including external coiled valve shells or internalized shells, and have a variety of ecological roles and play a key role in nutrient recycling in aquatic and terrestrial environment, and include herbivores, carnivores, filter feeders, and detritivore species (Ponder et al.,

2019; Wanninger and Wollesen, 2019).

The Mollusca phylum is divided into several classes, the most commonly recognized classes are the Gastropoda (snails and slugs), Bivalvia (clams, oysters, and mussels), Cephalopoda (squid, octopus, and nautilus), Polyplacophora (chitons), Scaphopoda (tusk shells), and Monoplacophora (deep-sea limpet-like molluscs) (Figure 1.1) (Ponder et al., 2019; Vinther, 2015). Each class within the Mollusca phylum is characterized by unique anatomical and physiological features, including variations in shell morphology, nervous system complexity, and feeding mechanisms. Despite the differences, molluscs share certain defining characteristics, such as a soft, unsegmented body that is often protected by a hard outer shell, a radula (a ribbon-like organ used for feeding), and a muscular foot used for locomotion (Stöger et al., 2013).

Their shell provides protection from predators and from environmental aggression and helps to maintain the animal shape (Marek and Yochelson, 1976). However, some gastropod molluscs, such as nudibranchs and slugs, have lost their shells entirely, while others, such as squid and octopus which are cephalopods, have internalized their shells to form a rigid structure known as the pen (Carlini et al., 2000; Martynov and Schroedl, 2011).

All molluscs possess a muscular foot, which is used for movement, attachment, and feeding (Marek and Yochelson, 1976) that is highly

variable in shape and function across different mollusc groups (Ponder and Lindberg, 2008). In addition, all molluscs have a mantle, a specialized tissue that surrounds the animals soft-body and in shell-bearing species is responsible for secreting the biomineralized shell (Vinther et al., 2017). In some molluscs, such as bivalves, the mantle is also partially responsible for helping to filter food from the water column, while in others, such as cephalopods, the muscular mantle cavity is involved in jet propulsion for locomotion (Fields et al., 1976; Morton, 1983). Molluscs also have a well-developed digestive system, with a mouth, stomach, and anus, and a complex nervous system, which includes a centralized brain and a network of nerve cells throughout the body and a complex sensory systems, with eyes, tentacles, and chemosensors for detecting food and other stimuli (Haszprunar and Wanninger, 2012; Vinther, 2015).

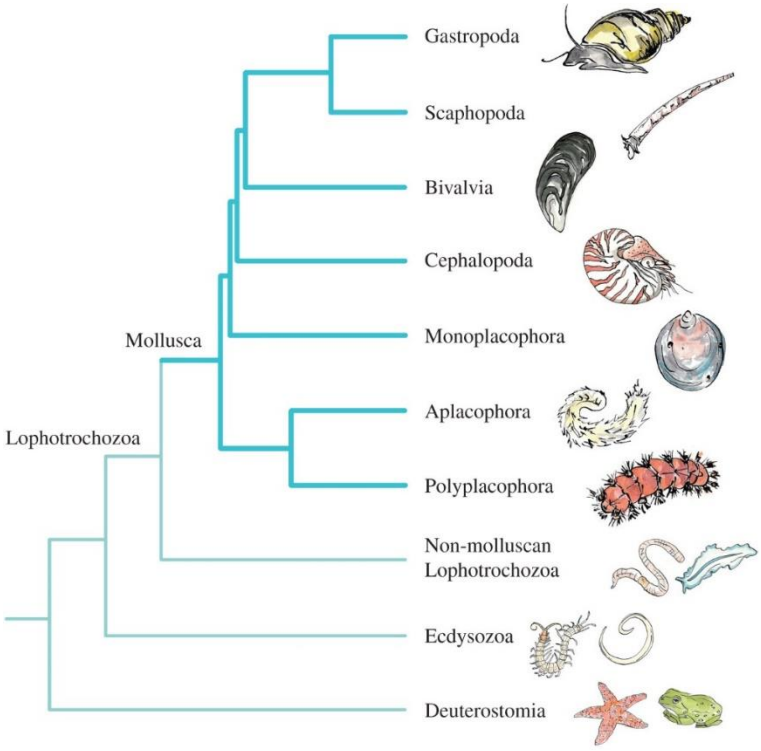

Figure 1.1. Evolutionary relationships of the seven major lineages of Mollusca, relative to other Lophotrochozoans, Ecdysozoans and Deuterostomes. Image was taken from (Davison and Neiman, 2021).

1.2.2 The class Bivalvia

The class Bivalvia are a diverse group of the Mollusca phyla and all members are characterized by having two hinged shells, or valves, that encase the soft body of the animal. The bivalve class contains about 30,000 extant species that inhabit a wide range of environments, including marine, freshwater, and terrestrial ecosystems (Gosling, 2008). The biological characteristics of bivalves, including their anatomy, physiology, behavior, and ecology, have fascinated scientists for centuries, as they represent a remarkable example of their evolutionary diversification and adaption to a wide range of ecological niches and

environmental stressors.

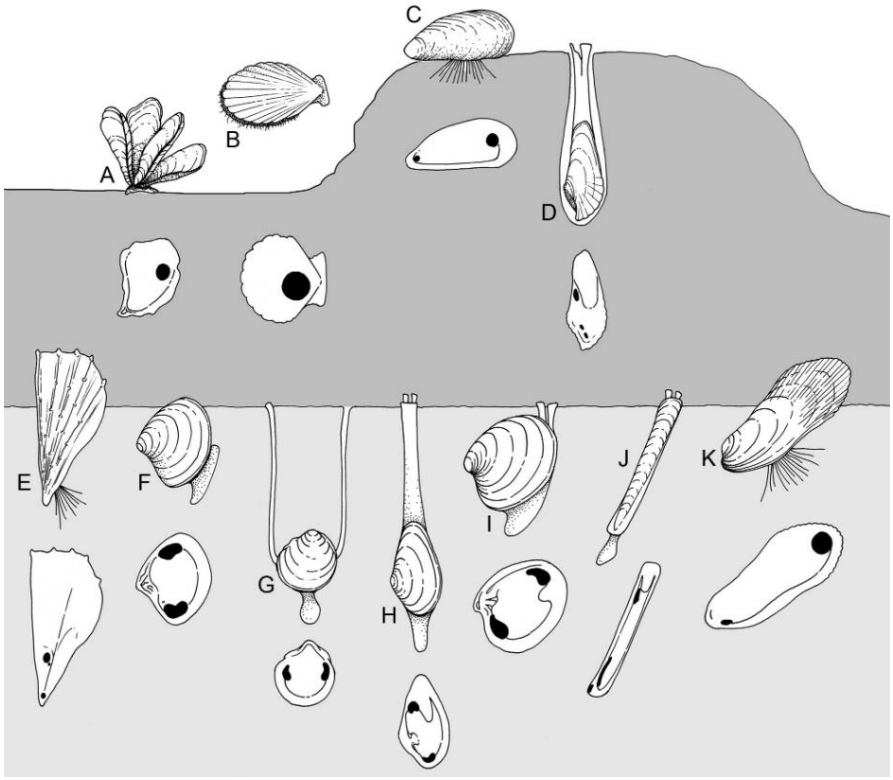

Figure 1.2. Diverse lifestyles of various benthic bivalve species. The interior side of one valve shows the position of the adductor muscle and pallial line. (Light gray = soft substrate; dark gray = hard substrate) **A.** *Crassostrea/Magallana* (Ostreidae), cemented. **B.** *Argopecten* (Pectenidae), epibenthic swimmer. **C.** *Mytilus* (Mytilidae), epibyssate. **D.** *Pholas* (Pholadidae), rock-borer. **E.** *Pinna* (Pinnidae), shallow burrower. **F.** *Astarte* (Astartidae), shallow burrower. **G.** *Phacoides* (Lucinidae), deep burrower with mucus siphons **H.** *Mya* (Myidae), deep burrower with fused mantle siphons. **I.** *Mercenaria* (Veneridae), shallow burrower. J. *Ensis* (Pharidae), deep burrower with fused mantle siphons. K. *Modiolus* (Mytilidae), endobyssate. Figure cited form Digital Encyclopedia of Ancient Life: https://www.digitalatlasofancientlife.org/learn/mollusca/bivalvia/ecology/.

The two valves are held together by a strong ligament, which allows the animal to open and close its shell by contracting its adductor muscles, which are their main musculature system that is attached to the shell. The shells of bivalves exhibit a remarkable diversity of shape, size, and

texture, and are composed mainly of calcium carbonate. The size and shape of the shells can vary widely between species, and can be influenced by factors such as environmental conditions, predation pressure, and life history traits (Harper, 2000; Mariani et al., 2002). In some species, such as the oysters, the shell is highly irregular, with deep grooves and ridges that provide attachment sites for other organisms and enhance resistance to wave action (Coen and Luckenbach, 2000). Other bivalve species, such as clams and mussels, have a more streamlined and symmetrical shell that facilitates burrowing in sediment or attachment to hard substrates (Barker, 2001). The internal structure of the shell can also vary between species, with some bivalves possessing highly complex microstructures that provide additional mechanical strength and resistance to fracture (Lopes-Lima et al., 2014). Understanding the shell structure and composition of bivalves is important not only for taxonomic classification, but also for studying their ecology, evolution, and biomineralization processes (Webb et al., 1991).

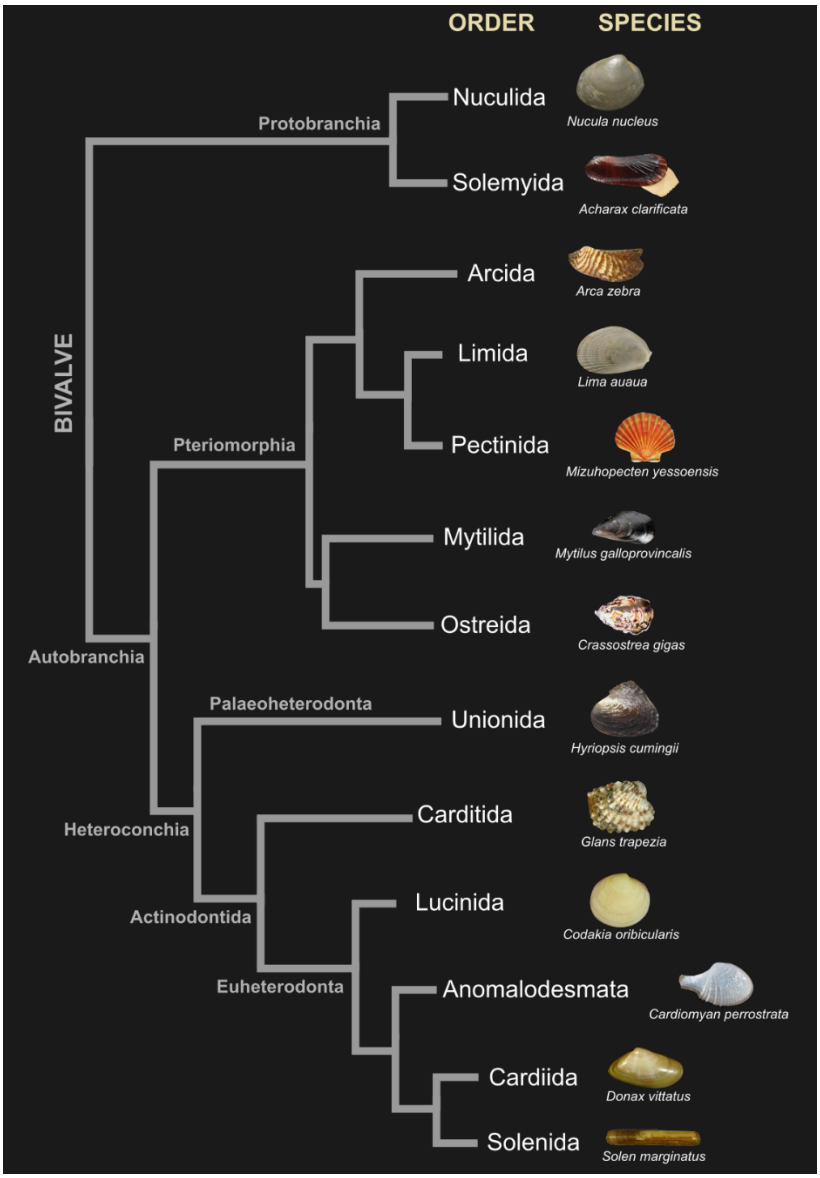

Figure 1.3. Evolutionary relationships of the class bivalvia members. Phylogenetic tree at the order level in the bivalvia class taken from (Ponder et al., 2019). The subclass, infraclass, and subterclass were identified in this tree based on data from the World Register of Marine Species (WoRMS，(WoRMS Editorial Board, 2023)). The species graph, *Mizuhopecten yessoensis*, *M. galloprovincalis*, *Hyriopsis cumingii* and *M. gigas* were from our studies; *Nucula nucleus*, *Arca zebra*, *Lima auaua*, *Glans trapezia*, *Codakia orbicularis*, *Cardiomyan perrostrata*, *Solen marginatus* and *Donax vittatus* cited form WoRMS; *Acharax clarificata* cited from (Walton, 2015).

The mantle is a key organ in the bivalvia class, with multiple important functions related to growth, reproduction, and survival. The

mantle is a specialized tissue that lines the inside of the shell, and is the main organ responsible for the production of the shell but it is also involved in respiration and feeding (Beninger et al., 1999; Morton, 1983). The mantle also plays a critical role in the formation of pearls, a valuable and sought-after gemstone naturally produced by some species (Fang et al., 2008). In addition to its physical functions, the mantle has also been described to play a major role in bivalve immune defense against pathogenic microbes (Allam and Espinosa, 2016). Furthermore, this tissue also plays a role in the detoxification of harmful substances, such as heavy metals, providing an additional mechanism for bivalves to cope with environmental stressors (Windoffer et al., 1999).

Bivalves exhibit a diverse array of feeding strategies, but the most common approach is filter-feeding. Bivalves use their gills to capture suspended particles, including phytoplankton, bacteria, and detritus, from the surrounding water. These particles are transported to the mouth by ciliary action or by the beating of the gills. This feeding strategy is highly effective and allows bivalves to exploit a wide range of ecological niches (Barker, 2001). They are also known for their ability to tolerate a wide range of environmental conditions, including variations in temperature, salinity, and oxygen concentration. Many bivalve species have developed physiological and behavioral adaptations to cope with environmental stressors. Some species can tolerate extreme fluctuations in salinity by

adjusting their physiology and behavior (Peng et al., 2019; Pourmozaffar et al., 2020) and in low-oxygen conditions they can reduce their metabolic rate or pump water through their gills more efficiently (De Zwaan et al., 1992; Gobler et al., 2014).

1.3 Ecological and commercial importance of bivalves

1.3.1 Ecological importance of bivalves

Bivalves, play a significant ecological role in aquatic environments. They are important members of marine and freshwater food webs, contributing to nutrient cycling and acting as a buffer against eutrophication. They can sequester environmental carbon in their shells, which contributes to long-term storage of carbon in the oceans. Furthermore, bivalves can modify their environment by creating habitats for other species, such as by forming reefs or beds that provide shelter and feeding opportunities for other animals. Their ecological value makes bivalves important indicators of aquatic ecosystem health.

Table 1.1. Distribution of bivalves in different aquatic environments. The table was taken form (Ponder et al., 2019). The • indicates the environment in which bivalves are found. They are notably absent from pelagic marine and aquifer freshwater environments.

Aquatic environment	Zone	Distribution of bivalves
Marine	Oceans	•
	Pelagic	
	Benthic	•
	Intertidal	•
	Vents & Seeps	•
	Coral Reefs	•
	Estuaries	•
Fresh water	Lakes & Ponds	•
	Springs & Seepages	•
	Aquifers	
	Swamps & Wetlands	•
	Rivers & Streams	•

Bivalves as filter feeders, are important for maintaining the balance of carbon and nutrients in the water column (Burkholder and Shumway, 2011; Dame, 1993; Welsh, 2003). They are involved in nutrient recycling, as they release nutrients back into the environment through their excretion and decomposition. They can also act as a buffer against eutrophication by removing excess nutrients from the water column through filter feeding, which can help to prevent harmful algal blooms (Brown et al., 2020; Rice, 2001).

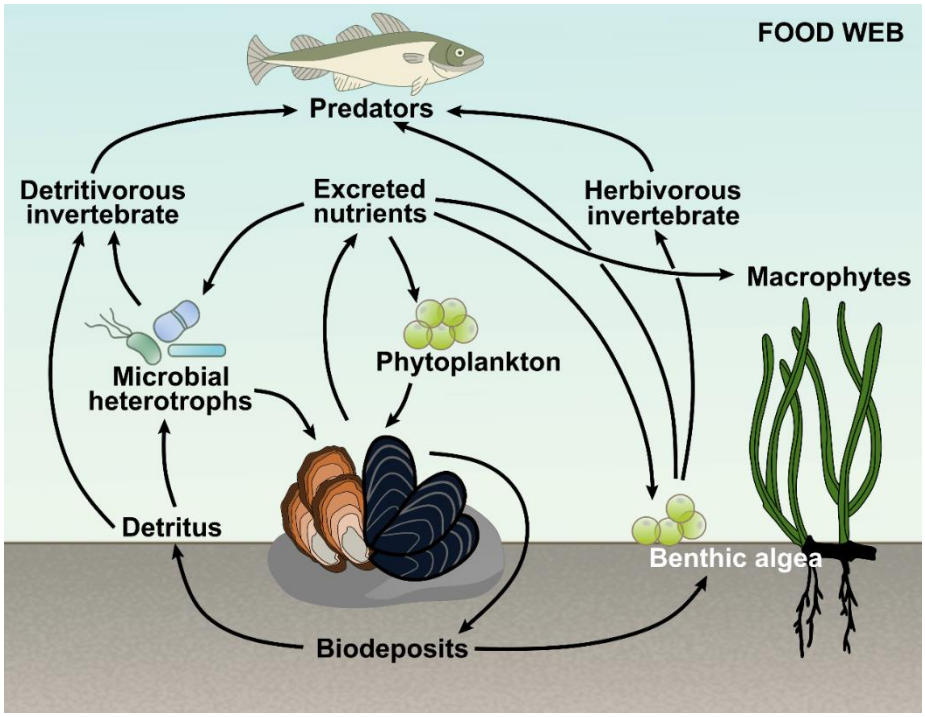

Figure 1.4. The role of bivalves in marine food webs. Bivalves feed on suspended seston and excrete and biodeposit nutrients that stimulate autotrophic and heterotrophic production. The increased secondary production of herbivorous and detritivorous invertebrates favoured by the action of bivalves supports fish production and predators. Figure modified from (Vaughn and Hoellein, 2018).

The bivalves ability to sequester carbon in their shells plays an important role in ecology, since it helps to remove carbon from the water column and contributes to the long-term storage of carbon in the oceans. In fact, bivalves are estimated to sequester as much as 13.6 million tons of calcium carbonate per year (Alonso et al., 2021; Chmura et al., 2003). This ability to sequester carbon makes bivalves an important part of the global carbon cycle and highlights their importance in protecting habitats and organisms.

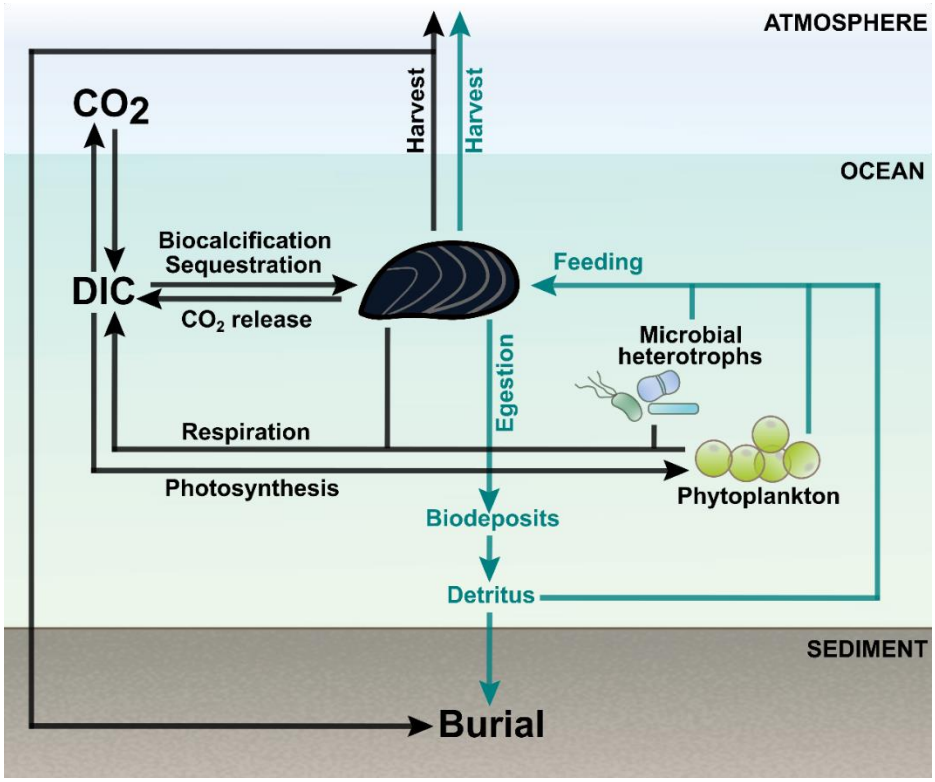

Figure 1.5. The role of bivalves in the carbon cycle. Blue and black lines represent organic and inorganic carbon fluxes. DIC- Dissolved inorganic carbon. The figure was adapted from (Filgueira et al., 2019) and was drawn in Inkscape software v1.2.

Bivalves have the ability to modify their environment by creating habitats for other marine species. Oysters and mussels can form reefs or beds that provide shelter and feeding opportunities for a wide range of other species (Coen et al., 1999; Fitzsimons et al., 2020). These habitats have important ecological and economic value, as they can support commercial fisheries and provide recreational opportunities for humans.

Furthermore, bivalves have been used as bioindicators of environmental quality. Their filter feeding behavior makes them particularly sensitive to contaminants in the water, and their tissues can accumulate these contaminants, making them useful for monitoring

pollution levels (Bonacci et al., 2004; Yap et al., 2021). Bivalves are also being explored for their use in bioremediation, as they can effectively remove pollutants such as heavy metals from environmental waters.

1.3.2 Commercial value of bivalves

Bivalves have been commercially harvested for centuries for their meat, pearls, and shells, making them an important economic resource in many countries. Global production of bivalves has increased over the years, with the Food and Agriculture Organization (FAO) reporting a record high of 17.3 million tonnes in 2018 (FAO, 2020).

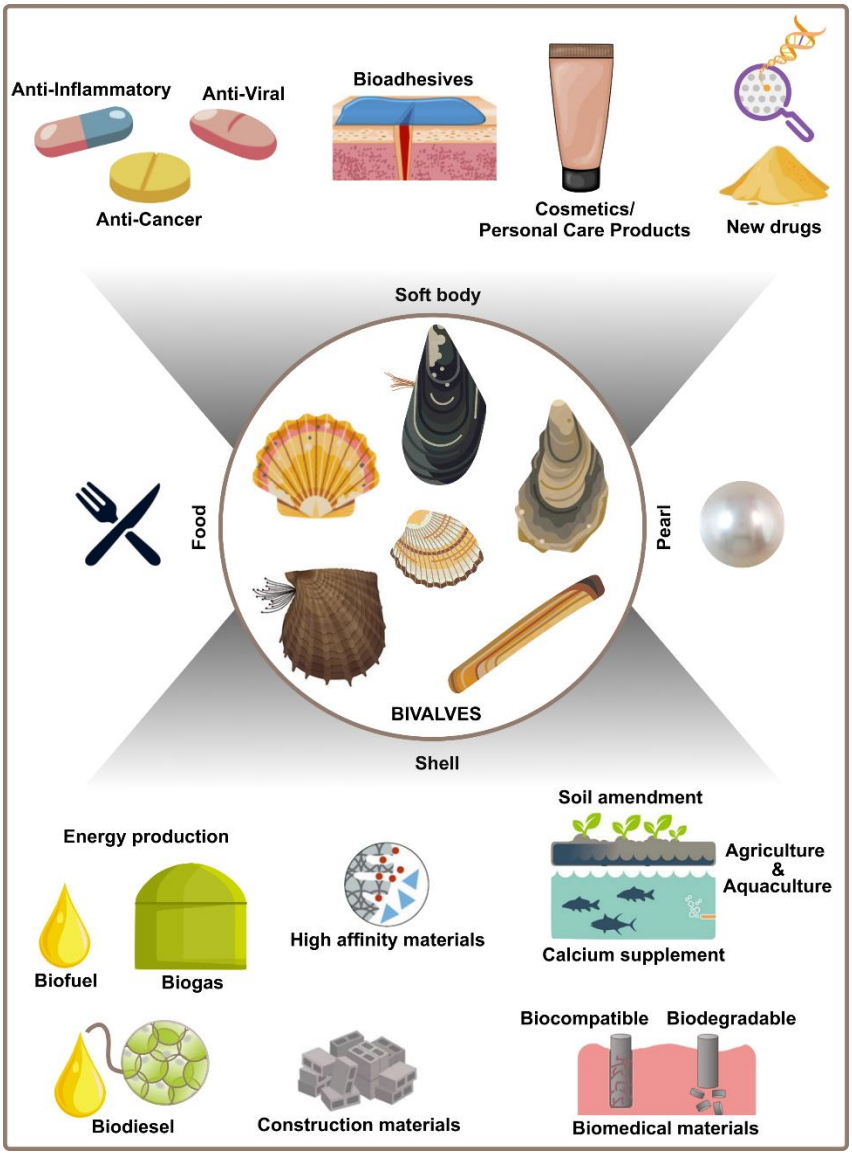

Figure 1.6. Commercial value of bivalves. Representative bivalves images cited from the Marine conservation society/Good fish guide (https://www.mcsuk.org/goodfishguide/) and (Zhang et al., 2022).

One of the primary commercial uses of bivalves is as a food source. They are widely consumed around the world and are particularly popular in Europe and Asia (Avdelas et al., 2021; Venugopal and Gopakumar, 2017). Bivalves such as oysters, mussels, clams and scallops are culinary delicacies. The global market for bivalve meat has been valued at over $23.9 billion and this is expected to grow in the coming years (Olivier et

al., 2020).

In addition to their popularity as food, bivalves are also used for pearl production and the major producers of cultured pearls are China, Japan, and other countries in the Asia-Pacific region, such as Australia and French Polynesia (Nagai, 2013; Taylor and Strack, 2008; Zhu et al., 2019). The pearl industry is an important sector of the global economy, valued at billions of dollars annually. Pearls have been highly prized throughout history for their beauty and rarity, and the demand for high-quality pearls remains strong today. Cultured pearls, which are produced by implanting a bead or tissue in a mollusc to stimulate pearl growth, now accounts for the vast majority of the pearl industry (Akamatsu et al., 2001; Li et al., 2018; Scarratt et al., 2000).

Bivalves are also an important source of industrial and pharmaceutical products for the development of new drugs and therapies (Eghianruwa et al., 2019). They contain bioactive compounds that have anti-inflammatory, anti-cancer, and anti-viral properties (Eghianruwa et al., 2019; Grienke et al., 2014; Zhukova, 2014). Bivalves such as the Pacific oyster contains heparin-like molecules that have potential applications as blood thinners (Dwivedi and Pomin, 2020). The blue mussel (*Mytilus edulis*) is widely used to produce adhesive materials, such as mussel adhesive protein (MAP) that can be used in the production of bioadhesives, coatings, and wound healing products with antimicrobial properties for medical

applications (Waite, 2017). It has been reported that oyster (*Saccostrea cucullata*) protein hydrolysates exhibit cytotoxic activity on colon cancer cells (HT-29) (Umayaparvathi et al., 2014) and are being explored for potential cancer therapy (Islam et al., 2022). Bivalves are also a source of bioactive compounds that can be used in the cosmetics and personal care product industry. For example, chitosan, a compound derived from the shells of crustaceans and bivalves, has moisturizing and anti-aging properties (Aranaz et al., 2018; Hosseini et al., 2022; Odeleye et al., 2019).

Bivalve shell waste is a valuable resource in a variety of industrial fields, ranging from agriculture to energy production. In agriculture farming, shell waste can be used o improve soil quality and promote plant growth (Alonso et al., 2021) as well as a fertilizers to increase crop yield and quality (Moon et al., 2000). In aquaculture, shell waste has been used as a calcium supplement in feed for farmed fish and shrimp, improving their growth and survival rates (Topić Popović et al., 2023) as well as a substrate for biofilm formation to improve water quality (Campanati et al., 2022). Shells can also be used for environmental remediation since they can remove heavy metals, phosphorus (PO_4^{3-}) and organic pollutants from contaminated water and soil (Roy, 2017). This application is particularly promising due to the abundance of bivalve shell waste and the high affinity of the shells for these type of contaminants (Olivier et al., 2020).

In the Biomedical industry the unique properties of bivalve shells, such as their high calcium content and porous structure, make them a promising material for tissue engineering and drug delivery (Morris et al., 2019; Scialla et al., 2020). Shell waste can also serve as an alternative material to traditional construction materials, such as cement and aggregates, due to its high compressive strength and low thermal conductivity (Summa et al., 2022; Yao et al., 2014) and it has also been explored as a potential source of biofuel and biogas production (Jović et al., 2019; Ramakrishna et al., 2018).

1.4 Representative economic bivalve species

Considering the diversity of bivalves, only a few species are of high commercial and economic importance and have been studied in most detail. These species are commonly used as a food source, as well as for the production of various industrial materials and pharmaceutical products. The most commonly exploited bivalve species include the Pacific oyster (*M. gigas*), pearl oyster (*Pinctada fucata*), blue mussel (*M. edulis*), Mediterranean mussel (*M. galloprovincialis*), scallop (*Pecten maximus*), soft-shell clam (*Mya arenaria*), razor clam (*Ensis directus*), Manila clam (*Ruditapes philippinarum*), cockles (*Cerastoderma edule*), geoduck clam (*Panopea generosa*), Atlantic surf clam (*Spisula solidissima*), and quahog clam (*Mercenaria mercenaria*).

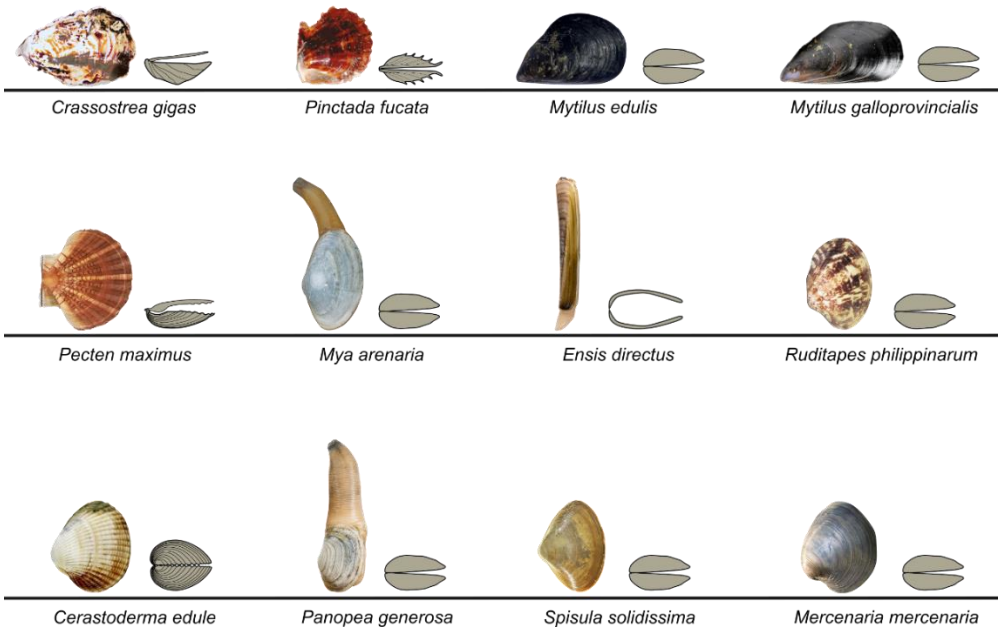

Figure 1.7. Examples of economically important bivalves.

The Pacific oyster, native to Asia, has become one of the most important bivalve species in world aquaculture due to its rapid growth and adaptability to different environments. The blue mussel and Mediterranean mussel (a target of the present thesis) are widely distributed along the coasts of Europe, North America, and Asia, and are a popular food sources and the shell is also used as a source of industrial materials. The scallop is highly valued for its delicate flavour and is commonly found in both wild and farmed environments. The soft-shell clam is an important commercial species in the eastern United States and Canada, while the razor clam is highly sought after in Asia and Europe.

The Manila clam, a species native to the western Pacific, has become a widely farmed species in many parts of the world. The cockles, geoduck clam, Atlantic surf clam, and quahog clam are also important species in different regions of the world, due to their significant economic value.

1.4.1 The Pacific oyster (M. gigas)

Originally from the Pacific coast of Asia, *M. gigas* was introduced in other parts of the world, including Europe and North America due for aquaculture purposes (Guo, 2009). It is one of the target species of the present thesis and is one of the most extensively farmed shellfish species worldwide, accounting for a significant portion of global aquaculture production (Olivier et al., 2020; FAO, 2020; Neves et al., 2021). *M. gigas* is a sessile bivalve that typically attaches to hard substrates such as rocks, pier pilings, and oyster shells. They have a wide tolerance to environmental conditions, including temperature, salinity, and wave exposure, which allows them to occupy a variety of intertidal and subtidal habitats. Oysters have a complex life cycle with separate male and female individuals that release sperm and eggs into the water column for fertilization. The fertilized egg develops into a trochophore larva, which is a ciliated, free-swimming stage. As the trochophore larva matures, it undergoes several changes, eventually developing into a veliger larva. The veliger stage is characterized by the development of a foot and is

when shell formation begins. The veliger larva undergoes metamorphosis to becomes a pediveliger larva with a well-developed foot and shell that settles on a suitable substrate and become a juvenile oyster (known as a spat) and subsequently acquires an asymmetric shell.

The shell of *M. gigas* is roughly oval or teardrop-shaped, with a flattened upper surface and a more rounded bottom surface (round valve settles on a suitable substrate). The size of the shell can vary greatly depending on the age and growth rate of the individual. Mature adults can reach up to 20 cm in length and weigh up to 1 kg. The shell of *M. gigas* is typically grayish-brown or whitish-gray in color, although it can also have shades of purple or green. The color of the shell may also change depending on environmental factors. The surface of the shell is rough and bumpy, with irregular growth lines that mark periods of growth and dormancy. The outer layer of the shell is composed of calcium carbonate. The edges of the shell are sharp and serrated, with small projections that help the oyster to attach itself to a substrate (Miossec et al., 2009).

M. gigas, has become a valuable model organism for investigating a wide range of research questions related to bivalve biology, ecology, and evolution. The species has been extensively studied for its genetic (species genome was sequenced and assembled in chromosome level) and physiological traits, which are of interest to both aquaculture and conservation scientists (Bayne, 1999; Penaloza et al., 2021; Qi et al.,

2021; Zhang et al., 2012). In *M. gigas*, previous studies have explored the genetic basis of growth, disease resistance, and stress tolerance, in order to develop more efficient breeding programs for aquaculture (De Melo et al., 2018; Gutierrez et al., 2018; Meng et al., 2019; Yang et al., 2022). Researchers have investigated the mechanisms by which *M. gigas* is able to resist environmental stressors, such as changes in temperature, salinity, and pH (Wei et al., 2015; Zhao et al., 2012). Studies have also focused on the ecology of *M. gigas*, including its interactions with other organisms, such as predators and competitors (Alfaro et al., 2019; Padilla, 2010). Furthermore, *M. gigas* has been used as a model for investigating topics such as biomineralization and bioremediation, due to its ability to secrete large amounts of calcium carbonate and remove particulate matter from the water column (Silva et al., 2012).

1.4.2 The mediterranean mussel (M. galloprovincialis)

The mussel *M. galloprovincialis*, belongs to the Mytilidae family. This species prefers to settle on hard substrates such as rocks, pier piling or on other mussels and can be found in both intertidal and subtidal habitats (Ceccherelli and Rossi, 1984). The life cycle of *M. galloprovincialis* is typical of most bivalve molluscs with separate sexes (identifiable at the spat larval stage) and external fertilization, with the byssus (secreted filaments) that attaches them to the substrate after metamorphosis (Lazo

and Pita, 2012).

The shell of *M. galloprovincialis* is elongated and the two valves are symmetrical, with a triangular or wedge-shaped outline. The size of the shell can vary depending on the age and growth rate and adults can reach up to 10 cm in length. The shell of *M. galloprovincialis* is typically dark purple or black in color, although it can also have shades of brown. The surface of the shell is smooth and shiny, with a thin outer layer that is composed of periostracum, a protein-based material that protects the underlying shell layers (calcium carbonate) (Krylova and Sahling, 2010; Waller, 1978).

This species is native to the Mediterranean Sea (where is the dominant mussel species) but has also been introduced to other regions, including the Atlantic coast of Europe, South Africa, Australia, and New Zealand for aquaculture proposes or mostly due to their successful invasiveness due to their adaptability (Wonham, 2004). The presence of *M. galloprovincialis* in these regions has a significant ecological and economic impacts, including changes in the structure of marine communities with displacement of native species (Suchanek et al., 1997; Wilkins et al., 1983; Wonham, 2004). This species is also an important aquaculture species worldwide, being farmed for its edible meat and due to its adaptability to a diversity of conditions.

The taxonomy and phylogenetic relationships of *M. galloprovincialis*

have been the subject of numerous studies. Molecular phylogenetic analysis revealed that *M. galloprovincialis* is closely related to other Mytilus species, such as *M. edulis* and *M. trossulus*, and has a complex evolutionary history with multiple hybridization events (Krylova and Sahling, 2010; Rey-Campos et al., 2021; Waller, 1978) and some authors suggest that they may represent a subspecies of *M. edulis* (Krylova and Sahling, 2010). The genetics of *M. galloprovincialis* have also been extensively studied (Gerdol et al., 2020), with the species serving as a model organism for population genetics and evolutionary ecology. Molecular markers such as microsatellites and mitochondrial DNA have been used to investigate the genetic diversity, structure, and connectivity of *M. galloprovincialis* populations across its range (Cao et al., 2004; Mizi et al., 2005).

M. galloprovincialis has been the subject of numerous scientific studies due to its ecological and economic importance, as well as its potential as a model organism for research, since species genome was sequenced and assembled in high quality. The species widespread distribution, adaptive traits, and strong genetic structure make it a valuable tool for studying various topics, including population genetics, reproductive biology, and adaptation to changing environments (Daguin and Borsa, 2000; Figueras et al., 2019; Robledo et al., 1995). Additionally, the filter-feeding behavior of the species and its ability to accumulate

pollutants make it a useful indicator of environmental health (Box et al., 2007; Fernández et al., 2010).

1.5 Bivalve shell biomineralization

1.5.1 Bivalve shell composition

The shell is an essential component of bivalves and protects, supports, and maintains body shape as well as providing a source of minerals. It is composed of a complex array of organic and inorganic molecules that interact to form a strong and durable structure. A major component of the shell is calcium carbonate, which is secreted by specialized cells of the mantle. Mantle cells secrete the ions and the organic shell matrix that forms the framework for the nucleation and formation of calcium carbonate crystals (Cuif et al., 2010). The shell organic matrix contains proteins, glycoproteins, and polysaccharides that play an important role in shell formation and organization. Some of these organic molecules are involved in controlling the nucleation and growth of the calcium carbonate crystals, while others are involved in regulating the size and shape of the crystals (Addadi et al., 2006). In addition, the shell also contains trace amounts of other minerals such as magnesium, strontium, and fluoride. Which have a significant impact on the properties of the shell, including its strength, durability, and resistance to erosion and dissolution (Keihan et al., 2020; Pilkey and Goodell, 1964; Sharma et al.,

2021; Wanamaker Jr and Gillikin, 2019).

Due to the difference in shell weight and composition, there are currently no reports indicating the physiological metabolic energy value spent by bivalves to build shells. In addition, this value also differs at different developmental stages of a single species. However, there are still people who have measured the source of shell carbon atoms in a specific state of a specific species, such as (Lu et al., 2018)reported that in normal seawater, the proportion of calcium carbonate derived from environmentally soluble inorganic carbon in *M. edulis* shells About 80.3%, with the remaining portion attributed to metabolism.

The shell composition and microstructure can vary significantly between different species and environmental factors such as temperature, salinity, and pH influence the shell microstructure. For example, changes in ocean chemistry due to OA can affect the ability of bivalves and other molluscs to form their shells (Doney et al., 2009; Grenier et al., 2020; Harayashiki et al., 2020).

1.5.2 Bivalve shell microstructure

The bivalve shell is composed by two valves and this structure plays a crucial role in their survival, protection, and adaptation to the environment (Dame and Kenneth, 2011). The shell is made up of three main layers, namely the outer layer or periostracum that is in direct

contact with the external aquatic environment, the middle layer, and the inner layer which is in contact with the extrapallial space, a cavity between the mantle epithelium and the shell, where shell biomineralization takes place (Kaplan, 1998; Kobayashi, 1969). Diverse shell structures are seen in bivalves. The shell shape, size, and thickness varies among the different bivalve species and is correlated with their mode of life, feeding habits, and habitat (McDougall and Degnan, 2018; Schneider and Carter, 2001).

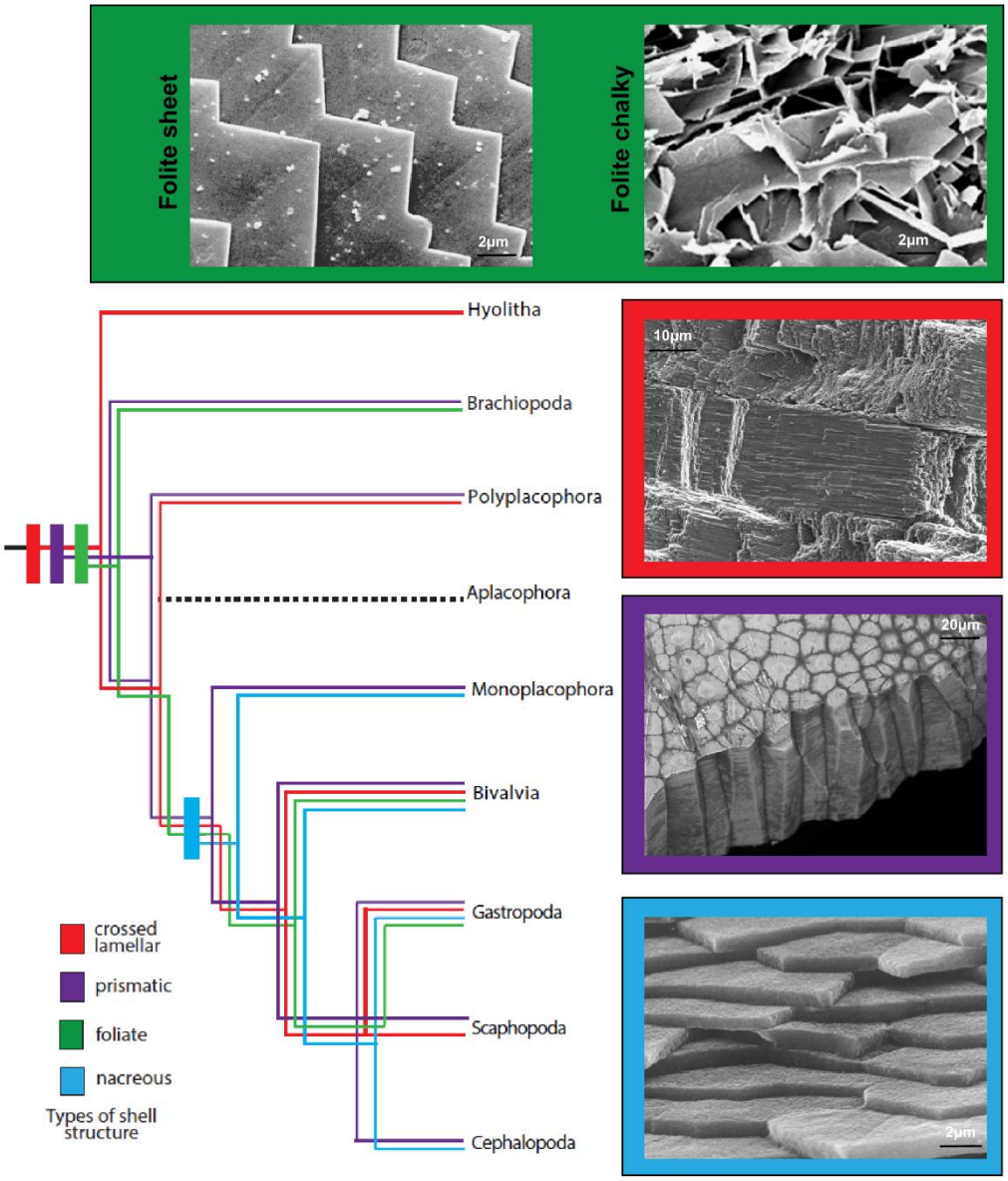

Figure 1.8. Diagrammatic of distribution of main types of shell microstructure in molluscan and Bivalvia class distributed crystal types presentation in SEM image. The figure of main types of shell microstructure in mollusc distribution and SEM images (folite sheet and nacreous) cited from Ponder et al., 2019. The dendogram branches are colour coded in accordance with the colour of the boxed crystal type. The SEM images prismatic and crossed lamellar cited from (Checa, 2018). The SEM image folite chalky was cited from (Lee et al., 2011) and was drawn in Inkscape software v1.2.

The outer layer or periostracum is a thin organic layer that covers the outer surface of the shell and protects it from erosion and abrasion

(Kniprath, 1981). The periostracum is composed of a matrix proteins and chitin, and the latter is a polysaccharide that plays a similar role as a matrix for the formation of the exoskeleton in insects (Bubel, 1973; Saleuddin and Petit, 1983; Saleuddin, 1974). The periostracum is also responsible for conferring the shells colour and texture, which varies substantially among different species of bivalves (Taylor et al., 1969).

The middle layer usually distributed with prismatic/crossed lamellar crystal is the thickest layer of the shell and is composed of calcium carbonate in the form of calcite/aragonite (Taylor et al., 1969). The middle layer is responsible for providing strength and rigidity to the shell, and it is composed of long, needle-like crystals that are oriented perpendicular to the surface of the shell (Taylor et al., 1969). The orientation of these crystals gives the shell its characteristic cross-hatch pattern, which is visible under a scanning electron microscope (Checa et al., 2005). (Schneider and Carter, 2001) believed that there may be a complex evolutionary relationship between the simple columnar arrangement of the prismatic structure and the crossed lamellar structure, because the crossed lamellar was the first to be discovered in ancient bivalve fossils.

The inner shell layer usually distributed with nacreous/foliate/crossed lamellar crystal is directly in contact with the extrapallial fluid and is composed of calcium carbonate in the form of calcite/aragonite (Checa,

2000). The inner (nacreous) layer is responsible for giving the shell its iridescent appearance and is composed of thin, overlapping layers of aragonite crystals (Dauphin et al., 2008). The inner layer has an important role in maintaining the structural integrity of the shell (Nudelman et al., 2008; Sun and Bhushan, 2012).

The micro-structure of the *M. gigas* shell, which is asymmetric, has been studied using various techniques, including scanning electron microscopy (SEM), X-ray diffraction, and Fourier transform infrared spectroscopy (FTIR). These studies revealed that the crystallographic orientation of the prism's changes with shell depth, and that the foliate layer is composed of calcite platelets that are approximately 40 nm thick (Sun and Bhushan, 2012). In addition to the prismatic and foliate layers, *M. gigas* shells contains organic material, which makes up approximately 1-2% of the shell by weight. This organic material is thought to control crystal growth and orientation, and to promote the adhesion between the prismatic and foliate layers (Dauphin et al., 2013). In *M. gigas* the prismatic layer crystal structure in the flat and round valves are different (Yamaguchi, 1994; Zamarreño et al., 1996) due to differences in the arrangement of the prismatic crystals, as well as differences in the organic matrix components that help with crystal mineralization. The prismatic crystals of the flat shell have a near-geometric crystal structure with regular boundaries and no cracks resembling the prismatic structure of

symmetric shells (Peng et al., 2021; Yamaguchi, 1994; Zamarreño et al., 1996). In contrast the crystals of the round shells have a ridge-and-furrow structure, which is associated with their rapid growth for substrate adherence (Yamaguchi, 1994). The prismatic layer of the round valve is composed of elongated crystals that are stacked perpendicular to the shell surface, forming columnar structures that are more tightly packed than those present in the flat valve (Zamarreño et al., 1996). In the flat valve, the prisms are oriented more parallel to the shell surface. The chemical composition of the prismatic layer can also differ slightly between the two valves. The flat valve has a higher magnesium content in the prismatic layer than the round valve, which may be related to its increased thickness and mechanical strength (Yamaguchi, 1994).

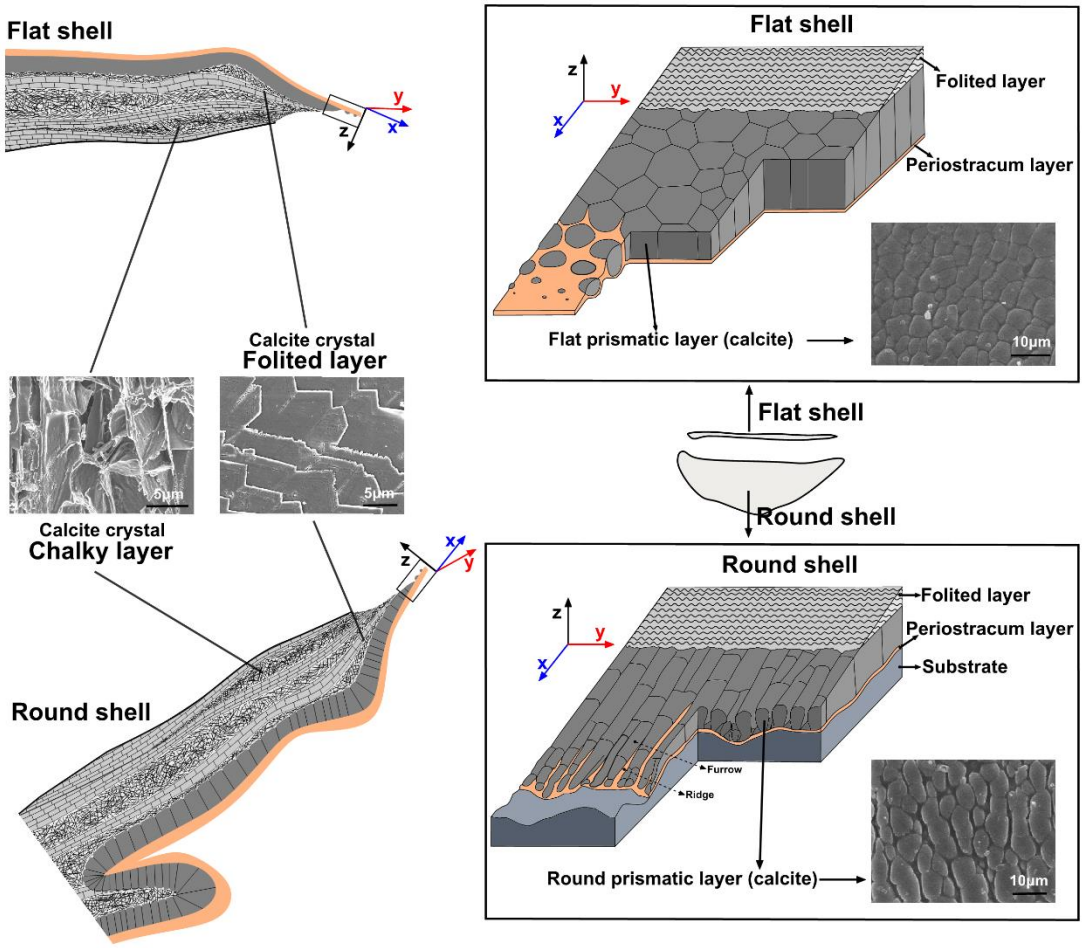

Figure 1.9. Schematic diagram of the *M. gigas* shell structure. The different shell layers are identified. The SEM figures of the foliated and chalky layer is cited from (Checa, 2018) and was drawn in Inkscape software v1.2.

The valves of *M. galloprovincialis* are symmetric and exhibit a similar micro-structure that differs from *M. gigas*. The outer layer, known as the periostracum, is a thin organic layer that covers the surface of the shell and provides protection against physical damage and chemical erosion (Furuhashi et al., 2009a). Underneath the periostracum is the prismatic layer, which is composed of calcium carbonate crystals that are arranged in a prism-like structure (Gillikin et al., 2008). The prisms are

oriented perpendicular to the shell surface and are separated by an organic matrix that helps to bind them together. Beneath the prismatic layer is the nacreous layer, which is composed of calcium carbonate platelets that are arranged in a highly ordered fashion (Frýda et al., 2010). The platelets are separated by thin layers of organic material, which helps to control the growth and orientation of the crystals.

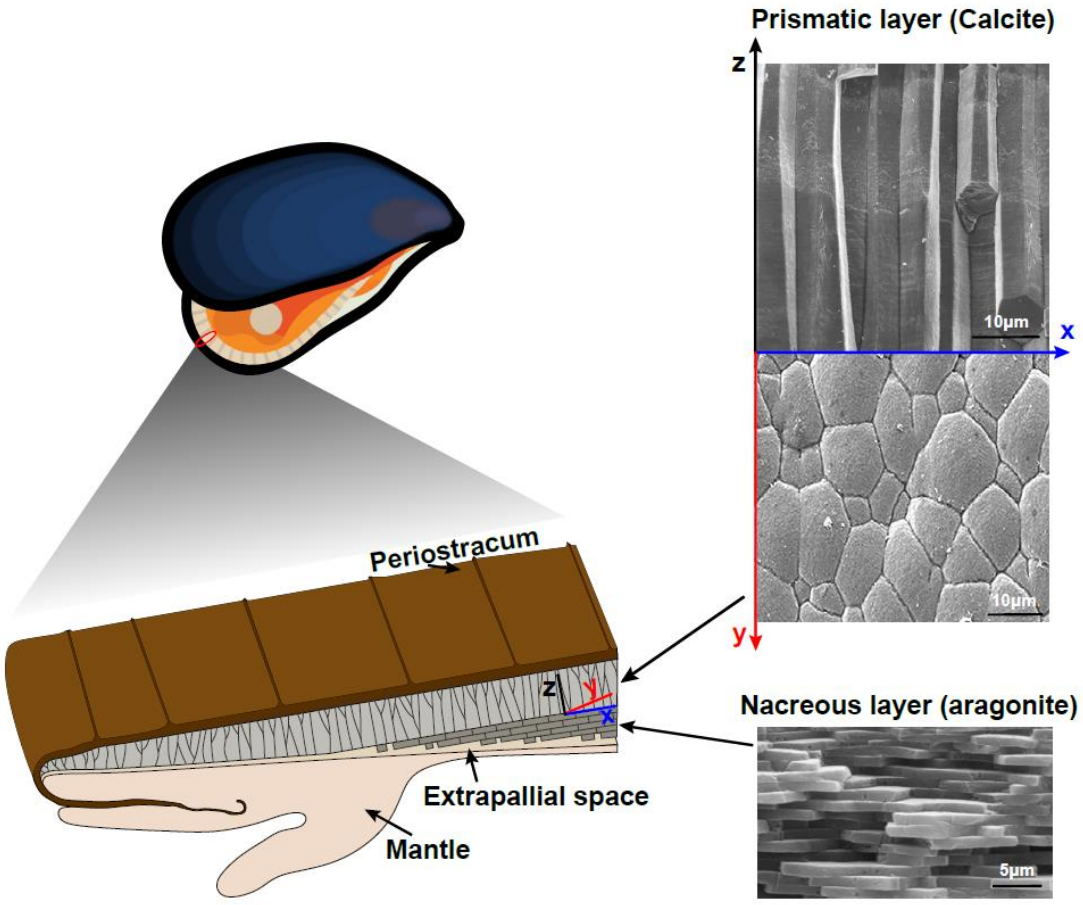

Figure 1.10. Schematic diagram of the *M. galloprovincialis* shell structure. The different shell layers are identified and a magnified image of the crystals is presented in the right hand image. The figure was adapted from (Checa, 2018) and was drawn in Inkscape software v1.2.

1.5.3 Biomineralization of bivalve shells

Shell formation is a complex process that involves the deposition of calcium carbonate crystals in a highly regulated manner. This process is mediated by a specialized tissue called the mantle, which lines the interior of the shell and secretes the material that are essential to form the shell (Marin and Luquet, 2004). This tissue is involved in shell formation, shell repair, and pigmentation. The circulating haemocytes (in the haemolymph with immune functions) have also been suggested to play a role in shell biomineralization through the transport of calcium and carbonate but this will not be described here (Ballina et al., 2022).

The mantle is a highly specialized tissue (it is a thin, membranous layer) that is composed of three layers or folds: the outer epithelial layer, a connective tissue middle layer, and the inner fold an inner secretory layer each of which have a distinct function in shell formation (Richardson et al., 1981). The outer fold is also named the pallial epithelium and is responsible for secreting the organic matrix (proteins, glycoproteins, and polysaccharides) that serve as a scaffold for the deposition of calcium carbonate crystals (Addadi and Weiner, 1992; Morton and Peharda, 2008). The epithelium layer of the mantle contains secretory cells that produce mucus and enzymes that are essential for shell maintenance (Audino et al., 2015a). The mantle epithelial cells are arranged in a continuous monolayer that lines the inner surface of the

mantle tissue. The cells are columnar in shape and are tightly packed, forming a dense layer of cells that extends over the entire mantle surface. The cells contain numerous organelles, including endoplasmic reticulum and golgi apparatus, which are involved in the synthesis and transport of the shell matrix components to the extrapallial space (Jacob et al., 2008).

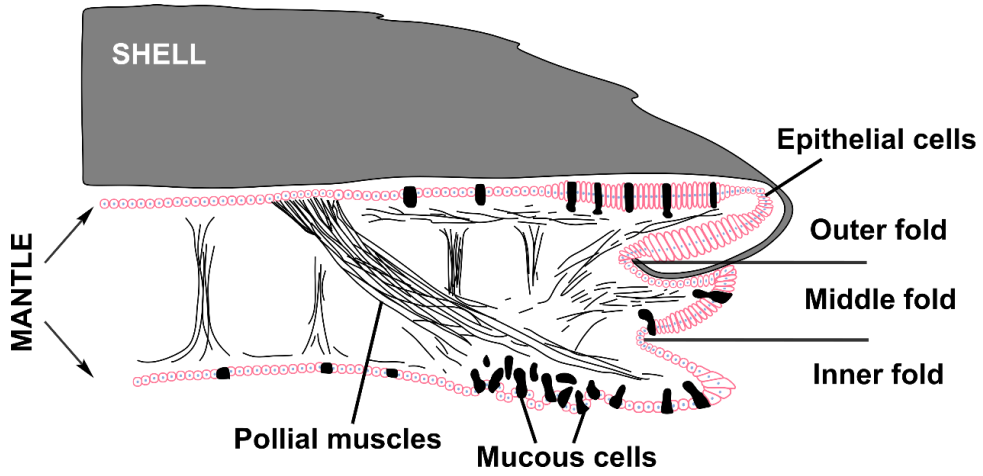

Figure 1.11. Schematic representation of the bivalve mantle showing the main structures and cell types. The image was adapted from (Kauffman, 1979) and was drawn in Inkscape software v1.2.

The connective tissue layer provides structural support to the mantle and facilitates the exchange of gases and nutrients between the mantle and the rest of the body (Audino and Marian, 2016). The inner fold of the mantle is also named the pallial musculature and is responsible for controlling the shape and size of the shell (Audino et al., 2015b; Audino and Marian, 2018). The inner mantle fold, on the other hand, plays a role in the movement of water in and out of the shell (Trueman, 1966). In addition the mantle tissue also contains specialized cells called epithelial

cells. These cells are involved in the secretion of enzymes that are necessary for shell formation.

As the shell grows, it undergoes a process of remodeling and repair, which is mediated by specialized cells called shell-forming cells. These cells are located within the mantle tissue, and are responsible for secreting new layers of calcium carbonate onto the existing shell (Marin and Luquet, 2004). In addition to secreting new layers of calcium carbonate, the shell-forming cells are also responsible for removing damaged or old shell material, and replacing it with new material (Weiner and Addadi, 1997).

The shell is a highly complex and dynamic structure that is continuously formed and remodeled throughout the life of the animal. In bivalves, shell formation begins during early embryonic development and continues throughout their life span. Shell formation is a complex biological process that involves the accumulation of calcium carbonate and the secretion of organic matrix proteins. Once the organic matrix has been secreted, calcium ions are transported from the haemocytes into the extrapallial space between the pallial epithelium or outer fold and the shell. The calcium ions combined with carbonate ions form the calcium carbonate crystals, which are deposited onto the organic matrix (Addadi and Weiner, 1992). The deposition of calcium carbonate crystals is highly regulated, and is mediated by a variety of proteins and enzymes that

control the size, shape, and orientation of the crystals (Weiner and Addadi, 1997).

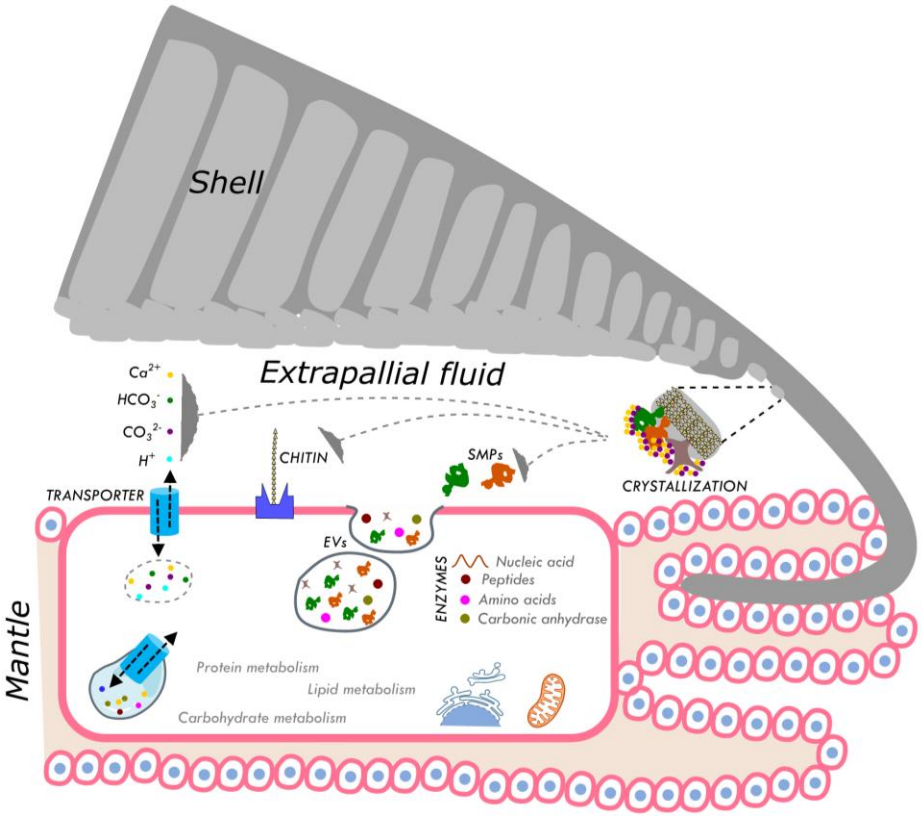

Figure 1.12. Schematic representation of the main mechanisms involved in shell biomineralization in bivalves. A largely amplified mantle epithelial cell shows the core processes that contribute to shell formation. The extrapallial space serves as a site for calcium carbonate crystal formation and brings together SMPs, chitin, enzymes, and inorganic salt ions secreted from epithelial cells. These substances use the self-assembled structure of chitin nanofibers as the skeleton and combine with enzymatic inorganic salt molecules under the action of SMPs to crystallize calcium carbonate. The figure was drawn in Inkscape software v1.2.

The first step in shell formation is the secretion of an organic matrix, which serves as a scaffold for calcium carbonate crystal deposition (Figure 1.12). The organic matrix is composed of various proteins, including chitinase, tyrosinase, and mantle-specific gene 1 (MSG1)

(Yarra et al., 2021). According to (Liao et al., 2021), chitinase is involved in the formation of the periostracum, which is the outermost layer of the shell. Tyrosinase, on the other hand, is responsible for the formation of the prismatic layer, which is the middle layer of the shell. Finally, MSG1 is essential for the formation of the nacreous layer, which is the innermost layer of the shell.

The deposition of calcium carbonate occurs within the secreted organic matrix. The initial deposition of calcium carbonate occurs in the form of amorphous calcium carbonate (ACC), which is then transformed into a crystalline form (Evans, 2019). According to (Gebauer et al., 2009), the transformation of ACC into the crystalline form is facilitated by the presence of acidic proteins, such as Asp-rich and perlucin. These proteins stabilize the ACC particles and prevent their aggregation, allowing them to transform into a stable crystalline form. Shell formation is regulated by various genes, including those encoding SMPs and carbonic anhydrase (CA) (Yarra et al., 2021). According to (Furuhashi et al., 2009b), SMPs are involved in the formation of the organic matrix and calcium carbonate crystals, while CA is involved in the regulation of pH levels in the shell-forming tissue. The expression of these genes is regulated by a diversity of environmental factors, such as temperature, salinity, and pH levels (Nudelman, 2015).

1.5.4 The biomineralization toolbox

Bivalves have developed a sophisticated set of tools to control the formation, composition, and morphology of their shells (Jackson and Degnan, 2016). The biomineralization toolbox of bivalves is a complex and dynamic system and one of the key components is the organic matrix that surrounds and guides the formation of the shell mineral phase but there are also other structures such as ion transporters, enzymes and extracellular vesicles that are suggested to play a key role in shell formation

1.5.4.1 Organic matrix

The organic matrix is a complex mixture of SMPs, polysaccharides and lipids (Weiner and Traub, 1984). It has been estimated that proteins represent 90% of the shell organic matrix, carbohydrates vary from 0.15 to 0.29%, while lipids vary from 0.8 to 2.9% (Goulletquer and Wolowicz, 1989).

1.5.4.2 Shell matrix protein (SMP)

The protein perlucin has been shown to promote the formation of aragonite, a particular form of CaCO3, in the shells of the pearl oyster *Pinctada margaritifera* (Suzuki et al., 2009). The SMPs of bivalve shells are highly diverse and can be classified into several groups based on their amino acid composition, structure, and function. One of the most abundant groups of SMPs is the acidic SMPs, which are rich in

phosphorylated residues (Yarra et al., 2021). These proteins play a critical role in regulating the nucleation and growth of calcium carbonate crystals by serving as templates for crystal formation (Marin, 2020). Another important group of SMPs is the basic SMPs, which are rich in positively charged amino acids such as lysine and arginine (Marie et al., 2013). These proteins are thought to play a role in regulating the morphology and orientation of crystals in the shell (Huang et al., 2021). SMPs, such as Shematrins and Pearlin, contain hydrophobic residues and are believed to be important for the adhesion of $CaCO_3$ crystals to the organic matrix (Marie et al., 2012). Glycine-rich SMPs, such as N16 and N19, are highly repetitive and are suggested to play a role in the control of crystal orientation (Liu et al., 2015). Additionally, several other groups of SMPs have been identified, including chitin-binding proteins, collagen-like proteins, lectins, glycosaminoglycans and metal-binding proteins (Marie et al., 2017, 2013; Suzuki and Nagasawa, 2013).

1.5.4.3 Polysaccharides

The composition of the polysaccharide in the organic matrix of bivalve shells varies among different species. In *M. gigas*, the main polysaccharide component is chitin, which makes up about 3.5 % of the total weight of the shell organic matrix (Chan et al., 2018; Dauphin et al., 2013; Peters, 1972). In contrast, the organic matrix of the mussel shell (*M. edulis*) is primarily composed of β-chitin and chitosan, with smaller

amounts of other polysaccharides (Addadi et al., 2006). Other bivalves, such as the clam (*M. mercenaria*), have a more complex polysaccharide composition in their shell organic matrix, which is primarily composed of chitin and chitosan, but also includes fucan, xylan, and other unidentified polysaccharides (Horan, 1983; Pallela, 2014).

1.5.4.4 Lipids

According to (Cobabe and Pratt, 1995), the lipid content of the shell organic matrix of the bivalve *Arac zebra* and *Codakia orbicularis* is rich in cholesterol, phytadiened and ketones. These lipids are thought to be involved in the formation and stabilization of the calcium carbonate mineral phase of the shell. Another study (Dreier et al., 2014) found that the lipid composition of the shell organic matrix of the bivalve *Fragum unedo* is also rich in octadecanoic acid and hexadecanoic acid, which contribute to the flexibility and resilience of the shell (Jacob et al., 2008). In addition to phospholipids and glycolipids, sphingolipids are also present in the shell organic matrix of bivalves (Li et al., 2018). These lipids are known to play a role in cell signaling and membrane structure in other biological systems, and may have important functions in the shell (Farre et al., 2008) and n-alkanes, n-alcohols, fatty acids and sterols have been detected in bivalve shell (Collins et al., 1995) and the contents and ratios of these components were suggested to be dependent on the environment and phylogeny. Lipids of the nacreous layer of *P. fucata* are

diverse, with cholesterol, fatty acids, triglycerides and other unknown components being described (Rousseau et al., 2006) and the lipid diversity was suggested to contribute to the mechanical properties of the shell, such as resistance to fracture and deformation.

Table 1.2. List of shell matrix protein (SMP) identified in bivalves shells. Data was obtained and from the Mollusca shell matrix proteins database Yarra, (2019, https://data.bas.ac.uk/full-record.php?id=GB/NERC/BAS/PDC/01132) and adapted for the thesis.

Shell matrix protein	Species	Interproscan Domain Name
Alpha carbonic anhydrase (Nacrein)	*Pinctada maxima, Pinctada fucata, Mytilus coruscus, Mytilus californianus, Crassostrea nippona, Mizuhopecten yessoensis, Magallana gigas, Mytilus galloprovincialis*	Alpha carbonic anhydrase; Carbonic anhydrase, alpha-class
Alveoline-like	*Pinctada fucata*	-
Amine oxidase	*Pinctada fucata, Pinctada margaritifera*	Copper amine oxidase; Copper amine oxidase, N2-terminal; Copper amine oxidase, C-terminal; Copper amine oxidase, N-terminal
Apextrin	*Mytilus galloprovincialis*	Apextrin, C-terminal domain
Beta-hexosaminodase	*Pinctada maxima, Pinctada margaritifera*	Carbohydrate-binding domain; Chitobiase/beta-hexosaminidase domain 2-like; Glycoside hydrolase superfamily; Chitobiase/beta-hexosaminidases, N-terminal domain;Cellulose-binding family II/chitobiase, carbohydrate-binding domain; Glycoside hydrolase, catalytic domain; Beta-hexosaminidase;Glycoside hydrolase family 20, catalytic domain
Beta-lactamase (Gigasin-6)	*Magallana gigas*	Beta-lactamase/transpeptidase-like;Beta-lactamase-related
THY domain-containing protein	*Mytilus galloprovincialis*	Beta-thymosin
BPTI/Kunitz domain-containing protein	*Pinctada maxima, Mytilus galloprovincialis, Pinctada fucata, Mytilus coruscus, Mytilus californianus, Crassostrea nippona, Mizuhopecten yessoensis, Magallana gigas*	Proteinase inhibitor I2, Kunitz, conserved site; Pancreatic trypsin inhibitor Kunitz domain

C1Q domain-containing protein	*Pinctada maxima, Mytilus galloprovincialis, Pinctada fucata, Mytilus coruscus, Mytilus californianus, Crassostrea nippona, Mizuhopecten yessoensis, Magallana gigas*	C1q domain; Tumour necrosis factor-like domain
Ca-binding glycoprotein	*Unio pictorum*	-
Calprismin	*Pinna nobilis*	-
Chitin binding	*Pinctada maxima, Mytilus galloprovincialis, Pinctada fucata, Mytilus coruscus, Mytilus californianus, Crassostrea nippona, Mizuhopecten yessoensis, Magallana gigas*	Chitin binding domain
C-lectin/(Perlucin)	*Pinctada maxima, Mytilus galloprovincialis, Pinctada fucata, Mytilus coruscus, Mytilus californianus, Crassostrea nippona, Mizuhopecten yessoensis, Magallana gigas*	C-type lectin-like/link domain; C-type lectin-like; C-type lectin fold
Concanavalin A	*Pinctada margaritifera, Pinctada fucata, Mytilus californianus, Mytilus galloprovincialis, Mytilus coruscus*	Concanavalin A-like lectin/glucanase domain
Conchiolin	*Pinctada maxima*	-
Dopamine B-hydroxilase	*Pinctada maxima, Mytilus galloprovincialis, Pinctada fucata, Mytilus coruscus, Mytilus californianus, Crassostrea nippona,*	Dopamine beta-hydroxylase-related; PHM/PNGase F domain; Copper type II, ascorbate-dependent monooxygenase, N-terminal; Copper type II ascorbate-

	Mizuhopecten yessoensis, Magallana gigas	dependent monooxygenase, C-terminal; Copper type II, ascorbate-dependent monooxygenase-like, C-terminal;DBH-like monooxygenase protein 2
EF-hand	*Ruditapes philippinarum, Pinctada maxima, Mytilus galloprovincialis, Pinctada fucata, Mytilus coruscus, Mytilus californianus, Crassostrea nippona, Mizuhopecten yessoensis, Magallana gigas*	EF-hand domain pair; EF-Hand 1, calcium-binding site; EF-hand domain
EGF-like domain-containing protein	All bivalve	EGF-like domain; EGF-like, conserved site
FAD/NAD	*Mytilus coruscus, Mytilus galloprovincialis, Mytilus coruscus, Mytilus californianus*	FAD/NAD(P)-binding domain; Amine oxidase
Fibronectin III (IG)	*Mytilus californianus*	Immunoglobulin-like fold; Fibronectin type III
Fibronectin III (IG)	*Pinctada margaritifera*	-
Filament/Filamin	*Mytilus galloprovincialis*	Intermediate filament protein
Fructose-bisphosphate aldolase	*Mytilus galloprovincialis*	Fructose-bisphosphate aldolase class-I active site; Fructose-bisphosphate aldolase, class-I; Aldolase-type TIM barrel
Gigasin	*Magallana gigas*	-
Glycoside hydrolase (Chitinase)	All bivalve	Glycoside hydrolase, catalytic domain; Glycoside hydrolase superfamily; Glycoside hydrolase family 18, catalytic domain; Chitinase II; Glycoside hydrolase, chitinase active site
Glycosyltransferase catalyzes (Chitin synthesis)	All bivalve	Myosin head, motor domain; Chitin synthase; P-loop containing nucleoside triphosphate hydrolase; Nucleotide-diphospho-sugar

		transferases
Peroxidase-like protein	*Pinctada margaritifera*	Haem peroxidase, animal;Haem peroxidase
Hic22	*Hyriopsis cumingii*	-
Immunoglobulin-like, Fibronectin III	*Pinctada fucata, Mytilus coruscus*	Immunoglobulin-like fold; Fibronectin type III
Insoluble matrix shell protein	*Ruditapes philippinarum*	-
Jacalin-like	*Pteria penguin*	Jacalin-like lectin domain
Kazal domain containing protein	*Ruditapes philippinarum*	Kazal domain
Liprin/alpha motif containing protein	*Pinctada fucata*	Sterile alpha motif/pointed domain; Sterile alpha motif domain; Liprin-alpha; LAR-interacting protein, Liprin
Mantle protein	*Pinctada maxima, Pinctada margaritifera*	-
Mucoperlin	*Pinna nobilis*	-
Mytilin	*Mytilus galloprovincialis, Mytilus californianus, Mytilus coruscus*	-
N14, N16, N19, N23	*Pinctada maxima, Pinctada fucata*	-
Nautilin	*Nautilus macromphalus*	-
Cathepsin-like protein	*Mytilus galloprovincialis*	Peptidase C1A, papain C-terminal; Peptidase C1A
Peroxiredoxin	*Pinctada fucata*	Peroxiredoxin, AhpC-type; Thioredoxin-like fold; Peroxiredoxin, C-terminal; Thioredoxin domain; Alkyl hydroperoxide reductase subunit C/ Thiol specific antioxidant
Prisilkin-39	*Pinctada fucata*	-
Prismalin-14	*Pinctada fucata, Pinctada margaritifera*	-
Prismin	*Pinctada fucata*	-
Rich single amino acids repeats protein	All bivalve	-
Shematrin	*Pinctada fucata,*	-

	Pinctada maxima, *Pinctada margaritifera*	
Sushi	*Pinctada fucata*	Sushi/SCR/CCP domain
Tissue inhibitor of metalloproteinase/NTR domain-containing protein	*Pinctada margaritifera*	Tissue inhibitor of metalloproteinases-like; Protease inhibitor I35 (TIMP)
TNFR/NGFR	*Pinctada margaritifera*	TNFR/NGFR cysteine-rich region
Transgelin-Calponin	*Mytilus galloprovincialis*	Calponin homology domain
Tyrosinase	All bivalve	Uncharacterised domain, di-copper centre; Tyrosinase copper-binding domain
Upsalin	*Unio pictorum*	-
VWA domain containing protein	All bivalve	von Willebrand factor, type A
WAP (Perlwapin)	All bivalve	WAP-type 'four-disulfide core' domain

1.5.4.5 Ion transporters

Another important component of the biomineralization toolbox is the presence of ion transporters that regulate the concentration of ions, such as calcium and carbonate, in the extracellular fluid surrounding the mineralizing tissue. These transporters help to create and maintain a supersaturated ion rich environment that promotes the formation of the mineral phase (Wilbur and Saleuddin, 1983). The sodium/proton exchanger NHE10 has been shown to play a critical role in maintaining the alkaline pH necessary for biomineralization in *M. gigas* (Ivanina et al., 2018). According to (Sleight et al., 2020), bivalves utilize a variety of ion transporters, including calcium channels, to control the concentration and

flux of calcium ions during shell formation. In particular, the Na^{+}/Ca^{2+} exchanger (NCX) is crucial for bivalve biomineralization, as it regulates the extracellular calcium concentration (Ramesh et al., 2019). Additionally, bivalves rely on proton pumps to control the pH of the extracellular fluid, which can influence the precipitation of calcium carbonate (Cao-Pham et al., 2019). The vacuolar H^{+}-ATPase (VHA) has been identified as a key proton pump in the shell-forming cells of *Tridacna squamosa* (Ip et al., 2018).

1.5.4.6 Enzymes

Bivalves also use enzymes to modify the chemistry of the extracellular fluid and regulate the biomineralization process. The representative composition of enzymes involved in this process includes acid phosphatase, alkaline phosphatase, carbonic anhydrase, and chitinase (Yarra et al., 2021). Carbonic anhydrase is an enzyme that catalyzes the conversion of CO_2 to bicarbonate ions, which are used in the formation of $CaCO_3$ (Le Roy et al., 2014). Carbonic anhydrase has been found in the mantle tissue of the *M. gigas*, where it helps to regulate the pH of the extracellular fluid during biomineralization (Ivanina et al., 2017). Acid phosphatase is an enzyme that catalyzes the hydrolysis of phosphate esters under acidic conditions. This enzyme plays a role in the formation of calcium phosphate minerals in bivalves (Cardoso et al., 2020; Jing et al., 2007). Chitinase is an enzyme that catalyzes the hydrolysis of chitin, a

polysaccharide found in the shells of bivalves. This enzyme is involved in the breakdown of old shells and the formation of new shells, which is critical for biomineralization (Zhang et al., 2019).

1.5.4.7 Extracellular vesicles

Bivalves also use extracellular vesicles (EVs), small membranous structures released by cells, to control the biomineralization process. Mineral-containing vesicles within specialized cells have been observed in many different tissues in molluscs (Watabe and Wilbur, 1976), including haemocytes thought to be involved in biomineralization. (Watabe and Wilbur, 1976) reported that the mineral phase in most of these vesicles was ACC or vaterite, both of which are highly unstable. In their study of shell regeneration, they concluded that the mineral phase was dissolved and transported to the site of shell formation and these EVs therefore function as ion storage sites. The vesicles contain acidic proteins, glycosaminoglycans, and lipids and they can influence the formation and morphology of the mineral phase (Mount et al., 2004). In the *Cristaria plicata*, EVs have been shown to play a role in the formation of the nacreous layer of the shell (Huang and Li, 1991). A study by (Li et al., 2016) found that the EVs isolated from the mantle tissue of the pearl oyster *P. fucata* contained a range of proteins, including shell matrix proteins and enzymes involved in biomineralization. EVs also contain nucleic acids that can regulate the expression of genes

involved in biomineralization. (Chen et al., 2019) identified several microRNAs (miRNAs) in the EVs isolated from the mantle tissue of *H. cumingii*. These miRNAs were found to regulate the expression of genes involved in nacre color formation, suggesting that EVs may play a crucial role in the post-transcriptional regulation of biomineralization in bivalves.

1.6 Environmental factors that challenge marine life

Climate change is a growing environmental issue, with anthropogenic activities causing an increase in atmospheric greenhouse gases, leading to significant changes in temperature and precipitation patterns (IPCC, 2018). From biodiversity loss and changes in migration and breeding patterns to increased wildfires, ocean acidification (OA), and changes in disease prevalence, the effects of climate change are widespread and multifaceted (Denman et al., 2011; Waldbusser et al., 2015; Widdicombe and Spicer, 2008). These changes have a profound impact on terrestrial and aquatic ecosystems worldwide, altering the behaviour, consortiums of species and interactions between them.

1.6.1 Ocean acidification

OA is caused by the uptake of excess CO_2 by seawater, leading to a rise in the partial pressure of CO_2 in seawater, resulting in a decrease in the pH levels. According to a study by (Doney et al., 2009), the ocean's

surface pH has already decreased by 0.1 units since the preindustrial era, but represents a 30% increase in acidity (Caldeira and Wickett, 2003). The reduction in Ocean pH reduces the concentration of carbonate ions available, and since these ions are essential for the formation of shells and the skeleton of marine cacifiers the consequences may be catastrophic (Gattuso et al., 2011). The effects of OA are widespread and they impact a range of marine organisms, from plankton to fish (Kroeker et al., 2013). OA can cause a decline in the growth and reproductive success of calcifying organisms such as corals, molluscs, and some planktonic species (Fabry et al., 2008). The reduction in pH and increased acidity can also lead to a decrease in the availability of carbonate ions, which are crucial for the formation of calcium carbonate ($CaCO_3$) structures such as shells and skeletons (Hoegh-Guldberg et al., 2007).

The reduction in the availability of carbonate ions can have cascading effects on the marine food web. For example, a study by (Riebesell et al., 2000) found that OA reduced the abundance of pteropods, a key food source for many species of fish, whales, and seabirds. The reduced availability of food can also affect the survival and growth of fish larvae, as demonstrated by (Munday et al., 2009), who found that the survival of clownfish larvae was reduced under conditions of high CO_2. A study by (Doney et al., 2012) found that OA can lead to a shift in the composition of marine communities, favoring non-calcifying species over calcifying

ones. This shift will have significant impacts on the functioning of marine ecosystems, and includes changes in nutrient cycling, primary productivity, and carbon storage (Waldbusser et al., 2015; Wang et al., 2022). A decline in fish stocks, as a result of OA, will have economic impacts on coastal communities that depend on fishing for their livelihoods (Cinner et al., 2016). Additionally, OA can impact human health through the consumption of contaminated seafood, as demonstrated by a study by (Talmage and Gobler, 2011), which found that the consumption of oysters grown under conditions of high CO_2 levels may cause neurological damage in humans.

1.6.2 Temperature changes

Rising temperatures due to global warming can have significant effects on marine ecosystems. A study by (Poloczanska et al., 2013) found that global warming may lead to the loss of 57% of the world's coral reefs by 2100. Elevated temperatures (marine heatwaves) induce acute and chronic stress in marine animal, compelling alterations in their habitat preferences and geographical ranges (Pinsky et al., 2020; Wernberg et al., 2011). Marine heatwaves significantly impact microalgae (importance primary trophic level in food web), since tiny organisms are highly sensitive to changes in temperature, by induced reduced growth, altered species composition and toxic blooms (Remy et al., 2017; Roberts

et al., 2019). Marine bivalves, as filter feeders, will be negatively affected. The rearrangement of species spatial distribution and abundance can disrupt established trophic interactions and interspecific relationships within food webs (propagate through multiple trophic levels, triggering cascading effects across the entire food web) (Gao et al., 2021). As species redistribute themselves, alterations in predator-prey dynamics, competition, and resource availability, invariably can engender imbalances in energy flow, nutrient cycling, and ecosystem resilience, compromising the overall ecological integrity of marine systems.

1.6.3 Ocean acidification and bivalve shell biomineralization

OA affects bivalve survival. According to a study by (Gazeau et al., 2010), the decrease in ocean pH due to OA reduces the calcification rates of bivalves up to 25%. This study was conducted in a controlled laboratory setting, where *M. edulis* were exposed to different pH levels during 6 months and showed that the decrease in pH resulted in a reduction in the shell length and thickness indicating that OA could lead to significant structural changes in the bivalves (Mackenzie et al., 2014; Wu et al., 2016) and make them more susceptible to predation (Barton et al., 2015).

The reduction in calcification rates due to OA has significant implications for the growth of bivalves. Bivalves grow by adding new

layers to their shells, and a reduction in calcification rates can lead to slower growth rates. A study by (Talmage and Gobler, 2009) showed that the growth rates of juvenile *M. mercenaria* were reduced by 50% under high CO_2 conditions when they were exposed to different CO_2 levels for 3 months. This study showed that the reduction in growth rates was due to a decrease in the energy available for growth, as the clams had to divert more energy towards calcification to maintain their shell structure under high CO_2 conditions. OA can also affect bivalves by reducing their ability to regulate their internal pH levels. Bivalves rely on the regulation of their internal pH levels to maintain normal physiological processes, such as metabolism and enzyme activity. However, OA can reduce the ability of bivalves to regulate their internal pH levels, leading to metabolic imbalances and decreased survival rates (Gazeau et al., 2011).

The reduction in growth rates due to OA have significant implications for the survival of bivalves. Bivalves that grow slower may take longer to reach maturity and reproduce, which can lead to population decline. A study by (Thomsen et al., 2015) showed that OA can decrease the survival of juvenile *M. edulis* by up to 50% when exposed to different pH levels for 4 months. The results showed that the decrease in survival was due to a combination of factors, including reduced calcification rates, increased metabolic rates, and a decrease in energy reserves.

OA can affect the biomineralization toolbox of bivalves by disrupting

the transport of ions and the secretion of organic matrices (Figure 1.13). The decrease in seawater pH affects the transport of calcium ions (Ca^{2+}) in the bivalve body, which is necessary for shell formation (Peng et al., 2017; Rajan et al., 2021). This leads to a slower shell growth rate and impaired shell quality (Thomsen et al., 2013). OA affects the secretion of organic matrices in bivalves by altering the expression of genes that code for SMPs (Gazeau et al., 2010). The alteration of SMP expression leads to changes in the organic matrix composition, affecting the biomineralization process (Zhang et al., 2012). However, considering the diversity of existing bivalves, their habitats, physiology and diversified exuberant shell shapes and composition it is an oversimplification to consider that OA will have the same impact on all bivalves. A better understanding of shell construction, the biomineralization toolbox and its regulation are required.

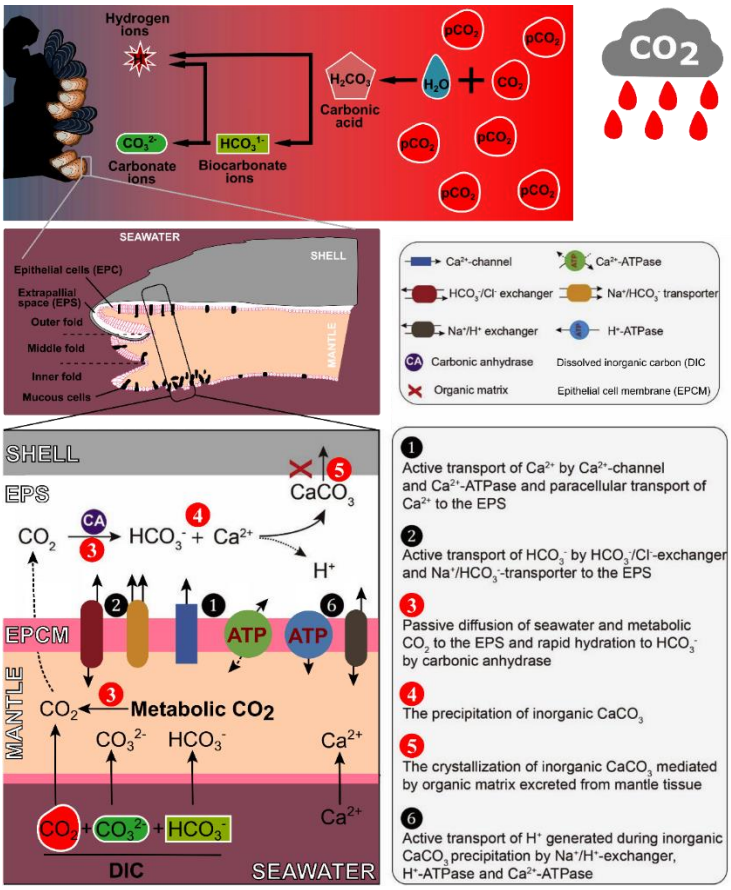

Figure 1.13. Schematic representation of the potential impacts of ocean acidification on bivalve shell biomineralization. The red circles (with white numbers inside) represents the potential impact of OA on chemical processes. EPS: Extrapallial space, EPCM: Epithelial cell membrane, dashed arrows in CO_2 transfer from cell to EPS represents osmotic transport. The figure was taken from (Zhao et al., 2020) and was adapted using Inkscape software v1.2.

1.7 Objectives

In bivalves, the mantle is the main tissue responsible for shell formation. The epithelial layer of the mantle promotes the production of the amorphous phase of calcium carbonate by transporting calcium (Ca^{2+}), bicarbonate (HCO_3^-) ions and secreting SMP into the extrapallial fluid to form the shell. The main aim of this thesis is to contribute to the understanding of the mechanisms that regulate bivalve shell formation and to understand the impact of OA on the homeostasis of shell maintenance considering the diversity of shell shapes, structures and composition in bivalves. The toolbox of bivalve is species-specific and comparative omics studies will provide understanding on the generality of bivalve shell biomineralization mechanisms, as well the specificity and evolution of shell biomineralization in the different species. The two bivalve species used as model species in this study were two important aquaculture species *M. gigas* (asymmetric bivalve) and the Mediterranean mussel *M. galloprovincialis* (symmetric bivalve) that possess different shell structures but occupy similar environmental niches, and are phylogenetically close, makes it possible to explore general and species-specific adaptations. This study used multi-omics methods with animal experimental verification to characterize factors involved in the regulation of shell growth and their composition and adaptation to environmental stressors. Specifically, it is divided into three mains

chapters:

1） Chapter 1: multi-species multi-omics analysis characterize the core "toolbox" of shell formation and verify the functional roles of some toolbox genes with functional experiments. For the toolbox genes identified, we further explore the toolbox genes related to the formation of asymmetric valves in bivalve, as well as explore the molecular evolution of asymmetric valve related genes and describe the molecular regulatory pathways.

2） Chapter 2: To explore the impact of global climate change (OA) on different species of bivalve, and to assess the potential impact of the model "bivalve physiology-shell-ocean carbon cycle".

3） Chapter 3: Describe the content of chitin in bivalves with different shell materials, the evolution of chitin metabolism-related enzymes (chitin synthase) in bivalves, and further explore whether OA has a general impact on bivalve shell organic matter-associated enzymes (chitin turnover).

CHAPTER 2

Core genes of biomineralization and cis-regulatory long non-coding RNA regulate shell growth in bivalves

Core genes of biomineralization and cis-regulatory long non-coding RNA regulate shell growth in bivalves

Published, Journal of Advanced Research,

https://doi.org/10.1016/j.jare.2023.11.024

Acknowledgements

The authors would like to thank to Dr. Telmo Nunes from the microscopy unit of the Faculdade de Ciências da Universidade de Lisboa for the shell SEM images. This study received Portuguese national funds from FCT - Foundation for Science and Technology through projects UIDB/04326/2020, UIDP/04326/2020 and LA/P/0101/2020.

Core genes of biomineralization and cis-regulatory long non-coding RNA regulate shell growth in bivalves

Maoxiao Peng[a], João C.R. Cardoso[a*], Gareth Pearson[b], Adelino VM Canário[a,c,d] and Deborah M. Power[*a,c,d]

[a] Comparative Endocrinology and Integrative Biology, Centre of Marine Sciences, Universidade do Algarve, Campus de Gambelas, 8005-139 Faro, Portugal

[b] Biogeographical Ecology and Evolution, Centre of Marine Sciences, Universidade do Algarve, Campus de Gambelas, 8005-139 Faro, Portugal

[c] International Research Center for Marine Biosciences, Ministry of Science and Technology, Shanghai Ocean University, Shanghai, China

[d] Key Laboratory of Exploration and Utilization of Aquatic Genetic Resources, Ministry of Education, Shanghai Ocean University, Shanghai, China

2.1 Abstract

2.1.1 Introduction

Bivalve molluscs are abundant in marine and freshwater systems and contribute essential ecosystem services. They are characterized by an exuberant diversity of biomineralized shells and typically have two symmetric valves (a.k.a shells), but oysters (Ostreidae), some clams (Anomiidae and Chamidae) and scallops (Pectinida) have two asymmetrical valves. Predicting and modelling the likely consequences of ocean acidification on bivalve survival, biodiversity and aquaculture makes understanding shell biomineralization and its regulation a priority.

2.1.2 Objectives

This study aimed to a) exploit the atypical asymmetric shell growth of some bivalves and through comparative analysis of the genome and transcriptome pinpoint candidate biomineralization-related genes and regulatory long non-coding RNAs (lncRNAs) and b) demonstrate their roles in regulating shell biomineralization/growth.

2.1.3 Methods

Meta-analysis of genomes, *de novo* generated mantle transcriptomes or transcriptomes and proteomes from public databases for six asymmetric to symmetric bivalve species was used to identify biomineralization-related genes. Bioinformatics filtering uncovered genes and regulatory modules characteristic of bivalves with asymmetric shells

and identified candidate biomineralization-related genes and lncRNAs with a biased expression in asymmetric valves. A shell regrowth model in oyster and gene silencing experiments, were used to characterize candidate gene function.

2.1.4 Results

Shell matrix genes with asymmetric expression in the mantle of the two valves were identified and unique cis-regulatory lncRNA modules characterized in Ostreidae. LncRNAs that regulate the expression of the tissue inhibitor of metalloproteinases gene family (*TIMPDR)* and of the shell matrix protein domain family (*SMPDR*) were identified. *In vitro* and *in vivo* silencing experiments revealed the candidate genes and lncRNA were associated with divergent shell growth rates and modified the microstructure of calcium carbonate ($CaCO_3$) crystals.

2.1.5 Conclusion

LncRNAs are putative regulatory factors of the bivalve biomineralization toolbox. In the Ostreidae family of bivalves biomineralization-related genes are cis-regulated by lncRNA and modify the planar growth rate and spatial orientation of crystals in the shell.

Keywords: Bivalve; mantle transcriptomes; lncRNA *cis*-regulation; shell asymmetry; shell biomineralization toolbox

2.2 Introduction

A renewed interest in mollusc shells and how they are produced has arisen because of current ocean acidification trends and its implication for shell calcification and mollusc survival, biodiversity and the burgeoning aquaculture industry (FAO, 2020; Kennedy et al., 1969; Wittmann and Pörtner, 2013). The biomineralized shell of the speciose molluscs contributed to their evolutionary success during and after the Cambrian explosion (Vinther, 2015; Wanninger and Wollesen, 2019). Shell microstructure and architecture has been characterised in a very small proportion of all bivalves but reveals they are extraordinarily diverse (McDougall and Degnan, 2018) and results from crystallization of calcium carbonate ($CaCO_3$) in a soft organic matrix made up of proteins, acidic polysaccharides and chitin (Jackson and Degnan, 2016). The shell gland in mollusc embryos and the outer mantle epithelium and haemocytes (responsible for calcium and carbonate ion transport (Alesci et al., 2023; Arivalagan et al., 2017; Li et al., 2016)) in the extrapallial fluid in subsequent stages produce the shell (Haszprunar and Wanninger, 2012). The mantle has been extensively studied as the main shell biomineralizing tissue and although the shell organic matrix accounts for less than 5% of its composition, shell diversity has been assigned to the rapidly evolving mantle secretome (Jackson and Degnan, 2016; Kocot et al., 2016; Saleuddin and Petit, 1983).

Asymmetrical shell growth has been mostly studied in the gastropods, the most specious class of molluscs, where most species have inherited one helical asymmetrical coiled shell (Ishikawa et al., 2020; Osterauer et al., 2010; Page, 2006, 2003; Wanninger et al., 1999). Although their soft body in common with other bilaterian organisms exhibits external left/right (LR) symmetry along the sagittal plane (Eble and Scro, 1996). Specialization of the shell-secreting mantle epithelium in gastropods controls shell morphology and structure. In the basket whelk (*Tritia obsoleta*) and ram's horn snail (*Planorbella sp*.) specialization of the mantle shell margin occurs during larval development and in *Tritia* is associated with regional expression of regulatory genes (Johnson et al., 2019). In the pond snail (*Lymnaea stagnalis*) asymmetric gene expression of shell matrix proteins (SMPs) by the mantle contribute to shell asymmetry (Ishikawa et al., 2020; Johnson et al., 2019). Overall, asymmetric shell growth in gastropods is a consequence of body torsion and differential gene expression during development, however in other mollusc, such as the bivalves, this process remains unclear.

Bivalve have a shell composed of two symmetric valves, although a few modern bivalves such as the oysters (Ostreidae), clams (Anomiida and Chamidae) and some scallops (Pectinida) have asymmetric valves indicating that shell asymmetry emerged at least twice during the bivalve radiation (Harper and Checa, 2020). Why oyster and scallop valves

deviate from the common symmetric pattern of bivalves is an evolutionary enigma (Savazzi, 2005). In most oysters, the right valve is flat, and the left valve attached to the substrate is convex (cupped or round) (Yamaguchi, 1994). The explanation for bivalve shell diversity is thought to lie in the recently characterized, highly evolved and diverse bivalve "biomineralization toolbox" (Aguilera et al., 2017; Jackson et al., 2006; Kocot et al., 2016; Song et al., 2019), which contains ion transporters, SMPs and enzymes (Arivalagan et al., 2017; Yarra et al., 2021; Zhao et al., 2018). But if there are master regulator genes is a mystery and it has been hypothesised that shell microstructure and diversity of shell shapes arose from a conserved upstream cis-regulatory network acting on the biomineralization toolbox genes in the bivalve mantle (Aguilera et al., 2017; Davidson, 2010). *Nacrein* and *SLC2A1* (Solute Carrier Family 2 Member 1) toolbox genes were proposed as candidates for shell asymmetry in the Hong Kong oyster *Magallana hongkongensis* (previously called *Crassostrea hongkongensis*) (Zhang et al., 2022). In contrast, in the adult Pacific oysters (*M. gigas*), factors regulating body plan asymmetry in vertebrates such as the Nodal cascade (Boorman and Shimeld, 2002; Yoshiba and Hamada, 2014) were associated with valve asymmetry (Wei et al., 2018).

Long non-coding RNAs (lncRNAs) are a group of non-coding RNAs (ncRNAs) that are generally defined as transcripts of more than 200

nucleotides that are not translated into protein (Ferre et al., 2016) and play an important multilevel regulatory role in various biological processes including development, cell differentiation, immune responses and tissue regeneration (Feng et al., 2018; Huang et al., 2018; Mu et al., 2016; Nam and Bartel, 2012; Wen et al., 2016; Yu et al., 2016; Zheng et al., 2020a, 2020b, 2019). To date only a few lncRNAs have been functionally characterized in Mollusca (Hongkuan et al., 2021). In the bivalve, *Pinctada fucata*, lncRNAs (lncMSEN1 and lncMSEN2) were reported to be associated with the response to poly I:C and LPS stimulation and with maintaining shell nacreous layer microstructure (Zheng et al., 2020a, 2020b, 2019). In addition, lncIRF-2 was also reported to play a role in the immune response (Huang et al., 2018). Protein-lncRNA interactions are reported to regulate pigment synthesis, shell colour and larval development in *M. gigas* (Feng et al., 2018; Yu et al., 2016) and although lncRNAs, are differentially expressed in the mantle of the cupped (round) and flat valves, their possible roles in shell shape and shell structure have not been considered (Wei et al., 2018; Zhang et al., 2022).

Following Krogh's principle (Krebs, 1975), we selected bivalves with completely asymmetric shells and bivalves with slightly asymmetric shells or totally symmetric shells as models and took a comparative approach to identify coding and non-coding RNA associated with the

regulation of shell matrix crystallization and growth. We reasoned that asymmetric shells arise from different rates of growth, but that the similar chemical composition of the valves means that the basic set of shell building genes in both mantles should be similar, and that by identifying differentially expressed genes in symmetric and asymmetric bivalves it should be possible to tease out the most important gene transcripts and regulatory factors for the trait. This was done using a step wise analysis of molecular resources from six symmetric to asymmetric bivalves to identify a) similarities and differences between mantle transcriptomes, b) core biomineralization-related genes and protein motifs in the mantle, c) biomineralization toolbox genes with biased expression in asymmetry and d) lncRNA and their putative binding partners. Using meta-analysis of available data, we identified collinear cis-regulatory regions and putative binding pairs composed of lncRNA and biomineralization toolbox genes in the evolutionary proximate asymmetric species *M. gigas*, *C. virginica* and *S. glomerata*. Targeted knock-down in *M. gigas* of the identified lncRNA *in vitro* down-regulated the expression of candidate biomineralization genes. Down-regulation of the genes by knock-down *in vivo* led to divergent rates of shell deposition and modified crystal growth. Overall, we conclude that valve asymmetry in *M. gigas* most likely results from cis-regulation by lncRNAs of specific biomineralization toolbox genes leading to their biased expression in the mantle, and

reduced rates of biomineralization in the flat valve.

2.3 Materials and Methods

2.3.1 Ethics statement

All experiments involving animals were conducted according to the ethical policies and procedures approved by the ethics committee of the Centre of Marine Sciences, University of Algarve, Portugal (Approval no. ICNF_327/2022/CAPT).

2.3.2 Animals, sampling, and experimental conditions

Adults from aquaculture production (length 9.2 ± 0.7 cm, width 5.0 ± 0.5 cm, ~1.5-years-old) and juveniles (length 2.5 ± 0.3 cm. width 1.8 ± 0.2 cm, ~ 5-month-old) *M. gigas* were kindly donated by Francois Hubert from the bivalve company located in the Ria Formosa, Olhão (Portugal). Wild adults (length 6.3 ± 0.1 cm, width 3.3 ± 0.2 cm, ~6-month-old) *Mytilus galloprovincialis* were captured by hand from the Ria Formosa (Faro, 37°00’32”N, 7°59’40”W). Animals were transported live to CCMAR experimental facilities and were acclimated for 3 days in 5 L tanks (25 (length) × 17 (width) × 15 (height), cm) filled with aerated seawater (37 ppt) collected from their natural environment before experimentation. All tanks were maintained at room temperature (20 - 23ºC) and animals were fed once a day (0.002 g / g body weight) with a

commercial mixture of dried microalgae (Phytobloom, Reef Feed, Portugal, Olhão). All experiments were run under similar conditions. Before tissue collection animals were anaesthetized with iced seawater and the mantles from both valves (right/flat and left/round or convex valve) were collected. The mantle margin from juvenile *M. gigas* was collected for transcriptome generation, expression analysis, and to assess the impact of *in vivo* shell damage-repair assays on target gene expression. The mantle margin from adult *M. galloprovincialis* was collected for transcriptome generation. The mantle margin from adult *M. gigas* was also collected for *ex vivo* siRNA experiments and for analysis of the subcellular localization of lncRNA. For the transcriptomics analysis, the mantle edge of animals was immediately sampled after collection, snap-frozen in liquid nitrogen and stored at -80ºC until RNA extractions. For details regarding RNA extractions, cDNA synthesis and small-scale gene expression analyses refer to SI Appendix.

2.3.3 Multi-omics analysis of bivalve mantle transcriptomes

The mantles from right/flat and left/round valves of juvenile *M. gigas* (n= 6/shell side) and adult *M. galloprovincialis* (n= 6/shell side) and were collected and RNA extracted. Library preparation and sequencing of *M. gigas* (n = 3, pools of RNA from 2 individuals) was performed at Shanghai Ocean University Sequencing Service (Shanghai, China) and

index codes were used to attribute sequences to individual samples (Supplementary Table 2.1). Library preparation and sequencing of *M. galloprovincialis* (n = 3, pools of RNA from 2 individuals) was performed at Novogene Europe Co., Ltd Sequencing Service and index codes were used to attribute sequences to individual samples (Supplementary Table 2.1). For details regarding protocols of library preparation (for *M. gigas* and *M. galloprovincialis*), transcriptome quality control, assembly, and the calculation of differentially expressed genes, see SI Appendix. To increase the robustness and data for the mantle transcriptome analysis publicly available mantle transcriptomes (raw data) from two other bivalves, the asymmetric shelled *Mizuhopecten yessoensis* (Ding et al., 2015) and the slightly asymmetric shelled *P. fucata* (Zhang et al., 2022) was obtained from NCBI (Supplementary Table 2.1). These two species were selected because of the public availability of sequencing data from libraries for flat and round valve mantles and the availability of reference genomes (*M. yessoensis* NCBI Accession: GCA_002113885.2 (Wang et al., 2017) and *P. fucata*, ver3.0 (Takeuchi et al., 2022), respectively) for mapping of reads using the same methods described for *M. gigas* and *M. galloprovincialis* (see SI Appendix). In this study, the flat valve, of the asymmetric bivalve, was assigned to the right valve of slightly asymmetric and symmetric bivalves, and the round (or cupped) valve (asymmetric bivalves) was assigned to the left valve (slightly

asymmetric and symmetric bivalve).

2.3.4 Identification of biomineralization toolbox genes and regulatory factors in mantle

DE coding (DEc) and DE non-coding (DEnc) transcripts were annotated. DEc were also annotated using blastp against NCBI (nr) and Swiss-Prot databases, respectively. DEc in *M. gigas*, *M. yessoensis*, *P. fucata* and *M. galloprovincialis* were annotated for subcellular localization using three programmes, for details see SI Appendix. Protein domains were identified using Pfam (ver 34.0) (http://pfam.xfam.org/) and compared with the *M. gigas* shell proteome (Arivalagan et al., 2017) to identify common domains. Protein motifs were identified using ProminTools (Skeffington and Donath, 2020) (Supplementary Figure 2.1), for details see SI Appendix. The *M. gigas* shell proteome was compared to secreted DEc of *M. yessoensis*, *P. fucata* and *M. galloprovincialis* to identify common asymmetric-related protein domains/motifs. DE lncRNAs (DEnc) were identified based on *M. gigas* and *M. galloprovincialis* genome annotations, respectively. Their full-length nucleic acid sequence and authenticity as non-protein coding gene transcripts was reconfirmed, for details see the SI Appendix. Confirmed DEnc of *M. gigas* were assigned an arbitrary name lncRNA 1-20, and lncRNA 3 and lncRNA 20 and after functional validation were named

TIMPDR and *SMPDR*, respectively. Publicly available bivalve transcriptome data from several tissues, larva at different developmental stages and shell damage-repair experiments of *M. gigas* (Zhang et al., 2012) was analysed and lncRNA candidates identified. Publicly available transcriptomes were downloaded from the SRA database of NCBI (Supplementary Table 2.1) and expression levels of candidate lncRNA were calculated in FPKM. DEnc that were a) abundant in the mantle and b) responded to shell-damage repair were considered putative candidates for shell formation. LncRNAs that were highly expressed in pediveliger larvae (before metamorphosis), spat and juvenile stages (after metamorphosis) were selected as candidates for shell shape transition/formation (from symmetry to asymmetry).

2.3.5 Detection of cis-regulatory modules in biomineralization toolbox genes

Mantle protein coding and non-coding DEGs were mapped in the *M. gigas* genome. Ten *M. gigas* chromosomes and two unassembled scaffolds were displayed using the advanced Circos program from TBtools (ver 1.0986) (Chen et al., 2020) and mapping was done with the chromoMap package (ver 0.3) (Anand and Lopez, 2020) in R-studio. DEc genes localized 100 kb upstream or downstream of DEnc genes were selected as cis-regulation candidates. Detailed mapping of candidate cis-

regulation modules (DEnc-DEc genes) was performed with the gggenes package (ver 0.4.1) (Wilkins, 2019) in R-studio. To identify if homologue cis-regulation modules were conserved in other bivalves, the *M. gigas* genome was used as a reference and aligned with the *M. yessoensis*, *P. fucata*, *M. galloprovincialis*, *C. virginica* (NCBI Accession: GCA_002022765.4) and *Saccostrea glomerata* (NCBI Accession: GCA_003671525.1) (Powell et al., 2018) genomes in Diamond (ver 2.0.11, parameters -sensitive; e value < $1e^{-5}$) (Buchfink et al., 2015). Gene synteny and collinearity were identified using MCscan (ver X, parameters s=5; k=50; m=20; e < $1e^{-5}$) (Wang et al., 2012) and gene synteny plots were visualized in dual synteny plot from TBtools (ver 1.0986) (Chen et al., 2020). Orthologues of *M. gigas TIMPDR* and *SMPDR* were identified in *C. virginica* and *S. glomerata* using blastn against the publicly available genome (Supplementary Table 2.1) and transcriptome (NCBI, Transcriptome Shotgun Assembly, TSA), respectively. The base sequence of the retrieved orthologue regions was aligned using Aliview with MUSCLE (ver 1.24), the percentage of sequence identity was calculated in GeneDoc (ver 2.7) and the non-coding potential confirmed using the defined criteria (indicated above). The candidate gene pairs (DEGnc-DEGc) and their neighbouring gene environments were performed using the gggenes package (ver 0.4.1) (Wilkins, 2019) in R-studio.

2.3.6 Shell growth, siRNA experiments and shell damage-repair assays

For the *in vivo* experiments to test the differential growth rates of flat and round valves, juvenile *M. gigas* (n = 13/group) were used in a shell damage-repair assay where 3 holes (~ 2 mm in diameter) were drilled in the posterior edge of the shell of juvenile *M. gigas*, for details see the SI Appendix. The rational for the assay was based on the predicted differential growth rates that maintain shell asymmetry throughout life in *M. gigas*. Targeted siRNAs were used to ablate specific lncRNA gene expression in juvenile *M. gigas* under a shell damage-repair challenge. The two siRNAs (*TIMPDR* and *SMPDR*) and control siRNA (negative control, NC) provided by GenePharma (Shanghai, China) were diluted in sterile seawater to obtain a working concentration (0.088 μg /μl) and 4.4 $\mu g_{(siRNAs)}$ /$g_{(soft\ body\ wet\ weight)}$ was injected into the adductor muscle of *M. gigas* in a 50 μl final volume. The concentration chosen was optimized *in vitro* using mantle cell cultures and injections were performed using a micro-syringe (Hamilton Gastight Syringes, Germany) (Supplementary Figure 2.2). Control (sham, injected with filtered (0.22 μm) sterilized seawater) and siRNA injected *M. gigas* were maintained under experimental conditions and 24h and 48h after injections the mantle underneath the damaged flat and round valves of randomly selected animals (n= 3) was sampled for molecular expression analysis. The shell

damage repair rate of each valve (flat and round, 3 holes/valve, 9 animals, a total of 54 holes /treatment) was determined to assess the effect of gene silencing by measuring the rate of hole repair at day 2. The area of the repaired shell and hole were calculated and a correlation analysis established for growth between the asymmetric valves. The experiments were repeated twice in independent experiments using the same protocol. No animals died during the experiments. To assess if siRNA treatments affected the shell structure the inner surface of the newly grown shells of siRNA treated and control animals were analysed by scanning electron microscopy (SEM), for details see SI Appendix.

2.3.7 Statistical analysis

For the statistical approaches used for omics-data see the relevant methods section. For other experimental treatments significant differences ($p < 0.05$) between groups were calculated with a two-tailed Student's t-test using GraphPad Prism ver 8.0.2. Data are presented as the mean ± SEM.

2.4 Results

2.4.1 Differentially expressed genes (DEGs) are more abundant in bivalve flat valve mantle transcriptomes

Mantle transcriptomes from *M. gigas* (asymmetric shell, this study)

and *M. galloprovincialis* (symmetric shell, this study) and from two other bivalve species *M. yessoensis* (asymmetric shell), *P. fucata* (slightly asymmetric shell), where mantle transcriptomes of both valves and an annotated genome exist, were used to identify differentially expressed genes (DEGs) in the mantle (Figure 2.1, Supplementary Table 2.1, 2.2). The correlation between intraspecies samples for each of the transcriptomes analysed was more than 0.8, indicating that the transcriptomes were of similar high-quality (Supplementary Figure 2.3). In *M. gigas*, a total of 129 DEGs were identified (~0.4% of the predicted genes in the species genome), of which 115 were unique to, or more abundant in, the mantle of the flat valve. In *M. yessoensis*, 133 DEGs were found of which 103 were unique to, or more abundant in, the mantle of the flat valve. In the mantle of the slightly asymmetric shell of *P. fucata*, 89 DEGs were identified, of which 37 DEGs were more abundant in the left mantle and 52 in the right mantle. But in the mantle of the symmetric shell of *M. galloprovincialis*, 44 DEGs were identified, of which 32 DEGs were more abundant in the left mantle and 12 in the right mantle (Supplementary Figure 2.3, Supplementary Table 2.3). In *M. gigas*, *M. yessoensis* and *M. galloprovincialis*, DEG protein coding and lncRNA genes were identified (Figure 2.2a).

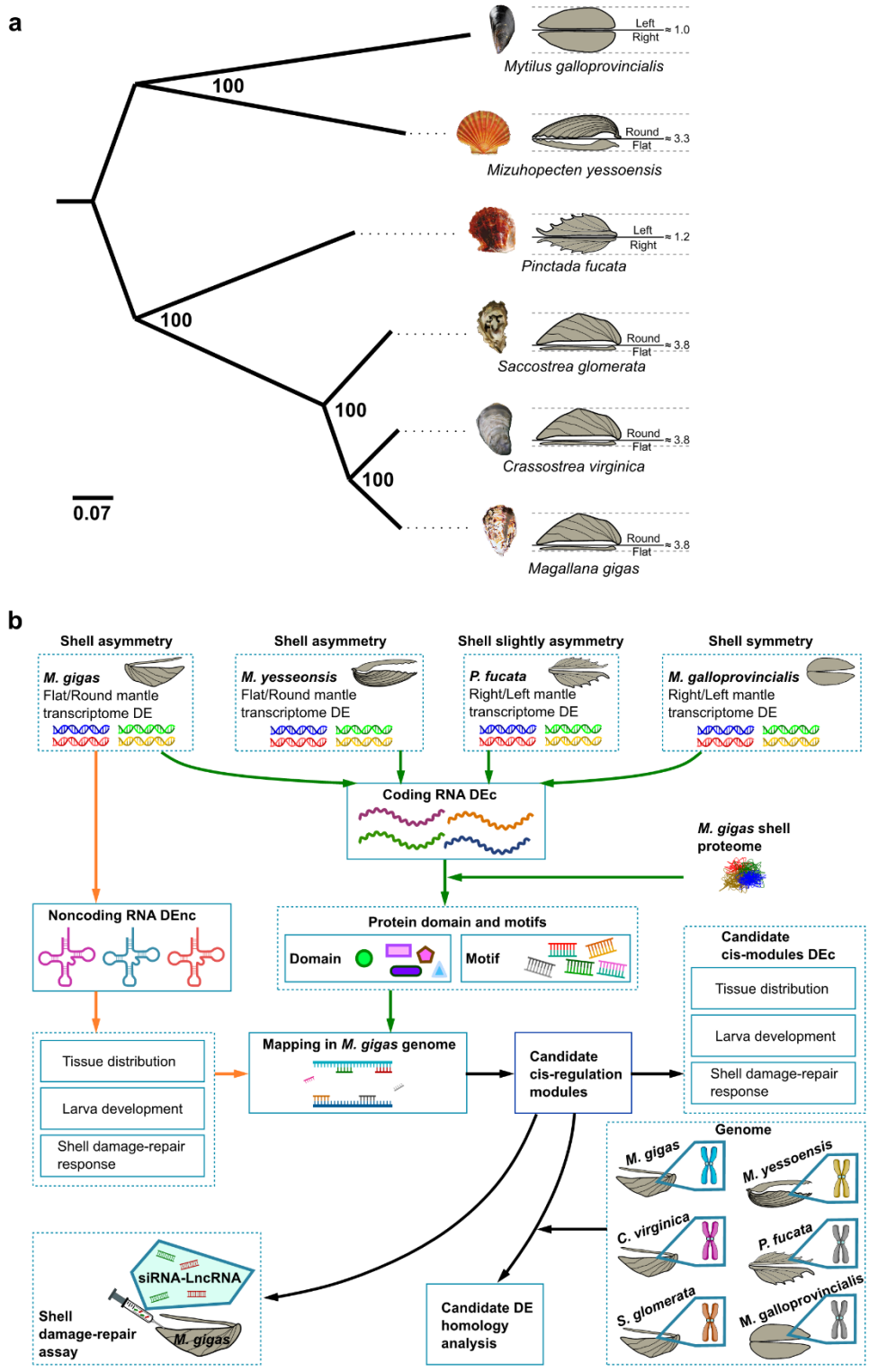

Figure 2.1. Workflow of the strategy to screen DEGs that regulate shell asymmetry of the bivalves in this study. (a) Phylogenetic relationship of the bivalves studied. The phylogenetic tree was constructed using the Orthofinder (ver 2.5.4, methods see SI Appendix) and the ML method. The shell height ratio and shell pattern plots are shown on the right side of the phylogenetic tree. Species with asymmetric shells (*M. gigas*, *C. virginica*, *S. glomerata*, *M. yessoensis*), slightly

asymmetric shell (*P. fucata*), and symmetric shell (*M. galloprovincialis*) are included in this study. Shell height ratio of *M. gigas* and *M. galloprovincialis* were measured in experimental specimens (n = 30), *M. yessoensis* shell height ratio data was provided by Xueshu Zhang, Dalian Ocean University (n = 30), *P. fucata* shell height ratio data was provided by Junlong Sun, Hainan University (n = 30), *C. virginica* and *S. glomerata* shell height ratio is measured using on-line resources (n = 10). (b) The overall workflow of the strategy taken to identify and characterize mantle DEG target genes that regulate shell growth and asymmetry in *M. gigas*. The DEc of the mantle transcriptome of symmetric, slightly asymmetric and asymmetric species was used to identify domains and motifs with the *M. gigas* deduced shell proteins as the reference, and the proteins predicted to be related to shell asymmetry in *M. gigas*. Available *M. gigas* public transcriptome data (normal tissues, larva development stages and shell damage-repair response) was used to predict the probable function of DEnc, and to screen for candidate DEnc related to *M. gigas* shell shape. Mapping *M. gigas* DEc and DEnc in the genome, obtained candidate cis-regulatory gene modules, which were analyzed to identify homologue gene modules across five bivalve species. Finally, the function of candidate lncRNA was assessed in gene silencing experiments using siRNA in *M. gigas* with damaged shells and the impact of gene silencing on crystal growth and shell repair rates determined in repaired shells.

2.4.2 Asymmetric expression of biomineralization toolbox genes in the mantle

DEGs encoding secreted proteins in the mantle associated with the flat or round valves corresponded to 80.73 % in *M. gigas*, 15.52 % in *M. yessoensis*, 45.45 % in the slightly asymmetric *P. fucata* and 37.08% in the symmetric *M. galloprovincialis* (Supplementary Figure 2.4, Supplementary Figure 2.5). In *M. gigas*, DE genes encoding proteins with a whey acidic protein (WAP, cl00156) domain were most abundant and were highly represented in the mantle transcriptome of the flat valve and in *M. yessoensis*, genes encoding proteins with a Calcium-binding Epidermal Growth Factor-like domain (EGF_CA, cl21504) were most

abundant and were highly represented in the mantle transcriptome of the flat valve (Supplementary Figure 2.6). The WAP domain in proteins has been proposed to inhibit crystal growth in the fast-growing c-axis and form platy geometrical aragonite crystals (Treccani et al., 2006). In *P. fucata*, genes encoding proteins of Solute carrier families 5 and 6-like; solute binding domain (SLC5-6-like_sbd, cl0045) were abundant in the mantle transcriptome of the left valve. SLC5-6-like_sbd domain functions as an ion transporter and is a member of the biomineralization toolbox genes. In *M. galloprovincialis*, proteins with a Low-Density Lipoprotein Receptor Class A domain (LDLa, cl00104), that are proposed to function as cell-surface receptors, were most abundant and were highly represented in the mantle transcriptome of the left valve. Comparison of the encoded proteins for the DEGs in the four species analysed indicated that six protein domains were restricted to the DEGs of *M. gigas* and *M. yessoensis* [C-type lectin domain (CLECT), EGF_CA, Carbonic anhydrase (Carb_anhydrase), PHA03247 superfamily, Copper type II ascorbate-dependent monooxygenases (Cu2_monooxygen) superfamily, Copper type II ascorbate-dependent monooxygenase C-terminal domain (Cu2_monoox_C) superfamily], and a bias in their expression between the mantle transcriptomes of the two valves was a characteristic of completely asymmetric valves as they were absent from *P. fucata* and *M. galloprovincialis* DEGs (Figure 2.2b).

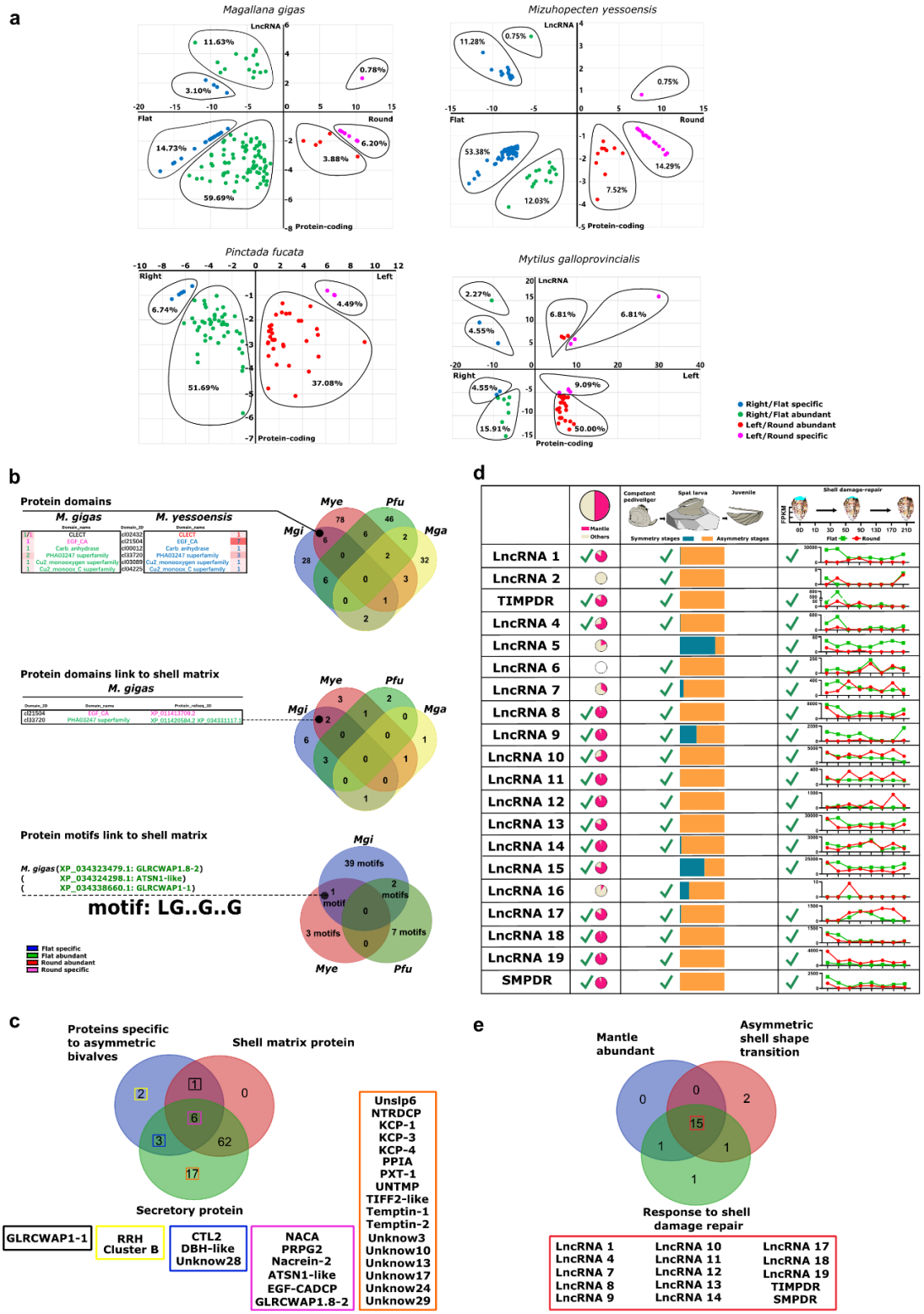

Figure 2.2. Potential lncRNA candidates regulating biomineralization toolbox genes in the mantle (selected by their deduced link with asymmetric shell-building). (a). Distribution and expression of DEGs (percentage in relation to all identified lncRNA) in the mantle of two bivalves with asymmetric shells, and one bivalve with slightly

asymmetric shells, and one bivalve with symmetric shells. The DEGs represented in the graphs for the four species are protein coding and lncRNA. The X-axes represent the significant change (log2 fold change) in DEGs in the mantle of each of the valves (flat or right/ round or left) and the Y-axes represents their abundance and distribution (log2 base mean). Dots are colour coded according to their abundance in the mantle: flat (right valve) is represented in blue (side-specific) and green (abundance) and round (left valve) is in pink (side-specific) and red (abundance). The percentage value indicates the proportion of the mantle DEGs in each species from each valve. (b) DEc deduced protein domains and protein motifs common in *M. gigas* and *M. yessoensis* and potentially associated with shell asymmetry. The Venn diagrams shows the mantle specific and overlapping deduced protein domains and SMP-domains and SMP-motifs identified. Domain names and the number of domains identified in deduced proteins are colour coded according to their relative abundance in expressed genes and localisation in the mantle of the round or flat valves. The protein motif LGXXGXXG (where X represent any amino acid residue) was found in both *M. gigas* and *M. yessoensis*. In *M. gigas* three DEc genes with an LGXXGXXG motif were found and were most abundant and enriched in the mantle transcriptome of the flat valve. (c) The Venn diagram shows the number and overlap of the DEc genes identified using the following criteria: 1) secretory proteins (green), 2) putative SMPs (red), 3) proteins with domains specific to the asymmetric bivalve mantle (blue). (d) Expression and distribution profile of the selected DE lncRNAs (lncRNAs 1 to 20) in the *M. gigas* mantle transcriptome of the flat and round valve. The pie chart represents the relative abundance in the mantle transcriptome in relation to other tissues. When transcript abundance was > 70% in the mantle they were considered as strong candidates for biomineralization “ √ ”. The rectangular chart represents the relative abundance in the asymmetric stages in relation to other symmetric stages. When transcript abundance was > 70% in the asymmetric stages they were considered as strong candidates for asymmetric shell biomineralization “ √ ”. Expression during shell damage-repair experiments (duration 21 days) in adult *M. gigas*. Transcript expression data for the mantle of the flat and round valves are represented by green and red lines, respectively. Transcripts marked “ √ ” were abundant and responded to shell damage-repair and were selected for further analysis. (e) The Venn diagram shows the number and grouping of lncRNAs by 1) regulated response to shell damage-repair (green), 2) regulation in larval stages associated with shell shape transition (red), 3) expression abundance in the mantle (blue).

To identify additional SMPs, *M. gigas* mantle transcriptomes were compared to their shell proteome (Supplementary Figure 2.7a). A total of 12 SMP-domains [WAP, Tyrosinase, GH20_hexosaminidase superfamily,

Glycoside hydrolase family 20 (GH20_hydro_20b) superfamily, putative carbohydrate-binding domain (CHB_HEX) superfamily, EF-hand calcium binding motif (EFh) superfamily, von Willebrand factor type C (VWC), EGF_CA, Lytic polysaccharide mono-oxygenase cellulose-degrading (LPMO_10), PHA03247 superfamily, PRK10263 superfamily, Topoisomerase II-associated protein PAT1 (PAT1) superfamily] were found in deduced proteins of the mantle transcriptome. Most of the proteins identified by proteomics were abundant or specific to the mantle transcriptome of the flat valve except the EGF_CA domain which was specific to the mantle transcriptome of the round valve (Supplementary Figure 2.7b). Only two SMP-domains (EGF_CA, PHA03247) were encoded by genes identified in the transcriptomes of *M. gigas* and *M. yessoensis* (Figure 2.2b). *In silico* analysis of gene transcripts also identified a novel SMP-motif “LGXXGXXG” (X represents any amino acid residue), present in asymmetric bivalves and abundantly expressed in the mantle of the flat valve (Supplementary Figure 2.8-9). Five groups of DEc genes with potential candidate functions in shell shape [GLRCWAP1-1 (group1); RRH and Cluster B (group2); CTL2, DBH-like and Unknow 28 (group3); NACA, PRPG2, Nacrein-2, ATSN1-like, EGF-CADCP and GLRCWAP1.8-2 (group4); Unslp6, NTRDCP, KCP-1/3/4, PPIA, PXT-1, UNTMP, TIFF2-like, Temptin-1/2 and Unknow 3/10/13/17/24/29 (group5)] were identified that complied with the criteria

"secretory protein", "putative SMP", and "proteins with domains specific to the asymmetric bivalve mantle" (Figure 2.2c). Overall, 66.06 % of *M. gigas* DE coding genes (DEc) were potential SMPs, of which 62.39 % were abundant or specific to the mantle of the flat valve (Supplementary Figure 2.10a) but only one DEc gene in *M. galloprovincialis* encoded an SMP. Genome mapping revealed that DE transcripts in *M. gigas* were widely distributed across the 10 chromosomes but were relatively more abundant on chromosome 2 and 3 (Supplementary Figure 2.10b).

2.4.3 Asymmetric expression of Long non-coding RNA genes in the mantle

LncRNAs accounted for 15.50 % of DEGs in *M. gigas* and 12.78 % in *M. yessoensis* and were most abundant in the mantle of the flat valve (Figure 2.2a). LncRNAs accounted for 19.44 % of DEGs in *M. galloprovincialis* and were more abundant in the mantle of the left valve. LncRNAs have been neither predicted nor documented in the latest release of the genome assembly of *P. fucata* (Takeuchi et al., 2022) and so were not analysed in the study (Figure 2.2a). Twenty-one lncRNAs were predicted in the genome of *M. gigas* and 20 were confirmed as authentic (lncRNA 1-20, Supplementary Table 2.4) and 19 were considered abundant or specific to the *M. gigas* flat valve mantle transcriptome. To select candidate lncRNA for functional studies publicly available mantle

transcriptomes (Supplementary Table 2.1, Supplementary Figure 2.11a), including transcriptomes of larval stages associated with shell/shape establishment (Supplementary Figure 2.11b), and transcriptomes of shell damage-repair (Figure 2.2d) were analysed and fifteen potential candidate lncRNAs associated with completely asymmetric shell-building were identified [*lncRNA 1*, *lncRNA 4*, *lncRNA 7-14*, *lncRNA 17-19*, *TIMPDR* and *SMPDR*] (Figure 2.2e).

2.4.4 Long non-coding RNAs are regulators of biomineralization toolbox genes

Six lncRNAs were assigned to potential cis-regulatory modules (Supplementary Figure 2.12a). Based on transcriptome evaluation, four candidate lncRNAs [*lncRNA 1*, *lncRNA 17*, TIMP (tissue inhibitor of metalloproteinases) domain regulator (*TIMPDR)*, SMP domain regulator (*SMPDR*)] were selected as likely regulators of DEc genes in the mantle (Supplementary Figure 2.12b). *LncRNA 1* and *lncRNA17* were excluded from further analysis because of high sequence similarity with the Acanthoscurrin-1-like (*ATSN1-like*) gene and extensive highly repetitive regions in the downstream regulatory protein, respectively, which precluded specific primer design.

The candidate cis-regulatory module of *TIMPDR* included uncharacterized shell protein 6-like (*Unslp6*) and NTR domain-

containing protein-like (*NTRDCP*), which encoded TIMP domain mantle proteins. The candidate *SMPDR* cis-regulatory module contained the gene *EGF-CADCP* (EGF-CA domain containing protein), that codes for an SMP (Figure 2.3a, Supplementary Figure 2.13). Expression analysis of cis-regulation module genes was evaluated using *in vitro* cultures of mantle tissue (Supplementary Figure 2.14).

Collinear cis-regulatory regions were conserved in the evolutionary proximate asymmetric shell species *C. virginica* and *S. glomerata* (Figure 2.3b-c, Supplementary Figure 2.15). No corresponding collinear regulatory modules were identified in the genomes of the asymmetric shelled *M. yessoensis* or slightly asymmetric shelled *P. fucata* or in the symmetric shelled *M. galloprovincialis*.

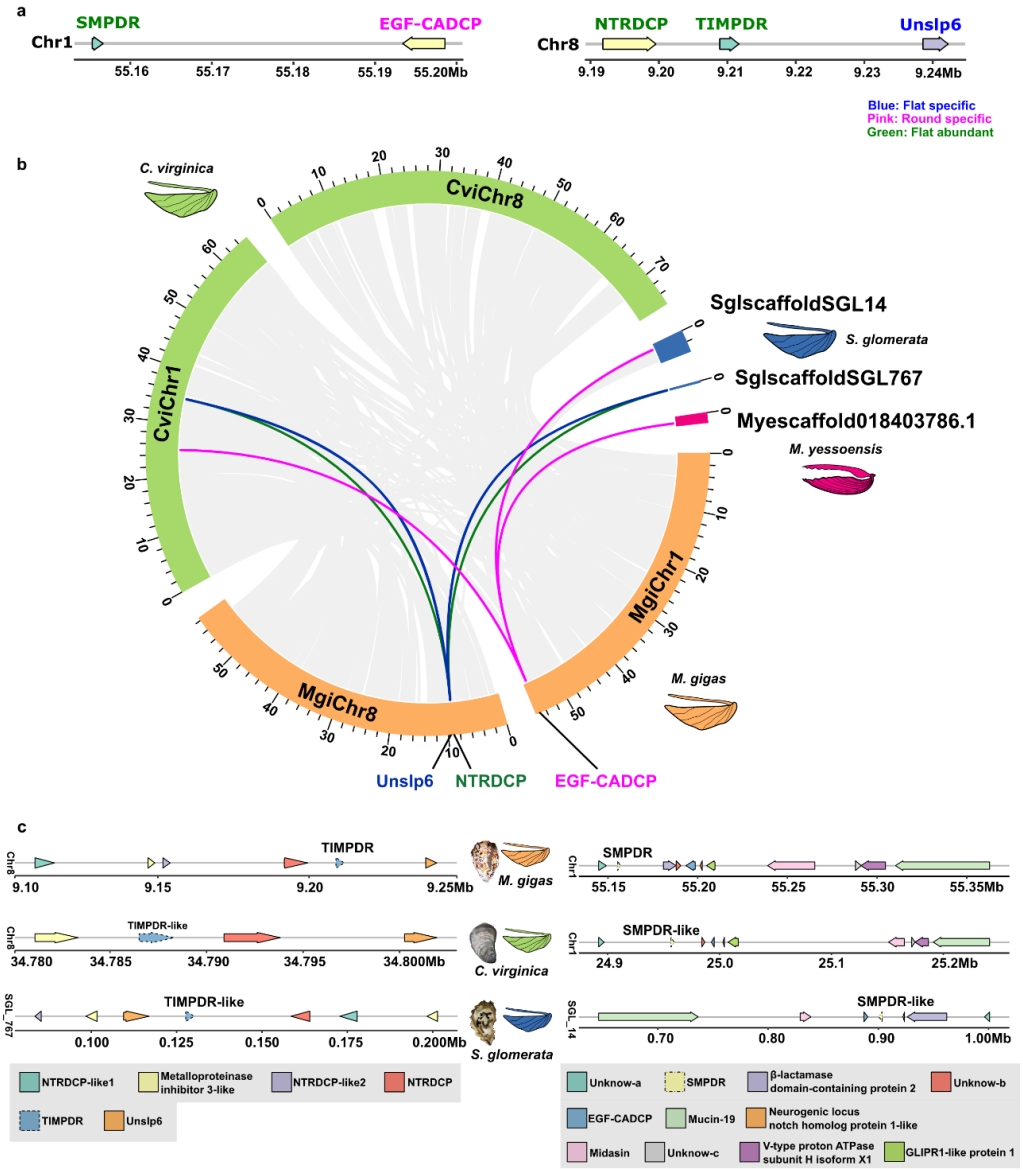

Figure 2.3. Mantle lncRNAs and candidate cis-regulation modules in bivalve/Ostreidae family. (a) Two candidate DEG cis-regulatory modules were selected in *M. gigas*. Arrows indicate gene orientation and gene position is provided (Megabases, Mb). Protein coding gene symbols and lncRNAs are indicated and are coloured according to distribution and abundance in the *M. gigas* mantle. The candidate cis-regulatory module of *TIMPDR* included uncharacterized shell protein 6-like (*Unslp6*) and NTR domain-containing protein-like (*NTRDCP*), which encoded TIMP domain mantle proteins, and are likely specific to *M. gigas*. The candidate *SMPDR* cis-regulatory module contained the gene *EGF-CADCP* (EGF-CA domain containing protein), that codes for an SMP and was common in the mantle transcriptome of the asymmetric bivalves studied. (b) Collinearity between *M. gigas* and homologue genome regions in other bivalves. Lines (grey) represent gene blocks with a minimum of five orthologue genes and lines (blue, green and pink) indicate collinear gene blocks that contain the candidate protein coding genes. Candidate protein coding genes are mapped to *M. gigas* chromosome 1 (*EGF-CADCP*) and

chromosome 8 (*NTRDCP* and *Unslp6*) and homologous collinear genome regions were found in *C. virginica* (chr 1 and 8) and in *S. glomerata* SGL_14 and SGL_767, respectively. No homologue regions containing the target coding genes were found in the genomes of *P. fucata* and *M. galloprovincialis* (slightly asymmetrical/symmetrical bivalves, Supplementary Figure 2.19) or the scallop *M. yessoensis* (asymmetrical bivalve) but a gene with a similar protein domain to *EGF-CADCP* (EGF_CA domain) was identified in the scallop genome, scaffold NW_018403786.1. (c) The *M. gigas* genes were taken as a reference to identify homologue genome regions in other members of the Ostreidae family with an asymmetric shell. Detailed characterization of the collinear gene blocks (> five homologue coding genes) containing the *M. gigas* candidate DEc genes and the lncRNAs for the homologue genome regions in the Ostreidae family members analysed, *C. virginica* and *S. glomerata* (see Supplementary Table 2.5). Lines represent the genome regions and arrows represent genes and arrow heads indicate gene direction according to the genome annotation. Arrow length is related to gene length. Gene names and their relative position in the genome (Mb) are indicated. Orthologue genes are indicated in the same colour and the gene symbol is given. The lncRNA genes analysed are represented by dashed arrows.

2.4.5 Non-coding RNAs regulate shell growth and crystal structure in oyster

To test the potential role of candidate lncRNAs on shell biomineralization, shell damage-repair assays in juvenile *M. gigas* were used. Shell damage-repair assays revealed that in juvenile *M. gigas* repair of damage to the round valve was faster than repair in the flat valve. Two days after shell perforation, 80.05 ± 20.82% of the 3 holes in each shell had been covered in the round valve compared to 12.84 ± 20.19% in the flat valve ($n = 13$, $p < 0.00001$, $Z=14.48$ (z-test), Supplementary Figure 2.16). To test the role of lncRNA in shell biomineralization, small interfering RNAs (siRNA) were applied in *M. gigas* damage-repair trials. The oysters of the control (no lncRNA, only seawater) and NC (negative

control, lncRNA control chain) experimental groups had a similar shell repair rate (mean value in round and flat valves were 79.71 % and 15.26 %, respectively) but the shell repair rate was altered in the siRNA-lncRNA treated groups. The damage-repair ratio in the round and flat valves of the group treated with siRNA-*TIMPDR* was similar (78.77 ± 25.48% and 76.09 ± 28.82%, respectively), and represented a significant increase in biomineralization of the flat valve compared to the normal flat valve repair rate in the control group ($p < 0.001$). Similarly, in siRNA-*SMPDR* treatments, flat valve repair rates (70.65 ± 20.87%) were significantly greater than in the negative control lncRNA ($p < 0.001$) (Figure 2.4a, b) groups. In the flat valve, siRNA-*TIMPDR* also caused a significant reduction ($p < 0.05$) in the expression of the target genes, *NTRDCP* and *Unslp6*, whereas ablation of *SMPDR* significantly up-regulated *EGF-CADCP* gene expression ($p < 0.05$) (Figure 2.4c). The results confirmed that the candidate lncRNAs affected shell repair of the flat valve by modifying expression of mantle and SMP genes.

The newly grown shell of the flat and round valve of the siRNA-*TIMPDR* oysters had a similar prismatic layer organization, which differed from the control groups (control and NC) (Figure 2.4d). In both valves, the boundaries between the crystals were narrower and the calcium carbonate crystals were flattened, had lost their typical convex shape and were larger than the normal crystals of the control groups

(Figure 2.4d-e, Supplementary Figure 2.17). The newly grown round inner shell valve of siRNA-*SMPDR* oysters, also modified shell structure, causing the prismatic crystals in the round valve to become larger without changing their shape compared to the control. In the flat shell the prismatic crystals were irregular with fissures and a horizontal orientation (Figure 2.4d-e).

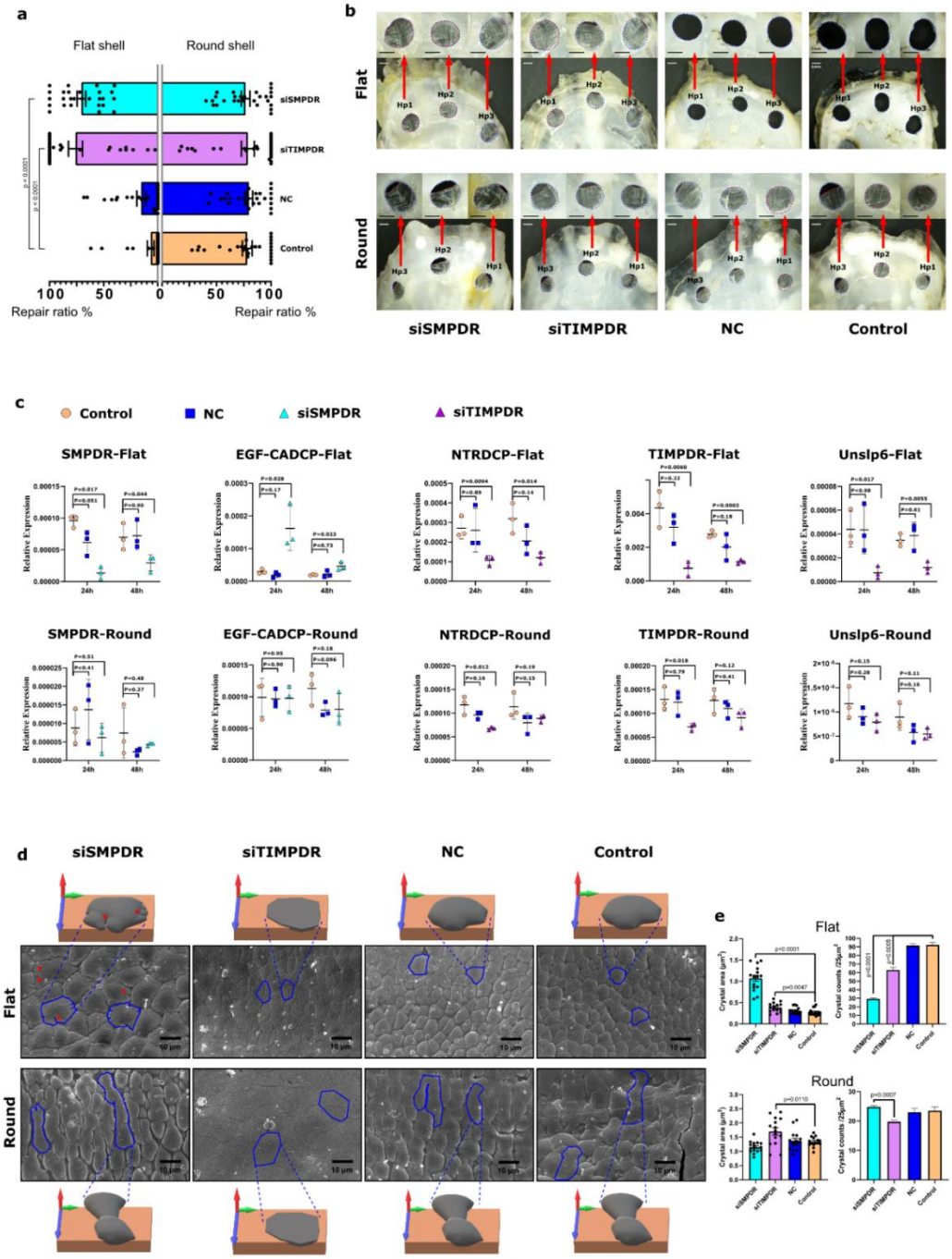

Figure 2.4. Effect of lncRNAs on mantle gene expression, shell damage-repair and shell structure of both valves in juvenile *M. gigas*. (a) Shell repair ratio in the flat and round valves 2 days after drilling: Control (seawater, no siRNA chain), negative siRNA chain (NC) and the two treatments groups (siRNA-*TIMPDR* and siRNA-*SMPDR*). Data is presented as the median and quartile ranges from 9 juvenile *M. gigas* for each treatment group (Control, NC, siRNA) where each valve (flat and round) was drilled with 3 holes (6 holes per animal, 54 holes in total/treatment). (b) Bright field digital photographs showing the recovery of the newly produced shell 2 days after drilling in juvenile *M. gigas* flat and round valves. A representative image from one individual/

experimental group is shown and was captured using a stereoscope (Motic, SMZ-171, China) equipped with a digital camera (Visicam 6 Plus, VWR, Portugal). Detailed magnification of the three-hole positions (Hp1, Hp2 and Hp3) is shown. The red-dashed line indicates the limit of the newly grown shell in each hole. The scale bar corresponds to 1mm. (c) Effect of shell damage on mantle gene expression. Data was obtained by quantitative expression (q-RT-PCR) and is shown as mean ± SEM, (n = 3 pooled samples: 3 individuals/pool). Significant differences in gene expression were calculated by comparison to the damaged group and control group using a Student t-test. The p values for the pairwise comparisons are shown. (d) Scanning electron microscope (SEM) images of the prismatic calcium carbonate crystals of the inner side of the recovered flat and round valves. Representative prismatic crystals are delineated with a blue line to highlight their structure and an illustrative 3D model of their structure was designed using Paint 3D (Microsoft, USA). The red arrowheads indicate slits at the periphery of calcium carbonate crystals in the flat valve of the siRNA-*SMPDR* group. (e) Prismatic crystal area of shell-repair in the flat and round valves was calculated from: i) the areas of randomly selected crystals (n = 15) or ii) the number of crystals present in a randomly selected 25 mm^2 area (n = 4).

2.5 Discussion

Shell biomineralization is tightly regulated by the mantle and haemocytes, and although some biomineralization toolbox genes are conserved across bivalves, its utilization for shell building is divergent across species and lineage-specific mantle secretomes are considered to underlie bivalve shell diversity and shape (Aguilera et al., 2017; Clark, 2020). Modern oysters and scallops, possess completely asymmetric shell valves and an asymmetric shell shape is acquired early in bivalve larval development when differential gene regulation begins (Liang et al., 2022; Stanton, 2012). Our meta-analysis of bivalve transcriptomes and proteomes suggests that asymmetric shell development is related to a small proportion of differentially expressed SMP genes that are most

actively expressed by the mantle producing the flat valve. The divergent gene expression between the mantle of the flat and round valves is orchestrated by a set of conserved non-coding RNAs that modify shell growth and the spatial organization of the crystals (Figure 2.5a).

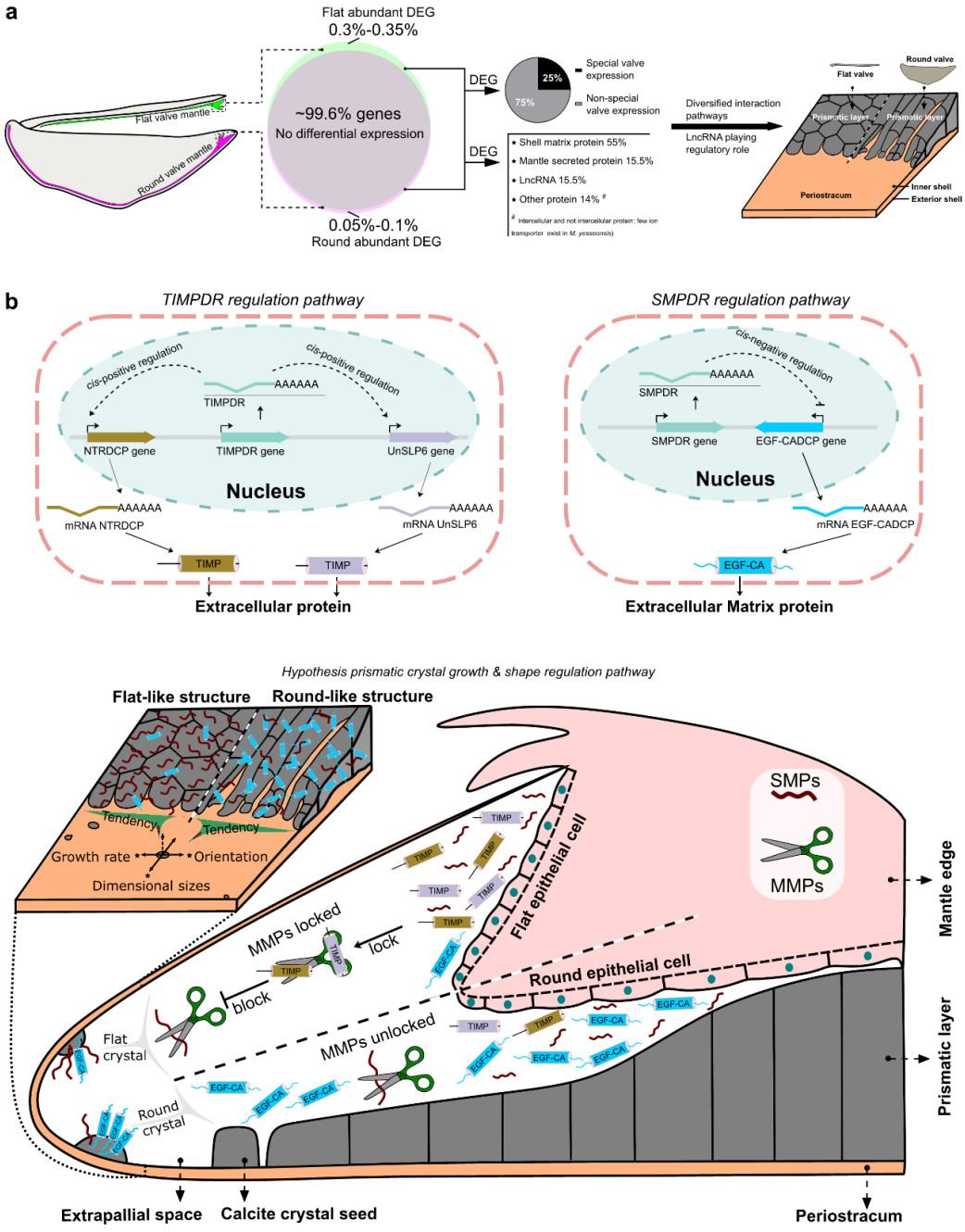

Figure 2.5. Putative regulatory model explaining the production of

asymmetric shells in oysters. (a) The shell shape is regulated by a very small number of DEGs in the mantle margin, the majority of which are biomineralization toolbox genes, and include lncRNA, and genes coding for secreted and intracellular proteins. Most DEGs are specific to the flat valve and twenty-five percent have valve-specific expression. (b) A putative model to explain how lncRNAs *TIMPDR* and *SMPDR* affect the expression of neighbouring protein coding genes. *TIMPDR* positive cis-regulation of the secreted non-matrix proteins *Unslp6* and *NTRDCP*, which contain a TIMP domain, explains their abundant expression in the mantle of the flat valve. *SMPDR* negative cis-regulation of the *EGF-CADCP* matrix protein (EGF-CA domain containing), which is abundantly expressed in the mantle of the round valve. It is hypothesized based on the siRNA experiments and SEM results for the prismatic calcium carbonate that i) expression of the SMP EGF-CA domain promotes the growth and area (shape) of the prismatic crystals in the round valve and b) expression of the TIMP domain protects SMPs from matrix metalloproteinases (MMP) and stimulates prismatic shell growth in the flat valve. The resulting differences in growth rate and shape of prismatic crystals causes shell asymmetry in oysters.

Despite the existence of relatively limited experimental evidence linking lncRNA to biological function in bivalves, previous transcriptome/genome screening identified them in the mantle, and they have been implicated in the regulation of shell pigmentation, larval development, the immune system, and shell formation (Feng et al., 2018; Guo et al., 2023; Le Franc et al., 2022; Núñez-Acuña et al., 2022; Sun and Feng, 2018; Yu et al., 2016). In bivalves, RNAi knockdown experiments indicated that lncRNAs regulate immune gene (IL-17) expression (Huang et al., 2018) stimulated by poly I:C (Zheng et al., 2020a). In *P. fucata,* expression of lncMPEG1 was stimulated by shell damage, alien invasion and temperature and hypoxia stresses. Furthermore, decreased lncMPEG1 expression is associated with irregular crystal growth on the inner surface of the prismatic layer and

nacre in *P. fucata* shells (Cai et al., 2022). In addition, RNAi knockdown experiments in *P. fucata* demonstrated that lncMSEN2 is related with the immune response and regulation of nacreous layer formation (Zheng et al., 2020b). None of the previous studies about lncRNA in bivalves considered their role in the regulation of shell growth or shape. In the present study we provide evidence that lncRNAs most likely regulate shell growth and shape in adults. Furthermore, we used publicly available transcriptomes from *M. gigas* early larval development stages and during the transition from a larva with symmetrical valves (free-swimming competitive pediveliger larvae) to a larva with asymmetrical valves (sessile spat) after metamorphosis to identify candidate genes involved in emergence and establishment of the shell. In bivalves, the shell emerges during the first stages of development and in *M. gigas* the shell gland starts to secret the shell 24 h post-fertilization (D-shape larvae) (Kniprath, 1981; Marin et al., 2007). After the shell is formed, the larvae develop into pediveliger larvae the last stage before settlement on a hard substrate and metamorphosis into a sessile juvenile spat with an asymmetric shell (Stenzel, 1963; Weiss et al., 2002). During larval stage transitions, the morphology, biochemistry, and composition of the calcifying tissue of oyster larvae changes and most studies of this ontogenetic stage have identified genes including lncRNA that change in expression and may be related to shell development (De Wit et al., 2018; Guo et al., 2023; Yu et

al., 2016; Zhang et al., 2012). In the present study by conducting meta-analysis of data from larvae developing a shell and the mantle from adults, novel biomineralization candidate genes and regulatory lncRNAs that regulate shell growth were identified. Although future studies are required to confirm binding partners and their common spatial-temporal expression and experiments to confirm they orchestrate shell development and growth in larvae. The involvement of lncRNAs in insect metamorphosis has been described and our results provide further support for the involvement of lncRNA during invertebrate development and emphasise their likely importance in Mollusca (Choudhary et al., 2021; Song and Zhou, 2020).

The differential distribution of lncRNAs between the mantle of flat and round valves, their proximity to SMP loci and the conservation of the cis-regulatory modules in other asymmetric oyster species indicates this regulatory mechanism probably emerged in the common ancestor of this taxonomic group. Using *M. gigas* as the model, we found that the number of DEGs between the mantle of the flat and round valves are relatively small, and differential gene regulation is likely to explain divergent rates of valve growth. To test if lncRNA modulated DEG expression and modified shell growth, small interfering RNAs (siRNA) were applied in *M. gigas* shell damage-repair trials. The results obtained confirmed that the candidate lncRNA (*TIMPDR* and *SMPDR*) affected shell repair

through modified expression of mantle (*NTRDCP* and *Unslp6*) and SMP (*EGF-CADCP*) genes.

The diversity of calcified shell types, despite the conserved “building blocks”, in extant bivalves is due to the deposition of crystalline and amorphous calcite crystals in an organic framework (Marin et al., 2012; Suzuki and Nagasawa, 2013) and the shell of asymmetric bivalves usually contain different microstructures (Carter, 1990). In *M. gigas* the flat and round valves have a different crystal structure (Yamaguchi, 1994; Zamarreño et al., 1996). The prismatic crystals of the flat shell have a near-geometric crystal structure with regular boundaries and no cracks resembling the prismatic structure of symmetric shells (Peng et al., 2021). In contrast the crystals of round shells have a ridge-and-furrow structure, which is associated with their rapid growth for substrate adherence (Yamaguchi, 1994). The explanation for the divergent shell growth and modified shell architecture in the asymmetric shell compared to the symmetric shell of the oysters (Pteriomorphia) may be explained by the unique bias in the expression of some biomineralization toolbox genes in the mantle of the asymmetric shells and the evolution of shared colinear cis-regulatory modules. When this is considered in the context of the vast diversity of bivalve species, and their complex phylogenetic relationships the consensus view is that the modern bivalves typically display bilateral symmetry both in shell and anatomy and only a few bivalves such as

oysters (Ostreidae), some clams (Anomiidae and Chamidae) and scallops (Pectinida) acquired valve asymmetry during evolution (Bieler et al., 2014; Carter, 1990; McDougall and Degnan, 2018; Ponder et al., 2019; Yonge, 1977). We propose based on the results of our study that the symmetry and round shells in bivalves is the default condition and that the flat valve of the asymmetric oysters is a more recent evolutionary innovation in the genome.

The new growth of damaged shells of both the flat and round valves in siRNA-*TIMPDR* treated *M. gigas* had a similar prismatic layer organization. To understand why modified expression of the non-SMPs, *Unslp6* and *NTRDCP*, affected the shell we analysed the characteristics of the deduced proteins. Both contained a TIMP domain and belonged to the NTR-like superfamily that has inhibitory matrix metalloproteinase activity in vertebrates (Bode et al., 1999) and in *P. fucata* (Kubota et al., 2017) (Supplementary Figure 2.18, Supplementary Table 2.6). In *P. fucata* metalloproteinases degrade extracellular matrices to produce the fine organic fibres that regulate the orientation of fibrous aragonite crystals (Kubota et al., 2018). siRNA-*SMPDR* also modified shell structure, causing the prismatic crystals in the round valve to become larger, although their shape was not changed and was similar to the control. The EGF domain containing protein in Pinctada shell was reported to only exist in the prismatic layers (Marie et al., 2011), which

implies that this domain may have an important role in specific crystal nucleation events and arrangements (Arivalagan et al., 2017; Beck et al., 1990). In the flat valve siRNA-*SMPDR* caused the prismatic crystals to be irregular with fissures and a horizontal orientation. The negative regulation of *EGF-CADCP* by *SMPDR* also had a positive effect on rapid planar growth of prismatic calcium carbonate crystals.

In summary, in our study we identify a conserved suite of enriched protein domains and regulatory factors of bivalve shell growth and propose a model to explain the origin of asymmetric valves in oysters and possibly other asymmetric bivalves. We propose that modified expression of SMP and non-SMP proteins regulates growth of prismatic calcium carbonate crystals and thus the shell (Figure 2.5b, Supplementary Table 2.7). Our results indicate that low expression of *SMPDR* in the mantle of the round valve upregulates the expression of EGF-CADCP (SMP), we hypothesise that this affects the deposition of secreted protein in the prismatic layer and promotes shell growth and the formation of crystals of calcium carbonate with an irregular spatial orientation. In contrast, high expression of *TIMPDR* in the mantle of the flat valve upregulates NTRDCP and Unslp6 (non-SMPs) expression, which we hypothesise increases secretion of proteins with a TIMP domain into the extrapallial fluid. High concentrations of TIMP domain proteins are likely to inhibit matrix metalloproteinase activity in the extrapallial fluid and decrease

degradation of SMPs to promote slower shell growth and a regular spatial orientation of the prismatic crystals.

In conclusion, we have demonstrated that valve asymmetry in oyster originates from the differential expression of some genes in the mantle of flat and round valves as a result or regulation by lncRNAs. The cis-regulatory modules identified explain the asymmetric expression in the mantle of some biomineralization-related SMP and secreted non-SMP genes that modulate prismatic crystal growth, by affecting the planar growth rate and spatial orientation of crystals in shells. The present study in oyster substantiates the hypothesis that shells are shaped by conserved upstream cis-regulatory factors and a highly evolved and diverse downstream regulatory network in the bivalve mantle (Aguilera et al., 2017; Davidson, 2010).

2.6 Supplementary materials

2.6.1 Supplementary material and methods (in Annex I, digital format)

All the supplementary material and methods (SI Appendix) are provided in the Annex I in digital format.

2.6.2 Supplementary Figures

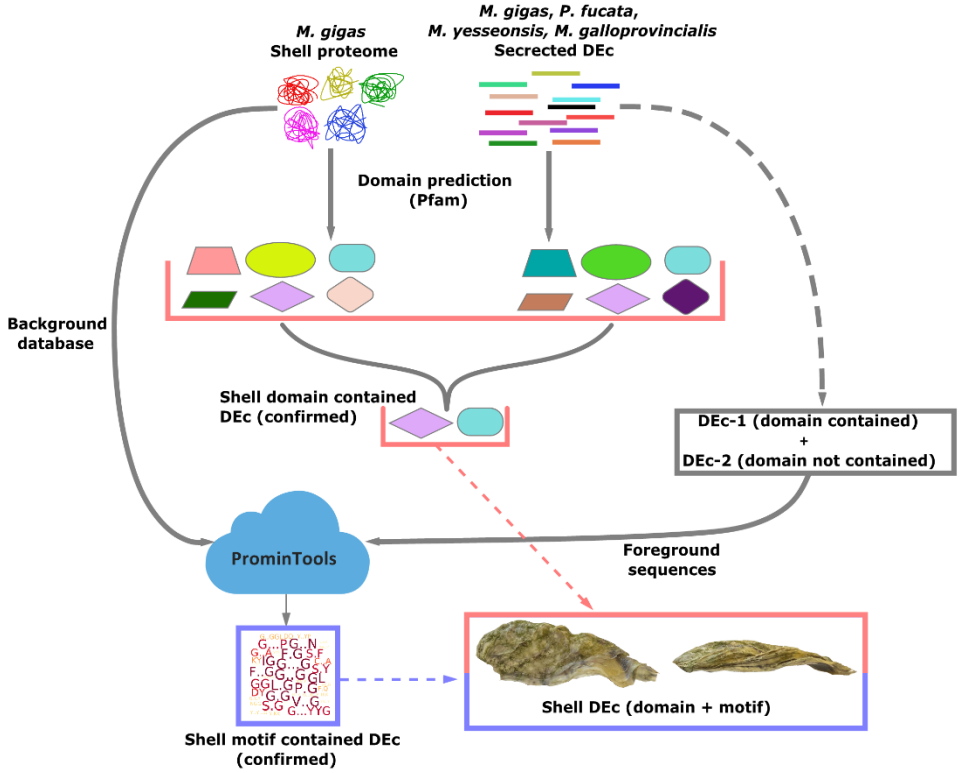

Supplementary Figure 2.1 Workflow of the strategy used to characterize the protein domains and motifs of deduced DEc protein genes in the mantle of the asymmetric valves of *M. gigas*, and *M. yessoensis*, and slightly asymmetric valve of *P. fucata* and the symmetric valve of *M. galloprovincialis*. The DEGs in the mantle transcriptome that code for proteins in *M. gigas* were compared to the shell proteome of *M. gigas* to identify specific protein domains associated with the asymmetric shell. To improve the identification of protein domains associated with bivalve SMPs, DEc genes in the mantle transcriptome that had no significant matches in the species-proteome were subsequently analysed using the ProminTools and employed as foreground groups and compared with the background group (*M. gigas* shell proteome). The dashed line represents DEc genes that had no SMP-domain identified or predict.

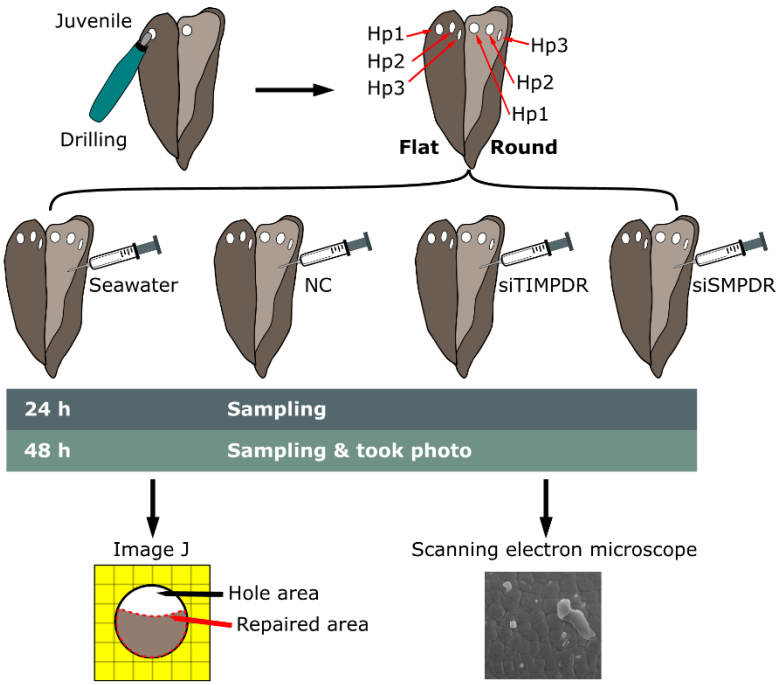

Supplementary Figure 2.2 Schematic representation of the strategy taken to test the effect of *SMPDR* and *TIMPDR* on the shell damage-repair process in juvenile *M. gigas*. Three holes were drilled in each *M. gigas* valve and the animals were divided into four experimental groups (n = 9 animals/ group – total 54 holes/group): two control (seawater and negative siRNA control chain) and two treatment groups (siRNA-TIMPDR and siRNA-SMPDR). Mantle samples were collected 24 h and 48h after shell damage and the progress of shell repair assessed by taking images of the drilled holes using a digital camera. The microstructure of the newly grown shell that filled the holes was analysed by SEM.

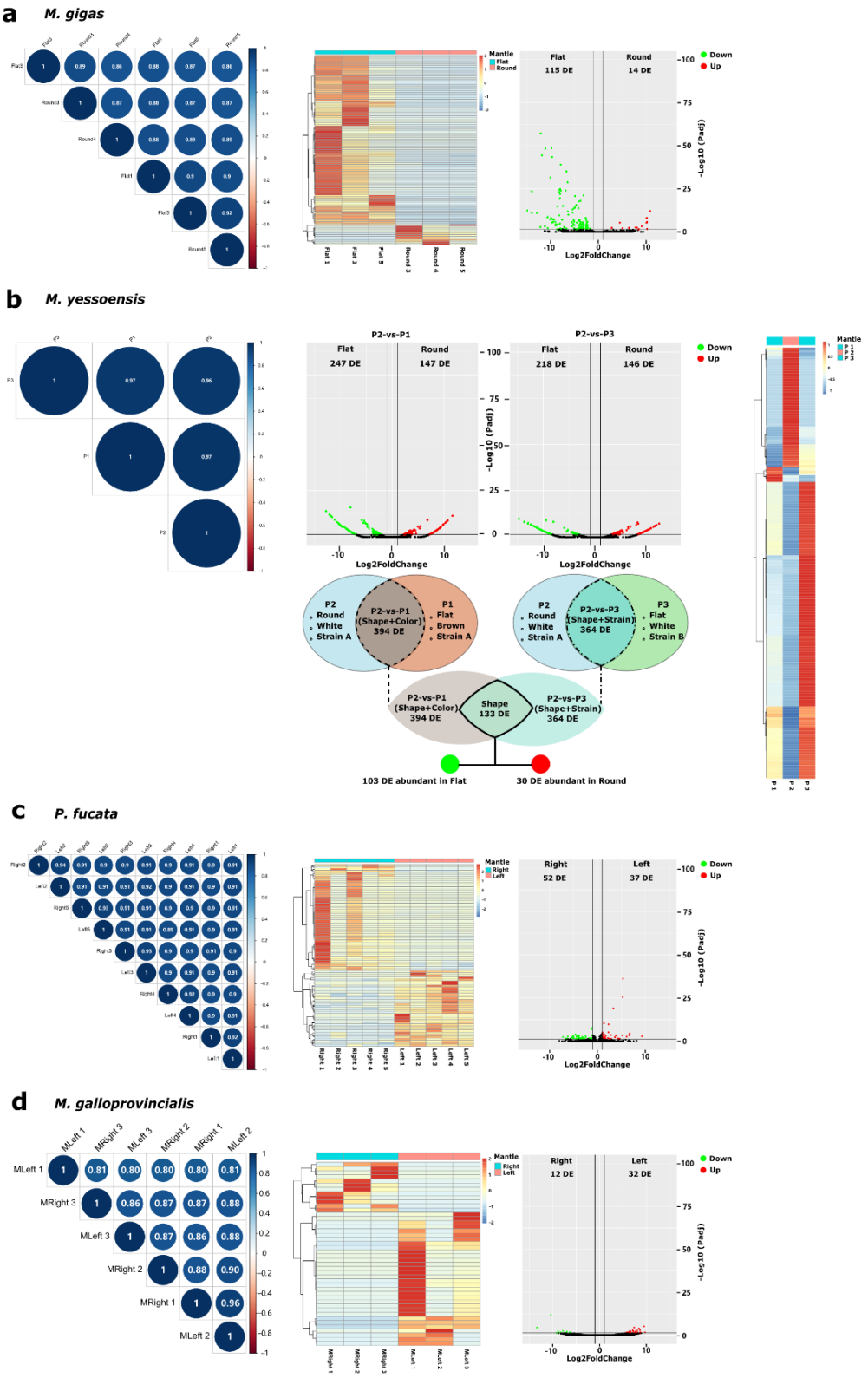

Supplementary Figure 2.3 Correlation analysis of the mantle transcriptome samples and volcano plots and heatmaps of differentially expressed genes. (a, b, c, d) DEGs in the mantle of two asymmetric bivalves, *M. gigas* (a) and *M. yessoensis* (b), in the slightly asymmetric bivalve, *P. fucata* (c) and in the symmetric bivalve, *M. galloprovincialis*

(d). Volcano plots were established with the transcriptome data and statistical significance (log10 adjusted p-value) versus the magnitude of change (log2 fold change) is represented. Heatmaps of the DEG that passed the threshold criteria, a Padj value < 0.05 and log2 fold change ≥ 1, were considered to be significantly modified. The green and red dots correspond to DEG significantly different in the flat (right) and round (left) valves, respectively. Black dots represent genes that were not significantly DE. The volcano plots were established using the ggplot2 package and the heatmaps using the pheatmap package in R Studio (see Materials and methods).

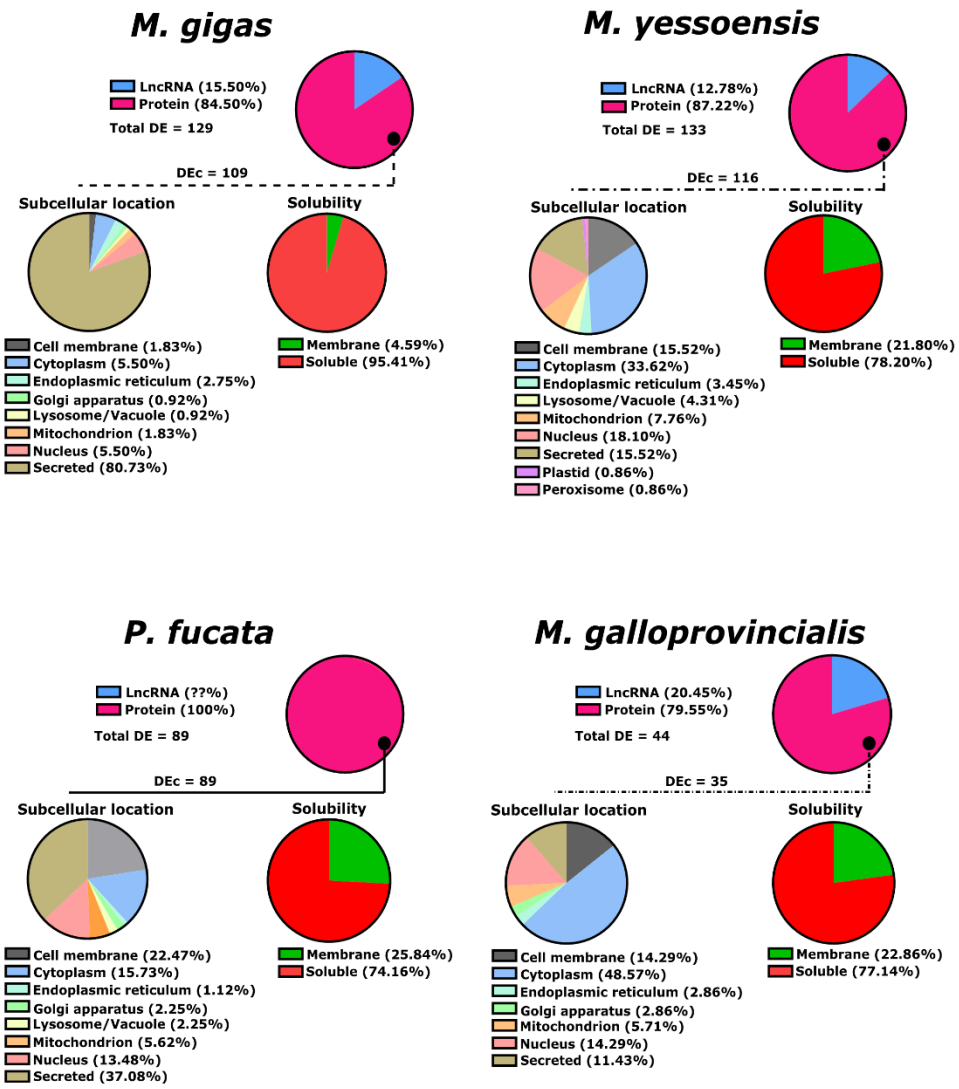

Supplementary Figure 2.4 Characterization of the differentially expressed protein coding genes (DEc) in the mantle and their subcellular localization. Subcellular localization and solubility of DEc genes were predicted using DeepLoc-1.0 (see Supplementary Table 2.9). The majority of the predicted DEc genes are soluble but subcellular localization is variable across the four species.

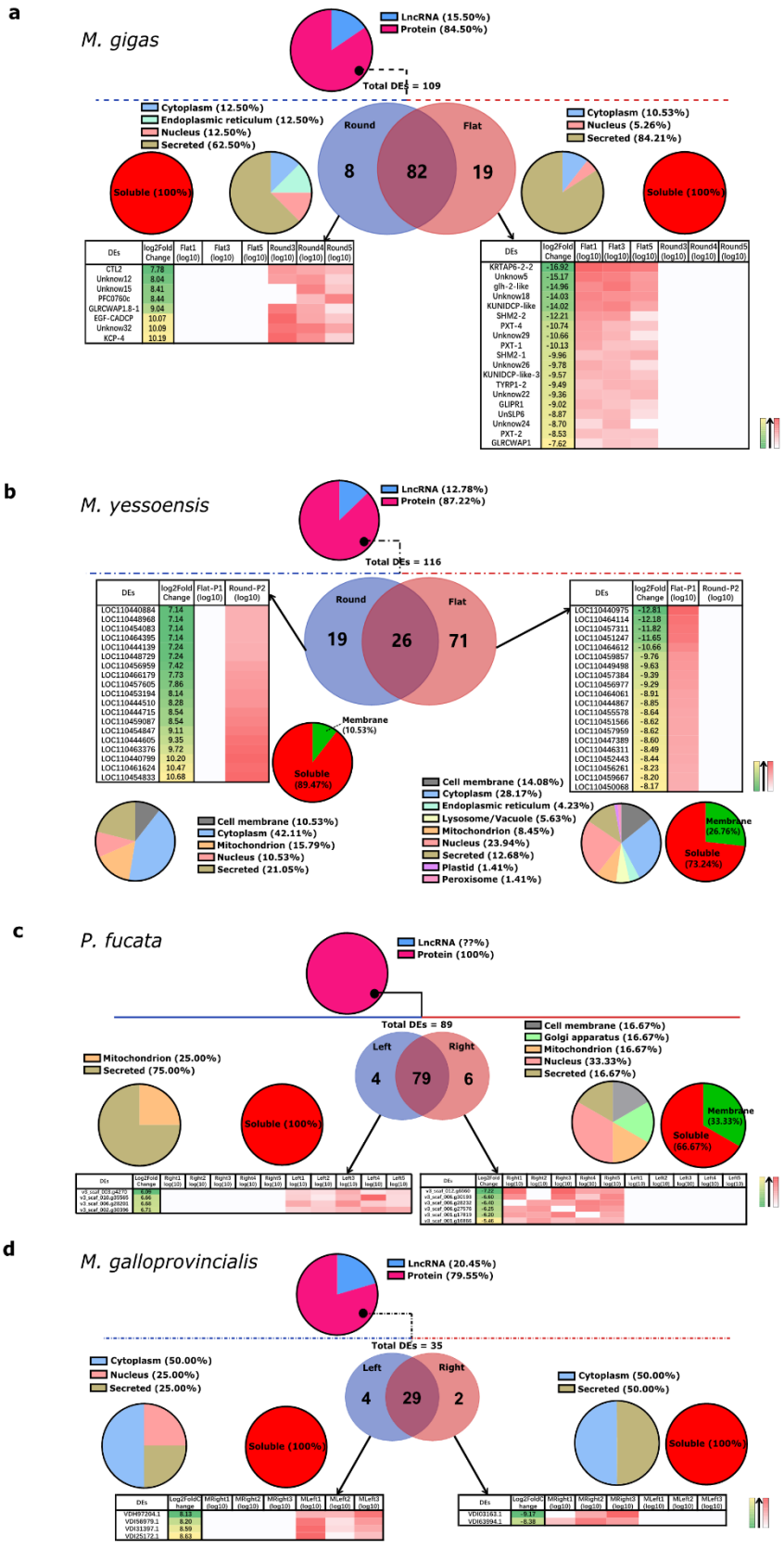

Supplementary Figure 2.5 Characterization of specific and common differentially expressed genes (DEG) in the mantle transcriptomes of the

flat and round valve. a-d) Analysis of *M. gigas*, *M. yessoensis*, *P. fucata* and *M. galloprovincialis* mantle transcriptomes. The *M. gigas* and *M. galloprovincialis* mantle transcriptomes were generated in the present study. The *P. fucata* and *M. yessoensis* mantle transcriptomes which are publicly available were downloaded from the SRA database (Supplementary Table 2.1). The Venn diagrams show the number of specific and shared DEG transcripts in the mantle of the flat or round shell. The percentage of DEc genes and lncRNA genes is presented in the pie chart at the top of the figure. DEc genes specific to the mantle of the flat (right) or round (left) valves are indicated in the table and their abundance (heatmap) and subcellular localization is provided.

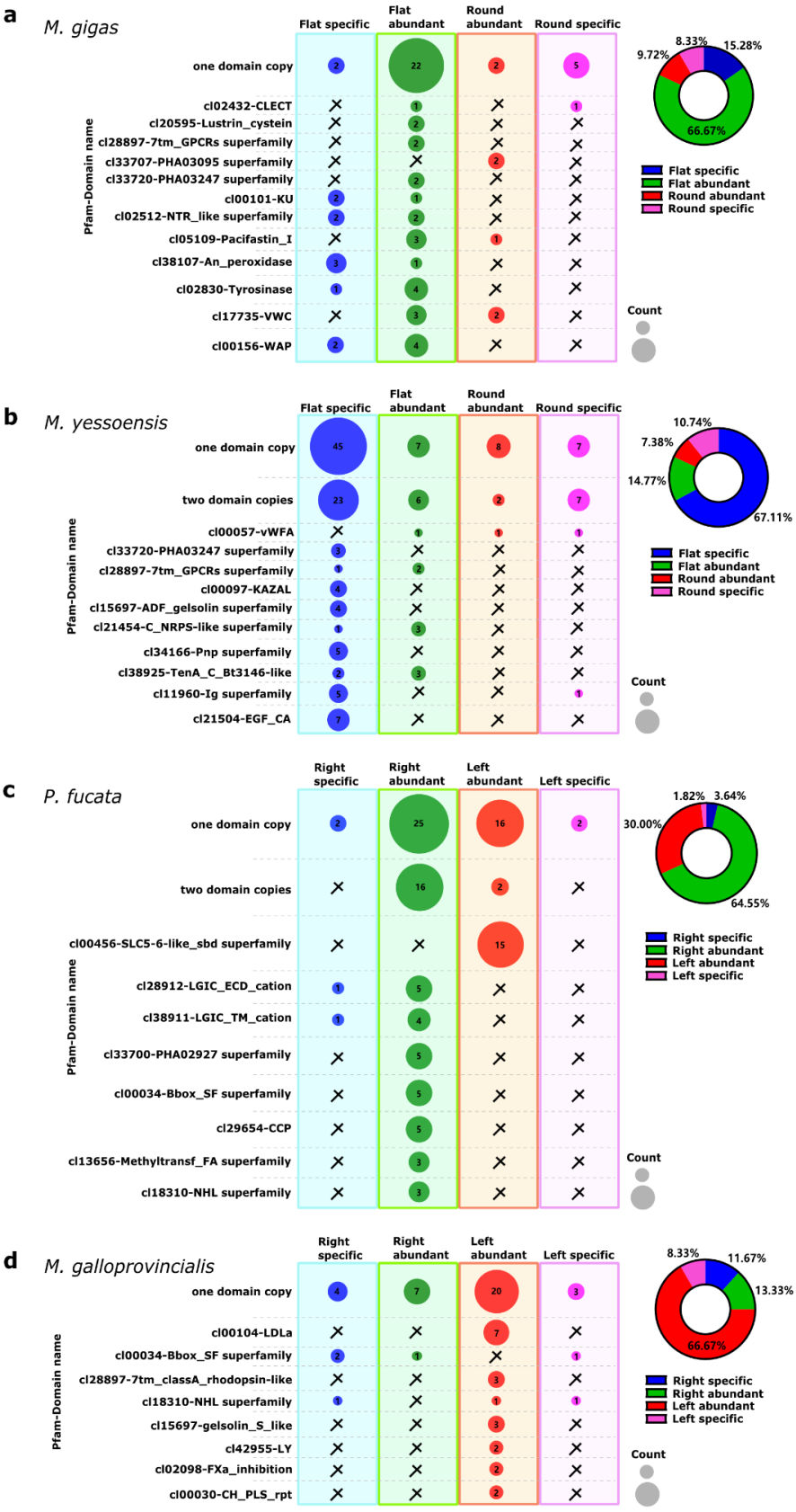

Supplementary Figure 2.6 Domain characterization of DE protein

coding genes. (a-d) Analysis of *M. gigas*, *M. yessoensis*, *P. fucata* and *M. galloprovincialis* mantle transcriptomes. Domain characterization of DEc genes was based on Pfam identification (see Supplementary Table 2.10). The protein domains found, and their IDs are provided, and their relative abundance (domain counts) is indicated by the bubble plots. Domains that scored once were grouped in the "one domain" category. For *M. yessoensis* due to the large number of domains found, domains that scored twice in the mantle were also grouped into a specific category, "two domains". The crosses represent domain absence, and the bubble size is proportional to the number of domains found and the numbers inside the bubbles indicate the domain count. Different colours represent the expression specificity and abundance of DEc genes in the flat and round mantle transcriptomes and the overall percentage of DE domains identified is indicated in the pie chart on the right.

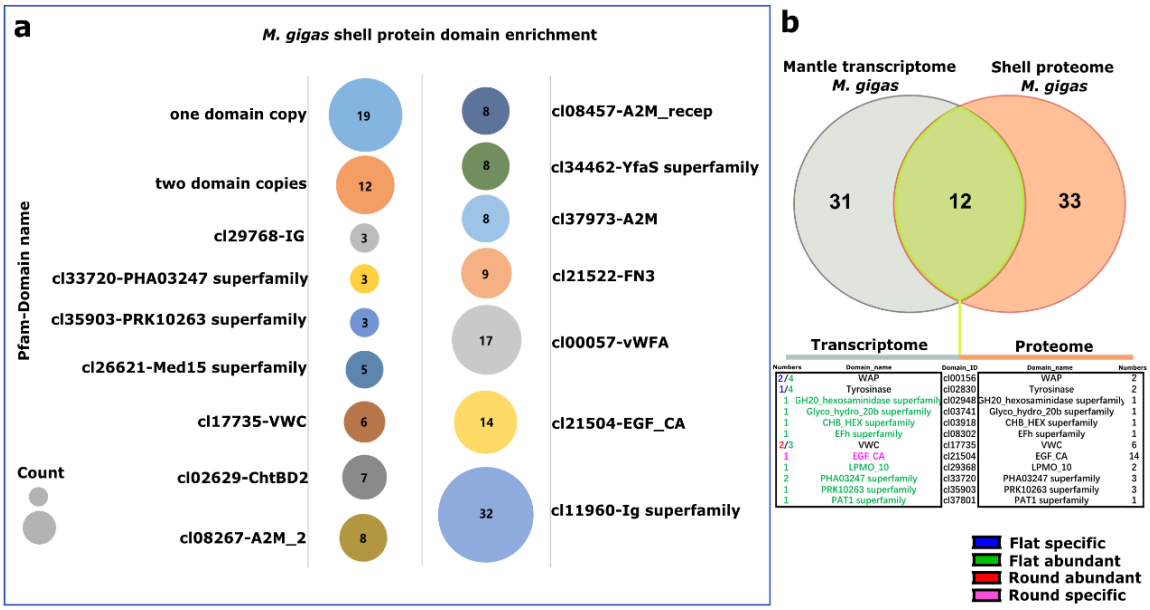

Supplementary Figure 2.7 Shell Matrix Protein (SMP) domains in DE protein coding genes in *M. gigas*. (a) Bubble plots representing the protein domains identified in the *M. gigas* shell proteome (data obtained from Arivalagan et al. 2017) (see Supplementary Table 2.11). Domains that scored once were grouped into the "one domain" category and domains that scored twice were grouped into the, "two domains" category. The bubble size is proportional to the number of domains found, and the count number is indicated. (b) A Venn diagram showing the specific and shared domains in DEc genes of the mantle transcriptome and the shell proteome (see Supplementary Table 2.12). The table presents 12-shared protein domains and their ID codes and the number of domain counts present in the DEc genes in the *M. gigas* mantle transcriptome and proteome. The colour code represents their expression and abundance in the mantle of the flat and the round valves.

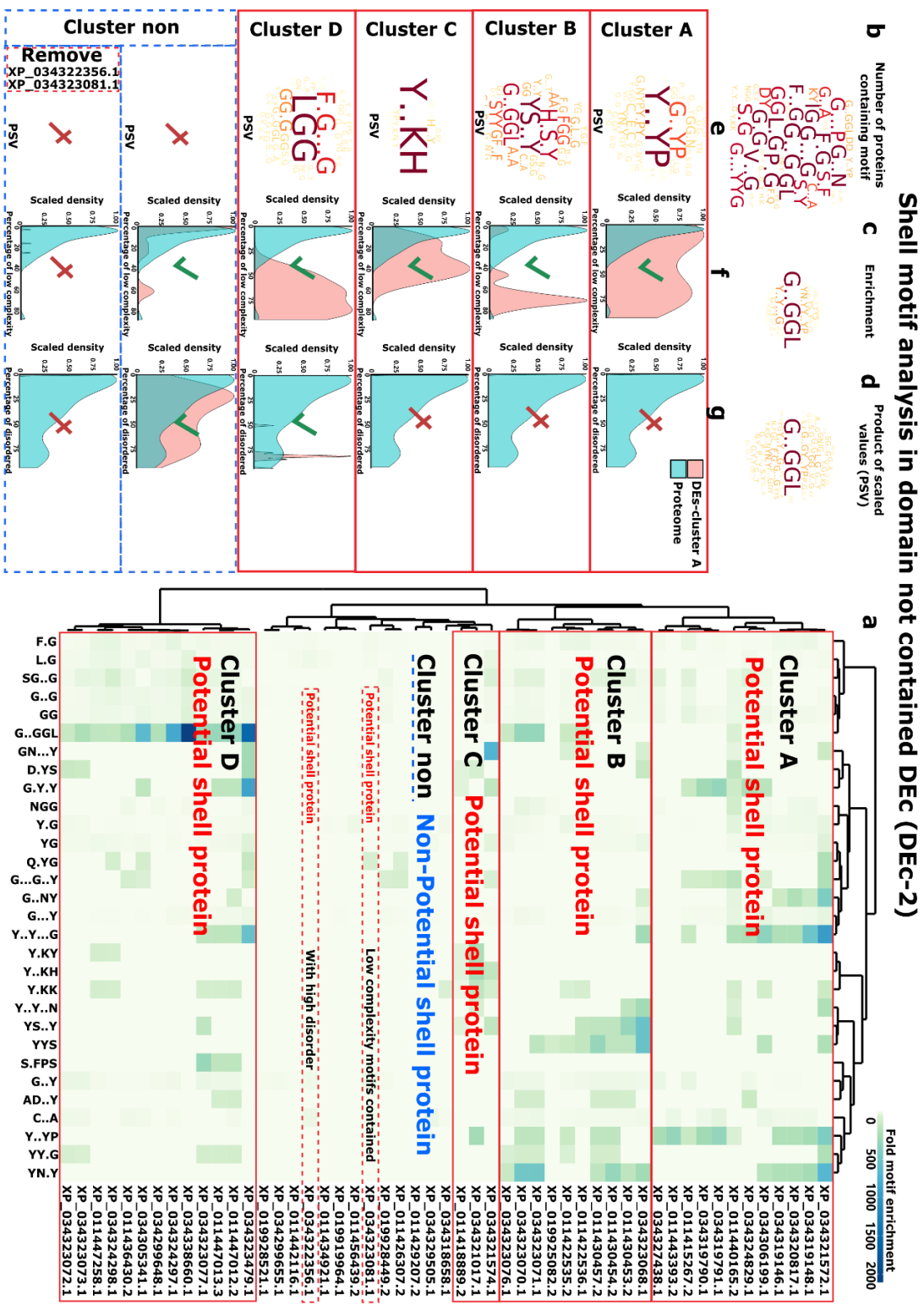

Supplementary Figure 2.8 Identification of putative SMP-motifs in non-annotated DE protein coding genes in the mantle transcriptome using ProminTools. (a) A heatmap showing the clustering of the predicted proteins (DE protein coding genes) based on motif enrichment analysis. Protein clustering was restricted to the 30 motifs with the greatest overall enrichment and according to the foreground knowledge proteins were

classified within clusters A to D, and proteins that were not enriched where classified as non-SMP. Proteins lacking enriched motifs were found but are not displayed in the figure. (b) predicted motifs and (c, d) enriched motifs present in at least 5% of all the predicted DEc genes in the mantle relative to the background established using the *M. gigas* shell proteome (Arivalagan et al. 2017). Font size in the word cloud is proportional to the overall motif abundance. Analysis of the deduced individual protein clusters according to enriched protein motifs in each protein cluster, (f) percentage of low complexity sequences (i.e, single amino acids repeats or short amino acid motifs) and (g) percentage of disordered sequence structure. The area below the curves corresponds to the distribution of the low complexity sequences in the proteins common to the foreground and background sequences. DE genes are in pink, and the shell proteome is in blue. Putative SMPs (see Supplementary Table 2.12) were designated when they met two of the criteria listed in e - g and are identified with √.

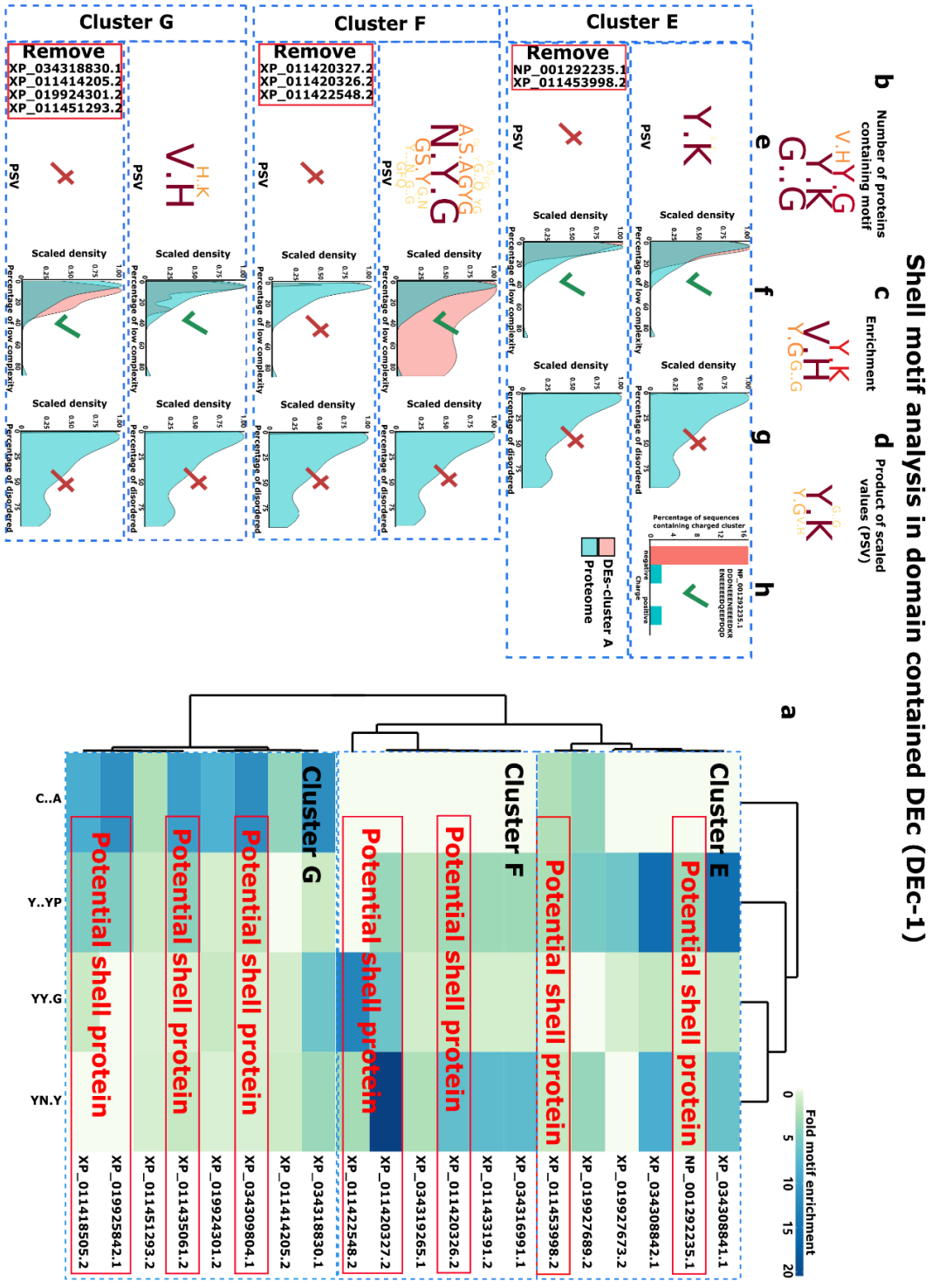

Supplementary Figure 2.9 Identification of SMP-motifs in annotated DE protein coding genes in the mantle using the ProminTools. (a) A heatmap showing the clustering of the predicted proteins based on motif enrichment analysis. Protein clustering was restricted to the 30 motifs with the greatest overall enrichment and based on comparisons with the foreground proteins (from proteomics) and were separated between clusters E to G. (b) predicted motifs and (c, d) enriched motifs present in

at least 5% of all the predicted proteins of the DEc genes in the mantle relative to the background established using the *M. gigas* shell proteome (Arivalagan et al. 2017). Font size in the word cloud is proportional to the motif abundance. Analysis of the individual protein clusters was based on (e) the enriched protein motifs in each protein cluster, (f) the percentage of low complexity sequences (i.e, single amino acid repeats or short amino acid motifs) (g) the percentage of disordered sequence structure and (h) the percentage of sequences containing charged clusters. The area below the curves corresponds to the distribution of the low complexity sequences in the proteins common to the foreground and background sequences. Deduced DE protein coding genes are in pink, and proteins of the SMP are in blue. DEc genes were designated as a putative SMPs (see Supplementary Table 2.12) when they met two of the criteria listed in e - h and are identified with √.

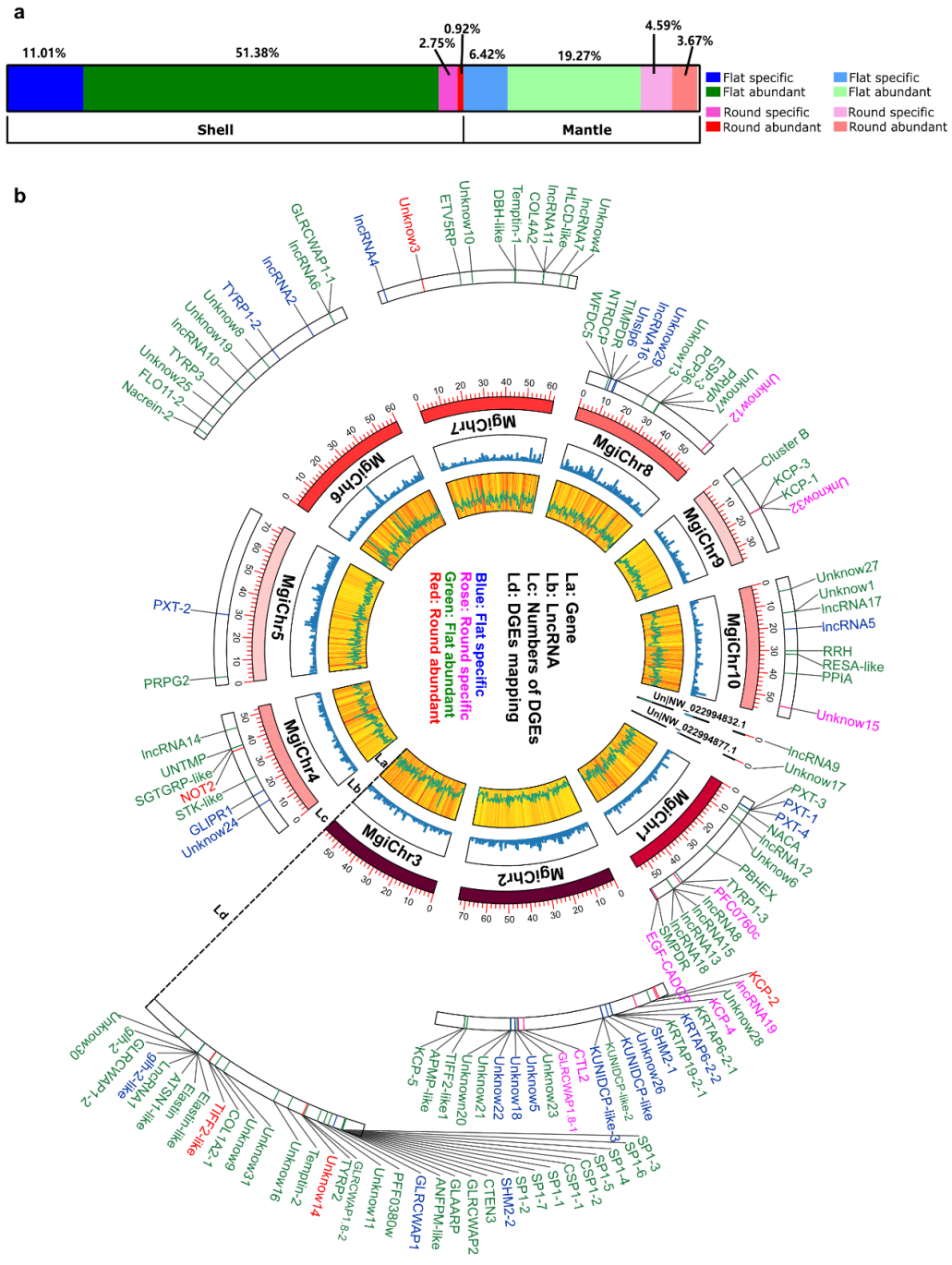

Supplementary Figure 2.10 The relative abundance of DEc genes between the mantle of the flat and round valve and their position in the genome. (a) Overall description and relative abundance of the DEc genes in the *M. gigas* mantle. The percentage of transcripts and their relative abundance were grouped into putative SMPs or other non-SMP proteins of the mantle. Most DEc genes are related to SMPs and abundant or specific to the *M. gigas* flat valve mantle. (b) Genome mapping of the DE transcripts (protein coding and lncRNAs) identified between the mantle of the flat and round valves in *M. gigas*. The interior circle (La) represents the mapping of all genes, the outer circle (Lb) the mapping of

the long non-coding (lncRNA) genes and the red bars (Lc) above the chromosomes represent the mapping of the mantle DEGs with the colour intensity indicating their relative abundance. A large percentage of the mantle DEGs mapped to *M. gigas* chromosome 2 and 3 (dark red). The relative position (Ld) of all the DEGs from the mantle transcriptome comparison within each chromosome is presented and gene names are coloured according to their specificity and abundance in the mantle of the flat and round valves.

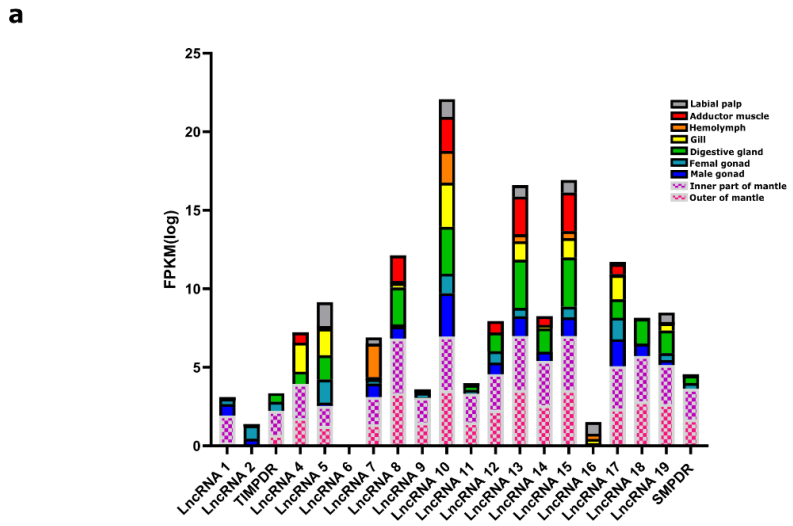

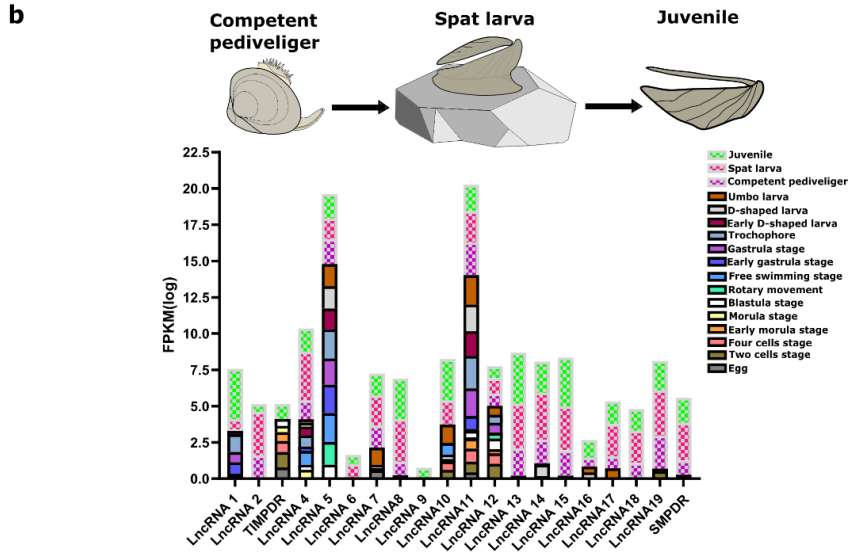

Stage of larva	LncRNA 1	LncRNA 2	TIMPDR	LncRNA 4	LncRNA 5	LncRNA 6	LncRNA 7	lncRNA 8	LncRNA 9	lncRNA 10	lncRNA 11	LncRNA 12	LncRNA 13	LncRNA 14	LncRNA 15	lncRNA 16	lncRNA 17	lncRNA 18	lncRNA 19	SMPDR
Egg	0.00	0.00	0.77	0.00	0.00	0.00	0.59	0.00	0.00	0.00	0.44	0.00	0.00	0.00	0.00	0.00	0.00	0.00	0.00	0.00
Two cells stage	0.28	0.00	0.59	0.00	0.00	0.00	0.00	0.00	0.00	0.60	0.73	1.03	0.00	0.00	0.00	0.00	0.00	0.00	0.53	0.00
Four cells stage	0.00	0.00	0.76	0.00	0.00	0.00	0.00	0.00	0.00	0.59	0.90	0.72	0.00	0.00	0.00	0.00	0.00	0.00	0.00	0.00
Early morula stage	0.00	0.00	0.62	0.00	0.00	0.00	0.15	0.00	0.00	0.16	0.69	0.28	0.00	0.00	0.00	0.00	0.00	0.00	0.00	0.00
Morula stage	0.00	0.00	0.43	0.61	0.00	0.00	0.00	0.00	0.00	0.00	0.10	0.00	0.00	0.01	0.00	0.00	0.00	0.00	0.00	0.00
Blastula stage	0.00	0.00	0.47	0.35	0.97	0.00	0.00	0.00	0.00	0.31	0.44	0.73	0.00	0.00	0.00	0.00	0.00	0.00	0.00	0.00
Rotary movement	0.06	0.00	0.00	0.00	1.56	0.00	0.00	0.00	0.00	0.00	0.00	0.39	0.00	0.00	0.00	0.00	0.00	0.00	0.00	0.00
Free swimming stage	0.00	0.00	0.00	0.95	1.99	0.00	0.00	0.00	0.00	0.78	0.14	0.00	0.00	0.00	0.00	0.00	0.00	0.00	0.00	0.00
Early gastrula stage	0.78	0.00	0.00	0.31	1.95	0.00	0.00	0.00	0.00	0.00	0.87	0.00	0.00	0.00	0.00	0.00	0.00	0.00	0.00	0.00
Gastrula stage	0.72	0.00	0.00	0.00	1.82	0.00	0.00	0.00	0.00	0.00	1.92	0.69	0.00	0.00	0.00	0.00	0.00	0.00	0.00	0.00
Trochophore	1.22	0.00	0.00	0.78	2.01	0.00	0.00	0.00	0.00	0.00	2.24	0.56	0.00	0.16	0.00	0.00	0.00	0.00	0.00	0.00
Early D-shaped larva	0.22	0.00	0.00	0.59	1.43	0.00	0.00	0.00	0.00	0.00	1.70	0.00	0.00	0.00	0.00	0.00	0.00	0.00	0.00	0.00
D-shaped larva	0.00	0.00	0.00	0.27	1.53	0.00	0.22	0.00	0.00	0.00	1.84	0.00	0.00	0.79	0.00	0.44	0.00	0.00	0.16	0.00
Umbo larva	0.00	0.00	0.00	0.23	1.52	0.00	1.18	0.24	0.00	1.27	2.02	0.62	0.21	0.09	0.21	0.40	0.72	0.00	0.00	0.27
Competent pediveliger	0.09	1.60	0.00	1.31	1.72	0.00	1.52	0.94	0.00	0.00	2.28	0.85	1.87	1.65	1.74	0.63	0.82	1.08	2.28	0.98
Spat larva	0.73	3.00	0.00	3.37	1.44	1.00	2.08	2.92	0.00	1.68	2.13	1.06	3.09	3.23	3.03	0.00	2.22	2.24	3.13	2.59
Jubenile	3.45	0.54	1.03	1.58	1.68	0.64	1.50	2.80	0.75	2.84	1.83	0.82	3.51	2.14	3.35	1.21	1.55	1.48	2.02	1.73

Supplementary Figure 2.11 Expression and distribution profile of the selected DE lncRNAs (lncRNAs 1 to 20) in the *M. gigas* mantle of the flat and round valve. Transcriptome data was obtained from public databases and the SRA accession numbers are provided in Supplementary Table 2.1 and transcript expression is given in logFPKMs. (a) The expression and abundance in adult *M. gigas* tissues. The colours represent the different tissues analysed. (b) Expression and abundance in different stages of developing *M. gigas* larvae. The coloured bars represent different larval stages. Transcripts with a significantly modified

expression in larval stages associated with the establishment of the shell and its shape (competent pediveliger, spat larva and juvenile) compared to other stages were considered as candidates for further studies. The heatmap represents relative transcript abundance in different developmental stages and the candidate transcripts selected are boxed in green.

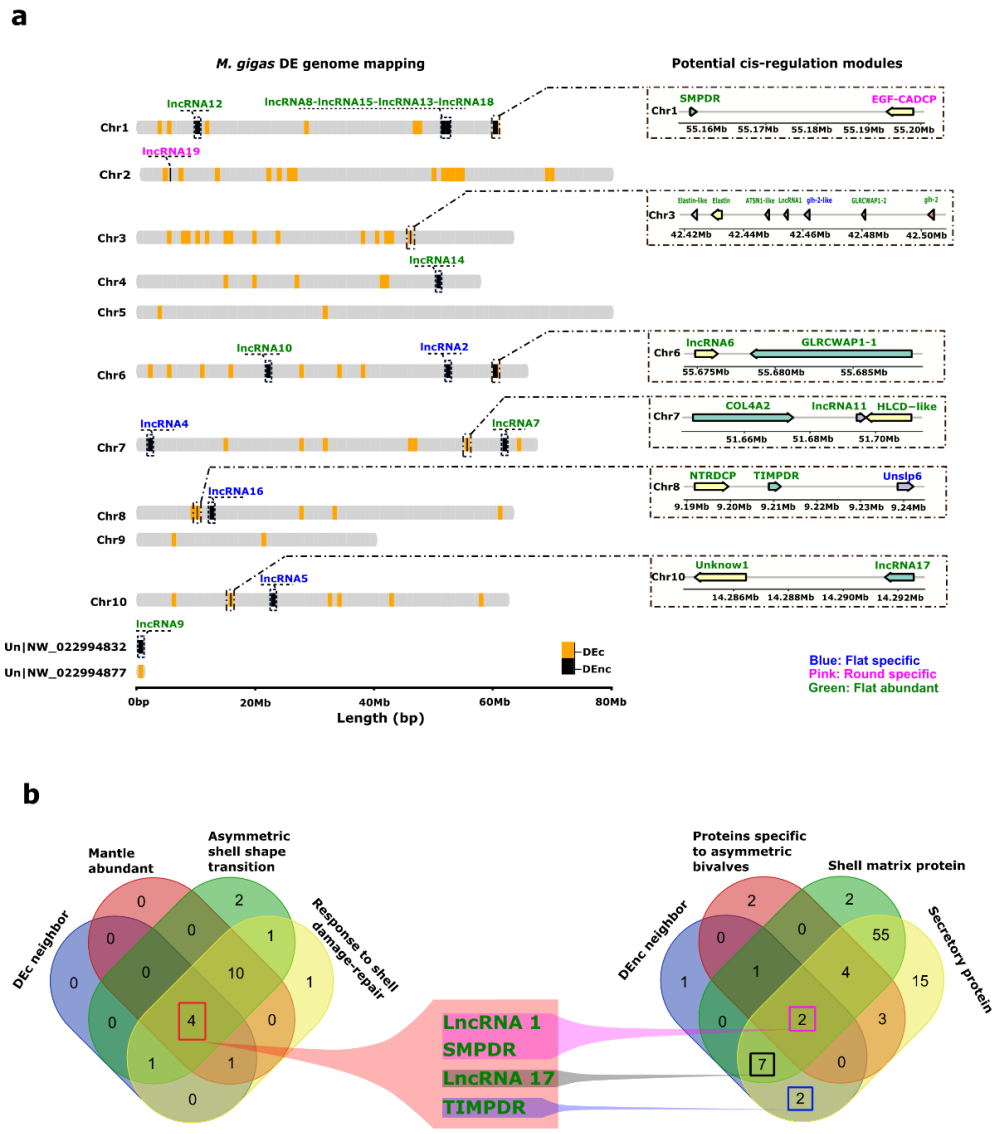

Supplementary Figure 2.12 Mantle lncRNAs and candidate cis-regulatory modules in *M. gigas*. (a) Mapping of DEGs in the *M. gigas* genome and identification of potential cis-regulation modules were based on the distance (kb) between protein-coding and lncRNA genes in the genome (located < 100 kb distant). DEc genes are represented by yellow bars and lncRNA genes by back bars. Six DEG candidates with transcriptional regulatory activity (cis-regulatory modules) were identified. Arrows indicate gene orientation and gene position is provided (Megabases, Mb). Protein coding gene symbols and lncRNAs are indicated and are coloured according to distribution and abundance in the *M. gigas* mantle. (b) The criteria for the identification of candidate lncRNAs putatively assigned as cis-regulatory factors was based on their expression profile and position in the genome. The Venn diagram shows the number and grouping of lncRNAs by 1) regulated response to shell damage-repair (yellow), 2) regulation in larval stages associated with shell shape transition (green), 3) expression abundance in the mantle (red)

and 4) proximity with a DEc gene (< 100 kb distance) (blue). LncRNA1, lncRNA17, *TIMPDR* (TIMP Domain Regulator) and *SMPDR* (Shell Matrix Protein-Domain Regulator) were identified across the 4 analysed conditions and were abundant in the mantle of the *M. gigas* flat valve (green). Characterisation of DEc genes potentially regulated by the candidate lncRNAs. The Venn diagram shows the number and overlap of the DEc genes according to the criteria previously used: 1) secretory protein (yellow), 2) putative SMP (green), 3) proteins with domains specific to the asymmetric bivalve mantle (red) and 4) localized in the neighbourhood (< 100 kb distance) of a DE lncRNA (blue). *EGF-CADCP* (EGF-CA domain containing protein) (under potential regulation of *SMPDR*) is specific to the mantle of the round valve and ATSN1-like (under potential regulation of lncRNA1) is abundant in the mantle of the flat valve and both are likely to be secretory SMPs, and common in the mantle of bivalves with an asymmetric shell. The *NTRDCP* gene is abundant in the mantle of the flat valve and *Unslp6* gene is a mantle specific gene associated with the flat shell, and both are potentially under the regulation of *TIMPDR* and are likely to encode putative secretory proteins.

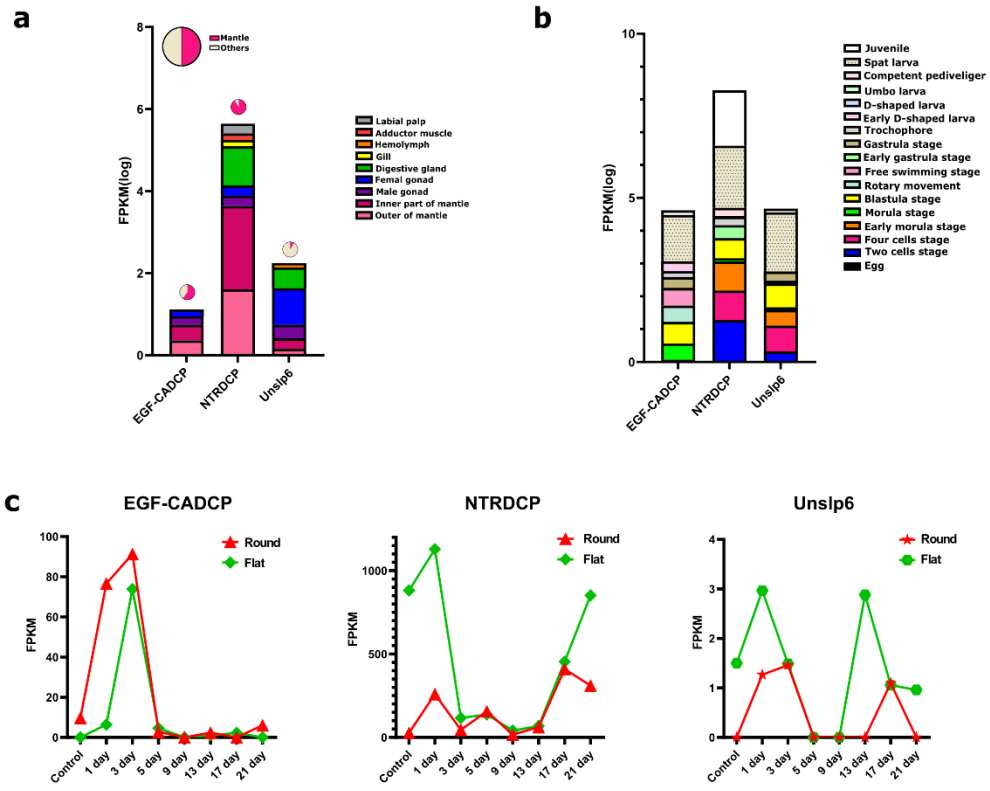

Supplementary Figure 2.13 Expression and profile of the tissue distribution of the candidate protein coding genes regulated by lncRNA. The candidate protein coding genes are *EGF-CADCP*, *NTRDCP* and *Unslp6*. Transcriptome data of the mantle from the flat and round valves was obtained from publicly available data and their SRA accession numbers are available in Supplementary Table 2.1. Transcript expression is given as logFPKM (a) Transcript expression and abundance in adult *M. gigas* tissues. The colours represent the different tissues and the pie chart at the top of each bar represents the relative representation of transcripts in the mantle compared to other tissues. (b) Transcript expression and abundance in different *M. gigas* developmental stages. The coloured bars represent different larval stages. (c) Transcript expression during shell damage-repair (after 21 days recovery) in adult *M. gigas*. Transcripts in the mantle from the flat or round valve are represented by green and red lines, respectively.

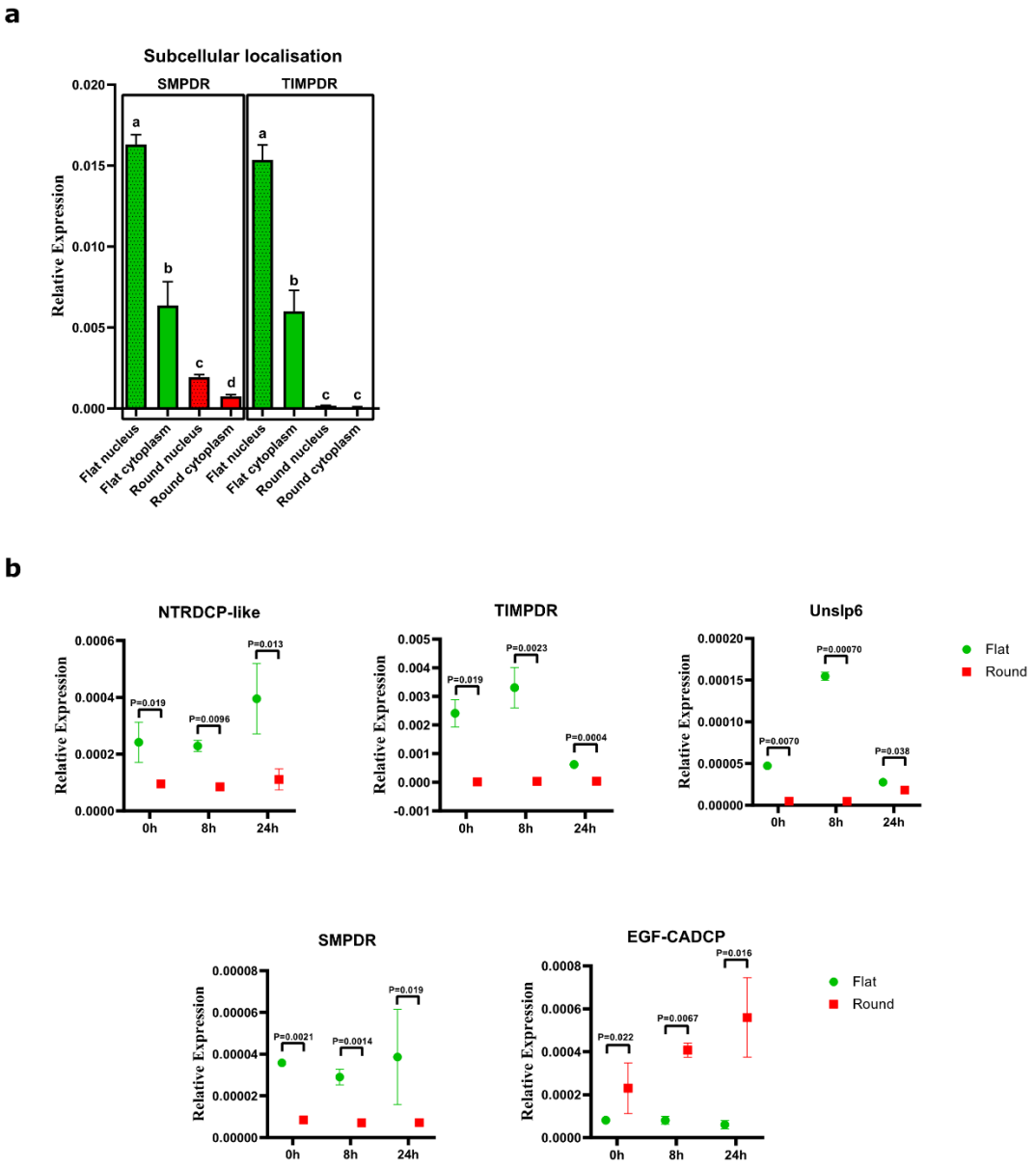

Supplementary Figure 2.14 Expression of lncRNA and protein coding candidate genes in the *M. gigas* mantle. (a) Subcellular localization (nucleus, N or cytoplasm, C) of the target lncRNA transcripts (*TIMPDR* and *SMPDR*) in *M. gigas* mantle from the flat or round valve. The mantle from the flat (green) and round (red) valve were collected from adult *M. gigas* and both lncRNA transcripts were more abundant in the flat mantle and predominantly found inside the nucleus. The relative gene expression level was determined by qRT-PCR and calculated as the fold change after normalization by the average expression of the reference genes (EF1α and RL7). Data represents the mean of n = 3 biological replicates (each biological replicate represents a pool of 3 individuals) and is shown as the mean ± SEM. One-way ANOVA was performed to detect significant differences between samples and different letters indicate significant differences ($p < 0.05$). (b) Expression of lncRNA transcripts in the mantle of the flat (green) and round (red) valves of juvenile *M. gigas*. Mantle tissue fragments were collected from an *ex-vivo* tissue culture at different

time points (0, 8 and 24h). Gene expression was determined by qRT-PCR and calculated as the fold change after normalization by the averaged expression of the reference genes (*EF1α* and *RL7*). Data is the mean ± SEM of 3 biological replicates (each biological replicate represents a mixture of ± 20 mantle fragments from 6 individuals) and One-way ANOVA was performed to identify significant differences between samples. The p value is shown, and significance was considered at $p < 0.05$. No differences in the abundance of gene transcripts existed between the samples at 8 hours compared to 0h in the control.

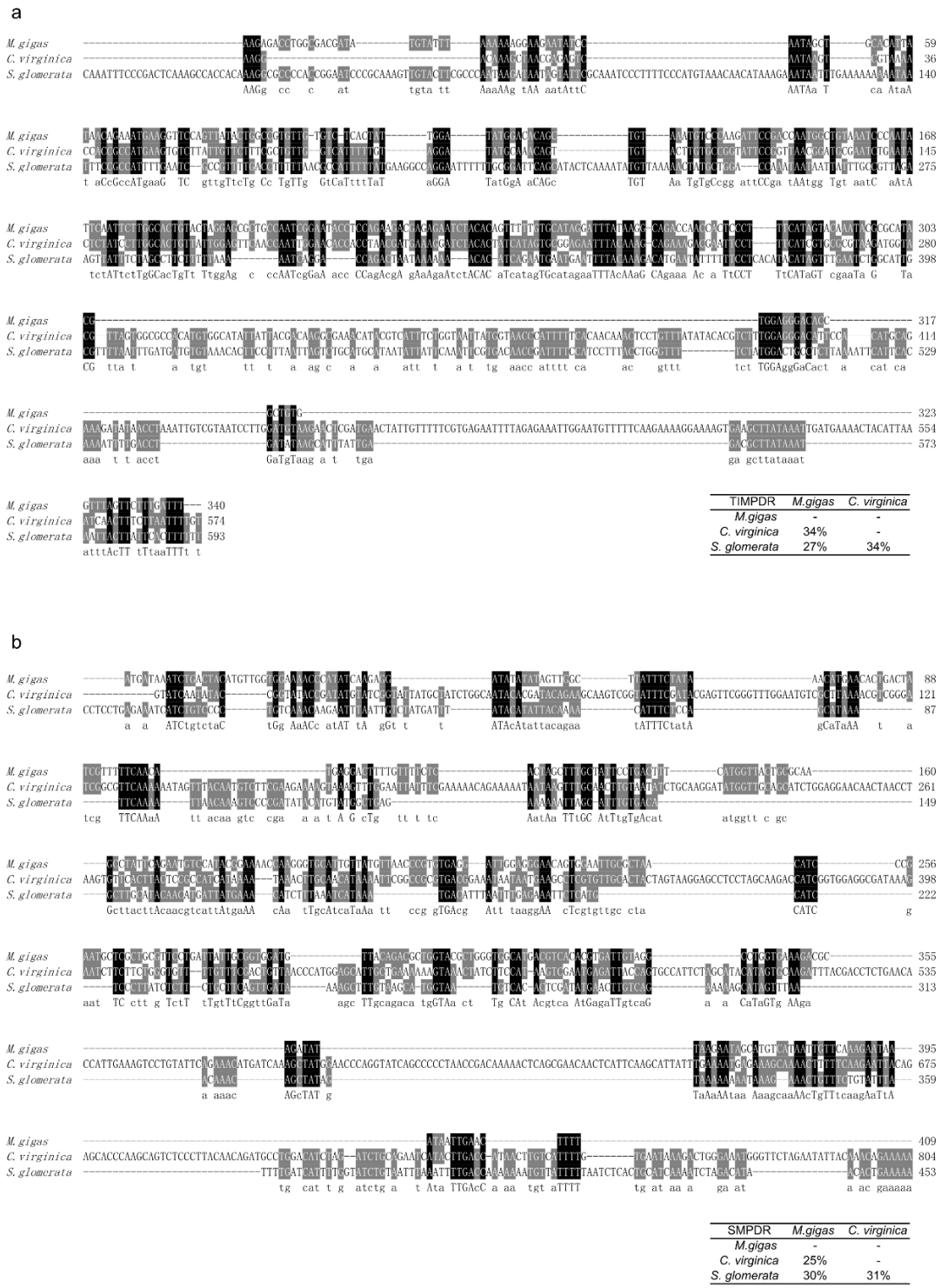

Supplementary Figure 2.15 Multiple sequence alignment of the *M. gigas TIMPDR* and *SMPDR* and homologues in *C. virginica* and *S. glomerata*. Multiple sequence alignments of the nucleotide sequence of (a) *TIMPDR* and (b) *SMPDR* from *M. gigas* and the homologues in *C. virginica* and *S. glomerata*. The *C. virginica* sequences were obtained from the annotation of the genome with predicted gene transcripts (GCA_002022765.4) and from the *S. glomerata* by searching against the SRA data. The sequences retrieved were predicted to be lncRNAs

Supplementary Table 2.13. Sequence alignments were performed in Aliview with MUSCLE and the aligned sequences were edited and the percentage of sequence identity calculated in GeneDoc.

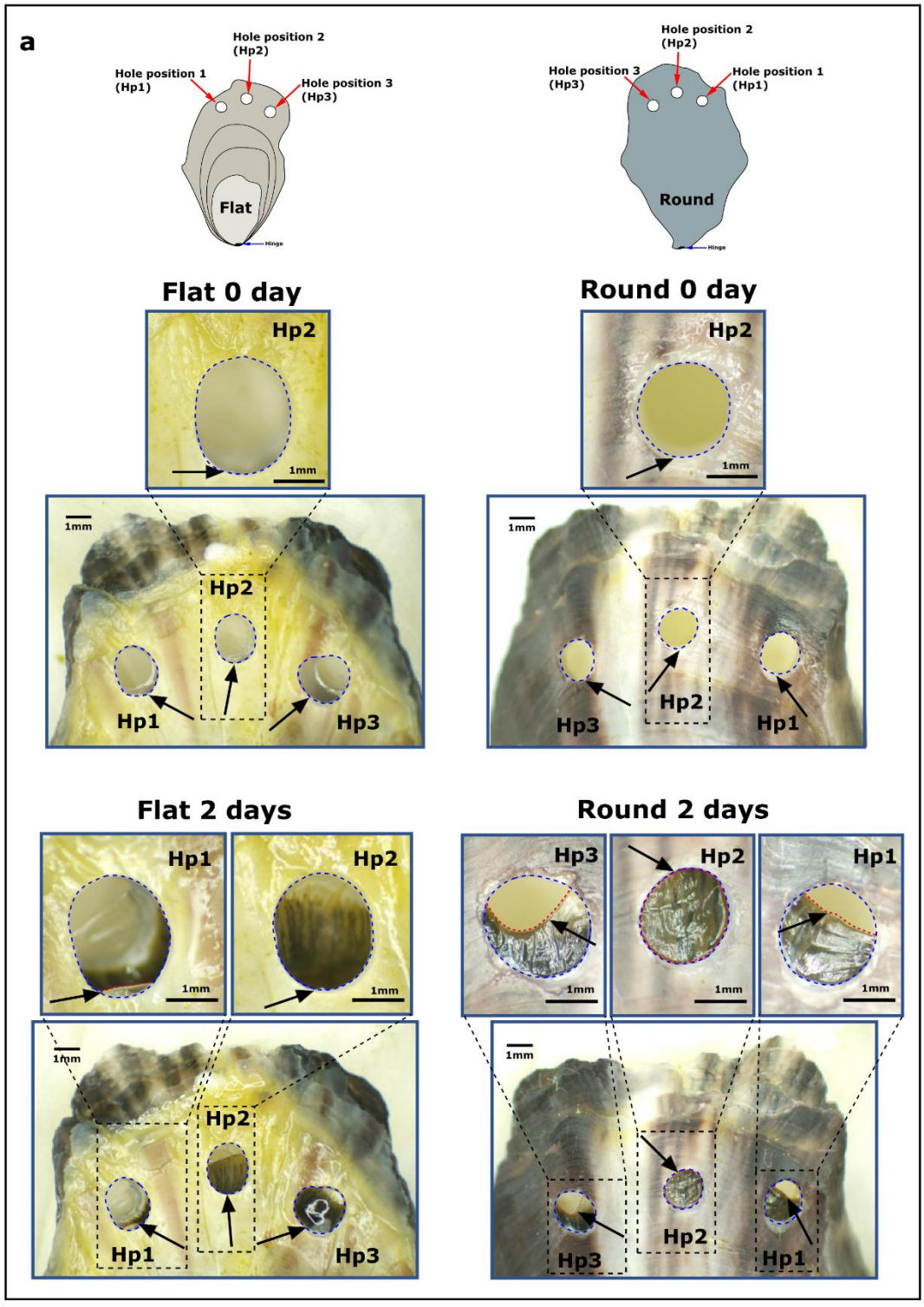

b

Shell repair ratio (2 days) %

Study or Subgroup	Round Mean%	Round SD	Round Total	Flat Mean%	Flat SD	Flat Total	Weight	Mean Difference IV, Fixed, 95% CI
Hole position 1	75.08	20.58	13	12.79	16.23	13	40.4%	62.29 [48.04, 76.53]
Hole position 2	78.83	23.62	13	13.28	21.47	13	27.2%	65.55 [48.20, 82.90]
Hole position 3	86.24	18.26	13	12.47	22.86	13	32.4%	73.78 [57.87, 89.68]
Total (95% CI)			39			39	100.0%	66.90 [57.85, 75.95]

Heterogeneity: Chi² = 1.14, df = 2 (P = 0.56); I² = 0%
Test for overall effect: Z = 14.48 (P < 0.00001)

Supplementary Figure 2.16 Shell damage-repair assays in juvenile *M. gigas*. (a) A schematic representation of the shell damage drilling experiment. Three holes (Hp1, Hp2 and Hp3) were drilled at the edge of the shell of each animal using a handheld electric drill (DIATOOLS, China) with a 2 mm metal drill head. The shell was pierced through, and three identical holes were introduced in approximately the same position (Hp) in the flat and round shell of each individual in the experiment. Care was taken to avoid damaging the mantle during drilling. Bright field digital photographs were taken of the holes in the flat and round shells of *M. gigas* at day 0 and day 2 during recovery. Images were taken using a stereoscope (Motic, SMZ-171, China) equipped with a digital camera (Visicam 6 Plus, VWR, Portugal). The arrows in the images indicate the side of the hole that is closer to the shell hinge. For day 0 a magnified image of a typical hole is provided using a selected image of Hp2 in the flat and round side of the shell. For day 2 detailed images of Hp1 and Hp2 are shown for the flat valve and for the round valve Hp1, Hp2 and Hp3 are shown. The red-dashed lines delimit the newly growth shell in each hole. (b) The shell damage-repair ratio of the holes punctured in the flat and round valves. Analysis was performed after 2 days shell regrowth and the area of the newly grown shell (repaired shell) in relation to the total hole area n = 13 individuals/3 holes/valve was calculated using ImageJ ver 1.52a software. The mean and standard deviation of the percentage of repair for each hole (Hp1, Hp2 and Hp3) in the flat and round valves are presented in the table. The mean difference in repair for the three holes made in each of the valves was used to draw a forest plot (RevMan 5.0 software). In the forest plot the x-axis represents the shell valves and the different hole position in the shell is plotted as a green box and the line indicates the 95% confidence interval. The diamond at the bottom shows the averaged combined data from all the individuals. Heterogeneity and overall effects are highlighted by the underlined red line. The scale bar in the photographic images represents 1mm. The statistical analyses presented in the figure were obtained from the software output (RevMan 5.0).

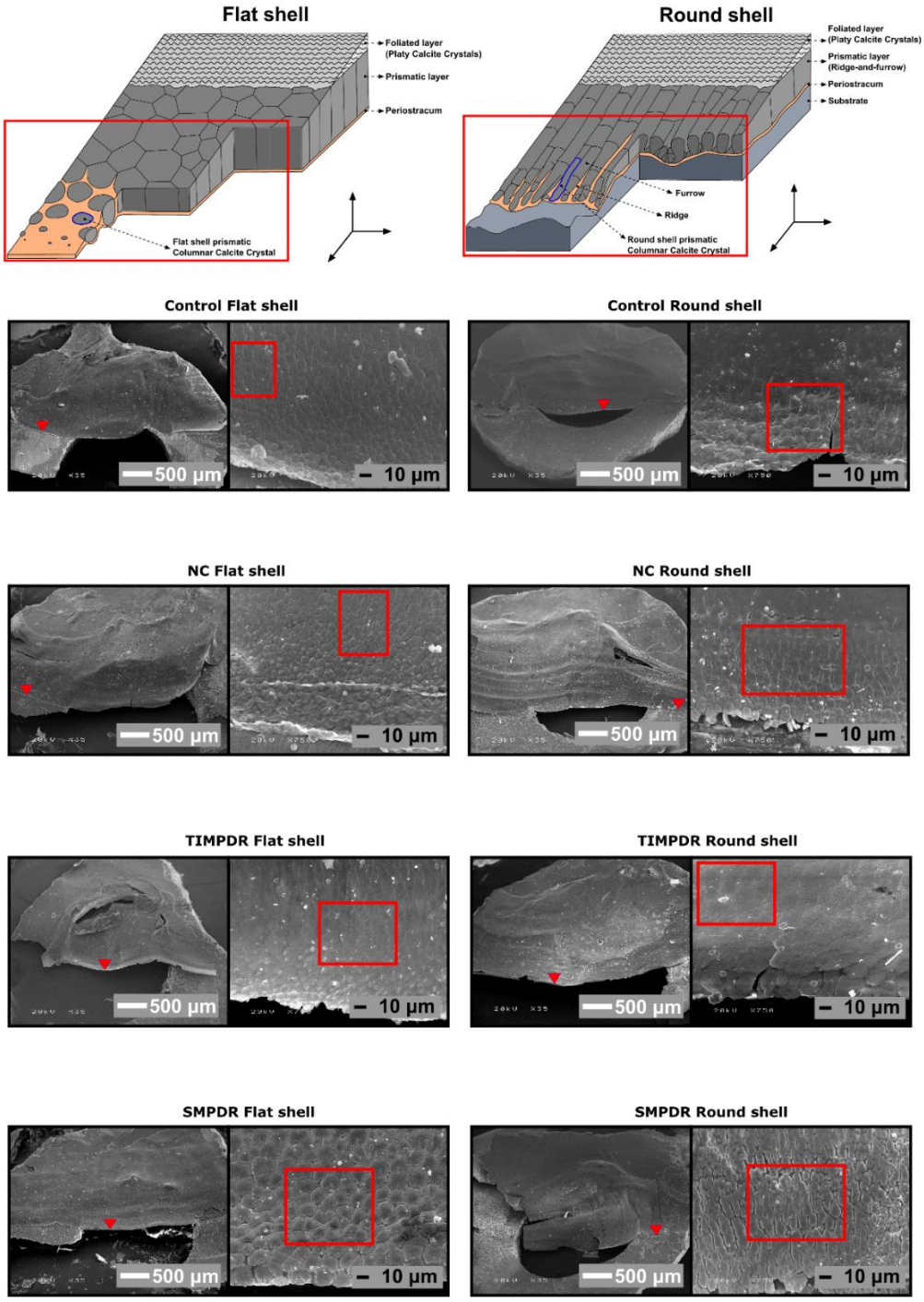

Supplementary Figure 2.17 Scanning electron microscopy (SEM) images of the prismatic layer of the recovered shell of the flat and round valves after drilling. The 3D models at the top of the figure represent the micro structure of the normal flat and round valve near to the edge (modified scheme from (Yamaguchi, 1994)). The 3D models were designed using Inkscape ver1.1.2 (The Inkscape Team). Photos (×35) represent a panorama captured for each sample, with red triangles identify the position boxed in red in the higher magnification image of the captured area. The red rectangles identify the regions that are also shown in Figure 2.4d of the main article.

Supplementary Figure 2.18 Multiple sequence alignment of the *TIMPDR* candidate regulatory proteins and homologue genes containing TIMP domains in the genome of *M. gigas*. *TIMPDR* candidate regulatory NTRDCP and Unslp6 proteins, both contained one TIMP domain. Three copies of the *NTRDCP* gene occur in the genome, and two are expressed

in the mantle, but only one copy of *Unslp6* gene was identified (see Supplementary Table 2.11). In addition, 43 genes in the genome encoded proteins that contain only one TIMP domain, 30 of which are expressed in the mantle (see Supplementary Table 2.11). (a) a schematic representation of thea multiple sequence alignment of the deduced full-length proteins of genes containing a TIMP domain that are expressed in the mantle. Using the TIMP domain length recorded in Pfam as the alignment standard, 12 TIMP domains of differing lengths were identified. NTRDCP, NTRDCP-like2, Unslp6 and 12 proteins with different TIMP domain lengths were used for the multiple sequence alignment. *TIMPDR* candidate regulatory proteins are boxed within red dashes, and deduced proteins containing the full-length TIMP domain are boxed within blue dashes. (b) Multiple sequence alignment of the TIMP domain. Sequence alignments of the retrieved data was performed in Aliview with MUSCLE and the aligned sequences were edited and the consensus sequence obtained in Jalview v2.11.2.3. The identity threshold display of amino acid letters is 30, and the background colour is adopted from ClustalX. *TIMPDR* candidate regulatory proteins are marked within red dashed boxes, the protein containing a full-length TIMP domain is marked with a blue dashed box. The TIMP domain in the *Unslp6* gene is unique. Although the TIMP domain in the *NTRDCP* gene has only limited specificity, its gene expression level in the mantle is higher than that of *NTRDCP-like1* and *NTRDCP-like2*.

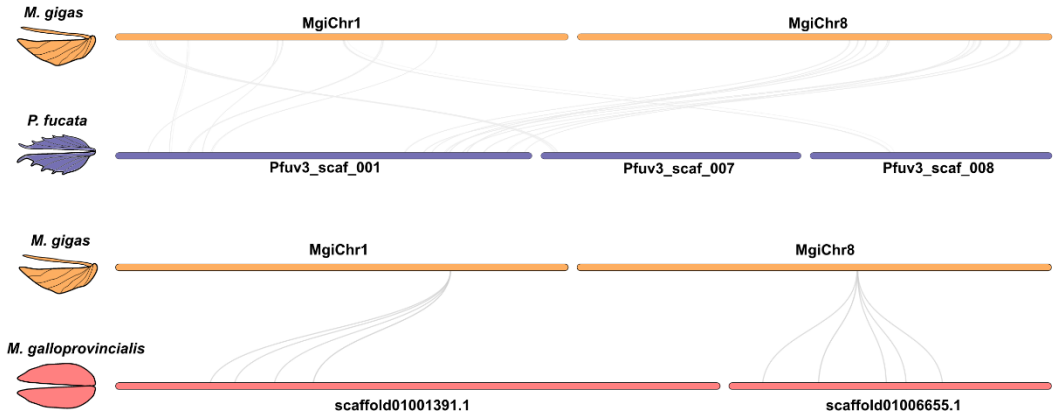

Supplementary Figure 2.19 Collinearity analysis of chromosomes that contain the target coding genes retrieved from *M. gigas*, *P. fucata* and *M. galloprovincialis*. Grey lines interconnecting chromosomes represent gene blocks with a minimum of five orthologue genes. No homologue regions containing the target coding genes were found in the genomes of *P. fucata* and *M. galloprovincialis* (slightly asymmetrical and a symmetrical bivalve, respectively).

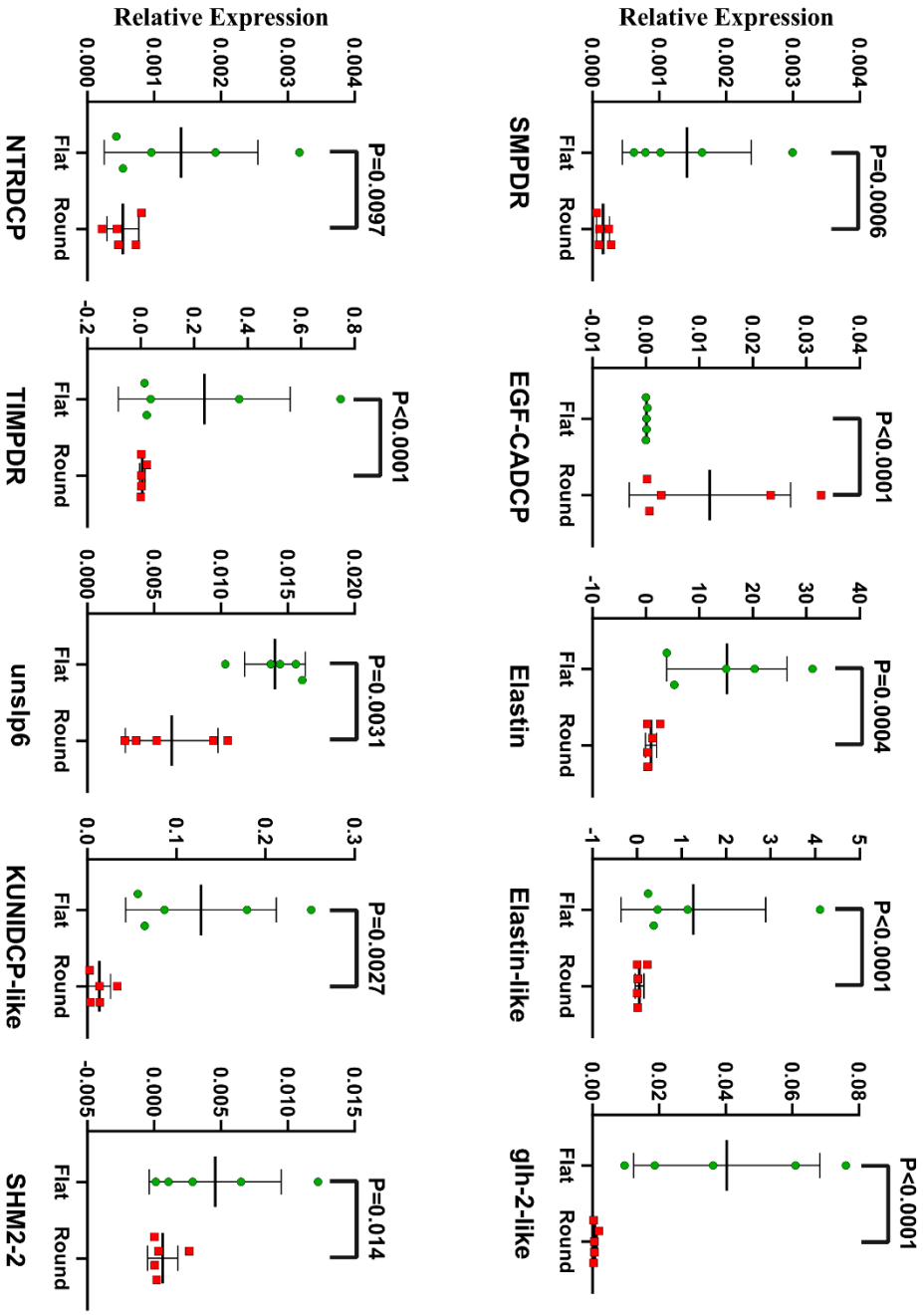

Supplementary Figure 2.20 Corroboration between differentially expressed candidate genes in the mantle transcriptomes and their analysis by qRT-PCR. Expression of the ten candidate genes selected (including the candidate non-coding and protein coding transcripts) in the mantle from the flat (green) and round (red) valves by qRT-PCR in the. Each graph represents the expression profile of each gene in the mantle of the two shell sides. Relative gene expression was calculated as fold change after normalization with the average expression of the reference genes (EF1α and RL7), that were not significantly different across the samples. Statistical analysis was performed using a student t-test and the presented data corresponds to the mean ± SEM of n = 5 biological replicate.

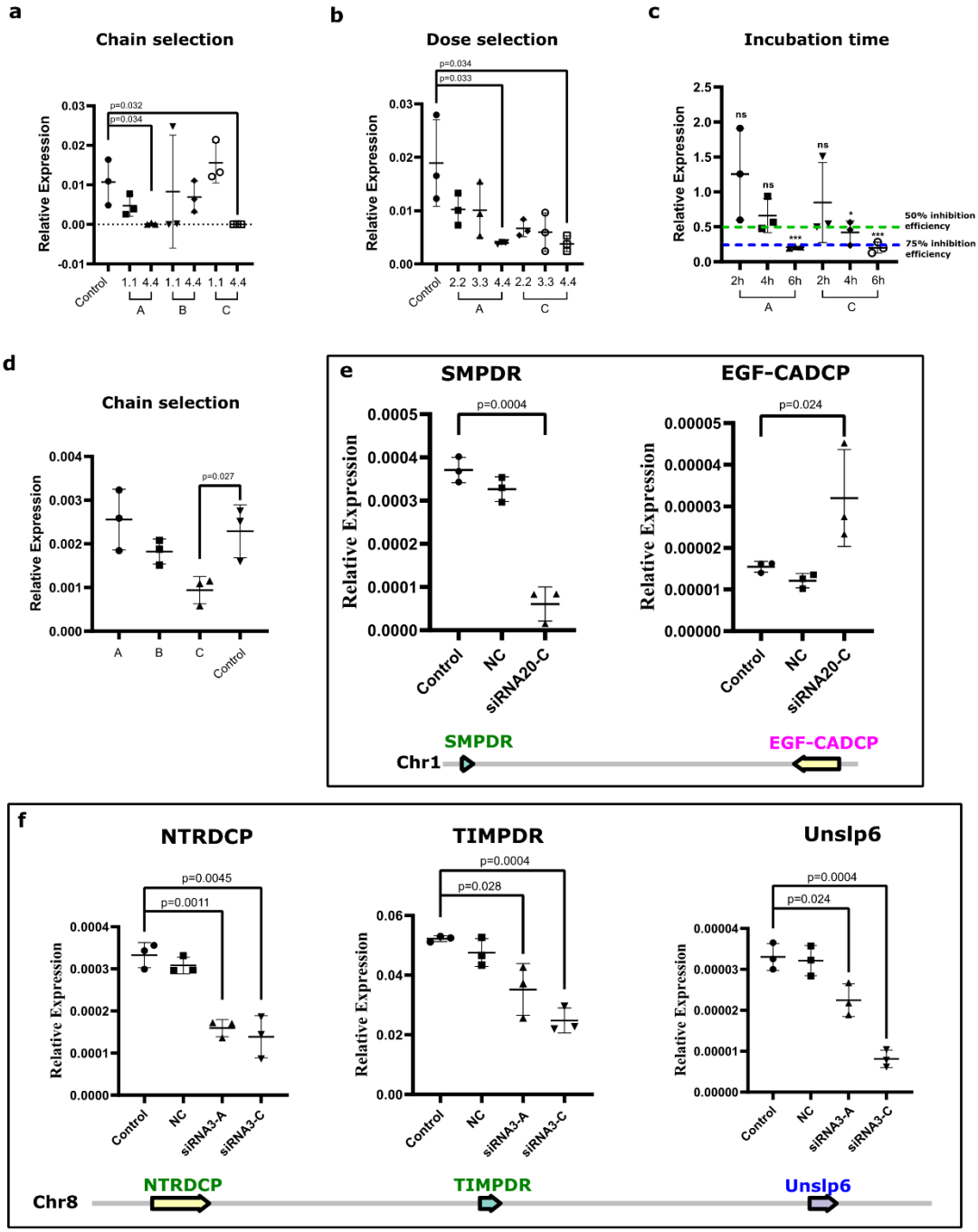

Supplementary Figure 2.21 Optimization of siRNA experiments (chain, dose, and incubation time) and effect of lncRNA ablation on candidate neighbour gene expression in *ex-vivo* mantle cultures. (a-c) Determination of the optimal siRNA experimental conditions for *TIMPDR* based on its effect on the expression of *TIMPDR* transcripts in mantle *ex-vivo* tissue culture. Selection of (a) chains, (b) dose and (c) incubation time. (a) the effect on *TIMPDR* transcript abundance of the different si RNA nucleotide chains A, B and C (11mg/ml and 4.4 mg/ml) and (b) the effect of *TIMPDR* chain concentration (2.2 mg/ml, 3.3 mg/ml and 4.4 mg/ml) after 8 h incubation with mantle *ex-vivo* tissue culture.

The expression data was determined by qRT-PCR and calculated as the fold change relative to the average of the expression of two reference genes (EF1α and RL7). The data is represented as the mean ± SEM of 3 biological replicates (each biological replicate represents a mixture of ± 20 mantle fragments from 6 individuals) and a student t-test was performed to determine the statistical difference between the Lnc-treated samples compared to the control. (c) Effect of incubation time (2, 4 and 6h) on the effectiveness of the candidate chains to ablate *TIMPDR* expression. Expression data was calculated as the fold change relative to the control. Data is represented as the mean ± SEM of 3 biological replicates (each biological replicate represents a mixture of ± 20 mantle fragments from 6 individuals) and a student t-test was performed to determine the statistical difference between the samples compared to the control. (d) Effect of the three siRNA chains (A, B and C) for *SMPDR* on the gene expression of *SMPDR* transcripts in mantle tissue fragments. The optimal conditions (dose and incubation time) previously obtained for *TIMPDR* were assessed for use with *SMPDR*. (e-f) Effect of the optimized siRNAs experimental conditions on the gene expression level of targeted lncRNAs and candidate regulatory protein coding genes in mantle ex-vivo cultures for e) *SMPDR* and f) *TIMPDR*. The gene expression data was obtained using qRT-PCR and calculated as the fold change relative to the average of the expression of the reference genes (*EF1α* and *RL7*). Data is represented as the mean ± SEM of 3 biological replicates (each biological replicate represents a mixture of ± 20 mantle fragments from 6 individuals) and a student's t-test was performed to determine if there were statistical differences between the lncRNA treated samples in relation to the control. The *p value* is shown, and statistical significance was considered when $p < 0.05$. The control group (seawater only) and the group incubated with the negative siRNA chain (NC) were used as negative controls.

2.6.3 Supplementary Tables (in Annex II, digital format)

CHAPTER 3

Species-specific responses of bivalves to ocean acidification

Species-specific responses of bivalves to ocean acidification

Manuscript submitted to Global Change Biology

Acknowledgements

This study received Portuguese national funds from FCT - Foundation for Science and Technology through projects UIDB/04326/2021, 2022 and 2023 and LA/P/0101/2020 and from the operational programs CRESC Algarve 2020 and COMPETE 2020 through the project EMBRC.PT ALG-01-0145-FEDER-022121.

Species-specific responses of bivalves to ocean acidification

Maoxiao Peng[1], João CR Cardoso[1*], Pol Sorigué[1,$], and Deborah M Power[1,2,3*]

[1]Comparative Endocrinology and Integrative Biology, Centre of Marine Sciences, Universidade do Algarve, Campus de Gambelas, 8005-139 Faro, Portugal

[2]International Research Center for Marine Biosciences, Ministry of Science and Technology, Shanghai Ocean University, Shanghai, China

[3]Key Laboratory of Exploration and Utilization of Aquatic Genetic Resources, Ministry of Education, Shanghai Ocean University, Shanghai, China

[$]Current address: Integrative and Behavioural Biology, Instituto Gulbenkian de Ciência, Oeiras 2780-156, Portugal

* Corresponding authors

3.1 Abstract

Ocean Acidification (OA) has direct impacts on calcifying organisms such as bivalves, but the diversity of shell architecture makes it unclear if OA will affect all bivalves equally. To explore this question, we compared the response of mussels (*M. galloprovincialis*) that have hard, aragonite-rich brittle shells and oysters (*M. gigas*) that have soft, calcite-rich chalky shells to 60 days of OA (pH 7.8), shell thinning (SS, to simulate shell dissolution), or the two challenges combined (SSOA). OA caused a significant reduction in soft body mass growth, shell growth and mantle enzyme activity that was more pronounced in *M. galloprovincialis*. OA, SS and SSOA elicited a bigger response in *M. galloprovincialis* than *M. gigas* as reflected by the number of DE genes in the new steady state of gene transcription in the mantle after 60 days of treatment. The gene transcripts identified in the two species indicated substantial differences exist in their response to the challenges particularly in relation to metabolic processes, shell building machinery and regulatory factors revealing a differing vulnerability to changes in their environment. The outcome was not due to the higher (3 times) number of protein coding genes in the genome of *M. galloprovincialis* since both species express a similar number of gene transcripts in the mantle and over 80% of them were homologous. Overall, our study revealed that under the same

stressors the mantle of *M. galloprovincialis* and *M. gigas* responded differently and this highlights the need for caution when generalising about the likely consequences of OA on the survival of calcifying organisms like bivalves.

Keywords: Climate change, aquaculture marine bivalves, mantle transcriptome, shell, biomineralization genes

3.2 Introduction

Bivalves belong to the molluscs, a highly diverse group of sessile filter-feeding aquatic invertebrates and the second most numerous animal phylum after insects (Wanninger and Wollesen, 2019). A characteristic taxonomic feature is the presence of two valves composed of calcareous biomineralized material that encloses and protects their soft body. Freshwater and marine bivalve species provide crucial ecosystem services and from a socioeconomic perspective their aquaculture production is an expanding and economically profitable industry accounting for approximately 60% of marine and coastal products (FAO, 2018). The sustainability of aquaculture production and bivalve biodiversity is at risk from rapidly changing seawater chemistry caused by climate change. It is estimated that due to increased pCO_2 and associated ocean acidification (OA) the pH of seawater by 2100 will drop to approximately 7.8 (Ken and Wickett, 2003; Sabine et al., 2004). Reduced seawater pH is known to modify the growth of the shell in bivalves and the calcified structures of other marine organisms although the consequences are controversial, and it is unclear if OA will affect all calcifying organisms in the same way (Hofmann et al., 2010; Ken and Wickett, 2003; Peck et al., 2015; Tan and Zheng, 2020).

Bivalve shells are composed primarily of calcium carbonate crystals

($CaCO_3$, is approximately 95% of the total shell weigh), which are generated in the extrapallial fluid and involve the activity of the enzyme carbonic anhydrase (CA) (Cardoso et al., 2019; Marie et al., 2010; Santini et al., 2011). Crystal nucleation and shell deposition occurs in an organic matrix (< 5% of the shell) secreted by the shell producing mantle, and is composed of proteins, polysaccharides and chitin (Kobayashi and Samata, 2006). The shell is important for bivalve survival, and it is first evident in D-shaped larvae stages where it is secreted by a specialised shell gland (Denny and Miller, 2006; Levine et al., 2014; Vermeij, 1995). The shell in juveniles and adults is secreted by the mantle tissue and the biomineralization toolbox identified so far includes enzymes, ion transporters and shell matrix proteins (SMPs) (Clark et al., 2020). Molecular data from shell and mantle proteomes, and mantle transcriptomes, have shed light on the proteins and other regulatory factors important in shell building and turnover although the mechanisms and dynamics of shell production remain enigmatic (Bjärnmark et al., 2016; Melody S. Clark, 2020; Marie et al., 2012). The exuberant shape and colour of shells is proposed to result from a high degree of species specificity in SMPs, although the core proteins and some protein domains/motifs of the shell biomineralization toolbox are conserved across bivalves (Clark et al., 2020; Peck et al., 2015).

The microstructure of bivalve shells is diverse, and the arrangement of different-shaped aragonite and calcite crystals results in a wide array of shell morphologies (Haszprunar and Wanninger, 2012; Ponder et al., 2019) and likely differing vulnerability to OA. For example, hard shells found in mussels, consists of longitudinally arranged calcite prismatic crystals (prismatic layer) and densely overlapped aragonite crystals in a planar fashion (nacreous layer) (Ren et al., 2009). While the softer and flakier shell of oysters have a prismatic layer structure similar to mussels, but the predominant structure is tightly overlapped and randomly stacked sheet-like calcite, which forms the foliated and chalky layers, respectively (Checa et al., 2018; Hamester et al., 2012). Research on calcium carbonate molecules indicates that crystallization in the form of calcite is more energy-efficient and stable than in the form of aragonite (Niu et al., 2022; Santos and Gerven, 2011; Shi et al., 2019). Construction in bivalves of different shell structures has different energy costs and means they are likely to be affected by OA in different ways (Kobayashi and Samata, 2006). This effect is likely to be compounded by species-specific and life-stage specific physiological responses to environmental change including OA (Kroeker et al., 2013, 2010; Ries et al., 2009).

The main way OA is proposed to affect shell growth is by modifying the composition of dissolved inorganic carbon (DIC) in the environment,

which changes the dynamics of its uptake and this is reflected in changed shell composition and structure (Fitzer et al., 2014; Rajan and Vengatesen, 2020; Timmins-Schiffman et al., 2014). OA impedes the development of the shell and reduces individual survival rates in early larvae stages of calcifying marine bivalves (Tan and Zheng, 2020). In-depth research reveals that the energy required for larval shell construction in early stages comes from the fertilized egg, while the raw materials (CaCO3) for the shell are sourced directly from the environment. The relatively low concentration of environmental CO_3^{2-} ions under OA increases the energy burden for larval shell construction. Individuals with limited energy reserves are unable to produce a shell or may produce a deformed shell, leading to death (Waldbusser et al., 2013). To date, research has mainly focused on the effects of OA on growth, immunity, and shell calcium carbonate crystal formation in marine bivalves.

Studies of bivalves under OA have evaluated relatively short-term energy balance, shell mineralization rates, ion transport protein activity, metabolism, calcium ion regulation-related enzyme activity, and immune system protein activity (Kroeker et al., 2014; Ren et al., 2020; Schwaner et al., 2023; Timmins-Schiffman et al., 2014; Young and Gobler, 2018). There have even been reports indicating that OA can erode the outer layer of shells, since it is believed that OA reduces the saturation point of

aragonite and calcite crystals (McClintock et al., 2009). The effects of OA and the resulting drop in pH are compounded by other changes in seawater, such as decreased salinity, increased temperatures and hypoxia, which all alter bivalve metabolism and energy requirements (Dickinson et al., 2012; Hiebenthal et al., 2013). OA imposes direct and combined effects on bivalves, requiring them to expend more energy to maintain normal physiological metabolism and shell construction (Lutier et al., 2022; Tan and Zheng, 2020). Therefore, the dynamic changes in microalgae availability and bivalve activity under OA have been considered in some studies to explain the consequences for the whole animal and tissue specific energy costs (Lassoued et al., 2019; Waldbusser et al., 2016). In addition, a change in the susceptibility of bivalves to pathogens has been proposed, due to modified bivalve immunity and shifting abundance and patterns of marine microbiota (Zhao et al., 2020). However, a significant knowledge gap is the lack of analysis from a comparative perspective of the responses/adaptability of different bivalve species to OA, as studies generally focus on individual species.

To test the hypothesis that the biological impacts of OA for bivalves will partly depend on their shell characteristics, a comparative analysis under a common experimental setup was performed for the

Mediterranean mussel (*Mytilus galloprovincialis*) and the Pacific oyster (*Magallana gigas*). The response of the bivalves was established after 60 days exposure to OA at the pH predicted for the year 2100 (pH 7.8; (Hönisch et al., 2012)). The exposure timeframe was chosen to permit assessment of whole animal and shell growth and to assess the new steady state of gene expression in the mantle by looking at global gene transcript patterns. The effects of OA on shell growth and shell architecture were studied, shell-related enzyme activity was determined in both species and in-depth comparative analysis of oyster and mussel mantle transcriptomes (gene expression) was established. To assess if shell thinning, proposed by some to be an outcome of shell erosion caused by OA, elicited a similar response to OA conditions alone, the shell edge was lightly sanded to thin it under control (seawater pH 8.2) and OA (seawater pH 7.8) conditions and the shell characteristics, enzymes and transcriptomes were analysed. Our data revealed that mussels and oysters respond differently to OA and to shell thinning and that mussels retained a more highly modified mantle transcriptome even after 60 days.

3.3 Materials and methods

3.3.1 Animals and experimental conditions

Juvenile Mediterranean mussels (*M. galloprovincialis*), of 3.0 - 3.5 cm shell-length and 8.62 - 10.11 g weight and the Pacific oysters (*M. gigas*), of 3.0 - 3.5 cm shell-length and 5.23 - 6.11 g weight was used. *M. gigas* oysters were obtained from a local company bivalve (Olhão, Portugal) and the mussels were collected from the Ria Formosa (Faro, Portugal, ICNF license 327/2022/CAPT). Animals were transported live to the experimental facilities of Ramalhete - CCMAR Experimental Marine Station (Faro, Portugal) and acclimated for one week before the start of the experiment to glass aquaria containing 5 L of aerated seawater collected from their natural environment. Experiments were performed in an open circuit system under normal environmental conditions of photoperiod and temperature (13-17ºC) for November-January in the Algarve (Portugal). Seawater was acidified in header tanks by pumping in CO_2 gas under controlled conditions to decrease the ambient pH value from, pH 8.2 to pH 7.8. The seawater temperature, oxygen and pH in the circuits were continuously monitored, and fluctuations automatically corrected (Aquatronica, Reggio Emilia, Italy).

To assess the impact of OA and shell thinning on the shell producing mantle and the shell four experimental groups were established for both

the mussels and oysters and were: 1) intact shell in ambient seawater pH 8.2 (control, SW), 2) intact shell at a lower seawater pH 7.8 (OA), 3) sanded shell at normal seawater pH 8.2 (SS) and 4) sanded shell at lower seawater pH 7.8 (SSOA). Triplicate aquaria were established for each experimental condition and for each species. Aquaria contained n = 10 mussels and n = 9 oysters. Shells were thinned by mechanical sanding of the external surface at the edge of the left valve in the mussel and the round (cupped) shell of oysters. Mussels and oysters were exposed to the challenge for 60 days in an open circuit supplied with aerated seawater (pH 8.19 ± 0.01) and with seawater gassed with CO_2 to achieve the desired pH, 7.8 ± 0.01. No mortality was observed in any of the experimental groups during the experiment.

Animals were fed every day with 10 mg of a commercial mixture of dried microalgae (PHYTOBLOOM, Necton, Portugal) that were prepared by resuspending them in 10 ml of seawater and then incubating for 30 min with occasional shaking to ensure complete hydration. The microalgae mixture was then added to each experimental tank to give a final approximate concentration of 0.2 mg of microalgae/individual. To avoid immediate loss of large quantities of microalgae from the aquaria the water throughflow was turned-off for one hour. After 60 days of exposure to the experimental conditions, samples from the mantle edge

were collected from the posterior region of the left valve in mussels and from the mantle from the round-cupped oyster shell for transcriptome, molecular and biochemical analyses. Samples were immediately frozen on dry ice and stored at -80ºC. *M. galloprovincialis* (n = 16, per experimental group) and *M. gigas* (n = 9, per experimental group) growth was measured by determining the shell area using digital images taken of both the right and left valves laid on graph paper using ImageJ (www.imagej.nih.gov) and by determining the dry weight (g) of the soft-body (*M. galloprovincialis* (n = 10, each experimental group) and *M. gigas* (n = 9, each experimental group)). The dry weight was determined by loosely wrapping the samples in aluminium foil and maintaining at 60 ºC until they achieved a constant weight in three successive measurements on an analytical balance (Sartorius, Gottingen, Germany).

3.3.2 Seawater chemistry

Seawater was pumped from the Ria Formosa into two (2,000 L) header tanks, where it was aerated with ambient air (control) or with CO_2 to achieve the desired pH (acidified water). The pCO_2 of the seawater in the CO_2 treated header tank was maintained at the target value of 1,000 µatm using a pH probe connected to an automated internal controller (EXAxt PH450G, Yokogawa Iberia, Portugal). Conditions in

the experimental system were stabilized for 1 month prior to initiation of the experimental trials. CO_2 and temperature were monitored and controlled in real time. Control and acidified CO_2 seawater were continuously supplied to the triplicate 5 L aquaria and seawater pH (Orion star A221, Thermo Scientific, Portugal), temperature (Orion star A221, Thermo Scientific, Portugal), and salinity (WTW, cond3310, Spain) were monitored every two days in each of the triplicate tanks of all experimental groups. Total alkalinity of seawater samples was analysed twice a week by Gran titration (DL15 titrator, Mettler Toledo, Portugal) using a certified acid titrant (0.1 M HCl, Fluka Analytical, Sigma-Aldrich). Carbonate chemistry parameters (Supplementary Table 3.1) were calculated in CO_2SYS (Pierrot et al., 2011) using the constants K1 and K2 from (Mehrbach et al., 1973) and refitted by (Dickson, 1990; Dickson and Millero, 1987) for KHSO4.

3.3.3 Microalgae filtration rate

The impact of the experimental conditions on the filtration rate of both *M. galloprovincialis* and *M. gigas* was measured by determining the change in concentration of microalgae (PHYTOBLOOM, prepared as outlined above) across time after addition of a known concentration to the seawater aquaria. So as not to disrupt the main experiment the feeding

rate experiment was carried out in parallel with the same stock of bivalves maintained under the same conditions and feeding regime as the experimental groups. The concentration of microalgae fed to the bivalves was assessed using the aquaria water and reading at a wavelength of 664 nm on a microplate reader (Biotek Synergy 4, USA) using a standard curve that related the density of the microalgae with absorbance. The feeding rate was established by measuring the microalgae filtration rate by the bivalves (n = 5 oyster/tank, n = 10 mussels/ tank in triplicate) by determining the absorbance in triplicate 2 ml seawater samples collected from each aquaria 30 minutes after microalgae addition. The bivalve filtration rate was calculated using the following formula.

Filtration rate (mg microalgae · g^{-1} · min^{-1}) = [A_i (initial microalgae concentration) - A_f (final microalgae concentration)] * V (volume of test water) / [W (wet body weight) * T (test time)]

3.3.4 Bivalve shell integrity and byssal secretion in M. galloprovincialis

The external appearance of *M. galloprovincialis* (n = 10) and *M. gigas* shells (n = 9) were visually inspected to identify differences in shell colour, shape, texture, or irregularities in the animals maintained under the four experimental conditions. In addition, the periostracum integrity and the number of byssal thread marks on the *M. galloprovincialis* shell

was scored.

3.3.5 Carbonic anhydrase enzyme activity in the mantle

CA activity gives a measure of shell formation since this enzyme accelerates the reversible hydration of metabolic carbon dioxide (CO_2) to bicarbonate (HCO_{3-}) and so contributes to regulate the formation of calcium carbonate crystals in the shell (Lindskog and Coleman, 1973; Tripp et al., 2001). Two different enzymatic activities were measured: esterase and hydratase. Esterase activity was quantified using a colorimetric assay that measures the conversion of the substrate 4-Nitrophenyl acetate to p-nitrophenolate according to (Cardoso et al., 2020, 2019). Briefly, 10 µl of the mantle protein extracts (0.1 mg/µl) were added in 190 µl of pCA working solution. Samples were assayed in duplicate, and the reactions were performed in 96-well plates (Greiner, Germany). Reactions were read with a microplate reader (Biotek Synergy 4, USA) at 405 nm. The amount of p-nitrophenolate produced was quantified using a standard curve constructed using p-nitrophenol (from 0 to 200 µM), and this permitted quantification of CA activity in the experimental samples. Bovine CA isoenzyme II (0.1 mg/ml) (Sigma-Aldrich) was used as a positive control.

Protonography on non-denaturing SDS-PAGE gels was performed to assess α-CA hydratase activity as described in (De Luca et al., 2015;

Perfetto et al., 2017). Briefly, a pool of mantle protein extracts of five individuals from each condition (SW, OA, SS and SSOA) was prepared and the pooled samples were run on 12% SDS-PAGE gels. The SDS-PAGE gels were washed with buffer (2.5% Triton X-100/Tris-HCl, pH 7.4) for 1 h, followed by two more washes of 10 min in 100 mM Tris-HCl (pH 7.4)/10% isopropanol. The gels were developed by incubation at 4ºC in 0.1% bromothymol blue (BTB, AcrosOrganic, USA) for 30 min and then revealed for 15 min in acidified ddH2O (saturated with CO_2, pH= 4.4 - 4.6) at room temperature. The α–CA activity was detected as a yellow product on the gel. A positive control, bovine α-CAII (Sigma-Aldrich), was included in the gel. Approximately 10 μg of total mantle protein extracts (mussel or oyster) and 5 μg of bovine CA isoenzyme II were loaded on SDS-PAGE gels. Gel images were captured using a SYBR green filter with a Chemidoc XRS (BioRad, USA) image analysis system.

3.3.6 RNA extraction and library sequencing

Total RNA (tRNA) from the mantle edge of 6 individuals from each of the triplicate tanks of the experimental groups was extracted for the construction of RNA-seq libraries. Before RNA extraction the black pigment of the mussel mantle edge, which can interfere with the quality of the RNA extracted, was manually removed using a surgical blade and

paper. The tRNA was extracted using an E.Z.N.A kit (VWR, USA). The mantle edge collected was homogenized by mechanical disruption using two iron beads (5 mm diameter) and a Tissue lyser II (Qiagen) with 1 cycle of agitation for 3 min at room temperature (RT). DNase treatment was performed after tRNA elution using a Precision DNase kit (Primer design, UK) and following the manufacturer's protocol. DNA-free tRNA was quantified using a Nanodrop (1000 Spectrophotometer, Thermo Fisher Scientific, USA) and the quality and integrity analysed by agarose gel electrophoresis (0.8%/1X TAE: Tris-acetate-EDTA). Samples used for RNA-seq library construction consisted of a pool of tRNA (2 µg) from two (2) individuals/ experimental group (1 µg of total RNA/animal) and three (3) replicate samples per treatment group were used for library preparation. Library preparation and sequencing were outsourced to the Experimental Department of Novogene (Beijing, China). Sequencing was carried out using an Illumina TrueSeq mRNA-Seq library Prep kit and sequenced on an Illumina Novaseq 6000 and 150 bp paired-end raw-reads were generated. Accession number of the raw data are PRJNA995578.

3.3.7 Transcriptome quality control, genome mapping and transcript counts

The *M. galloprovincialis* and *M. gigas* mantle raw sequenced data were uploaded to the Galaxy web platform https://usegalaxy.org (Afgan

et al., 2016) and the data was checked for quality, mapped against the species genomes and the reads counted. The quality of the raw reads from the sequenced libraries was assessed with FastQC (http://www.bioinformatics.babraham.ac.uk/projects/fastqc) and FastP (https://github.com/OpenGene/fastp) programmes using for quality evaluation “no contaminant or adapter”. The tool Trimmomatic (Bolger et al., 2014) was used to remove reads of low quality (short reads and reads without paired ends). The ‘Pair-ended reads’ option was used to join the forward and reverse read sense within the same individual sample. The mussel *M. galloprovincialis* (GCA_900618805.1 MGAL_10) and oyster *M. gigas* (GCA_902806645.1 cgigas_uk_roslin_v1) reference genomes were downloaded from the NCBI database (https://www.ncbi.nlm.nih.gov) and Hisat2 (Kim et al., 2019) was used to map the mantle transcriptome reads to the reference genomes, using the default parameters. The tool StringTie (Pertea et al., 2015) was applied to the BAM file provided by Hisat2 to assemble and quantify the transcripts. Gene expression was calculated using FPKM values. To verify the similarities between the samples during preliminary exploratory data analysis, a principal component analysis (PCA) was performed using psych, reshape2, factoextra and ggplot2 packages (Kassambara, 2017; Revelle, 2011; Wickham, 2009; Khetarpal et al., 2019), and correlation analysis plots were drawn using the corrplot package (Friendly, 2002) and a heatmaps

was generated using the pheatmap package (Kolde and Kolde, 2015) in Rstudio (version 3.1.6).

3.3.8 Differentially expressed genes (DEG)

The DESeq2 (Love et al., 2014) package in RStudio was used to calculate the differentially expressed genes (DEG) from the total counts of each library, where the screening thresholds were FDR (false discovery rate) <0.05, log2FC (log2-foldchange)>1 or log2FC<-1, respectively. Three comparative analyses were established: i) SW vs. OA (SW-OA) to determine the effect of OA on the mantle gene expression compared to control bivalves, ii) SW vs. SS (SW-SS) to study the effect of shell thinning on mantle gene expression and, iii) SS vs. SSOA (SS-SSOA) to differentiate the effect of OA and shell thinning on mantle gene expression. All gene transcripts that were only DE in one of the six libraries used for each comparison were considered non-significant and removed from further analysis. Volcano plots were constructed using the ggplot2 package in Rstudio (Wickham, 2016) and a heatmap of the DEGs was constructed using the pheatmap package (Kolde and Kolde, 2015). Non-protein-coding transcripts were excluded from the analysis.

3.3.9 Homology analysis of mantle epithelium DEGs between M. galloprovincialis and M. gigas

Significant genetic differences exist between different orders of bivalves (Zhang et al., 2012), and represents a challenge for comparative analysis. For this reason, a preliminary evaluation of the genetic differences between *M. galloprovincialis* and *M. gigas* particularly at the level of the protein coding genes characteristic of the mantle was made. First, the reference genome information (at the gene and protein levels) was extracted to compare the genetic backgrounds of the two species. Pfam (ver 34.0) (http://pfam.xfam.org/) was used to analyze protein-coding gene sequences and to identify mineralization-related domains in genes from each species using a mineralization toolkit library (https://data.bas.ac.uk/full-record.php?id=GB/NERC/BAS/PDC/01132). The genetic background alignment data was visualized using Inkscape (ver 1.2).

Deduced protein sequence databases were generated from the coding genes predicted in each species after removing variable splicing sequences using TBtools (ver 1.0986) (Chen et al., 2020) These databases were used as the background for blast (Diamond, ver 2.0.1) (Buchfink et al., 2015) analysis of mantle DE protein-coding genes. The strategy for comparative analysis of mantle DE genes was as follows: 1) DE protein-

coding genes from *M. gigas* mantle were blasted against the *M. gigas* deduced protein sequence library using Diamond (ver 2.0.1) to establish copy number. The same general procedure was applied to the DE protein-coding genes from the mantle of *M. galloprovincialis,* 2) gene homologues between *M. gigas* and *M. galloprovincialis* were identified by blasting the DE protein-coding genes from the *M. gigas* mantle against the protein coding genes deduced from the *M. galloprovincialis* genome (Diamond, ver 2.0.1). The same procedure was applied to the DE protein-coding genes of the *M. galloprovincialis* mantle. The mantle expression level of the obtained genes was determined using the control group transcriptome data of the respective species. The comparative expression data obtained for the mantle of *M. gigas* and *M. galloprovincialis* is presented as a heatmap and is based on the average FPKM values using the pheatmap package (Kolde and Kolde, 2015) in Rstudio (version 3.1.6).

The detection of cis-regulatory modules in DE mantle genes was obtained by mapping the protein coding and non-coding genes to the *M. galloprovincialis* and *M. gigas* genome, respectively. DE protein coding genes localized 100 kb upstream or downstream of DE non-coding genes were selected as cis-regulatory candidates. Mapping of candidate cis-regulation modules (DE non-coding – DE protein coding genes) was performed with the gggenes package (ver 0.4.1) (Wilkins, 2019) in R-

studio.

3.3.10 Protein coding annotation of DEGs and Gene Ontology (GO) enrichment analysis

The protein-coding annotation of DEGs were assigned by searching against the Swiss-Prot protein database using BLASTp in the Diamond software tools (v2.0.11, (Buchfink et al., 2015)) and the top ten hits with the lowest e-value (< 1.0 e^{-5}) were used to assign identity and were further confirmed by the prediction of protein domains using the SMART tool (http://smart.embl-heidelberg.de/). Shared genes identified in the mantle DE genes of both species under the same experimental conditions were identified using NCBI BLASTp software tools (local blast v2.9.0+). Gene Ontology annotation was performed using the ID mapping tool (https://www.uniprot.org/uploadlists/) and genes were classified within three categories: biological process (BP), cellular compartment (CC) and molecular function (MF). GO enrichment was performed using the OmicShare online platform (https://www.omicshare.com).

3.3.11 Protein subcellular localization and domain analysis

Protein subcellular localization was predicted using several tools: SignalP5.0 for the identification of a signal peptide sequence, TMHMM

v.2.0 (http://www.cbs.dtu.dk/services/TMHMM/) for the prediction of transmembrane domains and DeepLoc v1.0 (http://www.cbs.dtu.dk/services/DeepLoc/) was used to predict subcellular localization. DEGs were classified as membrane-spanning if at least one transmembrane region was predicted in the deduced proteins. The deduced putative extracellular and mollusc shell matrix proteins (SMPs, https://data.bas.ac.uk/full-record.php?id=GB/NERC/BAS/PDC/01132) were used to search the Pfam database (https://pfam.xfam.org) so that DE mantle genes encoding shell specific protein domains could be identified. To identify DEGs encoding membrane transporter proteins, searches were performed against the Transporter Classification Database (TCDB, https://tcdb.org/) using BLASTp. Deduced proteins of DE mantle genes expressed in the Nucleus were identified by searching against the Animal Transcription Factor Database (AnimalTFDB3.0, http://bioinfo.life.hust.edu.cn/AnimalTFDB/#!/) and putative transcription factors were verified using the Transcription Factor Prediction tool using the default parameters.

3.3.12 Small scale gene expression analysis

3.3.12.1 cDNA synthesis for quantitative-PCR

To corroborate the outcome of *M. galloprovincialis* and *M. gigas* mantle transcriptome gene expression, mantle cDNA from flat and round valves was prepared from 6 individuals of each experimental group. The cDNAs used for quantitative PCR (qPCR) were synthesized from DNase treated mantle tRNA (500 ng) denatured at 65ºC for 5 min and quenched for 5 min on ice. Reactions were carried out in a 20 µl final volume with 10 ng of pd(N)6 random hexamers (Jena Bioscience, Germany), 2 mM dNTPs (ThermoScientific, USA), 100 U of RevertAid Reverse Transcriptase and 8 U Ribolock RNAse inhibitor (ThermoScientific) and the reaction conditions were: 10 min, 20 ºC; 60 min, 42 ºC; 70 ºC, 5 min.

3.3.12.2 Quantitative-PCR (qPCR)

QPCR reactions were performed using SsoFast EvaGreen Supermix (Bio-Rad, Portugal) for a 10 µl final reaction volume containing 200 nM of candidate gene specific primer pairs (Supplementary Table 3.2) and 2 µl of cDNA template (diluted 1:2). Duplicate reactions were used for all samples (n = 6 for each experimental group) and controls (accepting < 5% variation between replicates) and all reactions were run on a CFX Connect Real-Time PCR Detection System for 96-well microplates (Bio-

Rad). Melting curves were performed to detect non-specific products and primer dimers. Reverse transcriptase (RT-) and PCR control (no template) reactions were included in all qPCR assays to confirm the absence of contaminating genomic DNA or technical-related contamination, respectively. Reaction efficiencies and R^2 (coefficient of determination) were established for each primer pair. The *M. galloprovincialis* elongation factor 1-alpha (EF1α) and 18S ribosomal RNA were used as reference genes for normalization (cDNA was diluted 1:100). The *M. gigas* EF1α and the ribosomal protein L7 (RL7) were used as the reference genes for normalization (cDNA diluted 1:100 and 1:10, respectively). Target gene expression was normalized using the geometric mean of the expression level of the respective reference genes, and quantification was based on the standard curve methods.

3.3.13 Statistical analysis

The statistical tests used for transcriptome analyses are indicated in the respective sections. The statistical analysis for shell area (*M. galloprovincialis* n = 16, *M. gigas* n = 9), soft body weight (n = 9 both species), CA enzyme activity assays (n = 9 for each condition), byssus markers (*M. galloprovincialis* n = 10) and the microalgae filtration rate assay (n = 5 tanks for each species and 10 individuals per tank) is

presented as the mean ± the standard error of the mean (SEM) for each condition. To identify significant differences between the experimental groups, a One-Way Anova Tukey's multicomparison test was performed. The cut-off for significance (p-value) was set at 0.05. The analysis was performed using GraphPad Prism (version 8.0 for Mac OS X, USA, www.graphpad.com).

For the qPCR analysis the results are presented as the mean of 6 replicates ± SEM for each condition. To identify significant differences in gene expression between the experimental groups, a two-tailed Student's *t*-test was performed between the treatment groups and the control. The p-value cut-off for significance was set at 0.05.

3.4 Results

3.4.1 Water chemistry

For the duration of the experiment the seawater parameters (salinity, temperature, alkalinity, and pCO_2) of all experimental group were maintained within the set experimental range. The pCO_2 was maintained at 1050 (µatm) in the acidified seawater tanks and 300 (µatm) in the normal seawater groups (Supplementary Table 3.1).

3.4.2 Phenotypic changes in M. galloprovincialis and M. gigas

The total shell area of *M. galloprovincialis* and *M. gigas* kept under OA conditions (OA and SSOA) was significantly decreased ($p < 0.001$) in relation to the specimens maintained in SW (SW and SS) (Figure 3.1 A-C). The *M. galloprovincialis* maintained in OA conditions had a more significant reduction in shell growth compared to the *M. gigas* maintained under the same OA conditions. In the bivalve specimens in which the shell was thinned, SS and SSOA, the surface damage was fully recovered in *M. galloprovincialis* after 60 days irrespective of the sea water conditions (e.g., SW and OA) but in *M. gigas* shell sanding marks were still visible (Figure 3.1 C).

The soft body dry weight in *M. galloprovincialis* significantly increased in the SS group and decreased in the OA group compared to the SW group ($p < 0.05$) but in *M. gigas* the soft body dry weight was only significantly changed ($p < 0.05$) in the OA group (Figure 3.1 D). The microalgae filtration rate was assessed daily up to day 7 in *M. galloprovincialis* and *M. gigas* and was similar in all groups after 5 days of exposure to OA or shell thinning and was maintained throughout the experiment. Since the supplied microalgae were common for all experimental groups this suggests that the differences observed in body weight were unlikely to be due to differences in the nutritional contents of

the microalgae or in the feeding rates between the experimental groups (Supplementary Figure 3.1 A).

In *M. galloprovincialis*, the number of byssus scars was significantly increased ($p < 0.001$) on the shells of the specimens kept under OA conditions (OA and SSOA, Supplementary Figure 3.1 B-C**).** This suggests that OA increased the secretion of byssus filaments. Moreover, the periostracum membrane showed corrosion and breakage and the inner surface of the shells of mussels exposed to OA were slightly lighter in colour that than mussels kept at normal SW pH (Figure 3.1 A, Supplementary Figure 3.1 C). No visible changes were detected in the integrity or colour of the periostracum in *M. gigas* but the inner shell surface of the flat valve under OA conditions was slightly paler than the shell from SS and SW animals (Figure 3.1 C)

3.4.3 Carbonic anhydrase enzyme activity in the mantle

CA activity was measured in the mantle by determining its esterase and hydratase activities. There was significantly increased esterase activity in *M. galloprovincialis* exposed to OA conditions compared to the other experimental conditions, SW and SSOA ($p < 0.05$). The *M. gigas* mantle esterase activity was significantly higher in the control (SW) group compared to the three other conditions, OA, SS and SSOA ($p <$

0.05). Positive hydratase activity signals were detected in the protonation assay for several proteins in *M. galloprovincialis* and *M. gigas* mantle protein extracts (Figure 3.1 F, G, I and J). The modified CA enzyme activity in the mantle of the different experimental groups was consistent with the presence and abundance of CA gene transcripts in the DE genes of the transcriptome analysis (Figure 3.1 E and H**)**.

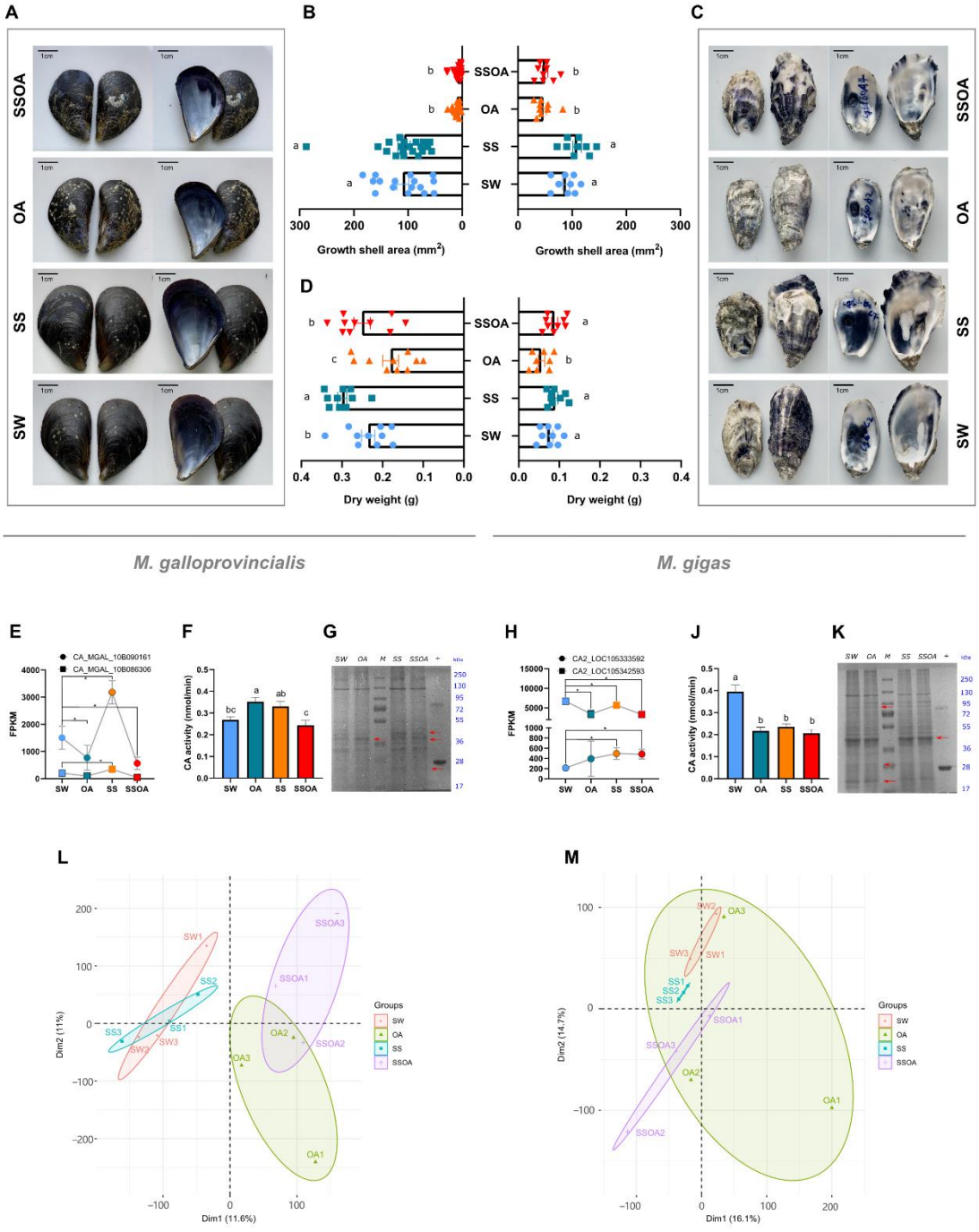

Figure 3.1. Bivalve growth, enzyme activity and global gene transcriptome changes under experimental conditions. (A-D) Shell growth rate after 60-day challenge. (A) Image of *M. galloprovincialis* inner and outer shell; (B) Shell growth area. Values represent the mean ± SEM (n = 16). Different letters indicate significantly different groups ($p < 0.05$); (C) Image of *M. gigas* inner and outer shell; (D) Soft body dry weight. Values represent the mean ± SEM (n = 10, *M. galloprovincialis*, n = 9, *M. gigas*). Different letters indicate significantly different groups ($p < 0.05$). (E) Significantly responding carbonic anhydrase (CA) transcript FPKM values in *M. galloprovincialis* and (H) *M. gigas* mantle

transcriptomes are shown in line graphs. Statistical analysis was performed using a t-test and the data represents the mean ± SD of n = 3 samples each containing RNA from 2 individuals. Asterisks indicate significant differences at $p < 0.05$. (F) CA enzyme activity in the mantle of *M. galloprovincialis* and (I) *M. gigas* are shown in bar plots. The values shown correspond to the results of 9 replicates ± SEM for each condition. Statistical significance was calculated using a One-Way ANOVA Tukey's multicomparison test. Different letters indicate significantly different groups ($p < 0.05$). (G) Images of Coomassie blue SDS-PAGE and protonogram of *M. galloprovincialis* and (J) *M. gigas* mantle protein extracts. The images on the left reveal the complexity of the total proteins in the mantle extracts (1 mg/well) after SDS-PAGE and staining with Coomassie blue. The positive control (+) corresponds to commercial bovine CA II (BCA II, 5 μg/well). The arrows indicate the bands that have higher hydratase activity. M: Molecular weight marker (PageRuler Plus, Thermo Scientific). PCA plots of global gene transcriptome of (K) *M. galloprovincialis* and (L) *M. gigas* experimental samples. Different colours represent the four experimental conditions, and each ellipse represents the 0.95 confidence range of the samples under that condition.

3.4.4 Mantle transcriptome under experimental conditions

This study obtained high-quality sequencing results with a minimum Q30 value greater than 92% for subsequent analysis (Supplementary Table 3.3). The correlation between the replicate samples analysed for each species across the treatments was greater than 0.8, revealing that there was an overall low variability between them (Supplementary Figure 3.2). The comparison of the expression pattern of transcripts across all samples are presented as a heatmap and clustered by treatment (Supplementary Figure 3.2). Principal component analysis (PCA) revealed that at a 0.95 confidence interval for the mantle transcriptomes of *M. galloprovincialis* the SW and SS groups partially overlapped and

clustered separately from OA and SSOA, while there was a partial overlap between OA and SSOA (Figure 3.1 K). PCA revealed that at a 0.95 confidence interval for the mantle transcriptomes for *M. gigas* SW, SS and SSOA samples did not overlap, while the dispersion maximum confidence intervals for the OA samples englobed the SW and SS samples and overlapped with two of the SSOA samples (Figure 3.1 L).

The volcano plot of the *M. gigas* mantle transcriptomes revealed a strongly conserved pattern of gene expression between the experimental groups and a low number of DEGs. A larger number of DEGs were found in *M. galloprovincialis* compared to *M. gigas* under the same experimental challenge (Figure 3.2 A). In the mantle transcriptome of *M. gigas* comparison of the SW and OA group identified 103 DEGs, 64 of which were up-regulated in OA. In *M. galloprovincialis* 787 DEGs were identified between SW and OA mantle transcriptomes and 234 were up-regulated in OA. Comparisons of the mantle transcriptomes of the shell-thinned group (SS) and the control group (SW) revealed a DEG response of a similar magnitude to the OA challenge. In *M. gigas* 126 DEGs were detected of which 90 were up-regulated in SS and in *M. galloprovincialis* 452 DEGs were identified of which 202 were up-regulated in SS. Shell thinning under OA (SS_vs_SSOA) identified 196 DE genes in the *M. gigas* mantle and 113 were up-regulated in SSOA. In *M. galloprovincialis*

mantle under shell thinning and OA, 364 DEGs were identified of which 177 were up-regulated (Figure 3.2 A). All the identified DEGs (SS_vs_SSOA) are presented as a list in Supplementary Table 3.4. To corroborate the outcome of the transcriptome analyses qPCR was used to analyse the expression levels of 8 of the DE genes of *M. galloprovincialis* and 8 of the identified genes of *M. gigas*. The gene expression determined by qPCR of selected candidates in mantle cDNA was consistent with the pattern of expression of DE genes identified in the transcriptome analysis (Supplementary Figure 3.3).

Long non-coding RNAs (lncRNA) are implicated in the regulation of bivalve biomineralization (Peng et al., 2023), and for this reason putative lncRNA cis-regulated gene modules were analysed. In the DE genes of both species, lncRNA were identified. In all experimental comparisons, the proportion of putative lncRNAs in *M. galloprovincialis* (34.18 - 42.86%) was higher than in *M. gigas* (8.67 - 13.49%), which may be a consequence of differences identified in the lncRNA content in their genomes (Figure 3.2 A). Within the DEGs of *M. gigas* 4 lncRNA and cis-modules were identified, while 34 lncRNA and cis-modules were identified in *M. galloprovincialis*, even though the reference genome of *M. galloprovincialis* is not assembled at the chromosome level (Supplementary Figure 3.4).

3.4.5 Homology analysis of mantle epithelium DEGs between M. galloprovincialis and M. gigas

To assess the comparability of the results from the DEG analyses in *M. galloprovincialis* and *M. gigas* the total number of protein-coding genes in their genomes and the sequence homology of DEGs between the two species was determined. Based on the available reference genome information, *M. galloprovincialis* has 14 chromosomes, and *M. gigas* has 10 chromosomes. The genome size of *M. galloprovincialis* is almost twice that of *M. gigas*, and it also possesses over three times the number of protein-coding genes (Gerdol et al., 2020). Nonetheless, despite the difference in their genome size the number of protein-coding genes was similar in the mantle transcriptomes of *M. galloprovincialis* and *M. gigas*, with 78,735 and 63,341 deduced proteins, respectively (Supplementary Figure 3.5 A). Approximately 40% of the protein-coding genes in the genome of *M. galloprovincialis* and *M. gigas* are homologues, and the conservation level of the known biomineralization toolkit gene domains between the two species was found to be high and exceeded 70%.

Comparison of the DE genes identified in the treatment specific mantle transcriptomes of the two species revealed 8.8% - 12.6% and 1.8% - 6.0% of the genes identified in the species-specific group comparisons,

were common between *M. gigas* and *M. galloprovincialis*, respectively (Figure 3.2 B). Taking into account the differences in the genetic background of *M. gigas* and *M. galloprovincialis*, the species homology of DEGs (coding genes) in the two genomes were explored and revealed the deduced proteins were highly conserved in both species, although gene copy number differed (Supplementary Figure 3.5 B, Supplementary Table 3.5), and the percentage of homologue genes identified in the mantle tissue of *M. gigas* and *M. galloprovincialis* under an experimental challenge was 82.78 - 91.14% in SW vs OA, 88.79 - 94.61% in SW vs SS and 88.79 - 94.61% in SS vs SSOA (Figure 3.2 C).

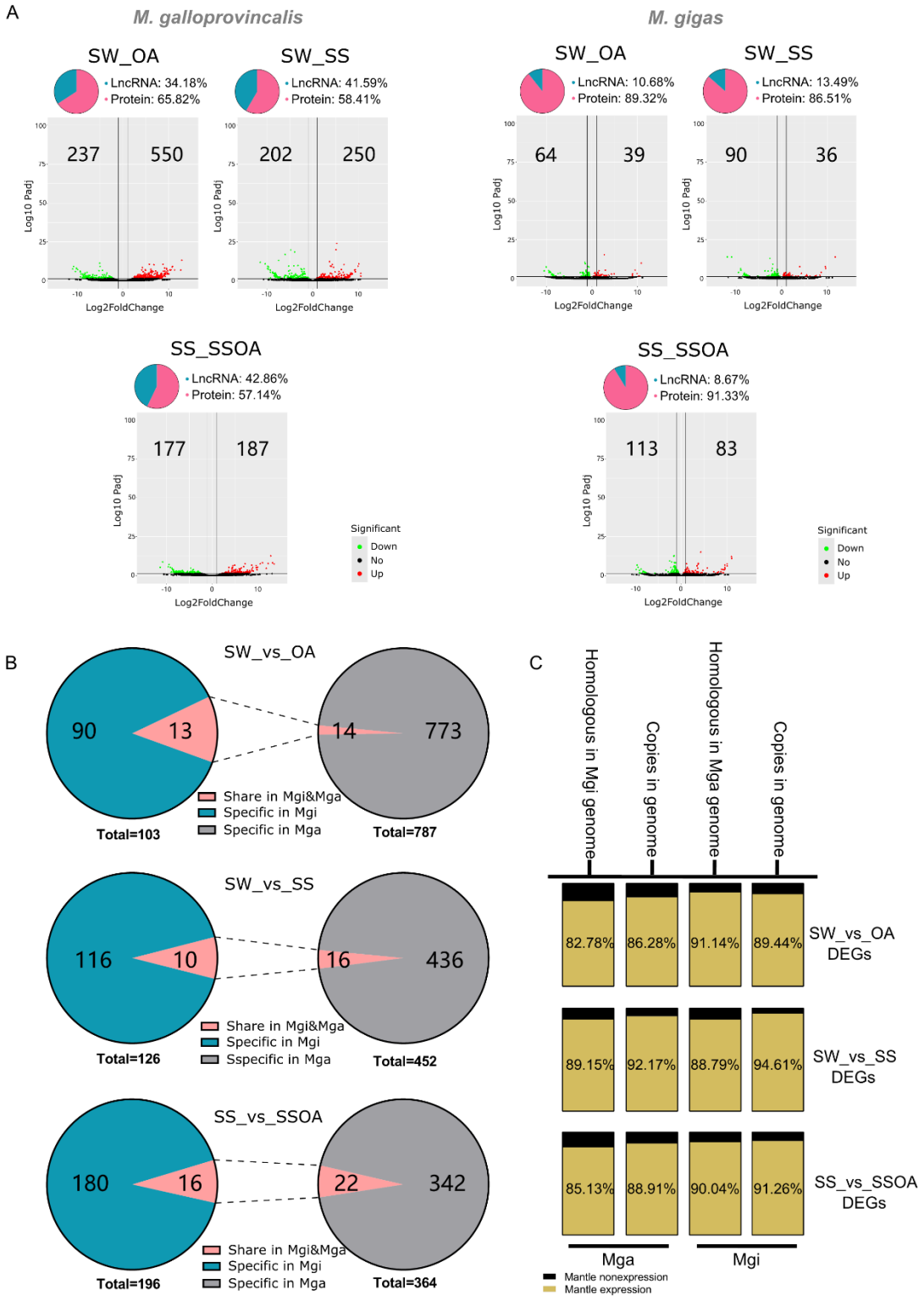

Figure 3.2. Differentially expressed genes (DEGs) in the bivalve mantle under OA, SS, SSOA and control conditions. (A) Volcano plots of *M. galloprovincialis* and *M. gigas* mantle transcriptome samples. Green, red and black dots indicate down-regulated, up-regulated and not significantly regulated (constant expression) genes, respectively. Values

on the non-coordinate axis represent the number of genes up-regulated or down-regulated. The pie chart shows the proportion of coding and noncoding genes represented in the DE genes identified. (B) Number of species-unique DE genes are represented by the blue background and the pink background represents the shared DE genes. The total of the DE genes identified are also indicated. (C) The graphical plot displays the mantle expression proportion of DE gene homologues identified (Supplementary Figure 3.5 B) in the respective genome of each species under each of the experimental conditions. The percent of the DE genes in the mantle is indicated in the brown shaded area.

3.4.6 Gene ontology (GO) functional characterization of mantle DEGs

GO annotation analysis was used to characterize the functional role of DEGs in the mantle of both bivalve species. The biological process (BP) categories represented by the DEGs identified in OA, SS and SSOA in *M. galloprovincialis* and in *M. gigas* were related to biological regulation, cellular and metabolic processes, response to stimulus, development and to immune system responses (Figure 3.3). In *M. gigas* most of the mantle enriched DE genes were down-regulated in OA vs SW and the GOs most affected were biological regulation and cellular process, but in *M. galloprovincialis* the same comparison (OA vs SW) revealed mantle enriched DE genes were mostly up-regulated and more than 50 genes associated with cellular process, metabolic process, biological regulation and response to stimulus were modified. In *M. gigas* in normal seawater after shell thinning (SW_vs_SS) most of the enriched genes were down-regulated and when shell thinning was coupled to OA (SSOA) biological process and cellular process were the most affected GOs. In *M.*

galloprovincialis the number of up-regulated and down-regulated DEGs in the mantle after shell thinning alone or coupled to OA was similar and the most affected GOs were cellular process and metabolic process (Figure 3.3).

GO enrichment of DE genes in the mantle revealed that only deoxyribonucleotide biosynthetic process was significantly enriched in OA challenged *M. gigas* but in *M. galloprovincialis* 28 GO items were significantly enriched and were mostly related to immune response and chitin metabolic process (Supplementary Figure 3.6) Twelve GO terms mainly related to developmental process were significantly enriched in the DE genes of the mantle in *M. gigas* with a thinned shell (SW_vs_SS). Significantly enriched GO terms for the DE genes identified between shell thinning and OA exposure (SS_vs_SSOA) were related to skeletal muscle cell proliferation/differentiation. In *M. galloprovincialis* no significantly enriched GO terms were identified for DE genes of the SW_vs_SS and SS_vs_SSOA groups (Supplementary Figure 3.6).

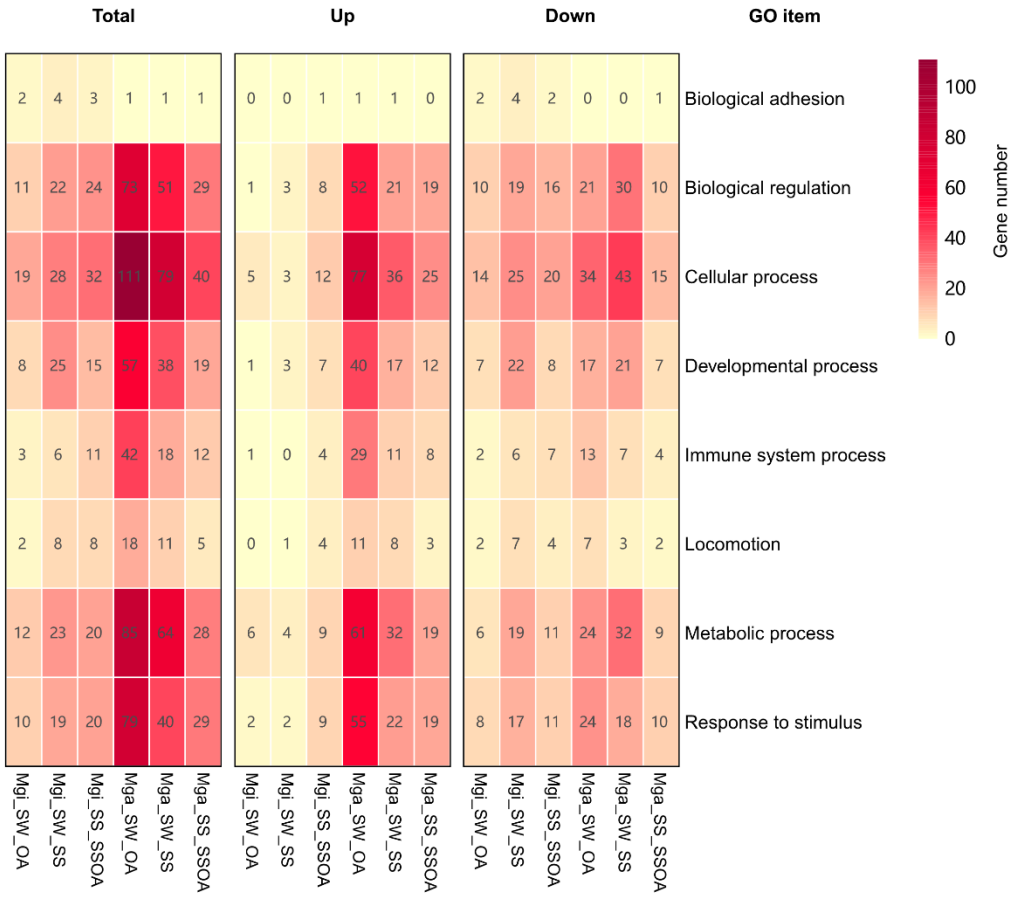

Figure 3.3. Heatmap of DEGs for GO item distribution. Each row represents a GO item, and the experimental conditions compared are in the columns (SW_vs_OA, SW_vs_SS, and SS_vs_SSOA). Graded colours from yellow to red indicates the relative number of DEGs attributed to each GO term. The numbers inside the boxes represent the number of DEGs. Total, up-regulated and down-regulated DEGs are shown.

3.4.7 Functional changes in the mantle epithelium inferred from gene expression

Analysis of the cell compartment to which protein coding DE genes in *M. gigas* and *M. galloprovincialis* were localized revealed extracellular (20 - 35%), cytoplasm (15 - 30%), nucleus (10 - 25%) and cell membrane (10 - 25%) were best represented (Supplementary Figure 3.7). Gene

transcripts in the *M. galloprovincialis* DE genes of the mantle epithelium categorised as core shell toolbox genes, transcription factors, metabolism and the immune response remained significantly modified after 60 days exposure to OA, shell sanding or a combination of these factors when compared to the control (Supplementary Table 3.7). In the case of *M. gigas* after 60 days exposure to OA, shell sanding or a combination of the factors the transcriptome of the mantle epithelium was similar to the control but with a few notably modified gene transcripts of the shell toolbox, and metabolism (Supplementary Table 3.7). Comparative analysis of the transcriptional profile of the mantle epithelium in *M. galloprovincialis* and *M. gigas* identified a species-specific transcriptional response to each of the challenges that may be linked to their differing shell composition and structure, physiology and ecology. To facilitate comparisons between the main transcriptional response to OA, SS and SSOA of *M. galloprovincialis* and *M. gigas*, models were constructed for each condition based on the identified DE gene transcripts and their deduced proteins (Figure 3.4 A – C).

For model construction the protein annotation of DE gene transcripts of *M. galloprovincialis* and *M. gigas* was established and detailed mapping of annotated genes to each of the experiments was established (see the supplementary results for more information). The main

categories used for mapping were as follows, transcription factors, shell matrix proteins (Supplementary Figure 3.9 A, D, Supplementary Figure 3.10 A and Supplementary Figure 3.11 A, D), ion pumps, receptors, and other cell membrane proteins (Supplementary Figure 3.9 B-C, F, Supplementary Figure 3.10 B-C, F and Supplementary Figure 3.11 B-C, F), and enzymes (Supplementary Figure 3.9 C, E-H, Supplementary Figure 3.10 C, E-H, and Supplementary Figure 3.11 C, E-H) and as appropriate the putative subcellular location of the deduced proteins. The condition causing the most significant changes in gene transcripts that were primarily linked to shell construction was OA in the case of *M. galloprovincialis* and SSOA in the case of *M. gigas*, which will now be briefly considered in more detail.

Mapping DE genes to specific processes identified the major responses elicited by OA (SW_OA) in *M. galloprovincialis* (Figure 3.4 A). From a shell construction perspective DE genes included, a) genes encoding chitin synthase protein isoforms (2 up-regulated and 2 down-regulated), b) genes encoding 34 shell matrix proteins (SMP) of which 26 were up-regulated and, c) genes encoding ion pumps related to H^+ and organic carboxylic acid, which were up-regulated and transporters involved in the exchange of amino acids, organic cations and metabolites, which were down-regulated (Figure 3.4 A). From a regulatory perspective

eight TF families (9 TFs), twenty-three lncRNA cis-regulatory gene modules and two GPCRs (GPCR-157 and adhesion-GPCR) were detected (Figure 3.4 A, Supplementary Figure 3.9 D). Metabolic related processes were well represented in the DE genes of the mantle epithelium in *M. galloprovincialis*, and genes related to carbohydrate metabolism, glucose metabolism, protein ubiquitination and cell adhesion were up-regulated, and genes related to lipid metabolism, cell growth and proteolysis were down-regulated (Figure 3.4 A).

In relation to M. *gigas* the SSOA (SS_SSOA) combined challenge elicited the greatest transcriptional response in the mantle epithelium. Shell toolbox related DE gene transcripts included a) 27 genes encoding SMPs 18 of which were upregulated, b) of the 5 genes encoding ion transporters identified, Na^+, K^+ and an anion exchanger were down-regulated as well as a Ca^{2+} exchanger on the lysosome/vacuole membrane (Figure 3.4 A), and c) the carbonic anhydrase 2 (CAH2) gene was down-regulated (Supplementary Figure 3.11 E). In relation to regulation two genes for TF families (THAP, TF_bZIP) (Figure 3.4 C, Supplementary Figure 3.11 D), and 5 lncRNA cis-regulatory gene modules were identified (Supplementary Figure 3.4) as well as 4 genes encoding GPCRs (GPCR83, GRL101, PTGFR and adhesion-GPCR). The Ca^{2+} receptor and ion exchange regulatory protein (DPP6) cell membranes

were down-regulated. From a metabolic perspective, genes related to transferase and hydrolysis were up-regulated and genes of carboxypeptidase, protein folding, glutamate/glutamine metabolism and carbonic anhydrase were down-regulated, and oxidoreductase genes were both up- and down-regulated (Figure 3.4 C, Supplementary Figure 3.11 C, E-H).

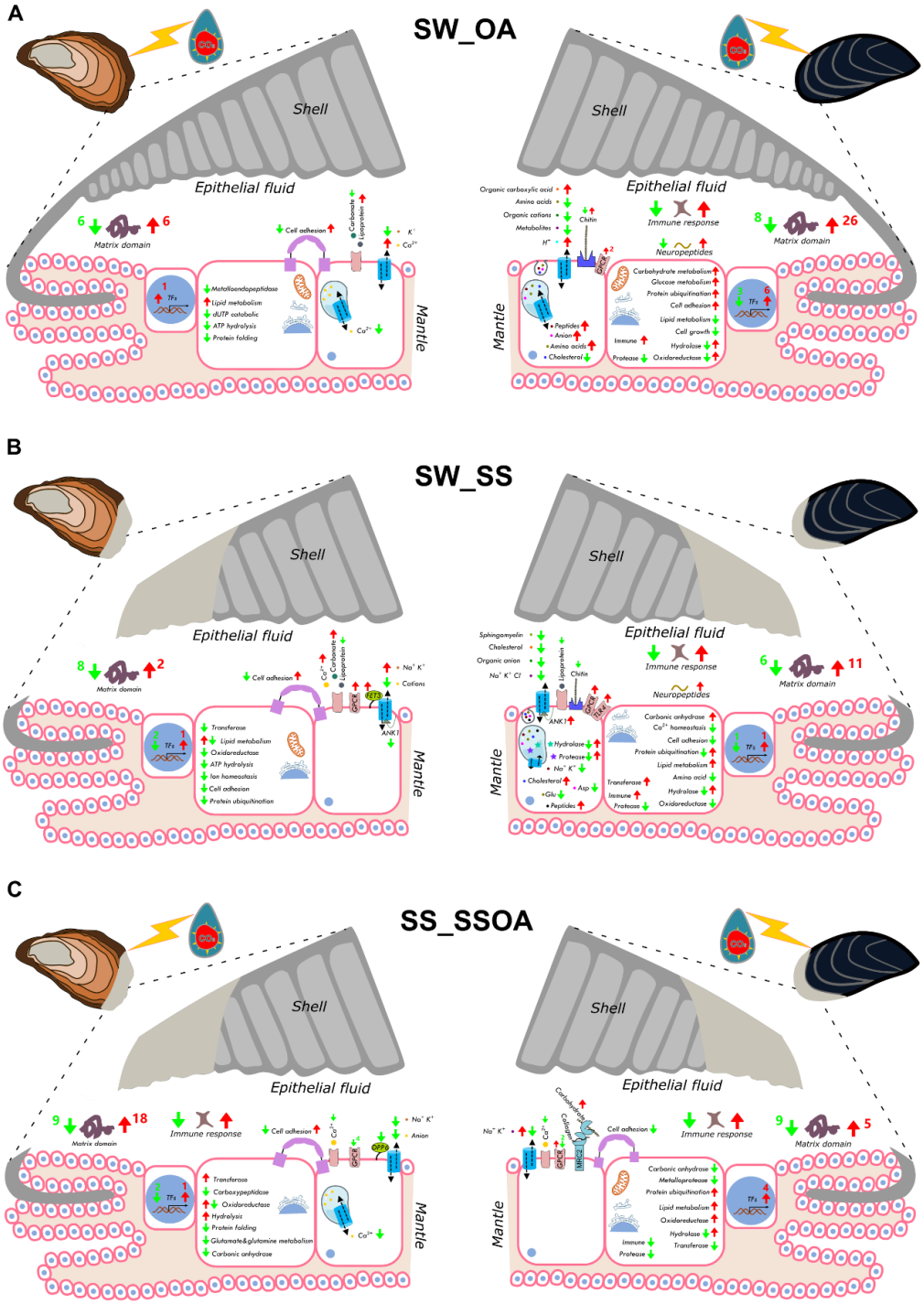

Figure 3.4. Schematic model established based on the DEGs in the mantle in response to SW_vs_OA (A), SW_vs_SS (B), and SS_vs_SSOA (C) stress in *M. gigas* and *M. galloprovincialis*. The red and green arrows appearing next to the text indicate up- or down-regulation of the function item/substance/domain/receptor, respectively. The presence of two-coloured arrows in an entry item means that there are both up- and down-regulated genes in that item. Cell-to-external exchange systems (cell membrane and lysosome/vacuole) is concentrated in a magnified cell representing the material exchange of the cell under

stress. Intracellular enzyme activities and biological processes are concentrated in a magnified cellular representation of intracellular responses. Transcription factors (TFs) are individually displayed in a cell with a magnified nucleus. Immune and biomineralized matrix protein domains are displayed in the epithelial fluid (in the extrapallial space). See supplementary Figure 3.9-11 for details of genes/domains distributed in organelles, and supplementary table 3.6 for gene information with abbreviated names.

3.5 Discussion

The commercially valuable bivalves, *M. galloprovincialis* and *M. gigas*, have a wide global distribution in coastal areas and understanding their response and adaptability to changing ocean conditions is crucial from both a socioeconomic and biodiversity perspective. Although *M. galloprovincialis* and *M. gigas* occupy nearly identical ecological niches that is, hard substrates in intertidal and subtidal habitats, they exhibit completely different shell shapes, shell calcium carbonate crystal types, and substrate attachment. Furthermore, although superficially *M. galloprovincialis* and *M. gigas* had a similar physiological response to 60 days of OA (pH 7.8) such as the significant reduction in their soft body mass and shell growth and changes in shell colour, the response of the mantle transcriptome in the two species was very different. The difference was further emphasised when the responsiveness of the mantle to shell thinning and OA (SS_SSOA) in *M. galloprovincialis* and *M. gigas* was compared. For example, a combined challenge (SS_SSOA) elicited a greater transcriptional response than all other treatments in *M.*

gigas but a combined challenge elicited the lowest response in *M. galloprovincialis* compared to other treatments. We propose that the differing response of the mantle to OA and SS revealed by the transcriptome reflects, i) a direct response by the mantle to elevated pCO_2 and a decrease in pH in the case of OA and ii) a hitherto unreported capacity of bivalves to sense and respond to shell thinning, which is known to occur under prolonged OA conditions (Gazeau et al., 2014), in corals that have calcium carbonate (aragonite) structures (Albright, 2011). Overall, the very different response of the two bivalve species in our study, highlights the need for caution when generalising about the likely consequences of OA on calcifying organisms like bivalves.

Previous studies on bivalves have reported that OA affects a plethora of processes including reproduction, survival, metamorphosis of larvae, growth, substrate attachment, and pathogen infection (Asplund et al., 2014; Kong et al., 2019; O'Donnell et al., 2013; Tan et al., 2020; Tan and Zheng, 2020; Zhao et al., 2020). The response of bivalves to elevated pCO_2 is species-specific and stage-specific during development (Gazeau et al., 2013; Tan and Zheng, 2020), and there are even cases where OA does not affect some bivalve species (Waldbusser et al., 2016). In the present study, the growth of both *M. galloprovincialis* and *M. gigas* was significantly inhibited under 60 days of OA exposure, and in concordance with previous studies *M. galloprovincialis* secreted more byssus threads

to compensate for byssus weakening (Zhao et al., 2017). OA has a well described inhibitory effect on the growth rates of *M. edulis* larvae and adults (Gazeau et al., 2010; Thomsen and Melzner, 2010), but in adult *M. gigas*, OA is not reported to modify shell growth (Lannig et al., 2010; Rajan et al., 2021), although it negatively affects the development and calcification of *M. gigas* larvae (Kurihara et al., 2007). Our results are not in entire agreement with previous OA studies since *M. galloprovincialis* and *M. gigas* juveniles maintained under OA conditions (pH 7.8) had a significant growth inhibition although the effect on *M. galloprovincialis* juveniles was more pronounced. Similar observations of a divergent response to OA between *M. gigas* and a mytilidea, *M. edulis*, has previously been reported (Gazeau et al., 2007), and the inhibition of shell calcification was approximately 2.5 times higher in *M. edulis*. Our study brings insights, that is currently lacking, into the molecular mechanisms that may explain the differing responsiveness of these bivalves to OA. Furthermore, we uncovered different molecular signatures in the mantle of each species after 60 days OA, shell thinning (mechanically, SS) or the combination of both challenges.

The genome and global mantle transcriptome of *M. galloprovinciallis* and *M. gigas* was compared to confirm that the different results obtained when each species was exposed to a similar experimental challenge was

not just a reflection of their very different genomes and protein coding gene content (e.g. *M. galloprovinciallis* has four times more genes than *M. gigas*). A comparison of the global mantle transcriptome revealed that the two species shared at least 82% of the gene transcripts expressed by the mantle (Figure 3.2 C) but that only 8 - 13% of the DE genes identified under OA, SS or SSOA were shared supporting the notion of a species-specific response to each challenge (Figure 3.2 B). Of note in both *M. galloprovinciallis* and *M. gigas* was the relatively small number of DE gene transcripts in the mantle after exposure for 60 days to OA, SS or SSOA. This may be explained by current understanding and concepts linked to eukaryotic gene regulation systems established by examining transient and steady state gene expression (Braun and Brenner, 2004). Such studies, although mainly on simple or single cell organisms reveal that following an environmental change, after an initial transient global change in gene transcript abundance, cells adapt to a new steady state, with a gene expression programme similar to the pre-environmental change state (Braun and Brenner, 2004; Gasch et al., 2000). The results of our study on *M. gigas* and *M. galloprovincialis* suggest that at the level of the mantle a new steady state was established in response to OA, SS and SSOA, since the bulk of the transcriptome was like the pre-environmental change state (or control in this case) but that in *M. galloprovincialis* a greater number of new genes linked to shell construction and metabolism

were recruited to the new steady state under OA (and other challenges). Species-specific differences in the subcellular location of DE protein-coding genes induced by OA were identified, but in both species, they were mainly assigned to the intracellular and extracellular regions of mantle cells. Further functional gene ontology (GO) annotations revealed that intracellular genes were primarily involved in metabolic processes, developmental processes, response to stimuli, and immune system functions. The largest difference between *M. galloprovincialis* and *M. gigas* was at the level of metabolic process-related genes.

At the molecular level OA has been proposed to inhibit metabolism-related gene transcripts in bivalves (Chapman et al., 2011; Clark et al., 2013; Johnson and Hofmann, 2017; Rajan et al., 2021), although the physiological energetics (e.g. increased ion pumping etc) and overall energy expenditure is increased (Gu et al., 2019; Pörtner et al., 2004). For example, Chandra Rajan et al., (2021) conducted a transcriptomic study on *Crassostrea hongkongensis* and found that OA inhibited metabolism-related genes. Similarly, in a study of *M. gigas*, OA reduced the content of metabolites in muscle and decreased alanine, glycogen, and ATP in the mantle (Lannig et al., 2010). In our study OA inhibited ATP metabolism-related functional genes in *M. gigas* and a metabolic-related effect was detected in the mantle DE transcriptome under OA, SS and SSOA in both

species. In *M. galloprovincialis* up-regulation of metabolism-related genes was observed in OA and this agrees with the results of other studies of the genus *Mytilus*. For example, it was shown that although there was decline in aerobic metabolism in *M. galloprovincialis* in response to high pCO_2, there was a parallel increase in ammonia excretion, which is indicative of enhanced protein catabolism (Michaelidis et al., 2005). The energetics of the physiological response to OA (and related challenges) need to be taken into account when interpreting transcriptome results since there is a consensus that cellular metabolism and gene expression are coupled (Braun and Brenner, 2004). In fact, since changes in metabolism occur in a shorter timeframe relative to gene expression, metabolism has been proposed to drive related adjustments in gene expression (Braun and Brenner, 2004).

However, Despite the apparent metabolism-related modifications in gene transcripts in OA, SS and SSOA experimental groups only the OA groups in *M. galloprovincialis* had a significantly reduced soft body growth and shell growth. The inhibition of growth under OA is presumably a consequence of the need to balance the increased metabolic demand at a whole organism level with the increased energetic needs for the construction of the crystalline structure of its hard shell (Ren et al., 2009). Overall, in both *M. galloprovincialis* and *M. gigas* it seems that

the experimental conditions modified energy demand and this was reflected by body growth inhibition and by some of the DE transcripts in the mantle and this metabolic phenomenon has previously been considered a major causative factor of shell growth inhibition (Kobayashi and Samata, 2006; Lannig et al., 2010; Ren et al., 2020). Nonetheless, in both *M. gigas* and *M. galloprovincialis* in our study the shell continued to grow, albeit more slowly, under OA and DE gene transcripts associated with the regulation and production of shell were identified. The greater recruitment of new gene transcripts to a "new steady state" in *M. galloprovincialis* compared to *M. gigas* under a modified environment may be indicative of increased plasticity in the former species, a factor proposed to favour adaptability and survival (Bateson, 2014).

An alternative hypothesis to explain the divergent response of the steady state gene expression observed between *M. galloprovincialis* and *M. gigas* exposed to OA, SS or SSOA may be linked to the characteristics of the shell. As bivalves have a limited ability to regulate extracellular pH (Michaelidis et al., 2005; Waldbusser et al., 2015), changes in the carbonate system in hemolymph and the extrapallial fluid are believed to affect the shell-forming process. This can occur either through inner shell surface dissolution or due to changes in extra-/intracellular ion composition, which affect cellular homeostasis and the precipitation of

amorphous calcium carbonate (Melzner et al., 2011; Thomsen and Melzner, 2010). Lu et al., (2018) reported that in comparison to normal seawater, the proportion of calcium carbonate derived from environmentally soluble inorganic carbon in *M. edulis* shells decreased from 80.3% to 62.3% under OA exposure, with the remaining portion attributed to metabolism. These findings suggest that *M. galloprovincialis* incurs a higher metabolic cost under OA exposure compared to *M. gigas* and this may explain the more pronounced inhibition of shell growth. The higher cost of shell growth in *M. galloprovincialis* may be associated with the construction of the energetically costly and more slowly growing thick nacreous layer (aragonite crystal structure), and we propose other bivalves with a similar shell structure will be affected by OA in a similar way (Waldbusser et al., 2016). The higher energetic cost of aragonite rich shells has been proposed to be a consequence of the lower stability of the crystals compared to calcite in natural environments (Niu et al., 2022; Santos and Gerven, 2011; Shi et al., 2019). This hypothesis is supported by studies that revealed exposure to 800 μatm or 1200 μatm pCO_2 decreased the ratio of aragonite-to-calcite in *M. galloprovincialis* shells to 7-8% and 18%, respectively (Lassoued et al., 2019). Interestingly, providing more food under modified pCO_2 (800 and 1200 μatm) did not modify the aragonite-to-calcite ratio in the shells of *M. galloprovincialis*, which contrasts with oysters (*C. virginica*) where increased food

availability restored shell mineralization inhibited by OA (Clements et al., 2017; Lassoued et al., 2019). Given that *C. virginica* and *M. gigas* have nearly identical shell structures, with low-energy-consuming calcite shells they are likely to be less affected by OA, which seems to be corroborated by its lesser effect on body growth, shell growth, enzyme activity and gene transcripts in *M. gigas* in our study.

A further observation coming from our study was the divergent response at the level of genes for SMPs, ion pumps, and enzymes in *M. galloprovincialis* and *M. gigas* under OA, SS and SSOA, which reiterates the idea of lineage- and species-specific evolution of biomineralization toolbox genes and regulation of shell construction (Clark et al., 2020). Considering the transcriptome data *M. galloprovincialis* exhibited a greater response to OA compared to *M. gigas*, with increased expression of ion pumps, chitin synthases, SMPs, and regulatory factors (TFs, and lncRNAs) involved in mineralization. A recent study identified lncRNAs, as new members of the bivalve mineralization toolbox, with strong lineage specificity (Peng et al., 2023) and acting as cis-regulatory factors of SMPs, that are involved in shell growth in *M. gigas*. Intriguingly, in the present study differential expression of lncRNAs was only identified in *M. galloprovincialis*, and this may contribute to explain the more negative impact of OA on the shell growth in *M. galloprovincialis*. An

example, of lineage-specific functional evolution comes from nacrein, the first discovered SMP, which plays a key role in the formation of aragonite crystals in the nacreous layer of the pearl oysters (Zhang et al., 2003), but in the oyster (*M. gigas*) where it is also highly expressed nacrein promotes the formation of calcite crystals (Oliveira et al., 2012).

Unexpectedly under all experimental conditions (OA, SS and SSOA) several G-protein coupled receptors (GPCRs) that are generally low abundance and therefore often missed in transcriptome studies were identified among the DE genes, e.g. Adhesion-GPCR, GPCR83, GRL101, PTGFR, 5HT-GPCR, GPCR157, Calcitonin-like-GPCR and GPCR158. Many of the GPCRs identified do not have a cognate ligand assigned and are considered orphans, although several peptide precursor gene transcripts e.g. small cardioactive peptides-like, APGW-amide-related neuropeptide and Thyrostimulin beta-5 subunit were also identified in mantle DE genes. Several recent studies in mussel (*M. galloprovincialis*) have identified neuropeptides (eg: calcitonin's) and their putative GPCRs as regulators of mantle function and shell growth (Cardoso et al., 2020, 2016; Li et al., 2021) and the identification of Calcitonin-like-GPCRs among the DE genes further highlights a role of the calcitonin system in bivalve shell construction (Cardoso et al., 2020). Although not identified in the present study other regulatory factors of the mantle include insulin-

like peptides that stimulate protein synthesis in mantle edge cells and regulate the growth of the mantle edge and the shell in the gastropods (*Otala lacteal* and *Helisoma duryi*), and in a bivalve (*M. gigas*) (Abdraba and Saleuddin, 2000; Gricourt et al., 2003; Saleuddin et al., 1992). Overall, the transcriptome results support the proposal of a conserved core biomineralization toolbox enriched with lineage- and species-specific genes and highlights the need for work in the neglected area of shell growth regulation.

The conjunction of OA with another stressor, shell thinning (SSOA), induced a much more pronounced response in *M. gigas* juveniles relative to other experimental conditions. In contrast, although overall *M. galloprovincialis* had a greater number of modified genes relative to *M. gigas*, compared to the other experimental treatments the response to SSOA was diminished. More work will be required to understand the factors explaining this difference (i.e. rapid resolution of shell thinning, different gene regulatory networks etc). The intriguing observation was a) that shell thinning induced a transcriptional response and b) there was a divergent transcriptional response between OA and shell thinning. We hypothesise that the response to OA is a direct effect of low pH on the mantle, while the response to shell thinning suggests the mantle senses a change in the calibre of the shell at the edge and this triggers a “repair”

response. The analysis of shell sanded transcriptomes (SS group) in our study revealed that the genes involved in shell repair in *M. galloprovincialis* were 4.5 times more abundant than in *M. gigas* (Figure 3.5). The main differences between the response of *M. galloprovincialis* and *M. gigas* were observed in the metabolic enzyme activity in the cytoplasm and molecular transport in the membrane system, along with a substantial number of species-specific lncRNAs and neuropeptides, suggesting the former species has an overall more complex shell growth process and regulation. We speculate that species that require a larger number of mineralization tools or invests more energy in constructing relatively unstable calcium carbonate crystals, the negative impact of OA on the metabolism of mantle cells and the energy cost will profoundly affect the utilization of mineralization tools and crystal formation.

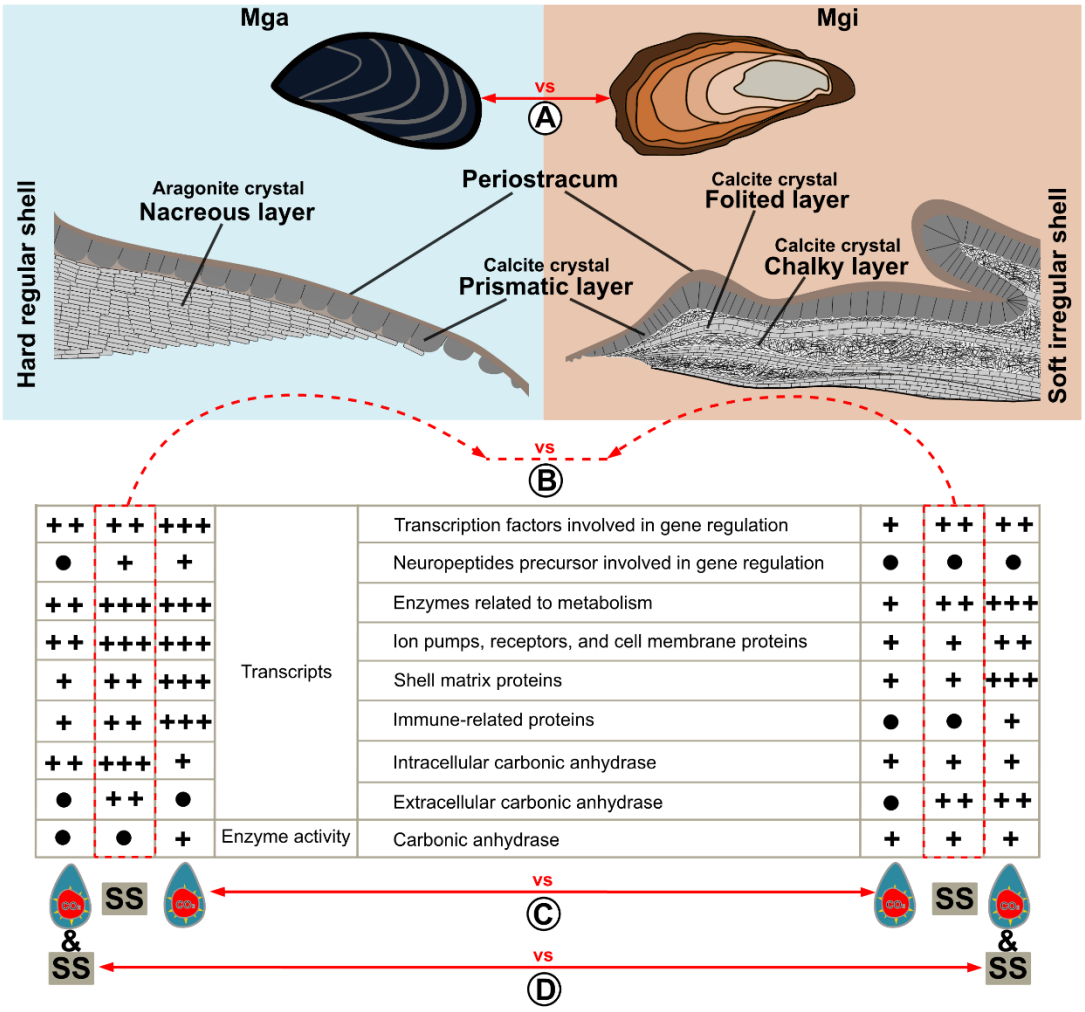

Figure 3.5. *M. galloprovincialis* and *M. gigas* respond differently to environmental change. There are differences in the genetic background, shell material, and microstructure of *M. galloprovincialis* and *M. gigas*. (A) Approximately 40% of the protein-coding genes in the genome of *M. galloprovincialis* and *M. gigas* are homologous between species. However, over 70% of the fundamental components (domains) in the known biomineralization tool genes are shared by both species. The experimental shell repair response suggests the existence of different biomineralization mechanisms between *M. galloprovincialis* and *M. gigas*. (B) This difference is reflected in the more significant reduction in growth (presumably due to increased energy expenditure) of *M. galloprovincialis* and the utilization of more genes to construct the intricately designed and regularly arranged calcium carbonate crystals. (C) Under OA stress, *M. galloprovincialis* mobilizes a greater number of genes compared to *M. gigas*, while consuming more energy to maintain the construction of energy-intensive calcium carbonate crystal shells. In an environment exposed to OA, if the shell is damaged, it further affects the shell-building behavior of the mantle. (D) Under OA stress, the damaged shell of *M. galloprovincialis* exhibits a greater mobilization of genes (primarily species-specific unknown genes) compared to *M. gigas*,

which are used for repairing the damaged shell and further shell construction.

3.6 Conclusion

OA is inevitable and it seems likely the 2100 predicted drop in seawater pH may be reached sooner with still unforeseen consequences for calcifying marine organisms. The insight provided by our study about the molecular processes in the mantle under OA, SS and SSOA indicates that *M. galloprovincialis* and *M. gigas* respond differently and suggests shell type will determine the response. The differing responsiveness of *M. galloprovincialis* and *M. gigas* to OA, SS and SSOA, as indicated by the new steady state of gene transcription from their biomineralization toolbox and energy-related and regulatory-related gene transcripts for shell production, shell composition, and microstructure suggests the plasticity of their response differs. This difference is not a consequence of the almost 3 times more protein coding genes in the genome of *M. galloprovincialis* compared to *M. gigas* as the number of genes expressed in the mantle of the 2 species was similar and over 80% of them were homologues. The bigger suite of regulatory factors (non-coding RNA, TFs, peptides) in the DEGs of *M. galloprovincialis* mantle transcriptomes exposed to OA, SS and SSOA may explain their greater capacity to regulate the biomineralization toolbox genes and may explain their

reduced growth as energy is diverted to the more costly process of building aragonite crystals and packing them into a regular arrangement.

The more plastic molecular and cellular response of *M. galloprovincialis* exposed to OA, SS or SSOA compared to *M. gigas* presumably explains the greater physiological adaptability reported for *M. galloprovincialis*, which is no doubt one factor explaining its reputation as *"one of the worst invasive species*" in the world (IUCN http://www.iucngisd.org/gisd/species, (Hockey and Schurink, 1992; Pickett and David, 2018). The importance of plasticity for adaptability to climate change is further emphasised by studies with genetically diverse *M. galloprovincialis* larvae exposed to OA, which showed that genetic and phenotypic variation was associated with better adaptation to declining seawater pH (Bitter et al., 2019). This suggests that from both an environmental and aquaculture perspective strategies that promote genetic diversity within bivalve populations will increase species' adaptability and survival under changing environmental conditions.

3.7 Supplementary materials

3.7.1 Supplementary results (in Annex III, digital format)

All the supplementary results are provided in the Annex III in digital format.

3.7.2 Supplementary Figures

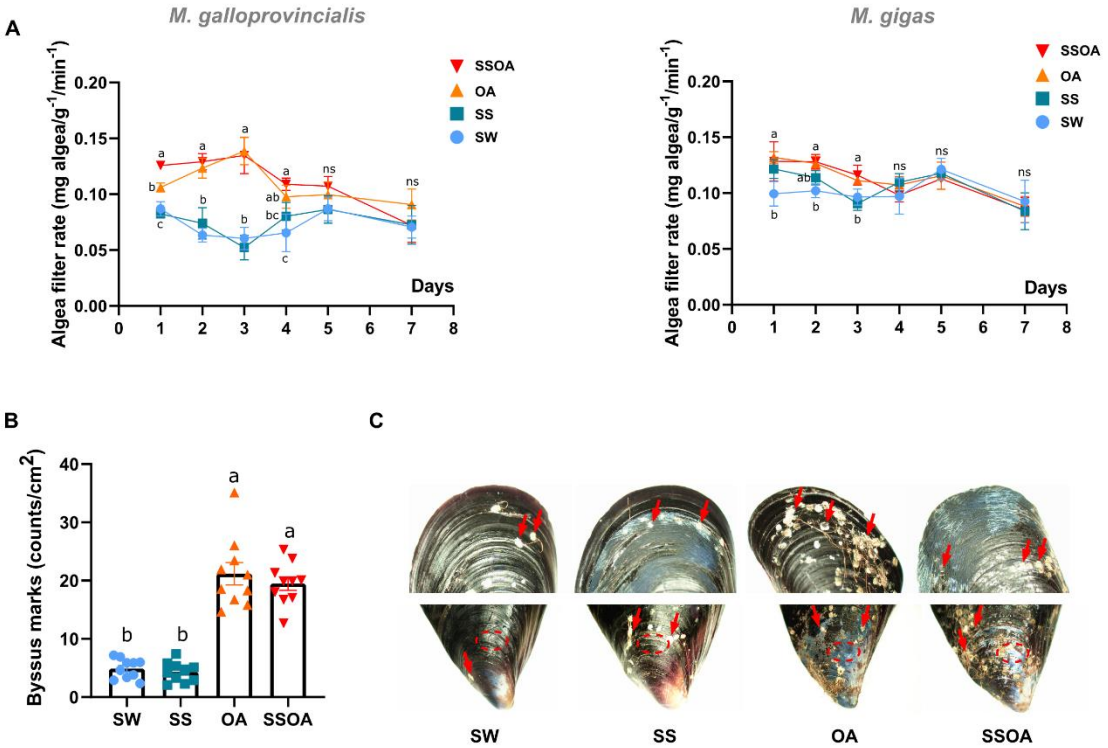

Supplementary Figure 3.1 Changes in feeding rates and shell outer surface of *M. galloprovincialis* and *M. gigas* under SW, SS, OA, and SSOA conditions. (A) Values represent the mean ± SEM (n = 4 assays with 10 mussels/assay and 5 oysters/assay). Different letters indicate significantly different groups ($p < 0.05$). (B) Number of byssus thread marks on the outer shell surface of *M. galloprovincialis*. Values represent the mean ± SEM (n = 10). Different letters indicate significantly different groups ($p < 0.05$). (C) Image of the *M. galloprovincialis* outer shell showing the byssus thread marks (red arrow) and changes in the periostracum organic layer (area around the red circle) after 60 days experiment.

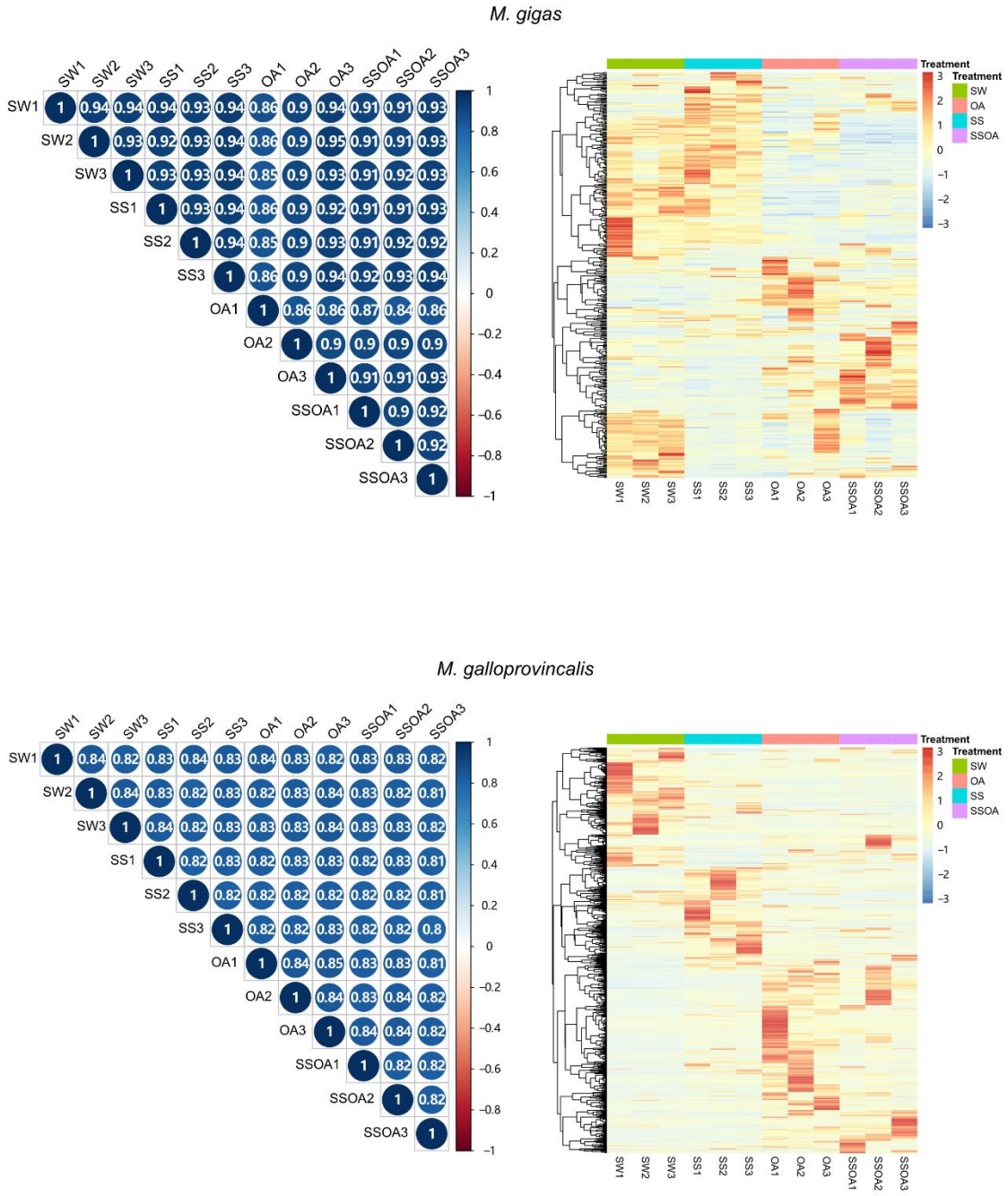

Supplementary Figure 3.2 Correlation analysis and heatmaps of the transcriptome samples. Gene transcript levels of transcriptome samples were used to draw correlation analysis plots (left). Correlation analysis plots were performed using the corrplot package and heatmaps using the pheatmap package in R Studio. Visual comparisons at the transcriptional level of sample biological replicates between treatment groups are shown using heatmap plots (right).

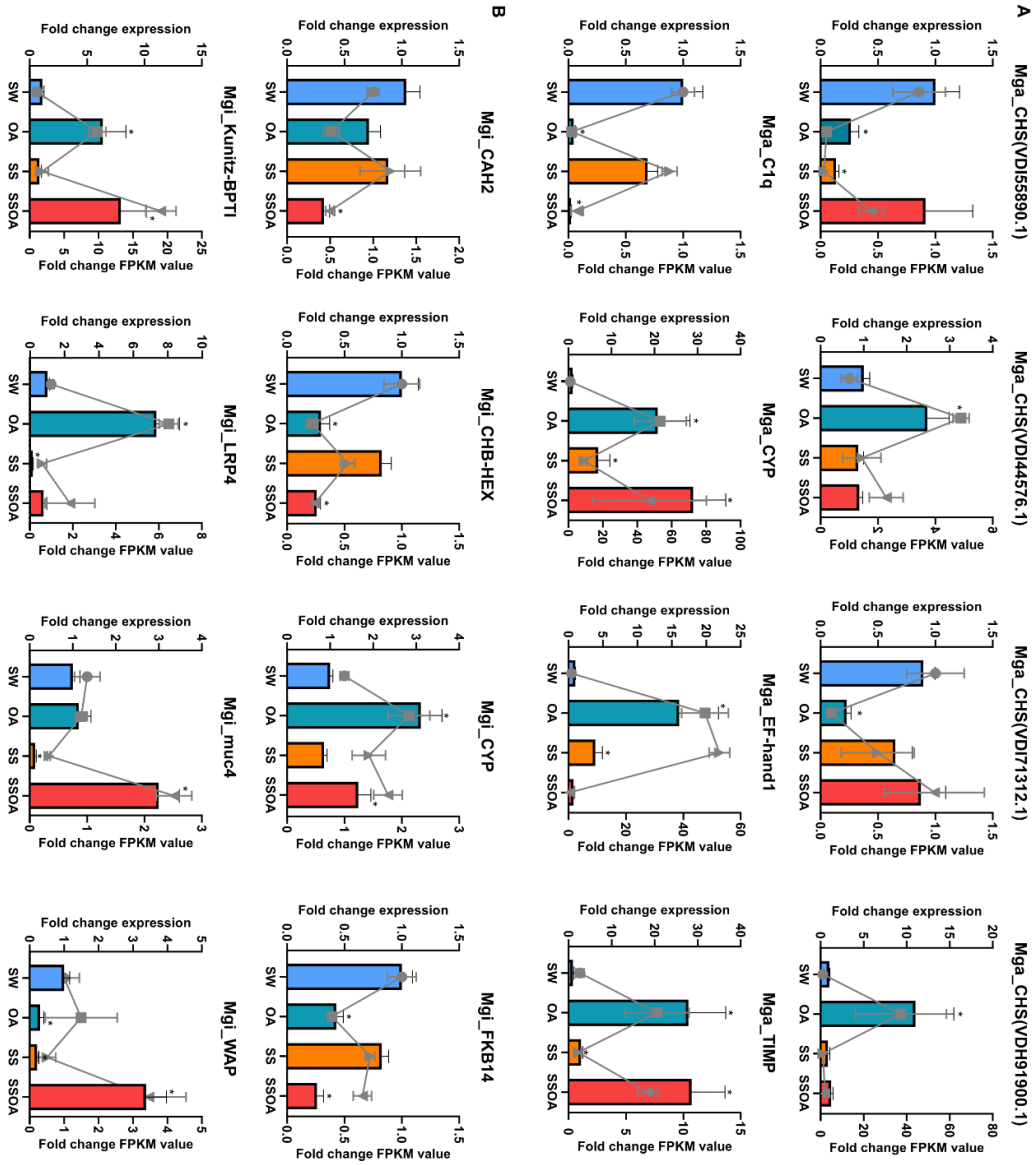

Supplementary Figure 3.3 Analysis by qPCR of selected differentially expressed genes in the transcriptome. Expression of sixteen candidate gene transcripts (corresponding to eight candidate *M. galloprovincialis* genes (A) and eight candidate *M. gigas* genes (B)) were assessed by qPCR of mantle edge RNA from the samples that were sent for RNA Seq (SW, OA, SS and SSOA). Each graph represents the expression profile of each gene. The histogram and the Y-axis coordinates on the left indicate the q-PCR results, and the line graph and Y-axis coordinates on the right indicate the transcriptome data. Relative expression was calculated by normalization using the average of the expression of two reference genes that did not vary in expression (EF1α and RL7 in *M. gigas*; EF1α and 18S in *M. galloprovincialis*). Fold change of expression was calculated by comparing the average normalized expression of the control (SW group) versus the treatment. The fold change FPKM value in the figure was calculated by comparing the average of the transcriptome FPKM value of each treatment group with the average of the FPKM value of the control

(SW group). Statistical analysis was performed for the qPCR results using a t-test and the data represents the mean ± SEM of n = 6 biological replicates. Asterisks indicate significantly different groups at $p < 0.05$.

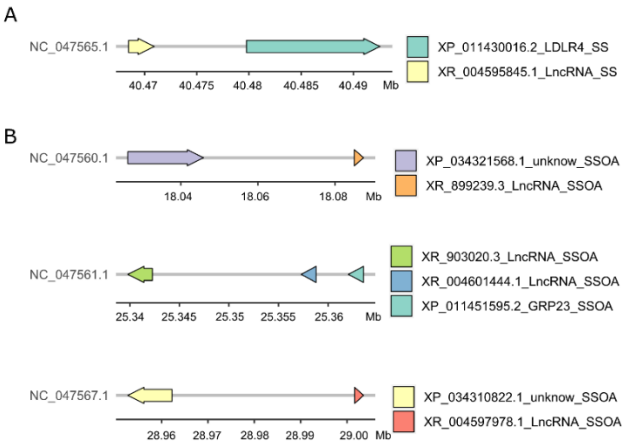
A
NC_047565.1
XP_011430016.2_LDLR4_SS
XR_004595845.1_LncRNA_SS
40.47 40.475 40.48 40.485 40.49 Mb
B
NC_047560.1
XP_034321568.1_unknow_SSOA
XR_899239.3_LncRNA_SSOA
18.04 18.06 18.08 Mb
NC_047561.1
XR_903020.3_LncRNA_SSOA
XR_004601444.1_LncRNA_SSOA
XP_011451595.2_GRP23_SSOA
25.34 25.345 25.35 25.355 25.36 Mb
NC_047567.1
XP_034310822.1_unknow_SSOA
XR_004597978.1_LncRNA_SSOA
28.96 28.97 28.98 28.99 29.00 Mb


C
UYJE01000478.1
ncRNA_MGAL_10NCA043414_OA
VDH93633.1_OA
UYJE01000980.1
VDH98173.1_OA
VDH98180.1_OA
ncRNA_MGAL_10NCA051954_OA
VDH98181.1_OA
ncRNA_MGAL_10NCA051956_OA
UYJE01001819.1
VDI05488.1_OA
ncRNA_MGAL_10NCA029248_OA
UYJE01001983.1
VDI06828.1_OA
ncRNA_MGAL_10NCA036154_OA
UYJE01001989.1
VDI06972.1_OA
ncRNA_MGAL_10NCA031909_OA
UYJE01002198.1
VDI08556.1_OA
ncRNA_MGAL_10NCA029334_OA
UYJE01002320.1
ncRNA_MGAL_10NCA016402_OA
VDI09649.1_OA
VDI09650.1_OA
UYJE01002738.1
ncRNA_MGAL_10NCA050293_OA
VDI13162.1_OA
UYJE01003330.1
ncRNA_MGAL_10NCA012833_OA
VDI18345.1_OA
UYJE01003556.1
ncRNA_MGAL_10NCA053185_OA
VDI20284.1_OA
UYJE01004632.1
VDI29805.1_OA
ncRNA_MGAL_10NCA016815_OA
UYJE01004638.1
VDI29943.1_OA
ncRNA_MGAL_10NCA059734_OA
UYJE01004694.1
ncRNA_MGAL_10NCA055184_OA
VDI30521.1_OA
UYJE01004727.1
VDI30893.1_OA
ncRNA_MGAL_10NCA035826_OA
UYJE01004850.1
ncRNA_MGAL_10NCA027131_OA
VDI31945.1_OA
UYJE01006065.1
VDI42692.1_OA
ncRNA_MGAL_10NCA009723_OA
UYJE01006504.1
VDI46553.1_OA
ncRNA_MGAL_10NCA055092_OA
UYJE01007037.1
ncRNA_MGAL_10NCA021504_OA
VDI51240.1_OA
UYJE01007303.1
VDI53483.1_OA
VDI53484.1_OA
ncRNA_MGAL_10NCA044634_OA
UYJE01010345.1
VDI82377.1_OA
ncRNA_MGAL_10NCA061633_OA
UYJE01010387.1
VDI82769.1_OA
ncRNA_MGAL_10NCA054162_OA
UYJE01010555.1
VDI84279.1_OA
ncRNA_MGAL_10NCA054188_OA

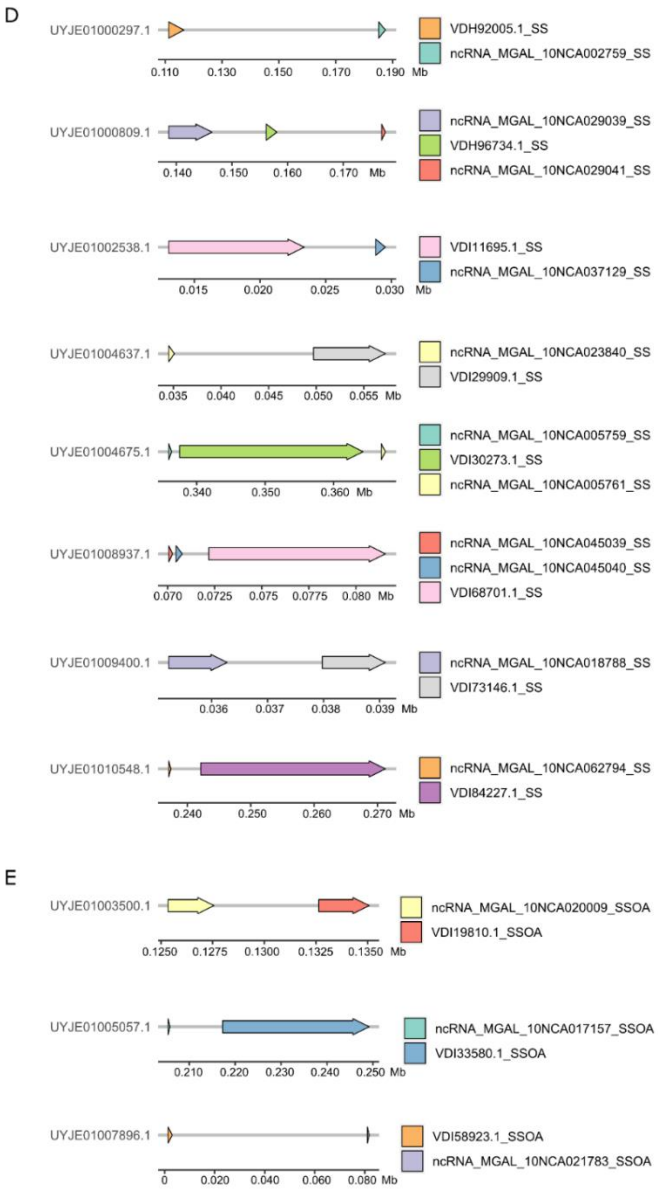

Supplementary Figure 3.4 Potential lncRNAs may participate in cis-regulation of genes and respond to experimental conditions. Mapping of DEGs in the *M. galloprovincialis* and *M. gigas* genomes and the identification of potential cis-regulatory modules were based on the distance (kb) between protein-coding and lncRNA genes in the genome (located < 100 kb distance). Chromosome accession numbers are shown on the left, and the black solid line shows the displayed chromosome region with a base distance scale. DEGs are represented by coloured arrows, the direction of the arrow represents the direction of the gene in the chromosome, and the length is based on the gene length. Gene transcript accession numbers and experimental conditions are shown on the right. The gene modules in the genome were identified using the gggenes package (ver 0.4.1) in R-studio (Wilkins, 2019). (A) *M. gigas*_SW_SS; (B) *M. giga*s_SS_SSOA; (C) *M. galloprovincialis*_SW_OA; (D) *M. galloprovincialis*_SW_SS; (E) *M. galloprovincialis* _SS_SSOA.

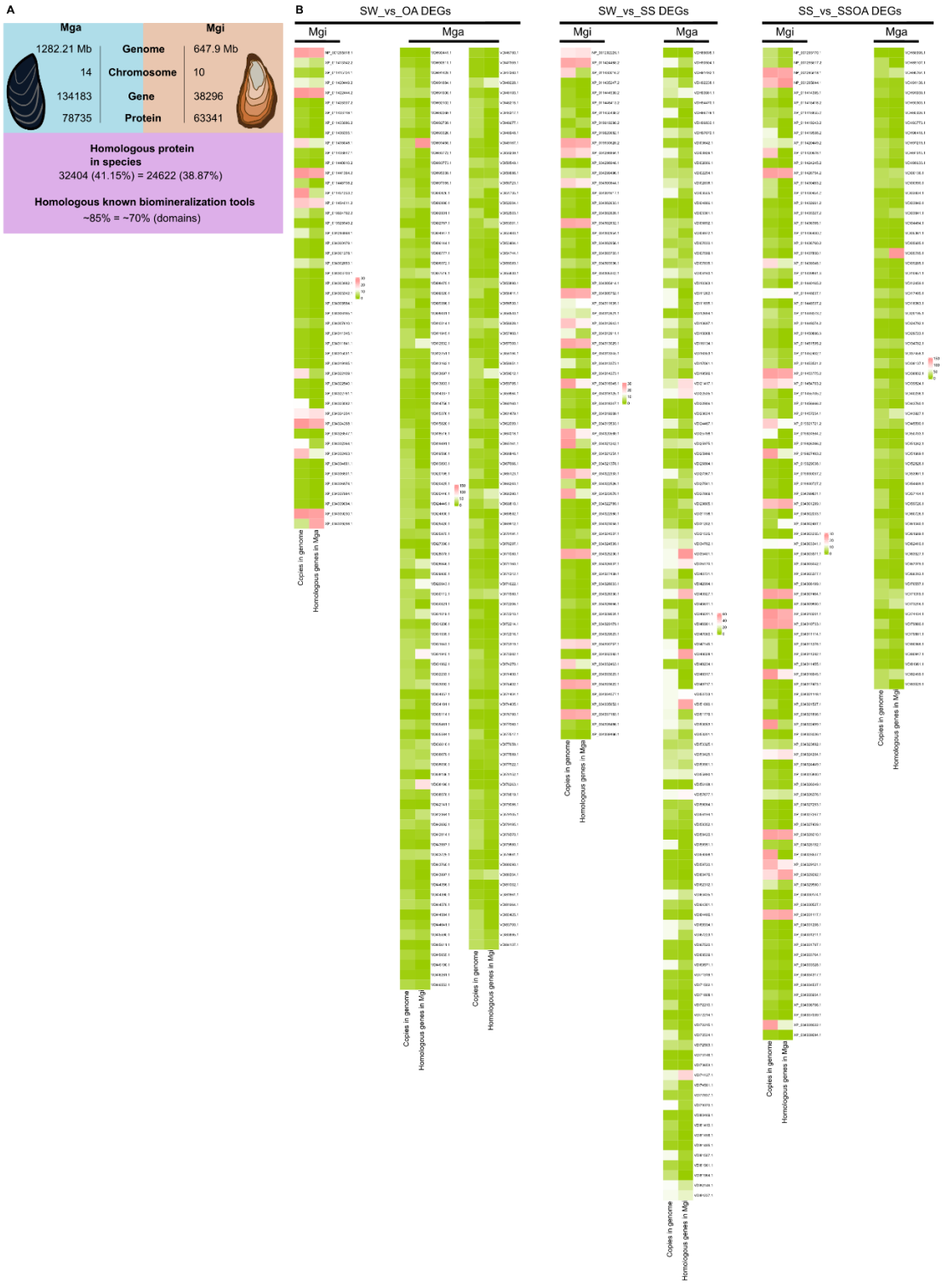

Supplementary Figure 3.5 *M. galloprovincialis* and *M. gigas* genetic background, interspecies homology comparisons of known DEGs and mantle expression profiles under experimental conditions. (A) The genetic background differences between *M. galloprovincialis* and *M. gigas* based on the reference genome information used. The numerical

value in parentheses indicates the percentage of homologue protein-coding genes between species taking into consideration the total number of protein-coding genes in each species genome. The percent of homologue genes coding biomineralization-related protein domains identified in each species and using published data to identify and annotate biomineralization-related genes in the genome. (B) Interspecies homology comparisons of identified DEGs under each experimental condition. The heatmap displays the copy numbers of known DEGs within and between species under each experimental condition.

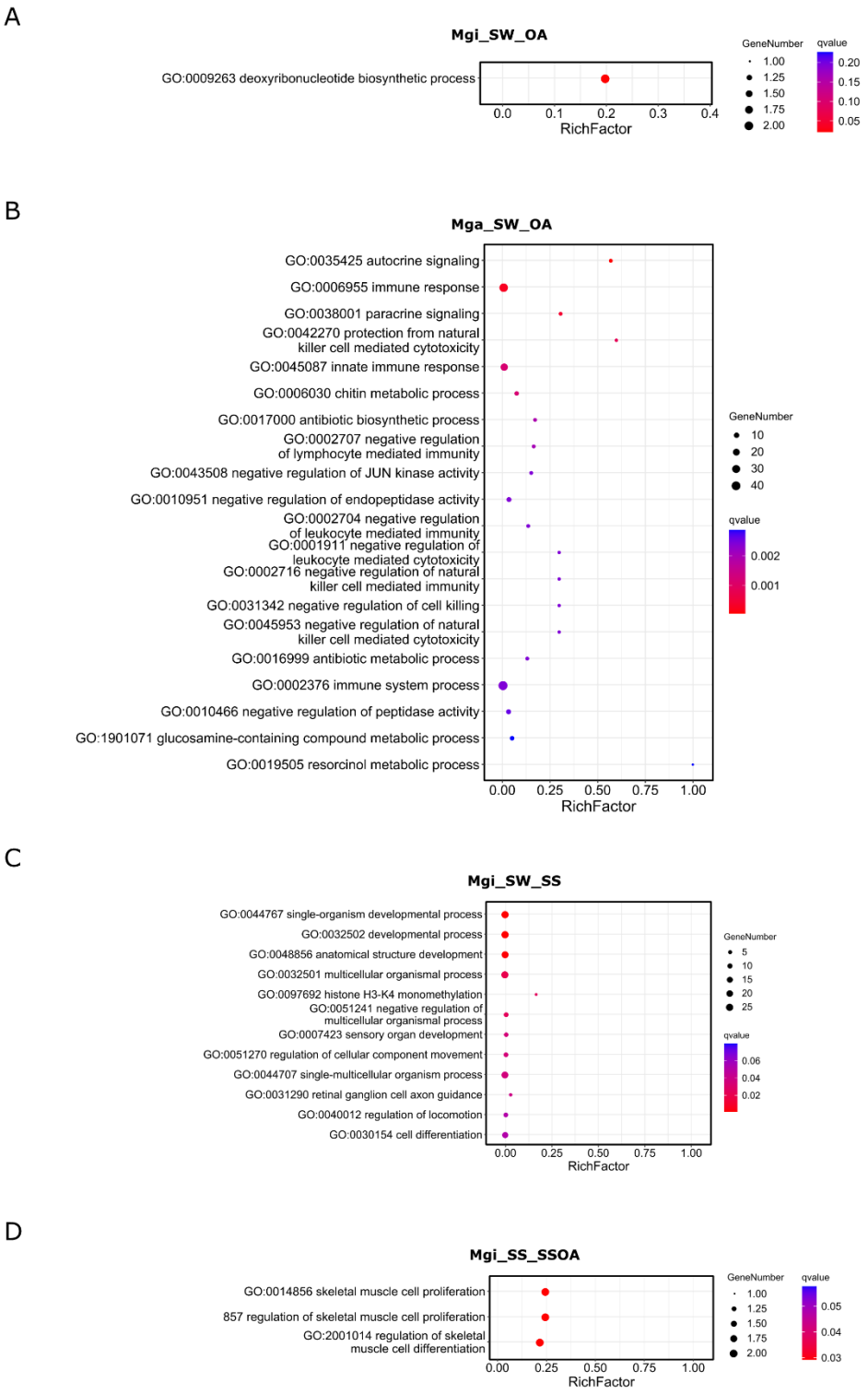

Supplementary Figure 3.6 GO enrichment distribution map of DEGs. (A) *M. gigas* SW_vs_OA 12h; (B) *M. galloprovincialis* SW_vs_OA; (C) *M. gigas* SW_vs_SS; (D) *M. gigas* SS_vs_SSOA. Different bubble volumes and colour depths represent different meanings. The larger the bubble volume, the greater the number of genes enriched in the pathway, and the darker the colour, the higher the degree of enrichment in the pathway. Horizontal axis represents the number of down-regulated genes,

and vertical axis represents the GO items. Experimental groups with no significant (qvalue < 0.05) enrichment of GO items is not shown.

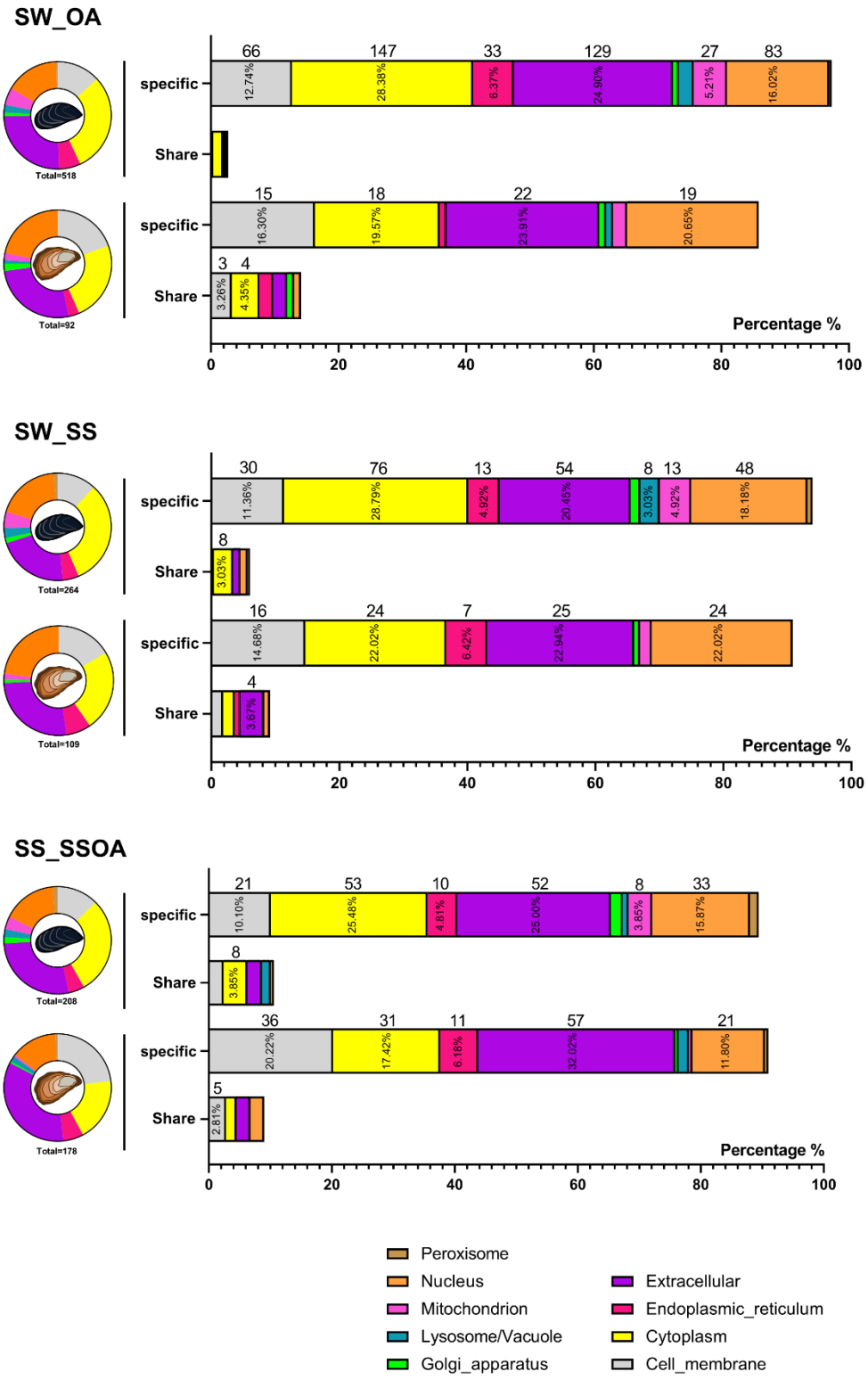

Supplementary Figure 3.7 Subcellar localization of the protein coding DE gene transcripts. Subcellar localization of protein coding gene transcripts was predicted by DeepLoc-1.0. Eight organelles and extracellular regions are shown using different colours. The doughnut plots represent the subcellar localization of coding DEGs in *M.*

galloprovincialis or *M. gigas* under each of the experimental conditions (SW_vs_OA, SW_vs_SS, and SS_vs_SSOA), while the bar plots independently show the subcellar localization of the shared DEGs (between oyster and mussel). The value inside the bar represents the relative proportion of the DEGs they represent, while the value above the bar represents the number of DEGs.

Supplementary Figure 3.8 Characterization of the *M. galloprovincialis* and *M. gigas* specific and shared extracellular domains of protein coding DE gene transcripts. (A-C) Analysis of SW_vs_OA, SW_vs_SS and SS_vs_SSOA comparisons. Domains were annotated based on Pfam identification. Domains found and IDs are indicated, and their relative

abundance (domain counts) is given by the bubble plot. Domains that scored only once or twice were grouped into the “one domain copy” and “two domain copies” category, respectively. The crosses represent absence, and the bubble size is proportional to the number of domains found and the numbers indicate the domain count number. Venn diagrams show the numbers of species specific and common DEGs in the mussel and oyster.

Supplementary Figure 3.9

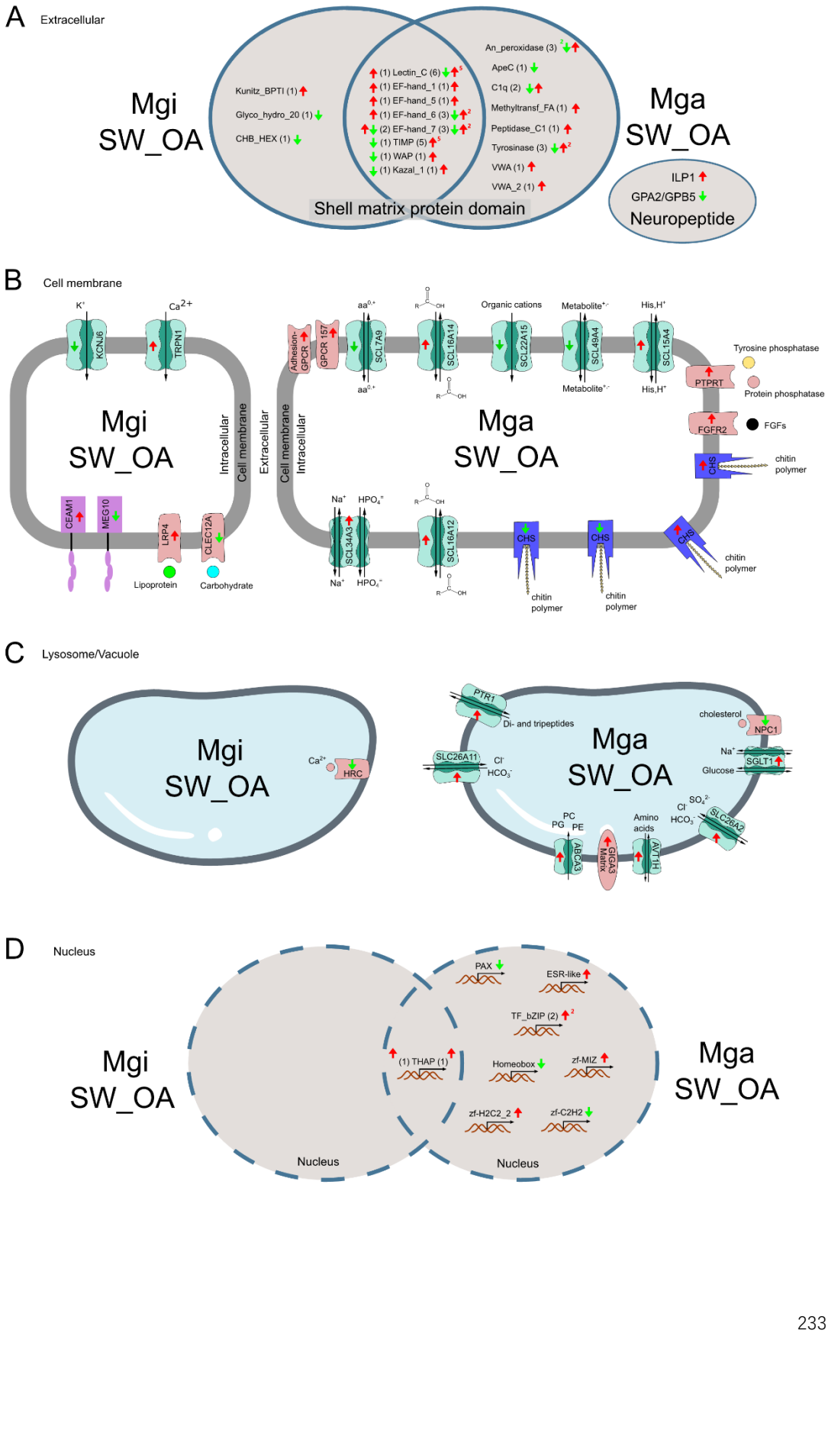

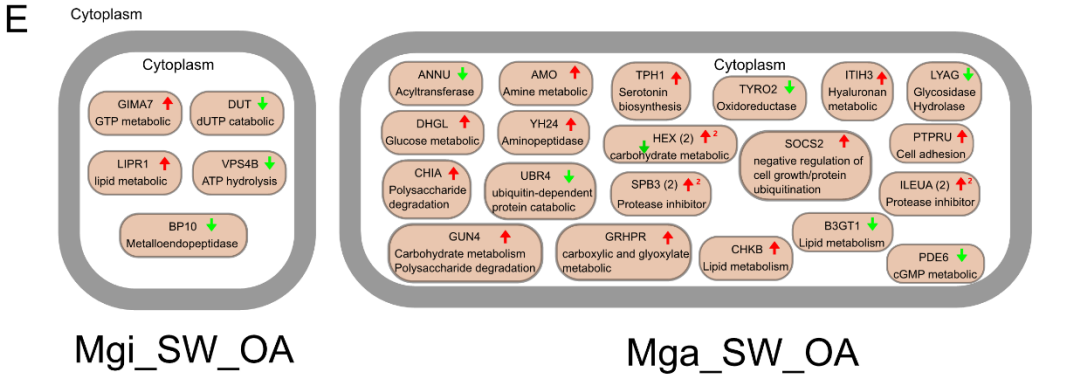
E
Cytoplasm
Cytoplasm
GIMA7
GTP metabolic
DUT
dUTP catabolic
LIPR1
lipid metabolic
VPS4B
ATP hydrolysis
BP10
Metalloendopeptidase
Mgi_SW_OA
Cytoplasm
ANNU
Acyltransferase
AMO
Amine metabolic
TPH1
Serotonin biosynthesis
TYRO2
Oxidoreductase
ITIH3
Hyaluronan metabolic
LYAG
Glycosidase Hydrolase
DHGL
Glucose metabolic
YH24
Aminopeptidase
HEX (2)
carbohydrate metabolic
SOCS2
negative regulation of cell growth/protein ubiquitination
PTPRU
Cell adhesion
CHIA
Polysaccharide degradation
UBR4
ubiquitin-dependent protein catabolic
SPB3 (2)
Protease inhibitor
ILEUA (2)
Protease inhibitor
GUN4
Carbohydrate metabolism
Polysaccharide degradation
GRHPR
carboxylic and glyoxylate metabolic
CHKB
Lipid metabolism
B3GT1
Lipid metabolism
PDE6
cGMP metabolic
Mga_SW_OA

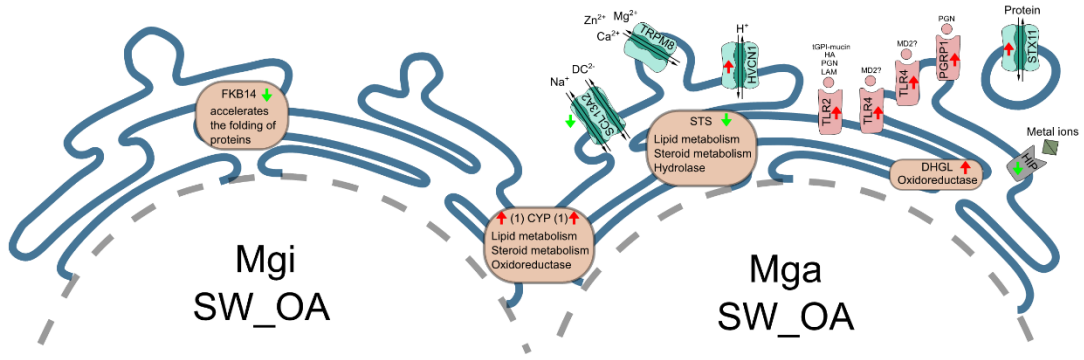
F
Endoplasmic reticulum
FKB14
accelerates the folding of proteins
Mgi
SW_OA
(1) CYP (1)
Lipid metabolism
Steroid metabolism
Oxidoreductase
TRPM8
HVCN1
SCN1/3/2
STS
Lipid metabolism
Steroid metabolism
Hydrolase
TLR2
TLR4
PGRP1
STX11
Protein
Metal ions
DHGL
Oxidoreductase
Mga
SW_OA

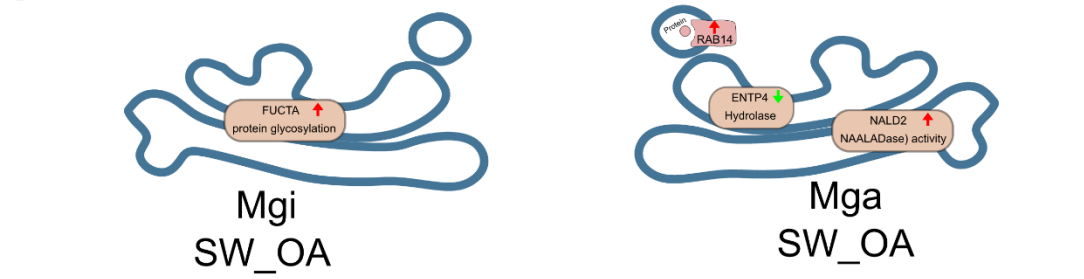
G
Golgi apparatus
FUCTA
protein glycosylation
Mgi
SW_OA
RAB14
ENTP4
Hydrolase
NALD2
NAALADase) activity
Mga
SW_OA

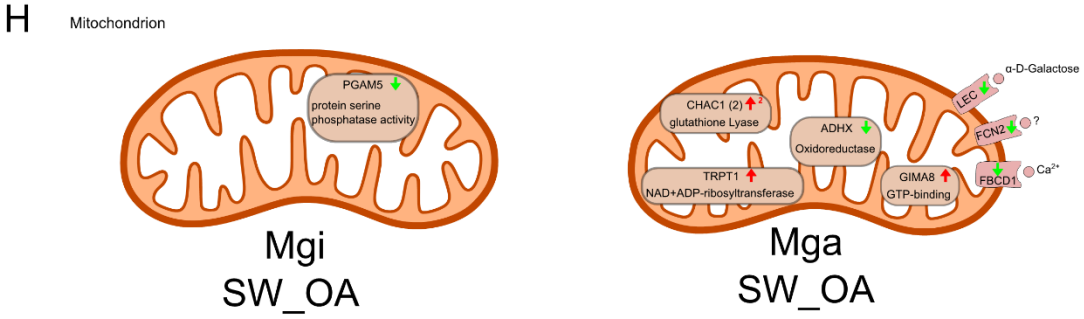
H
Mitochondrion
PGAM5
protein serine phosphatase activity
Mgi
SW_OA
CHAC1 (2)
glutathione Lyase
ADHX
Oxidoreductase
TRPT1
NAD+ADP-ribosyltransferase
GIMA8
GTP-binding
α-D-Galactose
LEC
FCN2
FBCD1
Mga
SW_OA

Supplementary Figure 3.10

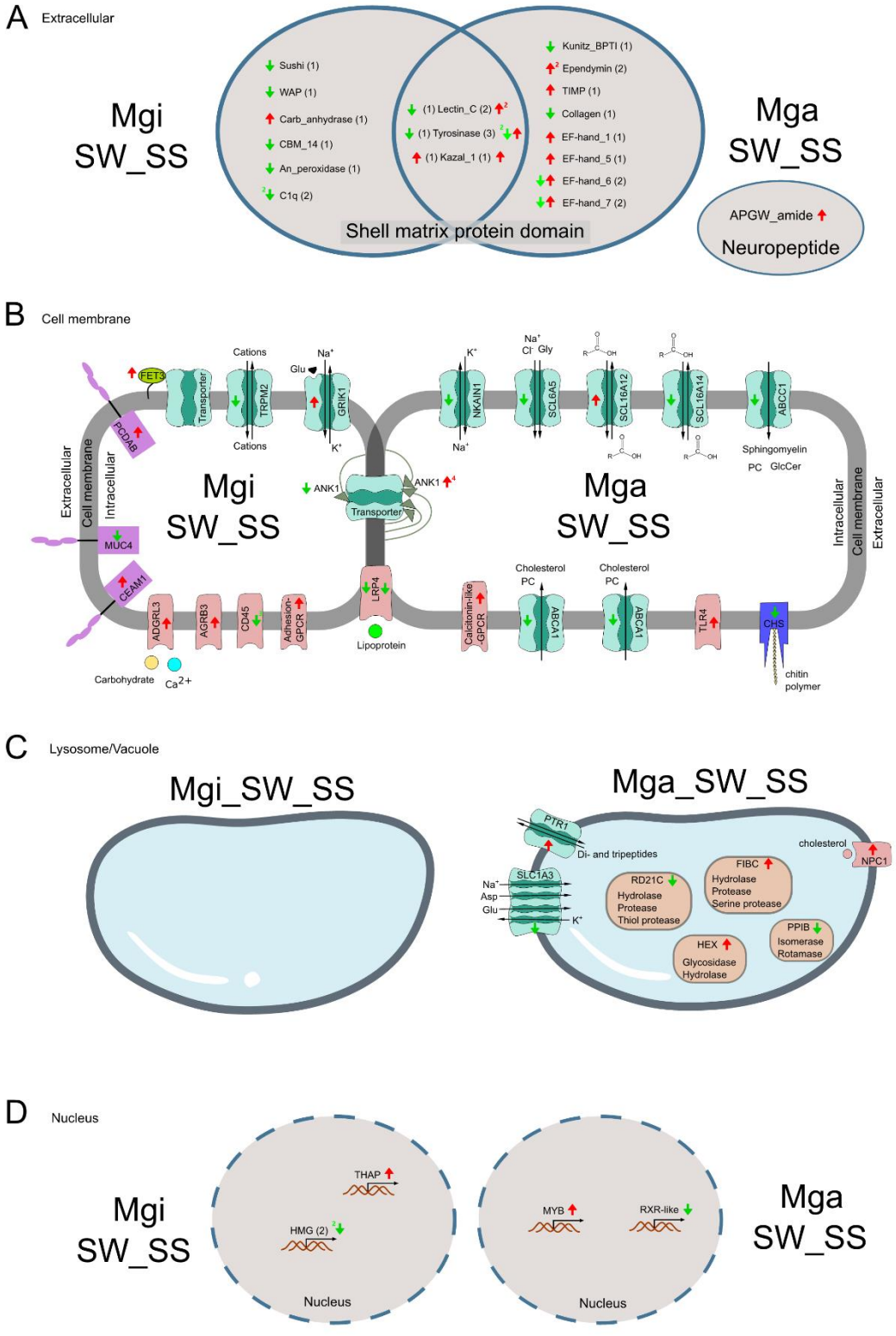

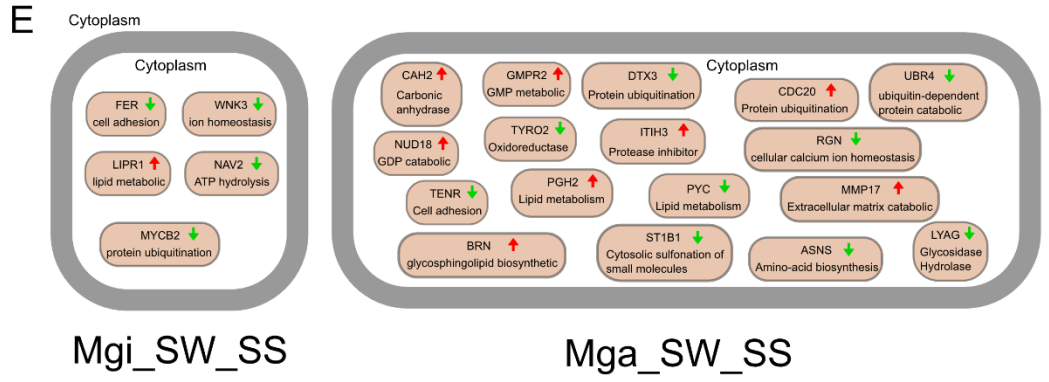
E
Cytoplasm
Cytoplasm
FER
cell adhesion
WNK3
ion homeostasis
LIPR1
lipid metabolic
NAV2
ATP hydrolysis
MYCB2
protein ubiquitination
Mgi_SW_SS
Cytoplasm
CAH2
Carbonic anhydrase
GMPR2
GMP metabolic
DTX3
Protein ubiquitination
CDC20
Protein ubiquitination
UBR4
ubiquitin-dependent protein catabolic
NUD18
GDP catabolic
TYRO2
Oxidoreductase
ITIH3
Protease inhibitor
RGN
cellular calcium ion homeostasis
TENR
Cell adhesion
PGH2
Lipid metabolism
PYC
Lipid metabolism
MMP17
Extracellular matrix catabolic
BRN
glycosphingolipid biosynthetic
ST1B1
Cytosolic sulfonation of small molecules
ASNS
Amino-acid biosynthesis
LYAG
Glycosidase Hydrolase
Mga_SW_SS

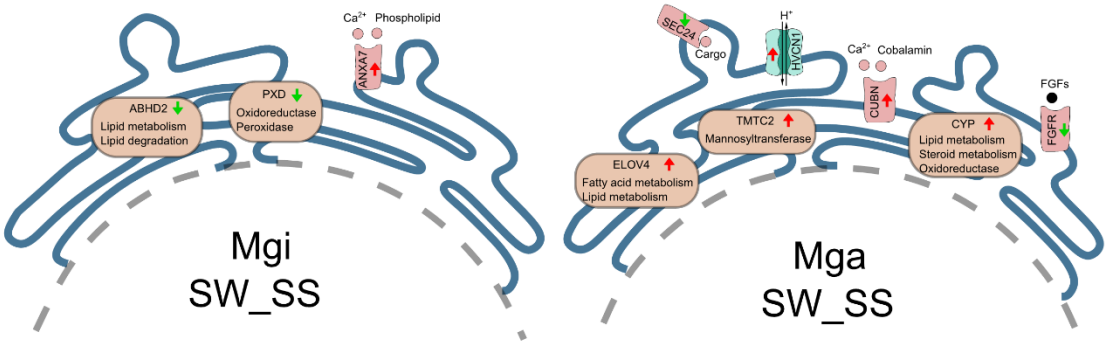
F
Endoplasmic reticulum
Ca2+ Phospholipid
ANXA7
ABHD2
Lipid metabolism
Lipid degradation
PXD
Oxidoreductase
Peroxidase
Mgi
SW_SS
SEC24
Cargo
H+
HVCN1
Ca2+ Cobalamin
CUBN
FGFs
FGFR
TMTC2
Mannosyltransferase
CYP
Lipid metabolism
Steroid metabolism
Oxidoreductase
ELOV4
Fatty acid metabolism
Lipid metabolism
Mga
SW_SS

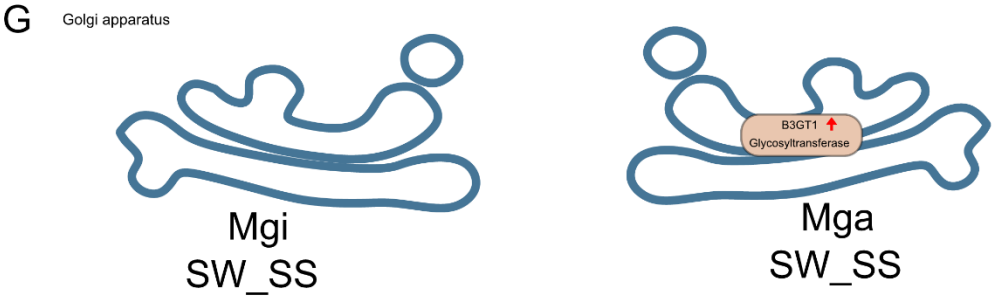
G
Golgi apparatus
Mgi
SW_SS
B3GT1
Glycosyltransferase
Mga
SW_SS

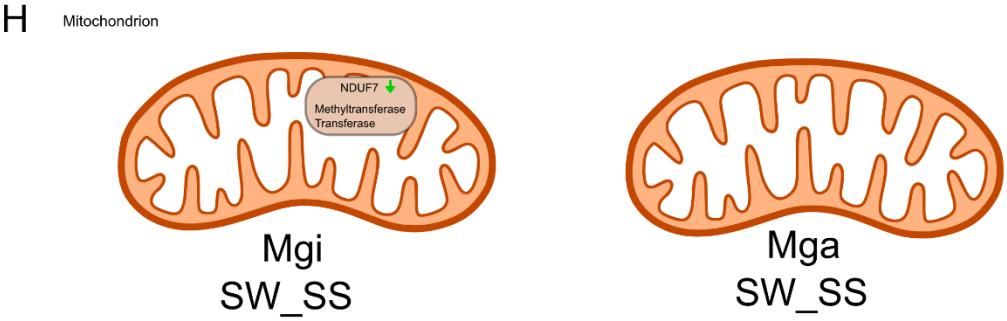
H
Mitochondrion
NDUF7
Methyltransferase
Transferase
Mgi
SW_SS
Mga
SW_SS

Supplementary Figure 3.11

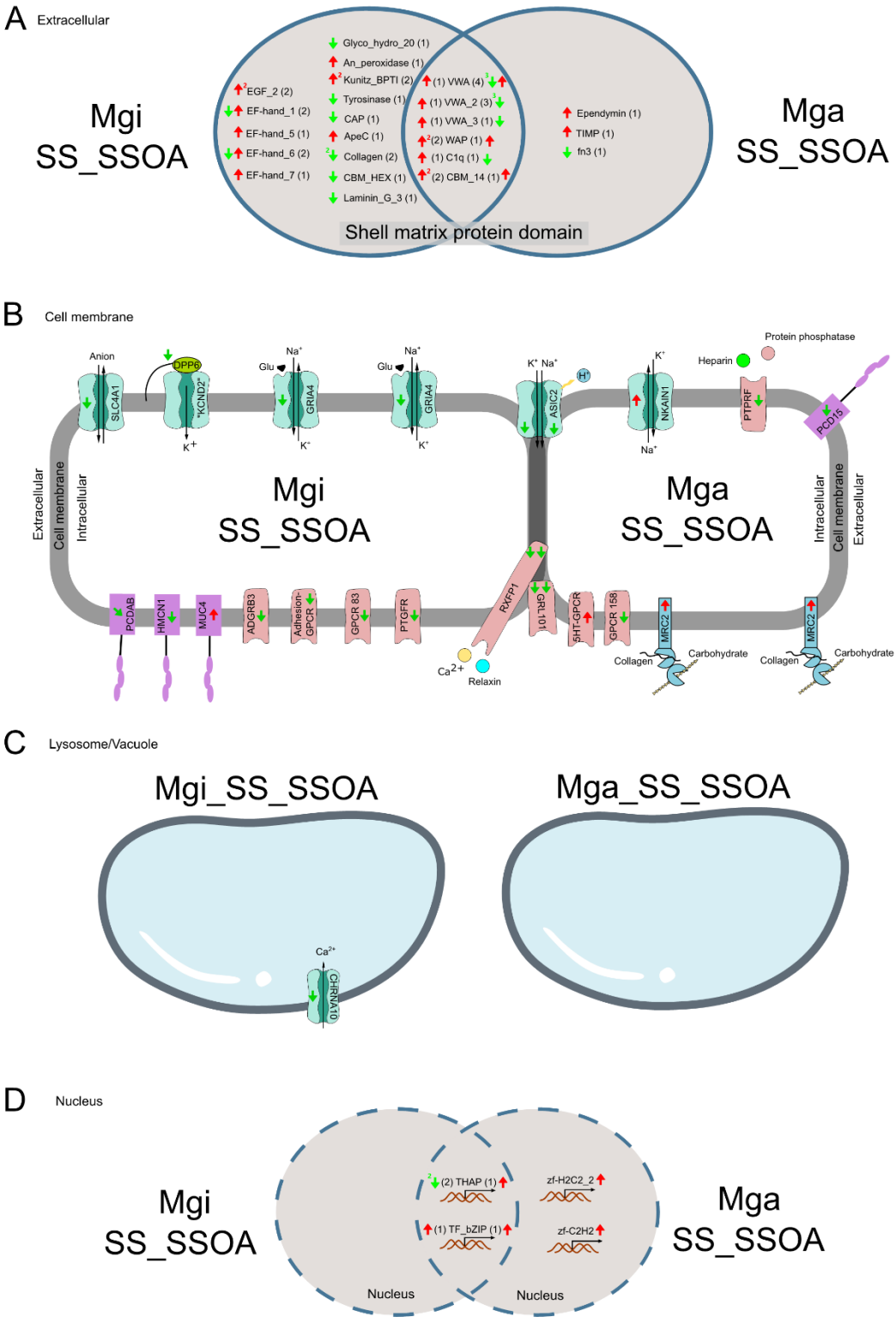

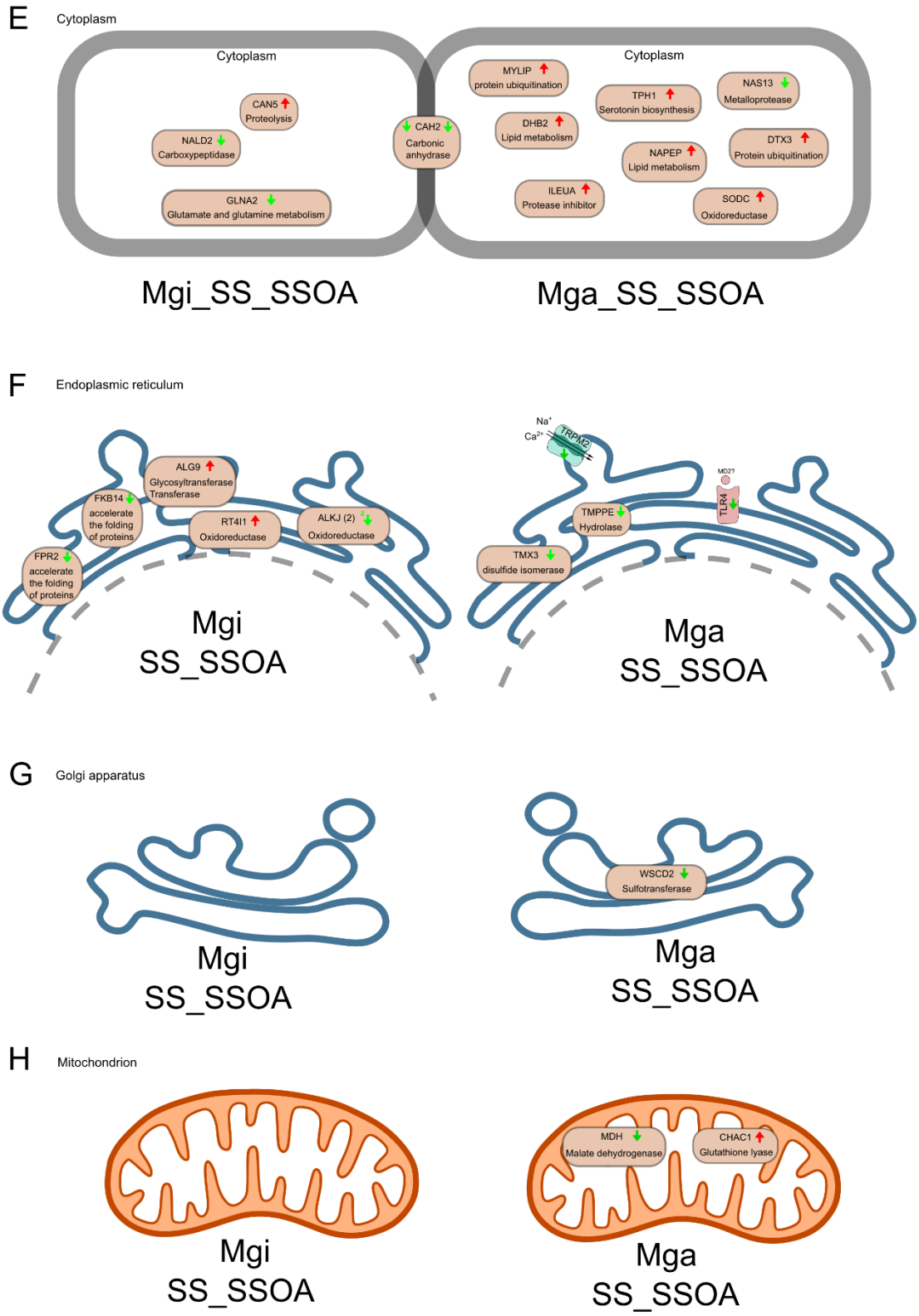

Supplementary Figure 3.9-11 Subcellular localization and functional model of protein coding DE gene transcripts. (9-11) Analysis of SW_vs_OA, SW_vs_SS and SS_vs_SSOA comparison. (A-H) Analysis

of extracellular matrix domain, cell membrane, nucleus, cytoplasm, endoplasmic reticulum, golgi apparatus, lysosome/vacuole, and mitochondrion. Domains were annotated based on Pfam identification (see supplementary table 3.4). Transcription factors (TF) are displayed in the form of the TF-family to which the gene belongs (see supplementary table 3.6). Venn diagrams show the specific and common domain/gene/TF-family in the mussel and oyster. Transporters, transporter regulatory proteins, chitin synthases, receptors and cell adhesion-related proteins are displayed in the cell membrane. The cytoplasmic fraction displays enzymes, matrix protein regulators, and cell adhesion-related proteins. Transporters, receptors and enzymes are displayed in the endoplasmic reticulum. Receptors and enzymes are displayed in the golgi apparatus and mitochondrion. The lysosome/vacuole fraction displays transporters, receptors, enzymes and matrix proteins. The red and green arrows indicate up- and down-regulation of the gene transcripts and encoded domain/family, respectively. The presence of green and red arrows in an entry item means that there are both up- and down-regulated genes represented in the transcriptome for that item. The superscript numbers next to the arrows indicate the number of genes/domains regulated, while the numbers in parentheses indicate the total number of genes/domains. All genes are indicated by abbreviated gene names (from Swiss-Prot database, see supplementary table 3.6). Enzymes display the abbreviation of the gene name and the corresponding function.

3.7.3 Supplementary Tables (in Annex IV, digital format)

CHAPTER 4

Evolution of chitin-synthase in molluscs and its response to ocean acidification

Evolution of chitin-synthase in mollusc and response to ocean acidification

Manuscript submitted to Molecular Phylogenetics and Evolution (2023)

Acknowledgements

This study received Portuguese national funds from FCT - Foundation for Science and Technology through projects UIDB/04326/2021, 2022 and 2023 and LA/P/0101/2020 and from the operational programs CRESC Algarve 2020 and COMPETE 2020 through the project EMBRC.PT ALG-01-0145-FEDER-022121.

Evolution of chitin-synthase in mollusc and response to ocean acidification

Maoxiao Peng[1], João CR Cardoso[1*] and Deborah M Power[1,2,3*]

[1]Comparative Endocrinology and Integrative Biology, Centre of Marine Sciences, Universidade do Algarve, Campus de Gambelas, 8005-139 Faro, Portugal

[2]International Research Center for Marine Biosciences, Ministry of Science and Technology, Shanghai Ocean University, Shanghai, China

[3]Key Laboratory of Exploration and Utilization of Aquatic Genetic Resources, Ministry of Education, Shanghai Ocean University, Shanghai, China

* Corresponding authors

4.1 Abstract

Chitin-synthase (CHS) is widespread among eukaryotes and known to have a complex evolutionary history. Research into CHS has mainly been in the context of biomineralization of mollusc shells. Exploration of CHS at the genomic level in molluscs, the evolution of isoforms, their tissue distribution, and response to environmental change are largely unknown. Exploiting the extensive molecular resources for mollusc species we reveal that bivalves possess between 12 to 22 CHS genes, which is the largest number of CHS genes discovered in eukaryotes to date. The evolutionary tree constructed suggests that the most recent common Molluscan ancestor had four CHS Type II isoforms (A-D), and further differentiation generated Type II-A (Type II-A-1/Type II-A-2) and Type II-C (Type II-C-1/Type II-C-2). Non-specific loss of CHS isoforms occurred at the class level, the myosin head domain in Type II (B-D groups) was not preserved in all isoforms despite its functional association with shell formation, the highly species-specific tissue expression of CHS isoforms suggest the potential for functional diversification or involvement in functions other than shell biomineralization. Analysis of transcriptome data uncovered species-specific potential of CHS isoforms in shell formation. The species-specific response of CHS to ocean acidification (OA) suggests the impact

of OA on CHS is not isoform-dependent but may be dependent on energy metabolism a decisive factor contributing to the consequences of OA in bivalves. In *Mytilus*, the Type I-B and Type II-D isoforms are influenced by OA-induced energy metabolism regulation, which in turn affects shell mineralization. In summary, these findings not only provide insights into the evolution of mollusc CHS but also lay the foundation for research into their function and contribute to the differing response of bivalves to environmental change.

Keywords: biomineralization, chitin-synthase evolution, mollusc, ocean acidification, species-specific functional diversification

4.2 Introduction

Chitin is the most widespread natural amino polysaccharide found in Nature. It a homopolymer of β-1,4-N-acetyl-D-glycosamine and part of the structure of many animal and plants tissues and provides resistance and strength. It is an important scaffolding material of the cell wall of fungi and yeast and is a major component of arthropod exoskeleton (20-30% of the crustacean carapace) (Kramer and Koga, 1986; Muzzarelli, 2013). In vertebrates, chitin is absent from mammals and birds but it exists in fish scales and has also been detected in fish and amphibian larvae suggesting that this polymer has multiple roles in vertebrate biology (Tang et al., 2015). The process by which animals synthesize chitin has raised a lot of interest not only because of its diverse application (Desbrières and Guibal, 2018) but also because of its role as a major component of the protective exoskeleton, and almost certainly is affected and determines the consequences of changes in the marine environment in shelled animals such as the molluscs.

The molluscs are the second-largest phylum of invertebrate animals after the arthropods and most mollusc species inhabit aquatic environments. The majority of molluscs possess a mineralized shell that confers protection and regulates internal ion homeostasis. The shell is secreted by the mantle and haemocytes; however the process of shell

production remains poorly elucidated. The shell is mostly composed of calcium carbonate crystals embedded in an organic matrix composed of proteins and chitin (Falini et al., 1996; Marin et al., 2012; Suzuki and Nagasawa, 2013). Chitin was present in the last common ancestor of the Conchifera and its abundance in the shell matrix depends on the differentiation of the shell (Furuhashi et al., 2009a). Chitin is proposed to constitute 3.5 % of the shell matrix (Chan et al., 2018; Heredia et al., 2007) and forms the framework for crystal mineralization (Falini et al., 1996). The calcium carbonate crystals in the shell are aligned with the chitin fibres (Weiner et al., 1983; Weiner and Traub, 1980) but how chitin is produced and regulated to form the cross-linked matrix essential for shell growth and maintenance remains poorly understood. Insights into the cellular regulation and evolution of the complex of proteins that determine chitin production or breakdown may contribute to understanding the role of chitin in mollusc shell formation.

Chitinases and CHS are two groups of enzymes that are responsible for the breakdown and formation of the chitin fibres, respectively. CHS is only found in species containing chitin but chitinases are widespread and exists in viruses through to mammals (Gooday, 1999). CHS are glycosyltransferase family 2 members (Merzendorfer, 2011) and are involved in the synthesis of the chitin polymer and play a key role in the addition of UDP-GlcNac units to the growing oligosaccharide chain

(Falini and Fermani, 2004). In vertebrates CHS has only been reported in fish and amphibians but they are common in invertebrate metazoans. In fungi CHS are very diverse and family members are grouped into seven distinct classes (Roncero, 2002) but in other metazoan they are less numerous, and their evolutionary relationship is complex. The fusion of different myosin types during the evolution of CHS is a common in some groups of metazoans and fungi and at least 5 gene duplication events are proposed to have occurred during CHS evolution in metazoan (Zakrzewski et al., 2014).

CHS have been isolated from relatively few molluscs and those in which they have include the rigid pen shell (*Atrina rigida*) (Weiss et al., 2006), the Japanese pearl oyster (*Pinctada fucata*) (Suzuki et al., 2007)and the pacific oyster (*Magallana gigas*) (Y. Zhang et al., 2019). *Lottia gigantea* is proposed to have the highest CHS gene number (10 isoforms), but recent research indicates that amphioxus has 11-12 CHS isoforms (Shi et al., 2020). Analysis of publicly available genome data for molluscs, reveals numerous CHS isoforms in bivalves. The extensive CHS diversification, and variety of chitinous structures in molluscs, makes them an interesting taxon in which to study CHS regulatory mechanisms, synergism, and functional divergence (Zakrzewski et al., 2014). (Weiss et al., 2013) first cloned a charged amino acid residue motif corresponding to the extracellular domain of mollusc myosin CHS (Ar-

CS1) and discovered assembly was pH-dependent and simulated the mineralization extrapallial space environment. This suggests that specific interactions of CHS with minerals may influence shell formation.

Relatively few studies have considered CHS functional dependence on the extracellular microenvironment (Weiss, 2012; Weiss et al., 2013; Zhang et al., 2019), the evolution of isoforms, tissue distribution, and how changes in the environment affect its activity. In this study CHS in molluscs was characterized and the enzyme's potential role in mollusc shell building determined. Taking advantage of assembled transcriptome data available for the Mediterranean mussel (*Mytilus galloprovincialis*) and publicly available data of the evolutionary proximate hard-shelled mussel (*Mytilus coruscus*) and Pacific oyster (*M. gigas*) CHS expressed in the mantle was characterized under control and OA conditions.

4.3 Material and Methods

4.3.1 Database searches and protein domain prediction

Oyster (*M. gigas*) CHS sequences were used as queries to retrieve putative CHS-like genes/transcripts (*e-value* $\leqslant$ $1e^{-40}$) from 39 representative species of different phyla (Fungi, Porifera, Cnidaria, Mollusca, Arthropoda, Chordata) available in public databases (Supplementary Table 4.1). Various sequence resources were further

identified by domain analysis (Pfam database (https://pfam.xfam.org)) including the identification of 1) the Chitin_synth_2 domain, and 2) a transmembrane domain. In addition, Pfam analysis was used to conduct a general scan for protein domains and they were displayed using Tbtools software (Chen et al., 2020).

4.3.2 Sequence alignments and phylogenetic analysis

Multiple sequence alignments (MSA) were made using the MUSCLE algorithm (Edgar, 2004) in the Aliview software (v 1.28). For the gene phylogenetic analysis removal of gaps and improvement of alignments was achieved by manual editing of the MSA and two tree-building methods were used: Maximum Likelihood (ML) and Bayesian Inference (BI). The ML tree was built in PhyML 3.0 from the ATGC bioinformatics platform (http://www.atgc-montpellier.fr/phyml/) using SMS automatic model selection for the study of protein evolution according to AIC (Akaike Information Criterion) with a 100 bootstrap replicates. The BI tree was built in MrBayes v3.2 using a VT substitution model (Aamodel = VT, obtained from SMS automatic model selection of ML tree) with 1,000,000 generations. Trees were displayed in FigTree 1.4.3 (http://tree.bio.ed.ac.uk/software/figtree), rooted with Fungi CHS and edited in the Inkscape program (https://inkscape.org). Functional motifs of the Chitin_synth_2 domain, the donor saccharide binding site (DSBS),

acceptor saccharide binding site (ASBS) and product binding site (PBS) were analysed in detail and displayed using Tbtools software (Chen et al., 2020).

4.3.3 Species orthogroup inference

Protein datasets from the genomes of seventeen bivalve species (Supplementary Table 4.2) were used for species phylogenetic tree analysis. Alternative transcripts were removed from the initial protein data set obtained for each species. Global orthogroup resolution was performed using Orthofinder (ver 2.5.4, parameters -M msa; -T raxml) (Emms and Kelly, 2019). The resulting tree was displayed in FigTree 1.4.3 (http://tree.bio.ed.ac.uk/software/figtree).

4.3.4 Acidification assay

Quantitative expression analysis (qPCR) was used to examine *M. galloprovincialis* CHS genes that significantly responded to OA. The experimental material was mantle samples obtained from a previous OA study with *M. galloprovincialis* (Peng et al., 2023). In brief, juvenile mediterranean mussels (*M. galloprovincialis*, 3.0 - 3.5 cm shell-length and 8.62 - 10.11 g weight) were collected from the Ria Formosa (Faro, Portugal, ICNF license 327/2022/CAPT). Experiments were performed in

an open circuit system under normal environmental conditions of photoperiod and temperature (13-17ºC) for November-January in the Algarve (Portugal). Seawater was acidified in header tanks by pumping in CO_2 gas under controlled conditions to decrease the ambient pH value from, pH 8.2 to pH 7.8. The seawater temperature, oxygen and pH in the circuits were continuously monitored, and fluctuations automatically corrected (Aquatronica, Reggio Emilia, Italy). Triplicate aquaria (each aquaria contained n = 10 mussels) were established for ambient seawater pH 8.2 (control, SW) and seawater at pH 7.8 (OA) conditions. Mussels were exposed to the challenge for 60 days in an open circuit supplied with aerated seawater (pH 8.19 ± 0.01) and with seawater gassed with CO_2 to achieve the desired pH, 7.8 ± 0.01. Animals were fed every day with 10 mg/aquaria of a commercial mixture of dried microalgae (PHYTOBLOOM, Necton, Portugal). After 60 days of exposure to the experimental conditions, samples from the mantle edge were collected from the posterior region of the left valve in mussels for qPCR analyses. Samples were immediately frozen on dry ice and stored at -80ºC.

4.3.5 Expression analysis

The experimental methods and steps for total RNA extraction (tRNA) and cDNA synthesis from samples were the same as in previous studies (Peng et al., 2023). Mantle cDNA was prepared from 6 individuals of

each experimental group. The cDNAs used for quantitative PCR (qPCR) were synthesized from DNase treated mantle tRNA (500 ng). Reactions were carried out in a 20 µl final reaction volume with 10 ng of pd(N)6 random hexamers (Jena Bioscience, Germany), 2 mM dNTPs (ThermoScientific, USA), 100 U of RevertAid Reverse Transcriptase and 8 U Ribolock RNAse inhibitor (ThermoScientific).

The qPCR experimental method used was as follows. qPCR reactions were performed using SsoFast EvaGreen Supermix (Bio-Rad, Portugal) for a 10 µl final reaction volume containing 200 nM of candidate gene specific primer pairs (Supplementary Table 4.3) and 2 µl of cDNA template. Duplicate reactions were used for all samples (n = 6 for each experimental group) and controls (accepting < 5% variation between replicates) and all reactions were run on a CFX Connect Real-Time PCR Detection System for 96-well microplates (Bio-Rad). Melting curves were performed to detect non-specific products and primer dimers. Reverse transcriptase (RT-) and PCR control (no template) reactions were included in all qPCR assays to confirm tRNA was absent of contaminating genomic DNA or technical-related contamination, respectively. Reaction efficiencies and R^2 (coefficient of determination) were established for each primer pair. The *M. galloprovincialis* elongation factor 1-alpha (EF1α) and 18S ribosomal RNA, which had a constant expression irrespective of treatment were used as the reference

genes for normalization, and quantification was based on the standard curve methods.

4.3.6 Statistical analysis

SPSS 19.0 was used for statistical analysis. For the qPCR analysis the results are presented as the mean of 6 replicates ± SEM for each condition. To identify significant differences in gene expression (qPCR data and FPKM value from transcriptome data) between the conditions, a two-tailed Student's *t*-test was performed between the treatment groups and the control. The p-value cut-off for significance was set at 0.05.

4.4 Results

4.4.1 Phylogenetic tree and distribution of chitin-synthase isoform

The genome of seventeen species belonging to 8 classes of the phylum Mollusca were used to construct a phylogenetic tree (Figure 4.1). The CHS gene family was expanded in mollusc species. Due to the limited availability in public database of DNA sequences for species of the Solenogastres, Caudofoveata, Polyplacophora, Scaphopoda, and Monoplacophora classes, a single species from each class was analyzed, and 4 to 7 CHS isoforms were identified. The genome of two species of the Cephalopoda class yielded 11 to 12 CHS isoforms, examination of the genome of four species of the Gastropoda class, yielded 8 to 12 CHS, and

analysis of the genome of six species of the Bivalvia class, yielded 17 to 22 CHS isoforms.

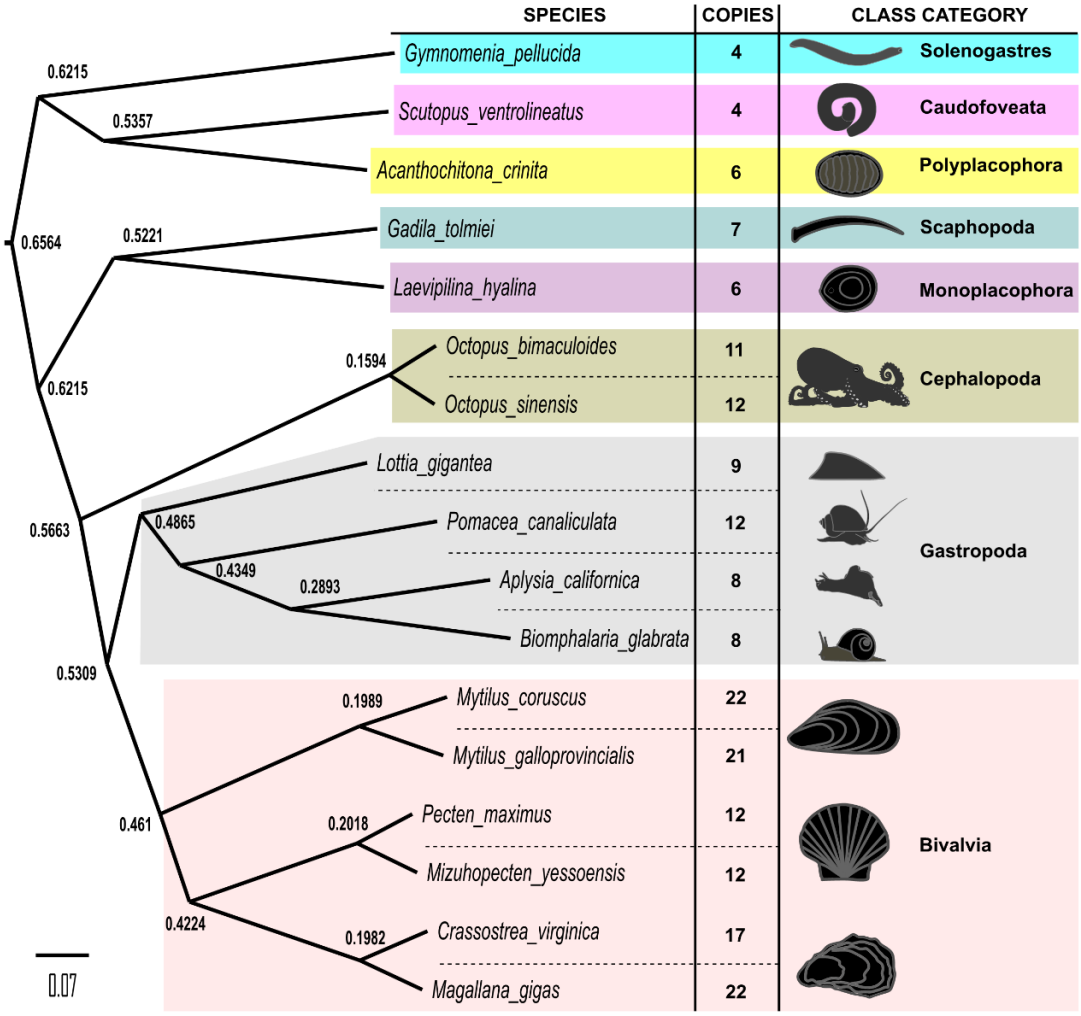

Figure 4.1. The phylogenetic relationship of the Mollusca species studied and copy number of the genes coding for chitin-synthase proteins. The species phylogenetic tree was constructed using Orthofinder (ver 2.5.4) and the ML method. The class level category is indicated by different background shading in the phylogenetic tree. The species name and the number of genes coding for CHS proteins are indicated.

A total of 228 deduced CHS amino acid sequences from the genomes of 39 species were used to construct a phylogenetic tree (Figure 4.2 and Supplementary Figure 4.1). The CHS sequences were from Fungi,

Porifera, Cnidaria, Arthropoda, Chordata (Leptocardii, Actinopterygii, Ascidiacea and Amphibia), and Mollusca (Bivalvia, Gastropoda, Cephalopoda, Polyplacophora, Monoplacophora, Scaphopoda, Solenogastres and Caudofoveata).

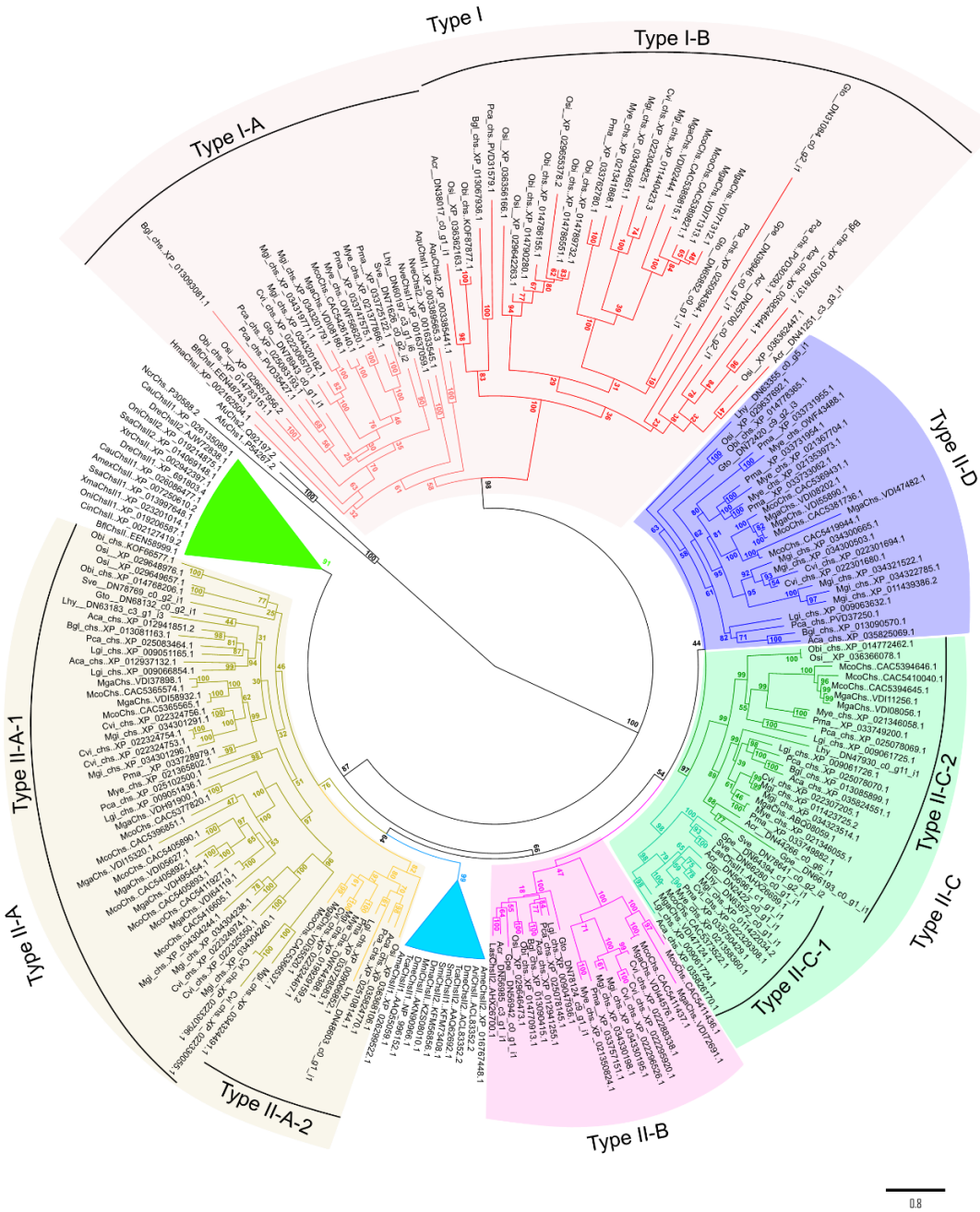

Figure 4.2. Phylogenetic ML tree of the mollusc, insect and vertebrate

chitin-synthases. The ML tree was built in PhyML 3.0 from the ATGC bioinformatics platform (http://www.atgc-montpellier.fr/phyml/) using SMS automatic model selection for the study of protein evolution according to AIC (Akaike Information Criterion). The tree was built with 100 bootstrap replicates and the support values for branching are indicated at the nodes. The accession numbers and name of the sequences used are indicated in Supplementary Table 4.1. The Fungi CHS were used to root the tree. The green and blue merged clades indicate the vertebrate and insect CHS, respectively. Colours background which non-merged clades represents the CHS genes of Mollusca phylum.

The CHS genes duplicated in the metazoans generating two major clades designated Type I and Type II, which expanded in molluscs. Type I and Type II in molluscs underwent a further round of duplication forming a Type I-A, Type I-B, Type II-A (Type II-A-1 and Type II-A-2), Type II-B, Type II-C (Type II-C-1 and Type II-C-2) and Type II-D clades. The CHS isoforms of the Porifera and Cnidaria phyla are exclusively distributed within the Type I-A branch. All Arthropod CHS isoforms cluster together and are near to Type II-A. The CHS isoforms of Chordata cluster together and are close to the Type II CHS of species of the Leptocardii class that have one CHS isoform distributed within the Type I-A branch.

Mapping the CHS isoforms of molluscs onto the evolutionary tree revealed that the Bivalvia and Gastropoda classes have all types and isoforms of CHS, while the Cephalopoda class loss the Type II-C-1 isoform (Table 4.1). The Monoplacophora class lost genes for Type I-B and Type II-B isoforms, the Scaphopoda class lost genes for Type II-A-2 and Type II-C-2 isoforms, and the Caudofoveata class loss genes for Type

I-B, Type II-A-2, Type II-B, and Type II-D isoforms. The Solenogastres and Polyplacophora classes lost genes for Type I-A, Type II-A, and Type II-D isoforms.

Table 4.1. Number of CHS isoforms identified in each type for each of the species analyzed

SPECIES	Type I		Type II					
	Type I-A	Type I-B	Type II-A		Type II-B	Type II-C		Type II-D
			Type II-A-1	Type II-A-2		Type II-C-1	Type II-C-2	
Gymnomenia pellucida	-	1	-	-	1	1	1	-
Scutopus ventrolineatus	1	-	1	-	-	1	1	-
Acanthochitona crinita	-	3	-	-	1	1	1	-
Gadila tolmiei	1	2	1	-	1	1	-	1
Laevipilina hyalina	1	-	1	1	-	1	1	1
Octopus bimaculoides	1	5	2	-	1	-	1	1
Octopus sinensis	1	5	2	1	1	-	1	1
Lottia gigantea	-	-	3	1	1	1	2	1
Pomacea canaliculata	2	3	2	1	1	-	2	1
Aplysia californica	-	1	2	1	1	1	1	1
Biomphalaria glabrata	1	2	1	1	1	-	1	1
Mytilus coruscus	1	2	9	1	2	1	3	3
Mytilus galloprocincialis	1	3	7	1	2	1	3	3
Pecten maximus	2	1	1	1	1	1	2	3
Mizuhopeten yessoensis	2	1	1	1	1	1	2	3
Crassostrea virginica	1	1	7	1	3	1	1	2
Magallana gigas	3	2	6	1	2	1	2	5

Note: The colour gradation from blue (low) to red (high) is correlated with the number of CHS isoforms identified.

4.4.2 Sequence analysis of chitin-synthase isoform

All the sequences used for the phylogenetic tree and sequence analysis shared a conserved core CS2 (Chitin_synth_2) domain (Supplementary Figure 4.2). The CHS of Fungi have different characteristics from the CHS of metazoan species analysed in this study, specifically, they possess the CS1 domain (Chitin_synth_1N and Chitin_synth_1). Fungi CHS only

have transmembrane domains on the C-terminal side of the CS2 domain and the amino acid sequence. However, the CHS of metazoan species used in this study not only shared the transmembrane structural domain characteristics of Fungi CHS but also possessed transmembrane domains at the N-terminus of the deduced protein (Figure 4.3). The C-terminal sterile alpha motif (SAM_1 and SAM_2) was only identified in the Type I-A sequences, and the SAM_1 and SAM_2 domains generally appeared together in the deduced protein seqeunces, with only a few exceptions e.g. AquChsI1 (XP_003389565.3) and AquChsI2 (XP_003385441.1). Type I, Type II-A, and Chordata phylum CHS isoforms did not have the Myosin_head domain in the N-terminal region of the deduced protein (Figure 4.3A). The Myosin_head domain was absent from all Type II-B, Type II-C, Type II-D, and Arthropoda phylum CHS isoforms (Supplementary Figure 4.2). In addition, in some species some CHS genes coded for proteins that contained other conserved domains.

The CS domain contained a donor saccharide binding site (DSBS), an acceptor saccharide binding site (ASBS) and a product binding site (PBS) (Figure 4.3B). Highly conserved ASBS (GEDRW) and PBS (QRRRW) motifs were found in all CHS isoforms of metazoan species included in this study. However, the conserved DSBS motif differed between Type I-A (DAD, GCFSVYR), Type I-B (DAD, GCFSLYR), and Type II (DGD, GCFSLFR) CHS isoforms (Figure 4.3B and Supplementary Figure 4.3).

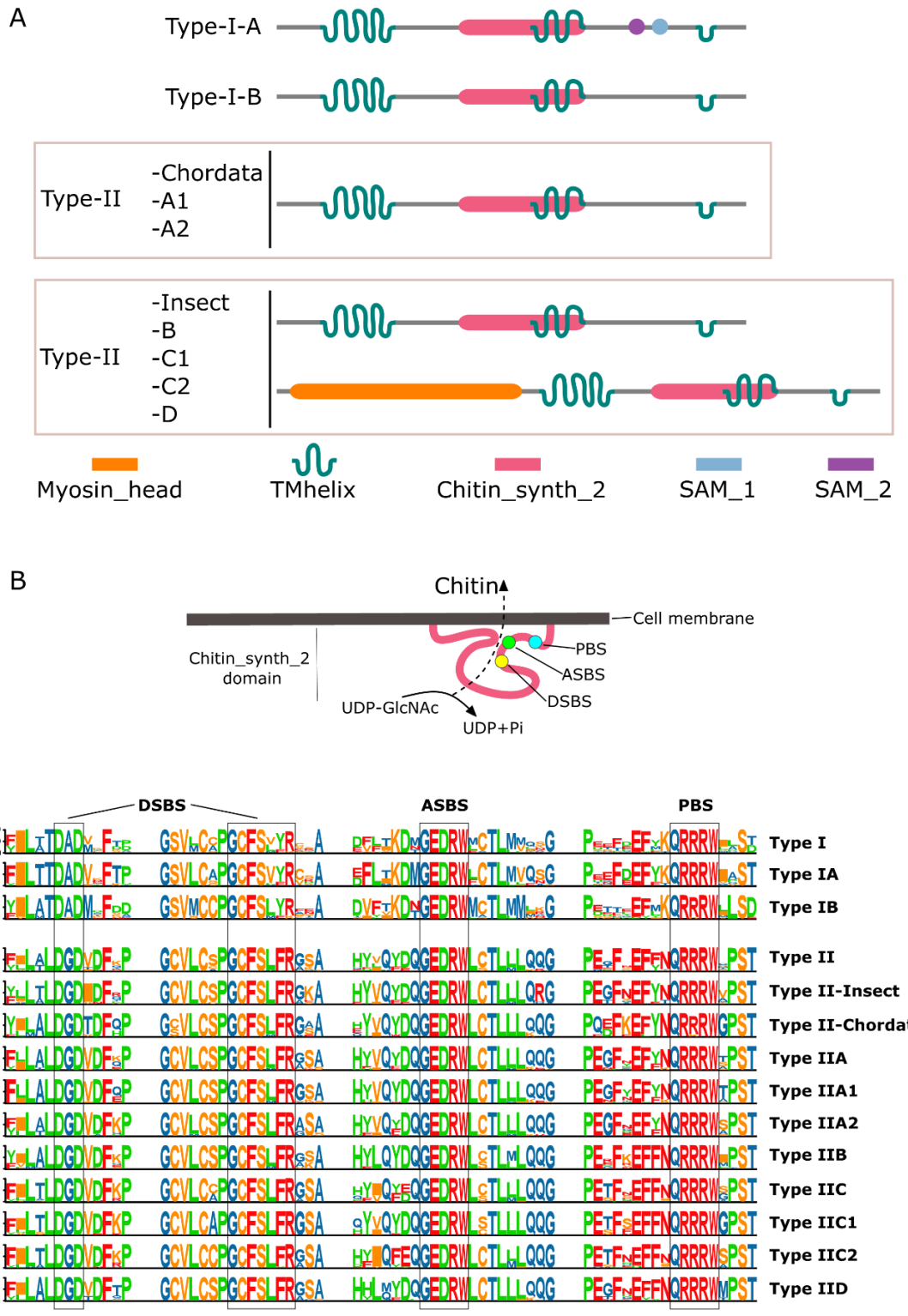

Figure 4.3. Schematic representation of the protein domains of the deduced chitin-synthase proteins. A) Linear representation of the domains elucidated from the Pfam prediction in different types of CHS. The deduced CHS protein possessed a unique Chitin_synth_2 domain

(pink shaded line) and the transmembrane regions (green shaded line). The presence or absence of the Myosin_head (in orange), sterile alpha motif, SAM_1 (blue shaded line) and SAM_2 (purple shaded line) domains is optional for types. **B)** Scheme of the catalytic center of the Chitin_synth_2 domain, modified from (Weiss, 2012), and highlighting the functional motifs including, the donor saccharide binding site (DSBS), acceptor saccharide binding site (ASBS) and product binding site (PBS). The full-length sequence alignment containing all collected sequences is available from Supplementary Figure 4.3 and indicating the functional motifs of the catalytic center in Chitin_synth_2 domain is represented. Amino acids were coloured using the MSA default settings and letters of different heights are indicative of amino acid residue conservation across sequences (the bigger the letter, the higher the sequence conservation).

4.4.3 Expression of chitin-synthase

In *M. gigas*, the digestive gland and mantle expressed the highest number (20 isoforms) of CHS, followed by the gonads (19 CHS isoforms), and then the muscles and gills (14 CHS isoforms). Haemocytes expressed the lowest diversity of isoforms, with only 10 CHS isoforms. However, this expression trend differed in *M. galloprovincialis* [haemocytes (19 isoforms) = gills (19 isoforms) > mantle (16 isoforms) = muscles (16 isoforms) > digestive gland (12 isoforms) > gonads (7 isoforms)] and *M. coruscus* [mantle (16 isoforms) > gills (13 isoforms) > gonads (6 isoforms)] (Figure 4.4). The genes MgiChs-IIA1_5, MgiChs-IIC1, MgaChs-IB_1, and MgaChs-IIA1_4 were not expressed in biomineralization-related tissues (haemocytes and mantle). Only data for the mantle was available for *M. coruscus* and revealed, McoChs-IB_1, McoChs-IIA1_4, McoChs-IIA1_6, McoChs-IIA1_8, McoChs-IIA2, and McoChs-IIC1 were not expressed. MgiChs-IID_2, MgaChs-IIC2_3, and

McoChs-IIC2_3 were the most abundantly expressed genes, respectively, in the biomineralization tissues of *M. gigas*, *M. galloprovincialis*, and *M. coruscus*.

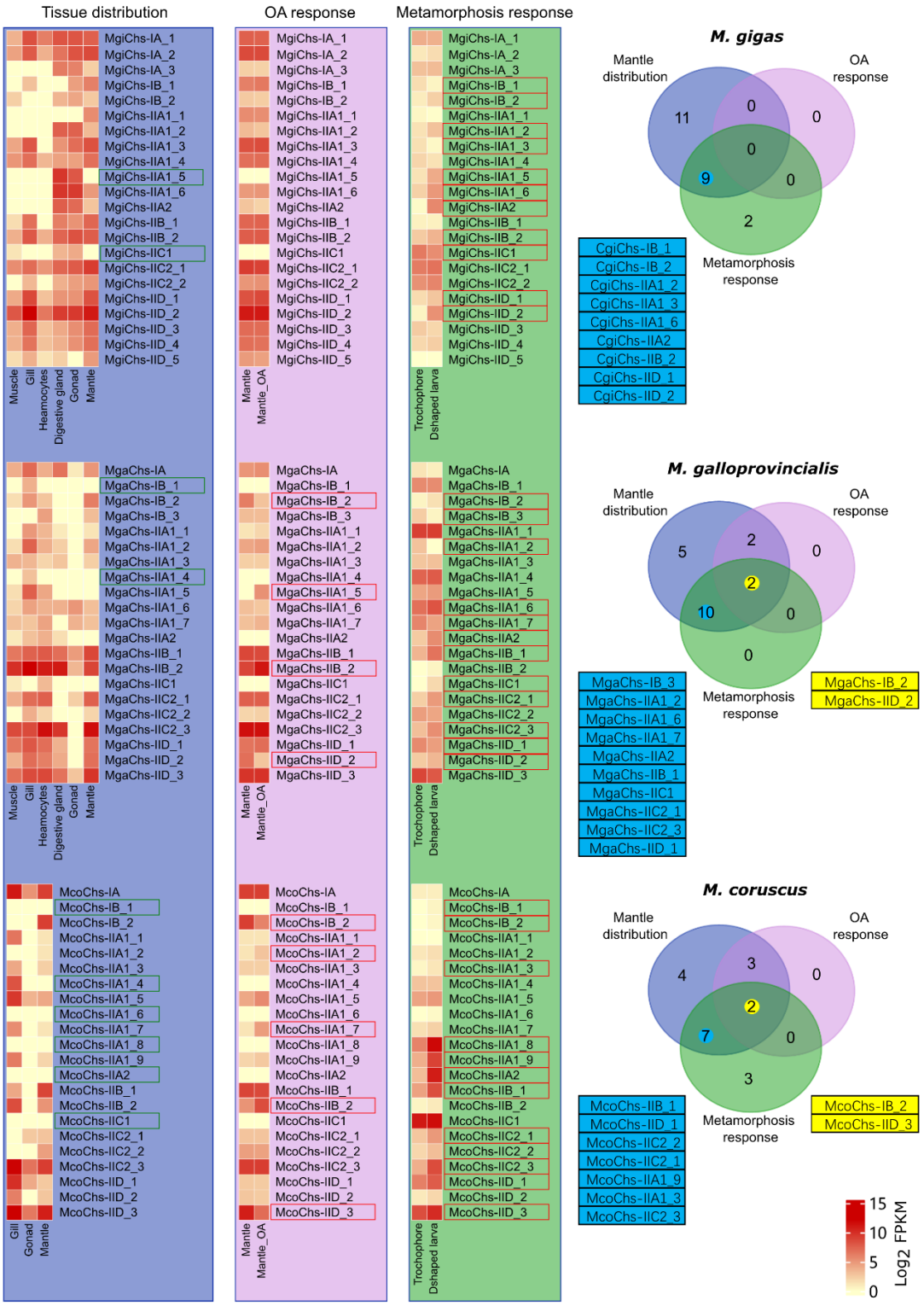

Figure 4.4. Heatmap of the CHS expression in different tissues, during larva metamorphosis and OA response in three bivalves. Each row represents an isoform of CHS. The tissues analysed were muscle, gill, haemocytes, digestive gland, gonad and mantle and the larva stages were Trochophore and D-shaped larva. Graded colours from yellow to red indicates the relative abundance of each isoform. The Venn diagram

shows the number and overlap of the CHS isoforms identified using the following criteria: 1) mantle distribution (deep blue), 2) OA response (purple), 3) shell biomineralization response (green). Genes within the tables with a blue or yellow background represent candidate CHS isoforms proposed to be involved in shell formation. Furthermore, OA-affected CHS isoforms putatively involved in biomineralization are highlighted in yellow.

In *M. gigas*, MgiChs-IID_5 was not expressed in pre- and post-shell formation larvae. The expression levels of MgiChs-IB_1, MgiChs-IIA1_3, and MgiChs-IIC1 were significantly downregulated during shell formation, while the expression levels of MgiChs-IB_2, MgiChs-IIA1_2, MgiChs-IIA1_5, MgiChs-IIA1_6, MgiChs-IIA2, MgiChs-IIB_2, MgiChs-IID_1, and MgiChs-IID_2 were significantly upregulated. In *M. galloprovincialis*, the expression levels of MgaChs-IB_3, MgaChs-IIA1_2, MgaChs-IIA1_7, and MgaChs-IID_1 was significantly downregulated during shell formation, while the expression levels of MgaChs-IB_2, MgaChs-IIA1_6, MgaChs-IIA2, MgaChs-IIB_1, MgaChs-IIC1, MgaChs-IIC2_1, MgaChs-IIC2_3, and MgaChs-IID_2 were significantly upregulated. In *M. coruscus*, McoChs-IIA1_1 was not expressed in pre- and post-shell formation larvae, while the expression levels of McoChs-IB_1, McoChs-IB_2, McoChs-IIA1_3, McoChs-IIA1_8, McoChs-IIA1_9, McoChs-IIA2, McoChs-IIB_1, McoChs-IIC2_1, McoChs-IIC2_2, McoChs-IIC2_3, McoChs-IID_1, and McoChs-IID_3 were significantly upregulated.

Exposure to OA conditions, caused a significant reduction in the

expression levels of MgaChs-IB_2, MgaChs-IID_2, McoChs-IB_2, and McoChs-IID_3, while the expression levels of MgaChs-IIA1_5, MgaChs-IIB_2, McoChs-IIA1_2, McoChs-IIA1_7, and McoChs-IIB_2 significantly increased. None of the CHS isoforms identified in *M. gigas* significantly responded to a 60 day OA challenge.

Using the distribution of CHS in biomineralization-related tissues and their changing expression in larvae during shell formation, a total of 9 (MgiChs-IB_1, MgiChs-IB_2, MgiChs-IIA1_1, MgiChs-IIA1_3, MgiChs-IIA1_6, MgiChs-IIA2, MgiChs-IIB_2, MgiChs-IID_1, and MgiChs-IID_2), 12 (MgaChs-IB_2, MgaChs-IB_3, MgaChs-IIA1_2, MgaChs-IIA1_6, MgaChs-IIA1_7, MgaChs-IIA2, MgaChs-IIB_1, MgaChs-IIC1, MgaChs-IIC2_1, MgaChs-IIC2_3, MgaChs-IID_1, and MgaChs-IID_2), and 9 (McoChs-IB_2, McoChs-IIA1_3, McoChs-IIA1_9, McoChs-IIB_1, McoChs-IIC2_1, McoChs-IIC2_2, McoChs-IIC2_3, McoChs-IID_1, and McoChs-IID_3) CHS isoforms were categorized as being related to shell biomineralization in the three species studied. Cross referencing of the CHS isoforms identified in biomineralizing larvae with those that change under an OA challenge identified a small number of common isoforms MgaChs-IB_2, MgaChs-IID_2, McoChs-IB_2, and McoChs-IID_3 in the genus *Mytilus* that were classified as shell formation-related genes that were influenced by OA. Expression levels of CHS which in transcriptomics analysis (Chapter 3) had a significant

response to OA in *M. galloprovincialis* mantle transcriptomes were analysed by qPCR analysis (Figure 4.5) in individual *M. galloprovincialis* and revealed the expression profile was similar with the two approaches.

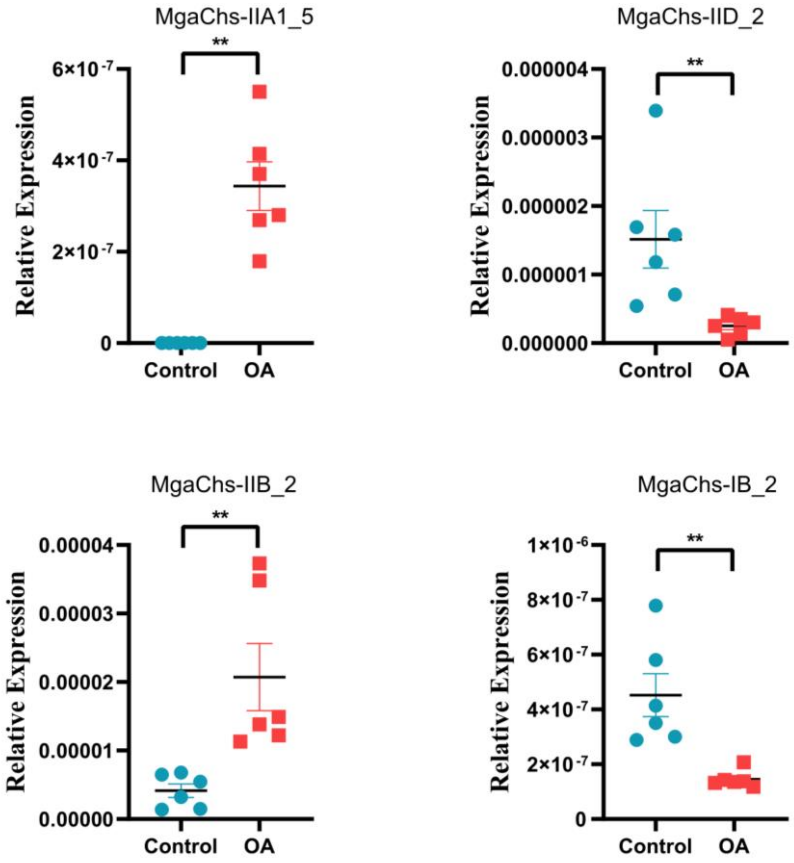

Figure 4.5. Analysis by qPCR of CHS gene isoforms that had a significantly different expression in the mantle transcriptome of control and OA challenged *M. galloprovincialis*. Differentially expressed CHS isoforms in the mantle were identified in the transcriptomes generated in Chapter 3. Relative expression was calculated by normalization using the average of the expression of two reference genes that did not vary in expression in the experimental groups (EF1α and 18S). Statistical analysis was performed using a students t-test and the data represents the mean ± SEM of n = 6 biological replicates. Asterisks indicate groups that were significantly different at $p < 0.05$.

4.5 Discussion

4.5.1 Expansion of CHS gene family in Mytilidae and Ostreidae

CHS enzymes are involved in chitin synthesis an important element that is part of the organic matrix of the shell and so these enzymes have long been the focus of studies about mollusc biomineralization (Ghatak et al., 2013; Han et al., 2016; Schönitzer and Weiss, 2007; Suzuki et al., 2007; Weiss, 2012). However, the evolution of CHS in mollusc is surprisingly poorly studied despite the significant amounts of genomic and transcriptomic data that have been made publicly available particularly for commercially important species belonging to the Cephalopoda, Gastropoda, and Bivalvia Classes (Gomes-dos-Santos et al., 2020; Takeuchi, 2017). To comprehensively describe the evolution of CHS in molluscs, we searched publicly available genome data for CHS genes. For the classes Cephalopoda, Gastropoda, and Bivalvia genes from several species were retrieved but for other taxonomic classes (Polyplacophora, Monoplacophora, Scaphopoda, Solenogastres and Caudofoveata) a single representative species was used. Previous studies proposed that the CHS family expanded in the phylum Mollusca, and it was thought that the gastropod *L. gigantea* possessed the highest number of CHS (10) isoforms (Zakrzewski et al., 2014). Recently, Shi et al. (2020) conducted a thorough reannotation of the genomes of amphioxus species

and identified new CHS genes, revealing that each amphioxus species has between 11 to 12 CHS isoforms (Shi et al., 2020). Based on homology alignment and Chitin_synth_2 domain analysis, we conducted an in-depth exploration of the genomes of 17 mollusc species. We found that bivalves, in particular those of the order Mytilidae (~22 isoforms), and Ostreidae (~17-22 isoforms), potentially suffered the most extensive gene family expansion and that their genomes possess the largest number of different isoforms across the mollusc.

4.5.2 CHS have a complex evolutionary history and different types may arise in a common ancestor of the molluscs

CHSs are widespread among eukaryotes and have a complex evolutionary history (Roncero, 2002). Independently formed paralogous groups are an important feature in the evolutionary history of CHS. According to study the evolution of CHS in eukaryotes can be divided into two main branches, with metazoan CHS forming one branch (Morozov and Likhoshway, 2016). Most of the fungi have several different CHS genes in their genomes and phylogenetic analysis revealed that fungal CHS form seven monophyletic classes, which form two clades (Roncero, 2002; Ruiz-Herrera and Ruiz-Medrano, 2004). Consistent with previous studies the metazoan CHS clustered in two main branches (Type I and Type II), and Porifera and Cnidaria CHS were restricted to Type I,

while Arthropod CHS isoforms were only found in the Type II branch (Shi et al., 2020; Zakrzewski et al., 2014), suggesting that Type I CHS may have been lost in Arthropods (Merzendorfer, 2011, 2006). Interestingly, the molluscs have retained Type I and Type II CHS, and considerable gene number expansion has I. Since all four CHS branches on the phylogenetic tree (Type II A-D) possess sequences from different lophotrochozoans (i.e., Mollusc, Brachiopods, Entoprocts, and Annelids) and based on previous evolutionary studies (Edgecombe et al., 2011; Helmkampf et al., 2008; Peng et al., 2022), we hypothesis that in the genome of their last common ancestor four CHS clusters (Type II A-D) were already present which is consistent with previous reports (Zakrzewski et al., 2014). In molluscs CHS gene isoforms further expanded and generated three different isoforms Type I, Type II A, and Type II C, although varying degrees of gene loss has occurred across the classes of Mollusca (Figure 4.6), and based on the pattern of loss appears to be unrelated to the presence or absence of a mineralized shell.

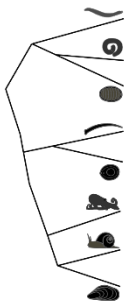

CLASSES	Type I		Type II					
	Type I-A	Type I-B	Type II-A		Type II-B	Type II-C		Type II-D
			Type II-A-1	Type II-A-2		Type II-C-1	Type II-C-2	
Solenogastres	-	•	-	-	•	•	•	-
Caudofoveata	•	-	•	-	-	•	•	-
Polyplacophora	-	•	-	-	•	•	•	-
Scaphopoda	•	•	•	-	•	•	-	•
Monoplacophora	•	-	•	•	-	•	•	•
Cephalopoda	•	•	•	•	•	-	•	•
Gastropoda	•	•	•	•	•	•	•	•
Bivalvia	•	•	•	•	•	•	•	•

Figure 4.6. Summary of the number of CHS genes identified in representatives of the different Mollusca classes. Cells shaded in green in the table indicate CHS isoform loss.

4.5.3 Chitin synthesized by CHS may be involved in multiple functions in molluscs

In Porifera and Cnidaria, that possess exclusively Type I CHS, most species have a mineralized exoskeleton, and this led to the hypothesis that Type I CHS is essential for the shell and synthesizes chitin (Bo et al., 2012; Ehrlich et al., 2007; Zakrzewski et al., 2014). Furthermore, this led to a general assumption that chitin was only used for exoskeleton formation. Recent research done by (Vandepas et al., 2023) on the tissue distribution and expression of CHS genes in the Cnidaria, which lack a hard exoskeleton, suggests that CHS and its product may have a diversity of roles, which are not restricted to mineralization, which is supported by studies on several soft-bodied molluscs (such as *Aplysia californica*) that lack a mineralized shell.

Current research on the function of CHS in molluscs mainly focused on its role in biomineralization (Ghatak et al., 2013; Schönitzer and Weiss, 2007; Suzuki et al., 2007; Weiss, 2012). However, the results of our study revealed that CHS are expressed in tissues and shell-less larvae stages further supporting the proposal that it has a much broader biological role. Currently there are relatively few reports that characterize the biological functions of CHS isoforms, and (Weiss et al., 2006) Type II CHS isoform

which contain a myosin head (corresponding to MgaChs-IIC2_3 in this study) was described to have a role in shell formation. Nonetheless, Type II CHS isoform in *Tegillarca granosa* was also suggested to play a role in regulating polyspermy since specific blockade of this enzymes activity in the oocytes significantly increased polyspermy (Han et al., 2016).

4.5.4 The diversity of mollusc CHS domains was independent of shell emergence

The myosin head domain, in CHSs, may be one of the core functional domains associated with shell formation in metazoans (Weiss, 2012). The presence of a complex transmembrane structure and myosin head domain in CHS suggests it may regulate the cellular cytoskeleton and membrane biophysics during assembly of organic matrices (Burridge and Wennerberg, 2004; Weiss et al., 2013). This was corroborated by studies on oomycete CHS, which integrates N-terminal microtubule interacting and trafficking domains (Guerriero et al., 2010). The evolutionary origin of the N-terminal myosin head domain present in some lophotrochozoan CHS and also in fungal CHS suggests that at least two independent gene fusion events occurred in fungi and lophotrochozoans, which yielded highly similar products (Zakrzewski et al., 2014), and a third gene fusion event has been proposed for diatom CHS as it also has a myosin head domain (Durkin et al., 2009). Furthermore, the results of this study make

it clear that the myosin head domain is not fully preserved in molluscs Type II (B-D groups) CHS suggesting functional differentiation has occurred.

The Chitin_synth_2 domain is a highly conserved structural domain in metazoan CHS, as are the complex N- and C-terminal transmembrane domains. The catalytic centre of the Chitin_synth_2 domain contains three highly conserved functional motifs on the intracellular side (Figure 4.3). Our study clearly identifies the donor saccharide binding site as the most prominent difference between Type I and Type II CHS in the conserved domain sequence. However, how this affects CHS enzyme function remains to be clarified. Furthermore, Type I-A CHS isoform also contains a SAM domain, which has been proposed to be very important for protein-protein interactions (Thanos et al., 1999) further revealing that functional differentiation most likely occurred during the evolution of Type I-A and Type I-B isoforms.

4.5.5 The impact of extracellular pH on CHS isoform expression is species-specific

The extracellular region of CHS plays a key role in the enzymes function and chitin polymerization (Yabe et al., 1998). However, this region shared low sequence conservation across the different isoforms in our analysis. (Weiss et al., 2013) reported that assembly mechanism of

Atrina rigida CHS (Ar-CS1) occurs via its extracellular domain ArCS1_E22. These experiments suggested that the extracellular domain ArCS1_E22 was involved in regulating the multiple enzyme activities of Ar-CS1 such as chitin synthesis and myosin movements by interaction with mineral surfaces and eventually protein assembly. The protein complexes could locally probe the status of mineralization according to pH unless ions and pCO2 are balanced with suitable buffer substances. Mollusc shell architectures could also be regulated via a cytoskeletal crosstalk based on transmembrane supramolecular arrays of myosin CHSs that are stabilized by self-assembly via an extracellular domain at appropriate extrapallial pH conditions (Weiss, 2012).

The results of the present study on the effects on CHS expression of OA suggest that CHS without the myosin head domain may also be influenced by changes in extracellular pH. Our results not only support the species-specific response of CHS to OA but also suggest a broad impact of OA on CHS isoforms in juvenile *Mytilus* when compared to the oyster. Previously it was described that two CHS isoforms in *M. gigas* larvae were significantly regulated under OA stress (Zhang et al., 2019). However, this is not contradictory to the results of this study because previously found significant differences in the response of *M. gigas* larvae and adults to OA. Larvae are more susceptible induced by OA due to limitations in their energy metabolism sources (Gazeau et al., 2013;

Tan and Zheng, 2020). We previously reported that molecular processes in the mantle under OA indicate that *M. galloprovincialis* and *M. gigas* respond differently and suggested that shell type may determine the response (Clements et al., 2017; Lassoued et al., 2019). The larger suite of biomineralization toolbox and energy-related and regulatory-related gene transcripts found in the *M. galloprovincialis* mantle transcriptomes when exposed to OA may explain their greater capacity to regulate biomineralization toolbox genes and their reduced growth as energy is diverted to the more costly process of shell growth by building aragonite crystals and packing them into a regular arrangement (Peng et al., 2023). Considering the species-specificity of the distribution of CHS in adult tissues, during larval shell formation, and in the response of the mantle to OA we propose a simple hypothesis that the response of CHS to OA is not isoform-dependent but might be dependent on energy metabolism. Interestingly, our results still suggest that the Type I-B and Type II-D isoforms in *Mytilus* are affected by OA-induced energy metabolism regulation, which, in turn, impacts shell mineralization.

4.6 Conclusion

This study, comprehensively explored the CHS isoforms and their evolution in the bivalve are currently found to have the highest number of

genes. Our evolutionary analysis supports the previous notions that all four CHS Type II (A-D) found in lophotrochozoan already existed in their last common ancestor (Zakrzewski et al., 2014) but we further confirm that the last common ancestor of molluscs diverged in Type II-A (Type II-A-1 and Type II-A-2) and Type II-C (Type II-C-1 and Type II-C-2) clades. At the class level, varying degrees of isoform loss were observed in mollusc, and gene losses were unrelated to the existence of mineralized shells suggesting that a much wider functional role for these large group of enzymes. Differences in the donor saccharide binding site of catalytic center of the chitin_synth_2 domain between Type I and Type II isoforms suggest potential functional differentiation. The myosin head domain is not conserved within all Type II (B-D groups) CHS, even it be seems functional importance in shell formation. and species-specific CHS isoform tissue expression was found suggesting that functional diversification exist and the Mollusca CHS may be involved in other functions beyond the production and maintenance of the biomineralized shell. Using transcriptome data from pre- and post-shell appearance larval stages and mineralization-related tissues, we have identified CHS isoforms potentially involved in shell formation and the species-specific response of CHS to OA leads us to hypothesize that the effect of OA on CHS expression may not be isoform-dependent and are probably dependent on energy metabolism which may impact on shell formation.

4.7 Supplementary materials

4.7.1 Supplementary Figures

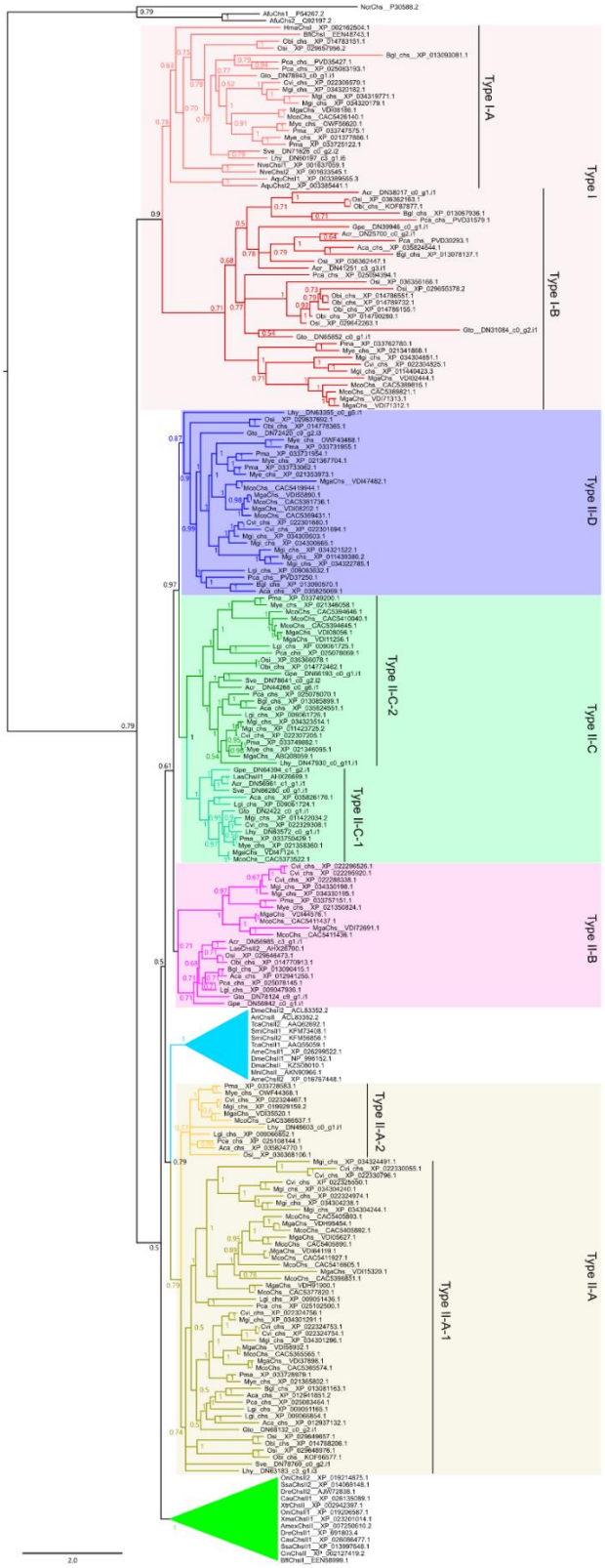

Supplementary Figure 4.1 Phylogenetic trees (BI tree) of the mollusc, insect and vertebrate chitin-synthases. Bayesian Inference tree with posterior probability value. The BI tree was built in MrBayes 3.2 using a VT substitution model (Aamodel = VT) with 1,000,000 generations. The accession numbers and give name of the sequences used are in Supplementary Table 4.1. The clade without background represents the Fungi CHS which is the root in phylogenetic tree. Green and blue merged clade indicate vertebrate and insect CHS respectively. Other colours background represents the CHS genes of Mollusc phylum.

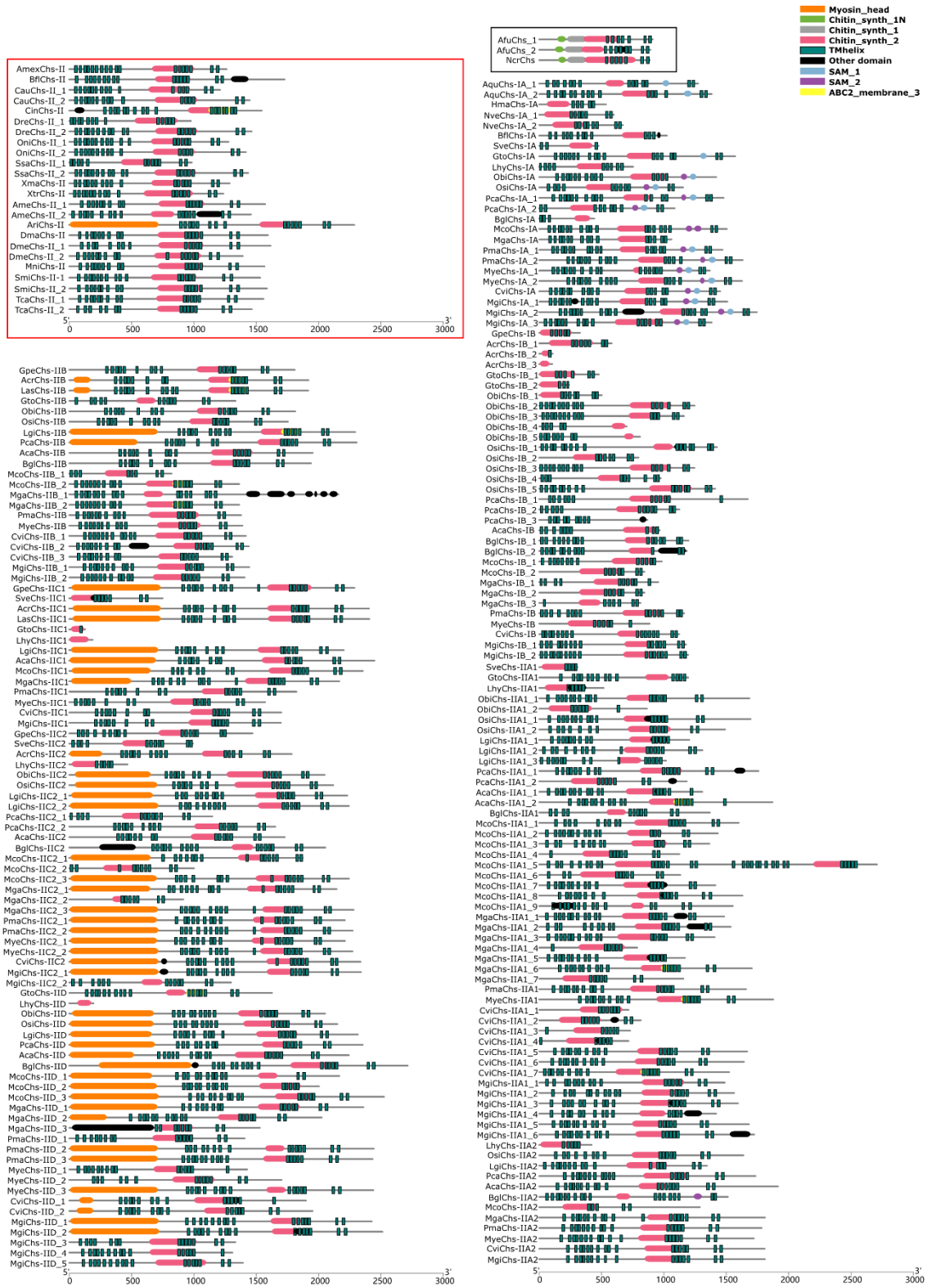

Supplementary Figure 4.2 Domain alignment of the deduced CHS proteins. The coloured bars represent the protein domains predicted by Pfam. The abscissa axis at bottom shows the amino acid length, the black line shows the protein amino acid length, and the domains are displayed with bars of different colors. The sources and accession numbers of the

sequences used are in Supplementary Table 4.1. Fungi and non-Mollusc CHS are shown in black and red boxes, respectively.

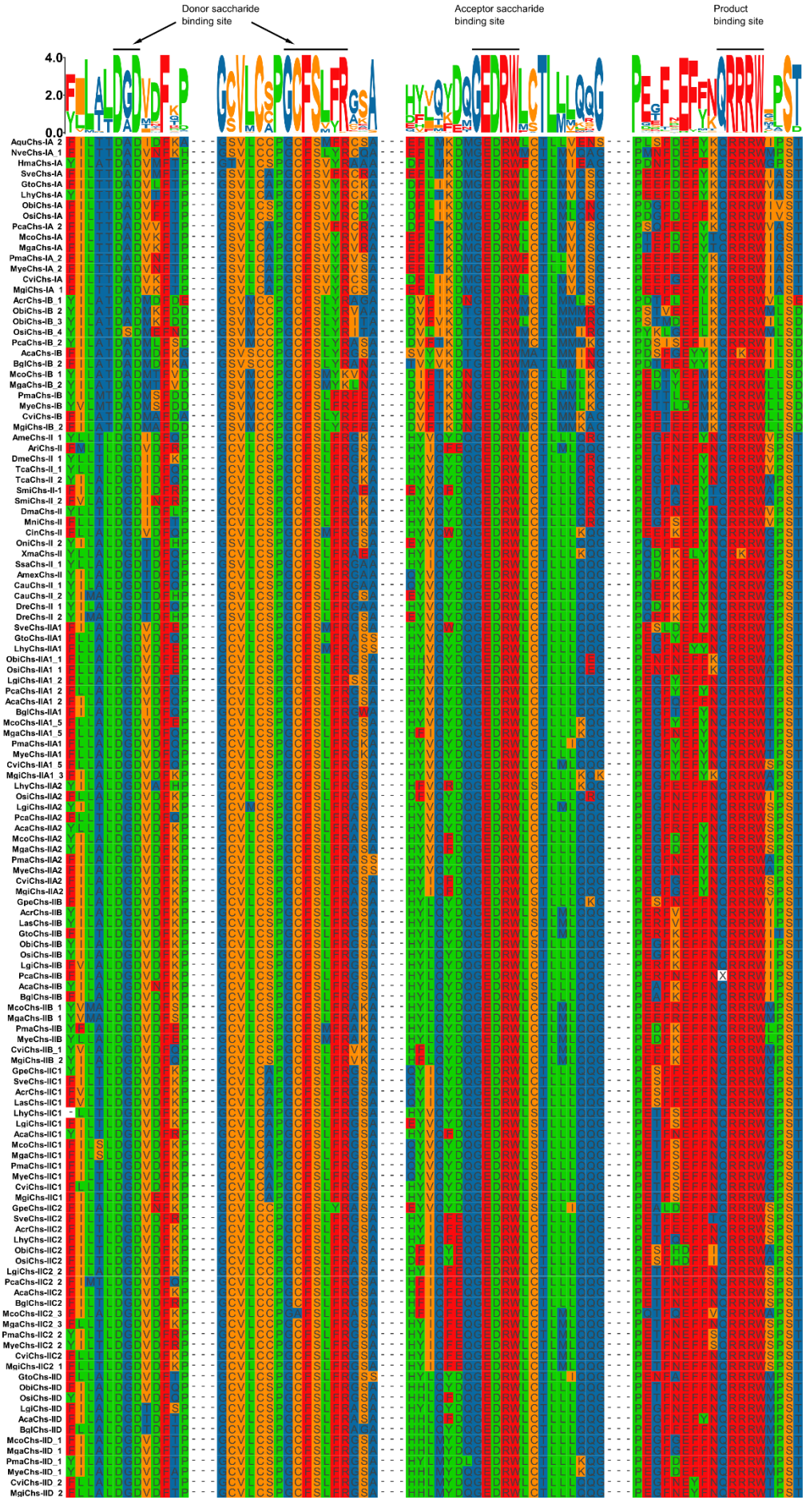
Donor saccharide binding site
Acceptor saccharide binding site
Product binding site
4.0
2.0
0.0
AquChs-IA 2
NveChs-IA_1
HmaChs-IA
SveChs-IA
GtoChs-IA
LhyChs-IA
ObiChs-IA
OsiChs-IA
PcaChs-IA_2
McoChs-IA
MgaChs-IA
PmaChs-IA_2
MyeChs-IA_2
CviChs-IA
MgiChs-IA_1
AcrChs-IB_1
ObiChs-IB_2
ObiChs-IB_3
OsiChs-IB_4
PcaChs-IB_2
AcaChs-IB
BglChs-IB_2
McoChs-IB_1
MgaChs-IB_2
PmaChs-IB
MyeChs-IB
CviChs-IB
MgiChs-IB_2
AmeChs-II_1
AriChs-II
DmeChs-II_1
TcaChs-II_1
TcaChs-II_2
SmiChs-II-1
SmiChs-II_2
DmaChs-II
MniChs-II
ClnChs-II
OsiChs-II_2
XmaChs-II
SsaChs-II_1
AmexChs-II
CauChs-II_1
CauChs-II_2
DreChs-II_1
DreChs-II_2
SveChs-IIA1
GtoChs-IIA1
LhyChs-IIA1
ObiChs-IIA1_1
OsiChs-IIA1_1
LgiChs-IIA1_2
PcaChs-IIA1_2
AcaChs-IIA1_2
BglChs-IIA1
McoChs-IIA1_5
MgaChs-IIA1_5
PmaChs-IIA1
MyeChs-IIA1
CviChs-IIA1_5
MgiChs-IIA1_3
LhyChs-IIA2
OsiChs-IIA2
LgiChs-IIA2
PcaChs-IIA2
AcaChs-IIA2
McoChs-IIA2
MgaChs-IIA2
PmaChs-IIA2
MyeChs-IIA2
CviChs-IIA2
MgiChs-IIA2
GpeChs-IIB
AcrChs-IIB
LasChs-IIB
GtoChs-IIB
ObiChs-IIB
OsiChs-IIB
LgiChs-IIB
PcaChs-IIB
AcaChs-IIB
BglChs-IIB
McoChs-IIB_1
MgaChs-IIB_1
PmaChs-IIB
MyeChs-IIB
CviChs-IIB_1
MgiChs-IIB_2
GpeChs-IIC1
SveChs-IIC1
AcrChs-IIC1
LasChs-IIC1
LhyChs-IIC1
LgiChs-IIC1
AcaChs-IIC1
McoChs-IIC1
MgaChs-IIC1
PmaChs-IIC1
MyeChs-IIC1
CviChs-IIC1
MgiChs-IIC1
GpeChs-IIC2
SveChs-IIC2
AcrChs-IIC2
LhyChs-IIC2
ObiChs-IIC2
OsiChs-IIC2
LgiChs-IIC2_2
PcaChs-IIC2_2
AcaChs-IIC2
BglChs-IIC2
McoChs-IIC2_3
MgaChs-IIC2_3
PmaChs-IIC2_2
MyeChs-IIC2_2
CviChs-IIC2
MgiChs-IIC2_1
GtoChs-IID
ObiChs-IID
OsiChs-IID
LgiChs-IID
AcaChs-IID
BglChs-IID
McoChs-IID_1
MgaChs-IID_1
PmaChs-IID_1
MyeChs-IID_1
CviChs-IID_2
MgiChs-IID_2

Supplementary Figure 4.3 Amino acid sequence alignment of the catalytic center of Chitin_synth_2 domain. Functional motifs donor saccharide binding site (DSBS), acceptor saccharide binding site (ASBS) and product binding site (PBS) were selected to display. The sources and accession numbers of the sequences used are in Supplementary Table 4.1. Amino acids were colored using the MSA default settings. At the top of the alignment letters of different heights indicate amino acid residues with different degrees of conservation, and the bigger the letter the higher the sequence conservation.

4.7.2 Supplementary Tables (in Annex V and VI, digital format)

CHAPTER 5

General discussion

5.1 General discussion

The phylum Mollusca comprises over 70,000 living species and is the second most diverse after the Arthropods. The large diversity of molluscs is attributed, at least in part, to their successful occupation of most habitats on Earth, including marine environments, freshwater lake and rivers, and even land. Throughout much of their history, particularly in the past 250 million years, bivalve have been one of the most diverse and ecologically important animal groups in the oceans. Today, they inhabit oceans and freshwater bodies worldwide, serving as a crucial food source for other organisms and playing a significant role in water filtration. Bivalves hold important ecological significance due to their role as a source of food and other products, as well as being potentially invasive species that can cause ecological disruption. Moreover, the heavily calcified shells of bivalves are also a vital component in the carbon cycle of the Earth. Currently, the mechanism behind shell formation requires extensive research for thorough exploration, especially in deciphering the functionality of the genetic "toolbox" responsible for shell formation. Additionally, the impact of environmental change, such as ocean acidification, on bivalves, lacks a well-established model, leading to contradictory results and conflicting viewpoints. Hence, understanding future trends in bivalve diversity, potential impacts on marine carbon

cycling, and assessing aquaculture production capacity in a continuously changing environment are crucial tasks at hand.

Based on the aforementioned, this thesis aims to focus on two bivalve species occupying the same ecological niche: the Pacific oyster (*M. gigas*), characterized by severely asymmetrical bivalves with shell containing irregularly arranged calcium carbonate crystals, and the Mediterranean mussel (*M. galloprovincialis*), a completely symmetrical bivalve shell featuring regularly arranged calcium carbonate crystals. This study investigated the composition of the biomineralization "toolbox" responsible for shell formation and the functional roles of candidate genes in these two target species. It also explored the universality and specificity of ocean acidification impact on bivalve species, along with the dynamic response of the "toolbox" genes. Specifically, the research is divided into four aspects: 1) Further development of the core "toolbox" for shell formation by exploring the transcriptomes and available genomes of multiple bivalve species (Chapter 2 and 3); 2) Through multi-omics analysis involving six species (including those with completely symmetrical, slightly asymmetrical, and severely asymmetrical shells), identified genes related to shell asymmetry and validation of the functional roles of some core genes through experiments (Chapter 2); 3) Explore and compare the impact of ocean acidification on the growth and

transcriptional levels of genes in the mantle in *M. gigas* and *M. galloprovincialis* (Chapter 3); 4) Explore the evolution of chitin synthase (responsible for synthesizing chitin, a fundamental framework used in the carbonate structure of bivalve shells) and its response to ocean acidification (Chapter 4).

5.1.1 The development of the core "toolbox" for shell biomineralization

Bivalves have developed a sophisticated set of tools to control the formation, composition, and morphology of their shells. The organic matrix, as the current focus of the shell biomineralization toolbox, is a complex mixture of SMP, lipids and polysaccharides (Weiner et al., 1983; Weiner and Traub, 1984). However, the organic matrix toolbox does not encompass all participants involved in shell formation; it should also include genes related to biomineralization regulation. We aimed to develop relevant regulatory genes and incorporate them into the toolbox. In this thesis, we have discovered and validated, for the first time, regulatory genes associated with biomineralization-related organic matrix, including lncRNA genes and non-organic matrix protein-coding genes.

The homogeneity of lncRNA genes is notably low among bivalve species, especially at taxonomic levels beyond the family level (Chapter 2). The number of genes on bivalve chromosomes varies, with mussels

having more lncRNA genes than oysters (Chapter 3). However, what remains consistent is the evidence from shell damage repair experiments, proving that lncRNAs are crucial members of the bivalve biomineralization toolbox (Chapter 3). Despite the existence of relatively limited experimental evidence linking lncRNA to biological function in bivalves, previous transcriptome/genome screening identified them in the mantle, and they have been implicated in the regulation of shell pigmentation, larval development, the immune system, and shell formation (Feng et al., 2018; Guo et al., 2023; Le Franc et al., 2022; Núñez-Acuña et al., 2022; Sun and Feng, 2018; Yu et al., 2016). One reason for the unclear understanding of the biomineralization mechanism in bivalves is the species diversity of SMP genes (Aguilera et al., 2017; Clark, 2020). This has captured major attention towards isolating and identifying the functional roles of SMP genes.

However, relatively little has been explored regarding the regulatory mechanisms. For instance, in the study of the biomineralization regulatory mechanisms in the *M. gigas*, non-organic matrix protein-coding genes (Unslp6, NTRDCP, KCP-1, KCP-3, KCP-4, PPIA, PXT-1, UNTMP, TIFF2-like, Temptin-1, Temptin-2, Unknow3, Unknow10, Unknow13, Unknow17, Unknow24, Unknow29) were identified and considered members of the biomineralization toolbox (Chapter 2). Identifying and developing toolbox genes from the perspective of

biomineralization regulation in bivalves poses both challenges and opportunities. This is due to the low homogeneity of non-protein-coding genes and the high homogeneity of non-organic matrix protein-coding genes.

5.1.2 Regulation by lncRNAs leads to asymmetry in the shells of bivalves

Most bivalve molluscs have a shell composed of two symmetric valves, modern bivalves such as the oysters (Ostreidae) and some scallops (Pectinida) have asymmetric valves indicating that shell asymmetry has emerged at least twice during the bivalve radiation (Harper and Checa, 2020). In most oysters, one shell is flat and the shell attached to the substrate is convex (cupped or round) (Yamaguchi, 1994). In this thesis, through multi-omics analysis of four species (highly asymmetric: *M. gigas*, *M. yessoensis*; mildly asymmetric: *P. fucata*; completely symmetric: *M. galloprovincialis*), we identified that only a small proportion of genes exhibited an asymmetric expression pattern in the mantle, approximately less than 0.4%. This suggests that the core group of genes regulating asymmetry in bivalve shells is relatively small, which could be advantageous for future analyses regarding the origin of asymmetry in bivalve shells. Previous studies on the limited number of asymmetric bivalves have tentatively suggested that the primary molecular pathway responsible for the asymmetry on both sides is

conserved, possibly similar to the TGF-β signalling pathway found in vertebrates (Wei et al., 2018; Zhang et al., 2022). However, such conclusions seem to overlook an established fact that vertebrates exhibit asymmetry in their body plans (tissue asymmetry), whereas bivalves display asymmetry in their shells (no reports of asymmetry in the soft body of bivalves). Furthermore, research does not appear to establish a connection between the genes in the mineralization toolbox and the asymmetry of the shell. Based on this, we used multiple-species analysis in this thesis to reveal distinctive features among DE genes in asymmetry: 1) 13-20% of differentially expressed genes are lncRNAs; 2) More DE genes have specific expression in the mantle of the flat shell of asymmetric bivalves; 3) Shared expression of DE genes more abundant in the mantle of the flat shell of asymmetry bivalves; 4) No significantly differentially expressed genes related to the TGF-β signalling pathway were found; 5) Taking *M. gigas* as an example, we demonstrate SMPs account for 66.06 % of *M. gigas* mantle DEc genes and that 62.39 % were abundant or specific to the mantle of the flat valve; 6) Only 12 proteins are specifically shared among asymmetric bivalves, linking to asymmetric shell formation, and 7 of these proteins belong to SMPs. These features imply that there might be differences in the signalling pathways associated with shell asymmetry at the order level. Additionally, differentially expressed lncRNA and SMP genes might predominantly

contribute to the formation of shell asymmetry. Protein-lncRNA interactions are reported to regulate pigment synthesis, shell colour and larval development in *M. gigas* (Feng et al., 2018; Yu et al., 2016). This supports the hypothesis that lncRNA may modulate shell shape by regulating asymmetric SMP/non-SMP expression.

This thesis conducted a multi-omic analysis using *M. gigas* as the representative species, identifying 6 candidate protein-lncRNA cis-regulatory modules linked to asymmetric shell formation. Further homology analysis across six bivalves revealed that 3 candidate cis-regulatory modules belong to taxa at or above the order level in Bivalvia, while the other 3 might be homologous to the oyster family level. Interestingly, among these, two cis-regulatory modules targeted proteins belonging to SMPs. Lineage-specific mantle secretomes are considered to underlie bivalve shell/shell microstructure diversity (Aguilera et al., 2017), since which overall conservation of SMP-domains and motifs (Arivalagan et al., 2017), and their utilization for shell building is divergent across species (Aguilera et al., 2017; Clark, 2020). Therefore, the above results suggest that protein-lncRNA cis-regulatory modules, homologous at different taxonomic levels, might be associated with differences in the proportions of calcite and aragonite content, as well as disparities in crystal arrangement in the shells of species at various order levels.

The prismatic crystals of the flat shell have a near-geometric crystal structure with regular boundaries and no cracks resembling the prismatic structure of symmetric shells (Peng et al., 2021). In contrast the crystals of round shells have a ridge-and-furrow structure, which is associated with their rapid growth for substrate adherence (Yamaguchi, 1994). This thesis, through experimental validation of the shell repair process in *M. gigas*, confirms the aforementioned points. Specifically, rapid shell growth significantly correlates with a round shell, suggesting that differences in the growth rates on both sides of the shell might be one of the phenotypes contributing to asymmetrical shells. Based on the morphological evolution and microstructure of bivalve shells we hypothesis that symmetry and round shells in bivalves is the default condition (McDougall and Degnan, 2018; Yonge, 1977) and that the flat and round valves of the asymmetric oysters are a more recent evolutionary innovation.

This thesis conducted functional studies on two candidate cis-regulatory modules, NTRDCP←TIMPDR→Unslp6 and SMPDR→EGF-CADCP, targeting these genes and using *M. gigas* shell growth and microscopic structure as assessment criteria. The newly grown damaged shell of both the flat and round valves in siRNA-TIMPDR treated *M. gigas* had a similar prismatic layer organization, the boundaries between the crystals were narrower and the calcium carbonate crystals had lost

their convex shape and were larger than the normal crystals in the controls. Both non-SMPs Unslp6 and NTRDCP contain a TIMP domain and belong to the NTR-like superfamily with inhibitory metalloproteinase activity in vertebrates (Bode et al., 1999) and in *P. fucata* (Kubota et al., 2017). In *P. fucata* metalloproteinases degrade extracellular matrices to produce the fine organic fibers that regulate the orientation of fibrous aragonite crystals (Kubota et al., 2018). siRNA-SMPDR also modified shell structure, causing the prismatic crystals in the round valve to be larger without changing shape compared to the control. In the flat shell the prismatic crystals were irregular with fissures and a horizontal orientation. The negative regulation of EGF-CADCP by SMPDR also had a positive effect on rapid planar growth of prismatic calcium carbonate crystal. Based on these observations, we propose a model in which lncRNAs modulate shell architecture and shape in asymmetric oysters by modifying expression of SMP and non-SMP proteins to regulate growth of prismatic calcium carbonate crystal.

5.1.3 Shell type determine species-specific response of bivalves under ocean acidification

As is well known, Ocean acidification (OA) is causing the dissolution of coral calcium carbonate structures, which has increased concerns about

the ocean carbon cycle (Albright, 2011). In bivalves, the main way OA affects shell growth and calcification is by modifying the elevated seawater pCO_2, which reduces the $CaCO_3$ saturation of aragonite and calcite in the environment. This alteration changes the dynamics of uptake and modifies shell deposition, shell composition, and structure (Kroeker et al., 2013, 2010). Although *M. galloprovincialis* and *M. gigas* occupy nearly identical ecological niches by settling on hard substrates in intertidal and subtidal habitats, they exhibit completely differentiated shell shapes, shell calcium carbonate crystal types (*M. galloprovincialis*: regularly arranged aragonite crystals and regularly arranged calcite crystals; *M. gigas*: irregularly arranged calcite crystals.), and attachment.

The response of bivalves to elevated pCO_2 is species-specific and stage-specific during development (Gazeau et al., 2013; Tan and Zheng, 2020), and there are even reported cases where OA has no negative impact on certain bivalve species (Waldbusser et al., 2016). In this study, the growth of both *M. galloprovincialis* and *M. gigas* juveniles was significantly inhibited under long-term OA exposure, and we observed that *M. galloprovincialis* secreted more byssus threads in response to the weakened impact caused by monofilament weakness (Zhao et al., 2017). (Gazeau et al., 2010) and (Thomsen and Melzner, 2010) reported that OA reduces the growth rates of *M. edulis* larvae and adults. Although most of

the literature reports no significant impact of OA on shell growth of adult *M. gigas* (Lannig et al., 2010; Rajan et al., 2021), (Kurihara et al., 2007) reported negative effects of OA on the development and calcification of *M. gigas* larvae. In our results, it is worth noting that under the same habitat background and experimental conditions, OA has a more significant growth inhibition effect on *M. galloprovincialis* juveniles compared to *M. gigas* juveniles. Similar findings have been reported by (Gazeau et al., 2007), who found that the rate of calcification inhibition by OA differs between *M. edulis* and *M. gigas*, with the former being approximately 2.5 times higher than the latter. Regardless of the species-specific response to OA, studies generally indicate adverse effects of OA exposure on bivalve larvae and adults.

Transcriptome PCA analysis in this study revealed that after OA exposure, the gene expression profile of the mantle in *M. galloprovincialis* juveniles deviated significantly from the seawater group (control group), while the OA group of *M. gigas* juveniles completely overlapped with the seawater group. This suggests that *M. galloprovincialis* exhibits a stronger physiological response and possesses a greater and more complex gene expression regulatory behavior compared to *M. gigas*. Both PCA clustering and the number of DEGs support that the presence of additional stressors (such as secondary stressors, SSOA) further triggers the response of *M. galloprovincialis* and

M. gigas juveniles to OA. Interestingly, others reported that OA increases the risk of bacterial infection in bivalves, negatively impacting immune-related signaling pathways (Liu et al., 2016; Su et al., 2017). DEGs induced by OA exposure in our study revealed species-specific differences and functional gene ontology (GO) annotations elucidated that these genes are involved in metabolic processes, developmental processes, response to stimuli, and immune system functions. The largest difference between *M. galloprovincialis* and *M. gigas* was observed in metabolic processes.

Our novel hypothesis that the high metabolic costs observed in *M. galloprovincialis* may be associated with its thicker nacreous layer (aragonite crystal structure), despite previous suggestions that species with slower growth and lower metabolic rates exhibit greater adaptability to OA (Waldbusser et al., 2016). This is because aragonite crystals are believed to be less stable than calcite crystals in natural environments, requiring more energy for their formation (Niu et al., 2022; Santos and Gerven, 2011; Shi et al., 2019). Additionally, the study by (Lassoued et al., 2019) strongly supports our viewpoint. They found that with increasing pCO_2, the ratio of aragonite-to-calcite in *M. galloprovincialis* shells exposed to 800 μatm pCO_2 and 1200 μatm pCO_2 decreased by 7-8% and 18%, respectively. Interestingly, their research also revealed that the aragonite-to-calcite ratio in the shells did not improve with increased food

availability, contrasting with findings in oysters (*C. virginica*) where sufficient food supply could restore shell mineralization inhibited by OA (Clements et al., 2017).

Considering the transcriptomic data demonstrating that *M. galloprovincialis* exhibits a greater response to OA compared to *M. gigas*, with increased expression of ion pumps, chitin synthases, SMPs, and regulatory factors (TFs, lncRNAs, and neuropeptides) involved in mineralization, we speculate that if a species requires the activation of a larger number of mineralization tools or invests more energy in constructing exquisite but relatively unstable calcium carbonate crystals, the negative impact of OA on the metabolism of mantle cells and the energy cost will profoundly affect the utilization of mineralization tools and crystal formation. This study provides the first answers regarding the differential adaptability and potential molecular mechanisms of bivalves with different types of calcium carbonate crystalline shells to OA.

5.1.4 Complex evolutionary history of chitin synthases in molluscs and species-specific responses to ocean acidification

In molluscs, chitin, a widespread natural amino polysaccharide, is an important organic structural polymer of the shell since it provides the framework for mineralization of calcium carbonate (Falini et al., 1996). The regulation of chitin turnover (synthesis/breakdown), evolution of

CHS in mollusc and how it affects shell growth is poorly understood. Furthermore, it is unclear if the effects of climate change on shell growth and mineralization are mediated by modifications in its organic framework. With a view to answering these questions the chitin-synthases (CHS) were investigated.

In previous studies, it was believed that CHS is expanded in the phylum Mollusca, and it was thought that the gastropod *L. gigantea* possesses the highest number of CHS (10 isoforms) although it was recently revealed that amphioxus species have 11-12 CHS isoforms (Shi et al., 2020). In this thesis we found that bivalve, in particular, the order Ostreoida (~22 isoforms), and oysters (~17-22 isoforms), have potentially the most extensive number of CHS isoforms in eukaryotes. Metazoan CHS can be divided into two branches (Type I and Type II) (Shi et al., 2020; Zakrzewski et al., 2014). Four branches (Type II A-D) of CHS contain sequences from different lophotrochozoans (i.e., Molluscas, Brachiopods, Entoprocts, and Annelids) suggest that the four different CHS type II (Type II A-D) already emerged in their last common ancestor (Zakrzewski et al., 2014). This study provides a straightforward hypothesis that the last ancestor of Mollusca may have further expanded in Type I (Type I-A and Type I-B), Type II A (Type II A-1 and Type II A-2), and Type II C (Type II C-1 and Type II C-2). However, there is

varying degrees of gene loss at the class level in Mollusca, and this loss phenomenon is unrelated to the presence of a mineralized shell.

CHS distribution in Cnidaria, vertebrates and shell-less molluscs (Vandepas et al., 2023), and the results of tissue and shell-less larvae CHS expression in this study all suggest that the relationship between CHS isoforms and function may be one-sided by solely considering the role of biomineralization. Instead, it may require more attention to the role of chitin as a polysaccharide itself (chitin possibly serving unknown functions in the role of polysaccharides in the biology) (Han et al., 2016). There are few reports that explicitly define the function of CHS isoforms.

CHS exhibits a complex structure with notable differences in structural domains among its isoforms. The distribution of crucial domains such as the Myosin head domain and Chitin_synth_2 domain in mollusc CHS isoforms demonstrates the intricate evolutionary history and functional divergence of CHS within this class (Durkin et al., 2009). Research show that the extracellular portion of CHS exhibits lower sequence conservation and assembly mechanism of the CHS (Ar-CS1) via its extracellular domain ArCS1_E22, which is involved in regulating the multiple enzyme activities of Ar-CS1 such as chitin synthesis and myosin movements by interaction with mineral surfaces and eventually by protein assembly (Weiss et al., 2013). The protein complexes could

locally probe the status of mineralization according to pH unless ions and pCO_2 are balanced with suitable buffer substances. Mollusc shell architectures could also be regulated via a cytoskeletal cross-talk based on transmembrane supramolecular arrays of myosin CHSs that are stabilized by self-assembly via an extracellular domain at appropriate extrapallial pH conditions (Weiss, 2012). The results of this study on the impact of OA on CHS suggest that CHS without the myosin head domain may also be influenced by extracellular pH. Furthermore, our results support the notion that the species-specific response (*M. galloprovincialis* and *M. gigas*) of CHS to OA suggests that the vulnerability of bivalve species to changes in the marine environment will not be uniform. Considering the species-specificity of CHS in tissue distribution, larval shell formation, and OA response demonstrated by the results of our study about CHS, we propose a simple hypothesis that the response of CHS to OA is not isoform-dependent but might be dependent on energy metabolism (Peng et al., 2023). Interestingly, our results still suggest that the Type I-B and Type II-D isoforms in *Mytilus* are affected by OA-induced energy metabolism regulation, which, in turn, impacts shell mineralization.

5.2 Conclusion and future perspectives

In summary, the results presented in this thesis further expand our current knowledge on the state-of-art of bivalve shell biomineralization by providing a comparative analysis of the molecular factors involved of shell regulation and growth by looking at the mantle, the main tissue involved in shell production. A molecular mechanism that explains the origin of asymmetric valves in oysters and possibly other asymmetric bivalves was identified. We uncover cis-regulatory modules that explain the asymmetric expression of biomineralization-related genes (SMP and secreted non-SMP), which change prismatic crystal growth and modify the planar growth rate and spatial orientation of crystals, culminating in asymmetric shells. LncRNA cis-regulatory modules exist in other asymmetric bivalves, indicating a conserved regulatory innovation and support the hypothesis that shells are shaped by conserved upstream cis-regulation and a highly evolved and diverse downstream regulatory network in the bivalve mantle. This work undoubtedly provides a novel research direction. In the future, we will verify the signaling pathways regulated by lncRNA, including upstream regulatory factors (intracellular factors such as transcription factors and membrane receptors; intercellular factors such as neuropeptides and hormones) and downstream protein interactions (signal transduction between downstream proteins and the

nucleation reaction of calcium carbonate crystallization).

Analysis of mantle transcriptomes suggest that *M. galloprovincialis* and *M. gigas* may have distinct biomineralization mechanisms. This difference is reflected in *M. galloprovincialis* consuming more energy and utilizing more genes to build more complex and costlier aragonite crystals, as well as their regular arrangement. OA exposure increases the construction cost of the shell. In an OA-exposed environment, shell damage further negatively affects the intracellular homeostasis, energy metabolism, and ion transport of mantle cells, thereby impacting bivalve calcification. This study provides novel insights and speculates that if a bivalve species needs to employ a greater number of mineralization tools or invest more energy in constructing relatively unstable calcium carbonate crystals, the negative impact of OA on mantle cell metabolism and the energy cost will more profoundly affect the use of mineralization tools and shell calcification. The implied conclusions from this study results are novel, yet further validation is required with more species of bivalves. In the future, we aim to incorporate a wider variety of bivalves with different shell compositions (aragonite and calcite ratios) for experiments to validate the nucleation dynamics of different calcium carbonate crystals under OA exposure. This research is challenging, undoubtedly, but also extremely compelling.

We comprehensively explored the CHS isoforms at the class level in

molluscs and constructed an evolutionary tree. Bivalves are currently found to have the highest number of CHS isoforms in eukaryotes and a complex evolutionary history. Identification of pronounced species-specific CHS isoform expression tissues and larval stage implies potential functional diversification or involvement in functions beyond shell biomineralization. The species-specific response of CHS to OA leads supports a hypothesis that the effects of OA on CHS are not isoform-dependent and may be dependent on energy metabolism. However, we found that the Type I-B and Type II-D isoforms in bivalves are affected by OA-induced energy metabolism regulation, which subsequently impacts shell mineralization. In terms of the evolutionary aspect, the distribution of available Mollusca genomes and the detection of CHS appears to be uneven. It is necessary in the future to conduct systematic analyses using a wider range of genomic information from more representation mollusc species. Additionally, investigating whether the specific response of CHS isoforms in the order of bivalves to OA exposure is related to specific motifs and functions of the protein remains a key focus for future work. The most significant questions revolve around the functional divergence among CHS isoforms in molluscs and whether there exist functionalities beyond shell construction.

Bibliography

Abdraba, A.M., Saleuddin, A.S.M., 2000. Protein synthesis in vitro by mantle tissue of the land snail Otala lactea: possible insulin-like peptide function. Can J Zool 78, 1527–1535.

Addadi, L., Joester, D., Nudelman, F., Weiner, S., 2006. Mollusk shell formation: a source of new concepts for understanding biomineralization processes. Chemistry–A European Journal 12, 980–987.

Addadi, L., Weiner, S., 1992. Control and design principles in biological mineralization. Angewandte Chemie International Edition in English 31, 153–169.

Afgan, E., Baker, D., Van den Beek, M., Blankenberg, D., Bouvier, D., Čech, M., Chilton, J., Clements, D., Coraor, N., Eberhard, C., 2016. The Galaxy platform for accessible, reproducible and collaborative biomedical analyses: 2016 update. Nucleic Acids Res 44, W3–W10.

Aguilera, F., McDougall, C., Degnan, B.M., Irwin, D., 2017. Co-option and de novo gene evolution underlie molluscan shell diversity. Mol Biol Evol. https://doi.org/10.1093/molbev/msw294

Akamatsu, S., Zansheng, L.T., Moses, T.M., Scarratt, K., 2001. The current status of Chinese freshwater cultured pearls. Gems Gemol 37, 96–113.

Albright, R., 2011. Reviewing the effects of ocean acidification on sexual reproduction and early life history stages of reef-building corals. Journal of Marine Sciences 2011.

Alesci, A., Albano, M., Fumia, A., Messina, E., Miller, A., Di Fresco, D., de Oliveira Fernandes, J.M., Spanò, N., Savoca, S., Capillo, G., 2023. Shell formation in two species of bivalves: the role of mantle cells and haemocytes. Zool J Linn Soc zlad099.

Alfaro, A.C., Nguyen, T. V, Merien, F., 2019. The complex interactions of Ostreid herpesvirus 1, Vibrio bacteria, environment and host factors in mass mortality outbreaks of Crassostrea gigas. Rev Aquac 11, 1148–1168.

Allam, B., Espinosa, E.P., 2016. Bivalve immunity and response to infections: are we looking at the right place? Fish Shellfish Immunol 53, 4–12.

Alonso, A.A., Álvarez-Salgado, X.A., Antelo, L.T., 2021. Assessing the impact of bivalve aquaculture on the carbon circular economy. J Clean Prod 279, 123873.

Anand, L., Lopez, C.M.R., 2020. chromoMap: an R package for interactive visualization and annotation of chromosomes. Biorxiv 605600.

Aranaz, I., Acosta, N., Civera, C., Elorza, B., Mingo, J., Castro, C., Gandía, M.D.L.L., Heras Caballero, A., 2018. Cosmetics and cosmeceutical applications of chitin, chitosan and their derivatives. Polymers (Basel) 10, 213.

Arif, M., Asif, M., Ahmed, I., 2017. Advanced composite material for aerospace application—A review. Int. J. Eng. Manuf. Sci 7, 393–409.

Arivalagan, J., Yarra, T., Marie, B., Sleight, V.A., Duvernois-Berthet, E., Clark, M.S., Marie, A., Berland, S., 2017. Insights from the shell proteome: biomineralization to adaptation. Mol Biol Evol 34, 66–77.

Asplund, M.E., Baden, S.P., Russ, S., Ellis, R.P., Gong, N., Hernroth, B.E., 2014. Ocean acidification and host–pathogen interactions: blue mussels, M ytilus edulis, encountering V ibrio tubiashii. Environ Microbiol 16, 1029–1039.

Audino, J.A., Marian, J., 2018. Comparative and functional anatomy of the mantle margin in ark clams and their relatives (Bivalvia: Arcoidea) supports association between morphology and life habits. J Zool 305, 149–162.

Audino, J.A., Marian, J.E.A.R., 2016. On the evolutionary significance of the mantle margin in pteriomorphian bivalves. Am Malacol Bull 34, 148–159.

Audino, J.A., Marian, J.E.A.R., Wanninger, A., Lopes, S.G.B.C., 2015a. Mantle margin morphogenesis in Nodipecten nodosus (Mollusca: Bivalvia): new insights into the development and the roles of bivalve pallial folds. BMC Dev Biol 15, 1–22.

Audino, J.A., Marian, J.E.A.R., Wanninger, A., Lopes, S.G.B.C., 2015b. Anatomy of the pallial tentacular organs of the scallop Nodipecten nodosus (Linnaeus, 1758)(Bivalvia: Pectinidae). Zoologischer Anzeiger-A Journal of Comparative Zoology 258, 39–46.

Avdelas, L., Avdic-Mravlje, E., Borges Marques, A.C., Cano, S., Capelle, J.J., Carvalho, N., Cozzolino, M., Dennis, J., Ellis, T., Fernandez Polanco, J.M., 2021. The decline of mussel aquaculture in the European Union: Causes, economic impacts and opportunities. Rev Aquac 13, 91–118.

Baag, S., Mandal, S., 2022. Combined effects of ocean warming and acidification on marine fish and shellfish: A molecule to ecosystem perspective. Science of The Total Environment 802, 149807.

Barker, G.M., 2001. The biology of terrestrial molluscs. CABI publishing.

Barton, A., Waldbusser, G.G., Feely, R.A., Weisberg, S.B., Newton, J.A., Hales, B., Cudd, S., Eudeline, B., Langdon, C.J., Jefferds, I., 2015. Impacts of coastal acidification on the Pacific Northwest shellfish industry and adaptation strategies implemented in response. Oceanography 28, 146–159.

Bayne, B.L., 1999. Physiological components of growth differences between individual oysters (Crassostrea gigas) and a comparison with Saccostrea commercialis. Physiological and biochemical zoology 72, 705–713.

Beck, K., Hunter, I., Engel, J., 1990. Structure and function of laminin: anatomy of a multidomain glycoprotein. The FASEB journal 4, 148–160.

Beninger, P.G., Veniot, A., Poussart, Y., 1999. Principles of pseudofeces rejection on the bivalve mantle: integration in particle processing. Mar Ecol Prog Ser 178, 259–269.

Bieler, R., Mikkelsen, P.M., Collins, T.M., Glover, E.A., González, V.L., Graf, D.L., Harper, E.M., Healy, J., Kawauchi, G.Y., Sharma, P.P., 2014. Investigating the Bivalve Tree of Life–an exemplar-based approach combining molecular and novel morphological characters. Invertebr Syst 28, 32–115.

Bitter, M.C., Kapsenberg, L., Gattuso, J.-P., Pfister, C.A., 2019. Standing genetic variation fuels rapid adaptation to ocean acidification. Nat Commun 10, 5821.

Bjärnmark, N.A., Yarra, T., Churcher, A.M., Felix, R.C., Clark, M.S., Power, D.M., 2016. Transcriptomics provides insight into Mytilus galloprovincialis (Mollusca: Bivalvia) mantle function and its role in biomineralisation. Mar Genomics 27, 37–45. https://doi.org/10.1016/j.margen.2016.03.004

Bo, M., Bavestrello, G., Kurek, D., Paasch, S., Brunner, E., Born, R., Galli, R., Stelling, A.L., Sivkov, V.N., Petrova, O. V, 2012. Isolation and identification of chitin in the black coral Parantipathes larix (Anthozoa: Cnidaria). Int J Biol Macromol 51, 129–137.

Bode, W., FERNANDEZ-CATALAN, C., Grams, F., GOMIS-RÜTH, F., Nagase, H., Tschesche, H., Maskos, K., 1999. Insights into MMP-TIMP interactions. Ann N Y Acad Sci 878, 73–91.

Bolger, A.M., Lohse, M., Usadel, B., 2014. Trimmomatic: a flexible trimmer for Illumina sequence data. Bioinformatics 30, 2114–2120.

Bonacci, S., Browne, M.A., Dissanayake, A., Hagger, J.A., Corsi, I., Focardi, S., Galloway, T.S., 2004. Esterase activities in the bivalve mollusc Adamussium colbecki as a biomarker for pollution

monitoring in the Antarctic marine environment. Mar Pollut Bull 49, 445–455.
Boorman, C.J., Shimeld, S.M., 2002. The evolution of left–right asymmetry in chordates. Bioessays 24, 1004–1011.
Box, A., Sureda, A., Galgani, F., Pons, A., Deudero, S., 2007. Assessment of environmental pollution at Balearic Islands applying oxidative stress biomarkers in the mussel Mytilus galloprovincialis. Comparative Biochemistry and Physiology Part C: Toxicology & Pharmacology 146, 531–539.
Braun, E., Brenner, N., 2004. Transient responses and adaptation to steady state in a eukaryotic gene regulation system. Phys Biol 1, 67.
Brown, A.R., Lilley, M., Shutler, J., Lowe, C., Artioli, Y., Torres, R., Berdalet, E., Tyler, C.R., 2020. Assessing risks and mitigating impacts of harmful algal blooms on mariculture and marine fisheries. Rev Aquac 12, 1663–1688.
Bubel, A., 1973. An electron-microscope study of periostracum formation in some marine bivalves. I. The origin of the periostracum. Mar Biol 20, 213–221.
Buchfink, B., Xie, C., Huson, D.H., 2015. Fast and sensitive protein alignment using DIAMOND. Nat Methods 12, 59–60.
Burkholder, J.M., Shumway, S.E., 2011. Bivalve shellfish aquaculture and eutrophication. Shellfish aquaculture and the environment 155–215.
Burridge, K., Wennerberg, K., 2004. Rho and Rac take center stage. Cell 116, 167–179.
Cai, C., He, Q., Xie, B., Xu, Z., Wang, C., Yang, C., Liao, Y., Zheng, Z., 2022. Long non-coding RNA LncMPEG1 responds to multiple environmental stressors by affecting biomineralization in pearl oyster Pinctada fucata martensii. Front Mar Sci 9, 1014810.
Caldeira, K., Wickett, M.E., 2003. Anthropogenic carbon and ocean pH. Nature 425, 365.
Campanati, C., Willer, D., Schubert, J., Aldridge, D.C., 2022. Sustainable intensification of aquaculture through nutrient recycling and circular economies: more fish, less waste, blue growth. Reviews in Fisheries Science & Aquaculture 30, 143–169.
Cao, L., Kenchington, E., Zouros, E., Rodakis, G.C., 2004. Evidence that the large noncoding sequence is the main control region of maternally and paternally transmitted mitochondrial genomes of the marine mussel (Mytilus spp.). Genetics 167, 835–850.
Cao-Pham, A.H., Hiong, K.C., Boo, M. V, Choo, C.Y.L., Pang, C.Z.,

Wong, W.P., Neo, M.L., Chew, S.F., Ip, Y.K., 2019. Molecular characterization, cellular localization, and light-enhanced expression of Beta-Na+/H+ Exchanger-like in the whitish inner mantle of the giant clam, Tridacna squamosa, denote its role in light-enhanced shell formation. Gene 695, 101–112.

Cardoso, J.C.R., Félix, R.C., Bjärnmark, N., Power, D.M., 2016. Allatostatin-type A, kisspeptin and galanin GPCRs and putative ligands as candidate regulatory factors of mantle function. Mar Genomics 27, 25–35.

Cardoso, J.C.R., Félix, R.C., Ferreira, V., Peng, M., Zhang, X., Power, D.M., 2020. The calcitonin-like system is an ancient regulatory system of biomineralization. Sci Rep 10, 1–18.

Cardoso, J.C.R., Ferreira, V., Zhang, X., Anjos, L., Félix, R.C., Batista, F.M., Power, D.M., 2019. Evolution and diversity of alpha-carbonic anhydrases in the mantle of the Mediterranean mussel (Mytilus galloprovincialis). Sci Rep 9, 10400.

Carlini, D.B., Reece, K.S., Graves, J.E., 2000. Actin gene family evolution and the phylogeny of coleoid cephalopods (Mollusca: Cephalopoda). Mol Biol Evol 17, 1353–1370.

Caron, J.-B., Jackson, D.A., 2008. Paleoecology of the greater phyllopod bed community, Burgess Shale. Palaeogeogr Palaeoclimatol Palaeoecol 258, 222–256.

Carter, J.G., 1990. Skeletal Biomineralization: Patterns, Processes and Evolutionary Trends: Volume I. Springer.

Ceccherelli, V.U., Rossi, R., 1984. Settlement, growth and production of the mussel Mytilus galloprovincialis. Marine ecology progress series. Oldendorf 16, 173–184.

Chan, V.B.S., Johnstone, M.B., Wheeler, A.P., Mount, A.S., 2018. Chitin facilitated mineralization in the eastern oyster. Front Mar Sci 5, 347.

Rajan, K.C., Meng, Y., Yu, Z., Roberts, S.B., Vengatesen, T., 2021. Oyster biomineralization under ocean acidification: From genes to shell. Glob Chang Biol 27, 3779–3797.

Chapman, R.W., Mancia, A., Beal, M., Veloso, A., Rathburn, C., Blair, A., Holland, A.F., Warr, G.W., Didinato, G.U.Y., Sokolova, I.M., 2011. The transcriptomic responses of the eastern oyster, Crassostrea virginica, to environmental conditions. Mol Ecol 20, 1431–1449.

Checa, A., 2000. A new model for periostracum and shell formation in Unionidae (Bivalvia, Mollusca). Tissue Cell 32, 405–416.

Checa, A.G., 2018. Physical and biological determinants of the fabrication of molluscan shell microstructures. Front Mar Sci 5, 353.

Checa, A.G., Harper, E.M., González-Segura, A., 2018. Structure and crystallography of foliated and chalk shell microstructures of the oyster Magallana: the same materials grown under different conditions. Sci Rep 8, 7507.
Checa, A.G., Rodríguez-Navarro, A.B., Esteban-Delgado, F.J., 2005. The nature and formation of calcitic columnar prismatic shell layers in pteriomorphian bivalves. Biomaterials 26, 6404–6414.
Chen, C., Chen, H., Zhang, Y., Thomas, H.R., Frank, M.H., He, Y., Xia, R., 2020. TBtools: an integrative toolkit developed for interactive analyses of big biological data. Mol Plant 13, 1194–1202.
Chen, X., Bai, Z., Li, J., 2019. The mantle exosome and microRNAs of Hyriopsis cumingii involved in nacre color formation. Marine Biotechnology 21, 634–642.
Chmura, G.L., Anisfeld, S.C., Cahoon, D.R., Lynch, J.C., 2003. Global carbon sequestration in tidal, saline wetland soils. Global Biogeochem Cycles 17.
Choudhary, C., Sharma, S., Meghwanshi, K.K., Patel, S., Mehta, P., Shukla, N., Do, D.N., Rajpurohit, S., Suravajhala, P., Shukla, J.N., 2021. Long non-coding RNAs in insects. Animals 11, 1118.
Cinner, J.E., Huchery, C., MacNeil, M.A., Graham, N.A.J., McClanahan, T.R., Maina, J., Maire, E., Kittinger, J.N., Hicks, C.C., Mora, C., 2016. Bright spots among the world's coral reefs. Nature 535, 416–9.
Clark, Melody S, 2020. Molecular mechanisms of biomineralization in marine invertebrates. Journal of Experimental Biology 223, jeb206961.
Clark, Melody S., 2020. Molecular mechanisms of biomineralization in marine invertebrates. Journal of Experimental Biology 223. https://doi.org/10.1242/jeb.206961
Clark, M.S., Peck, L.S., Arivalagan, J., Backeljau, T., Berland, S., Cardoso, J.C.R., Caurcel, C., Chapelle, G., De Noia, M., Dupont, S., 2020. Deciphering mollusc shell production: the roles of genetic mechanisms through to ecology, aquaculture and biomimetics. Biological Reviews 95, 1812–1837.
Clark, M.S., Thorne, M.A.S., Amaral, A., Vieira, F., Batista, F.M., Reis, J., Power, D.M., 2013. Identification of molecular and physiological responses to chronic environmental challenge in an invasive species: the P acific oyster, C rassostrea gigas. Ecol Evol 3, 3283–3297.
Clements, J.C., Bourque, D., McLaughlin, J., Stephenson, M., Comeau, L.A., 2017. Extreme ocean acidification reduces the susceptibility of eastern oyster shells to a polydorid parasite. J Fish Dis 40, 1573–

1585.
Cobabe, E.A., Pratt, L.M., 1995. Molecular and isotopic compositions of lipids in bivalve shells: a new prospect for molecular paleontology. Geochim Cosmochim Acta 59, 87–95.
Coen, L.D., Luckenbach, M.W., 2000. Developing success criteria and goals for evaluating oyster reef restoration: ecological function or resource exploitation? Ecol Eng 15, 323–343.
Coen, L.D., Luckenbach, M.W., Breitburg, D.L., 1999. The role of oyster reefs as essential fish habitat: a review of current knowledge and some new perspectives, in: American Fisheries Society Symposium. pp. 438–454.
Collins, M.J., Stern, B., Abbott, G.D., Walton, D., Riley, M.S., Von Wallmenich, T., Savage, N.M., Armstrong, H.A., Westbroek, P., 1995. Intracrystalline" organic matter in biominerals. Org Geochem 702–706.
Simon, C.M., 1985. The Middle Cambrian metazoan Wiwaxia corrugata (Matthew) from the Burgess Shale and Ogygopsis Shale, British Columbia, Canada. Philosophical Transactions of the Royal Society of London. B, Biological Sciences 307, 507–582.
Cuif, J.-P., Dauphin, Y., Sorauf, J.E., 2010. Biominerals and fossils through time. Cambridge University Press.
Daguin, C., Borsa, P., 2000. Genetic relationships of Mytilus galloprovincialis Lamarck populations worldwide: evidence from nuclear-DNA markers. Geological Society, London, Special Publications 177, 389–397.
Dame, R.F., 1993. The role of bivalve filter feeder material fluxes in estuarine ecosystems, in: Bivalve Filter Feeders: In Estuarine and Coastal Ecosystem Processes. Springer, pp. 245–269.
Dame, R.F., Kenneth, M.J., 2011. Ecology of marine bivalves: an ecosystem approach. Taylor & Francis.
Dauphin, Y., Ball, A.D., Castillo-Michel, H., Chevallard, C., Cuif, J.-P., Farre, B., Pouvreau, S., Salomé, M., 2013. In situ distribution and characterization of the organic content of the oyster shell Crassostrea gigas (Mollusca, Bivalvia). Micron 44, 373–383.
Dauphin, Y., Ball, A.D., Cotte, M., Cuif, J.-P., Meibom, A., Salomé, M., Susini, J., Williams, C.T., 2008. Structure and composition of the nacre–prisms transition in the shell of Pinctada margaritifera (Mollusca, Bivalvia). Anal Bioanal Chem 390, 1659–1669.
Davidson, E.H., 2010. Emerging properties of animal gene regulatory networks. Nature 468, 911–920.

Davison, A., Neiman, M., 2021. Mobilizing molluscan models and genomes in biology. Philosophical Transactions of the Royal Society B 376, 20200163.
Ballina, N.R.D. La, Maresca, F., Cao, A., Villalba, A., 2022. Bivalve haemocyte subpopulations: a review. Front Immunol 13, 826255.
De Luca, V., Del Prete, S., Supuran, C.T., Capasso, C., 2015. Protonography, a new technique for the analysis of carbonic anhydrase activity. J Enzyme Inhib Med Chem 30, 277–282.
De Melo, C.M.R., Morvezen, R., Durland, E., Langdon, C., 2018. Genetic by environment interactions for harvest traits of the Pacific oyster Crassostrea gigas (Thunberg) across different environments on the West Coast, USA. J Shellfish Res 37, 49–61.
De Wit, P., Durland, E., Ventura, A., Langdon, C.J., 2018. Gene expression correlated with delay in shell formation in larval Pacific oysters (Crassostrea gigas) exposed to experimental ocean acidification provides insights into shell formation mechanisms. BMC Genomics 19, 1–15.
De Zwaan, A., Cortesi, P., Van den Thillart, G., Brooks, S., Storey, K.B., Roos, J., Van Lieshout, G., Cattani, O., Vitali, G., 1992. Energy metabolism of bivalves at reduced oxygen tensions, in: Marine Coastal Eutrophication. Elsevier, pp. 1029–1039.
Denman, K., Christian, J.R., Steiner, N., Pörtner, H.-O., Nojiri, Y., 2011. Potential impacts of future ocean acidification on marine ecosystems and fisheries: current knowledge and recommendations for future research. ICES Journal of Marine Science 68, 1019–1029.
Denny, M., Miller, L., 2006. Jet propulsion in the cold: mechanics of swimming in the Antarctic scallop Adamussium colbecki. Journal of Experimental Biology 209, 4503–4514.
Desbrières, J., Guibal, E., 2018. Chitosan for wastewater treatment. Polym Int 67, 7–14.
Dickinson, G.H., Ivanina, A. V, Matoo, O.B., Pörtner, H.O., Lannig, G., Bock, C., Beniash, E., Sokolova, I.M., 2012. Interactive effects of salinity and elevated CO2 levels on juvenile eastern oysters, Crassostrea virginica. Journal of Experimental Biology 215, 29–43.
Dickson, A.G., 1990. Thermodynamics of the dissociation of boric acid in synthetic seawater from 273.15 to 318.15 K. Deep Sea Research Part A. Oceanographic Research Papers 37, 755–766.
Dickson, A.G., Millero, F.J., 1987. A comparison of the equilibrium constants for the dissociation of carbonic acid in seawater media. Deep Sea Research Part A. Oceanographic Research Papers 34,

1733–1743.
Ding, J., Zhao, L., Chang, Y., Zhao, W., Du, Z., Hao, Z., 2015. Transcriptome sequencing and characterization of Japanese scallop Patinopecten yessoensis from different shell color lines. PLoS One 10, e0116406.
Doney, S.C., Fabry, V.J., Feely, R.A., Kleypas, J.A., 2009. Ocean acidification: the other CO2 problem. Ann Rev Mar Sci 1, 169–192.
Doney, S.C., Ruckelshaus, M., Emmett Duffy, J., Barry, J.P., Chan, F., English, C.A., Galindo, H.M., Grebmeier, J.M., Hollowed, A.B., Knowlton, N., 2012. Climate change impacts on marine ecosystems. Ann Rev Mar Sci 4, 11–37.
Dreier, A., Loh, W., Blumenberg, M., Thiel, V., Hause-Reitner, D., Hoppert, M., 2014. The isotopic biosignatures of photo-vs. thiotrophic bivalves: are they preserved in fossil shells? Geobiology 12, 406–423.
Durkin, C.A., Mock, T., Armbrust, E.V., 2009. Chitin in diatoms and its association with the cell wall. Eukaryot Cell 8, 1038–1050.
Dwivedi, R., Pomin, V.H., 2020. Marine antithrombotics. Mar Drugs 18, 514.
Eble, A.F., Scro, R., 1996. General anatomy. The eastern oyster Crassostrea virginica 19–73.
Edgar, R.C., 2004. MUSCLE: multiple sequence alignment with high accuracy and high throughput. Nucleic Acids Res 32, 1792–1797.
Edgecombe, G.D., Giribet, G., Dunn, C.W., Hejnol, A., Kristensen, R.M., Neves, R.C., Rouse, G.W., Worsaae, K., Sørensen, M. V, 2011. Higher-level metazoan relationships: recent progress and remaining questions. Org Divers Evol 11, 151–172.
Kauffman, E.G., 1979. Bivalvia. Encyclopedia of Earth Science. Springer, Berlin, Heidelberg.
Eghianruwa, Q.A., Osoniyi, O.R., Maina, N., Wachira, S., 2019. Bioactive Peptides from Marine Molluscs–A Review. Int J Biochem Res Rev 27, 1–12.
Ehrlich, H., Maldonado, M., Spindler, K., Eckert, C., Hanke, T., Born, R., Goebel, C., Simon, P., Heinemann, S., Worch, H., 2007. First evidence of chitin as a component of the skeletal fibers of marine sponges. Part I. Verongidae (Demospongia: Porifera). J Exp Zool B Mol Dev Evol 308, 347–356.
Emms, M.D., Kelly, S., 2019. OrthoFinder: phylogenetic orthology inference for comparative genomics. Genome Biol 20, 1–14.
Evans, J.S., 2019. The biomineralization proteome: protein complexity

for a complex bioceramic assembly process. Proteomics 19, 1900036.
Fabry, V.J., Seibel, B.A., Feely, R.A., Orr, J.C., 2008. Impacts of ocean acidification on marine fauna and ecosystem processes. ICES Journal of Marine Science 65, 414–432.
Falini, G., Albeck, S., Weiner, S., Addadi, L., 1996. Control of aragonite or calcite polymorphism by mollusk shell macromolecules. Science (1979) 271, 67–69.
Falini, G., Fermani, S., 2004. Chitin mineralization. Tissue Eng 10, 1–6.
Fang, Z., Feng, Q., Chi, Y., Xie, L., Zhang, R., 2008. Investigation of cell proliferation and differentiation in the mantle of Pinctada fucata (Bivalve, Mollusca). Mar Biol 153, 745–754.
FAO, 2020. The State of World Fisheries and Aquaculture 2022, Towards Blue Transformation. FAO, Rome.
FAO, 2018. The State of World Fisheries and Aquaculture 2018 - Meeting the sustainable development goals [WWW Document]. https://www.fao.org/3/i9540en/i9540en.pdf.
Farre, B., Dauphin, Y., Cuif, J.P., 2008. Lipids of the mollusks shells, in: EGU. pp. 1607–7962.
Feng, D., Li, Q., Yu, H., Kong, L., Du, S., 2018. Transcriptional profiling of long non-coding RNAs in mantle of Crassostrea gigas and their association with shell pigmentation. Sci Rep. https://doi.org/10.1038/s41598-018-19950-6
Fernández, B., Campillo, J.A., Martínez-Gómez, C., Benedicto, J., 2010. Antioxidant responses in gills of mussel (Mytilus galloprovincialis) as biomarkers of environmental stress along the Spanish Mediterranean coast. Aquatic Toxicology 99, 186–197.
Ferre, F., Colantoni, A., Helmer-Citterich, M., 2016. Revealing protein–lncRNA interaction. Brief Bioinform 17, 106–116.
Fields, J.H.A., Baldwin, J., Hochachka, P.W., 1976. On the role of octopine dehydrogenase in cephalopod mantle muscle metabolism. Can J Zool 54, 871–878.
Figueras, A., Moreira, R., Sendra, M., Novoa, B., 2019. Genomics and immunity of the Mediterranean mussel Mytilus galloprovincialis in a changing environment. Fish Shellfish Immunol 90, 440–445.
Filgueira, R., Strohmeier, T., Strand, Ø., 2019. Regulating services of bivalve molluscs in the context of the carbon cycle and implications for ecosystem valuation. Goods and services of marine bivalves 231–251.
Fitzer, S.C., Phoenix, V.R., Cusack, M., Kamenos, N.A., 2014. Ocean acidification impacts mussel control on biomineralisation. Sci Rep 4,

6218.
Fitzsimons, J.A., Branigan, S., Gillies, C.L., Brumbaugh, R.D., Cheng, J., DeAngelis, B.M., Geselbracht, L., Hancock, B., Jeffs, A., McDonald, T., 2020. Restoring shellfish reefs: Global guidelines for practitioners and scientists. Conserv Sci Pract 2, e198.
Friendly, M., 2002. Corrgrams: Exploratory displays for correlation matrices. Am Stat 56, 316–324.
Frýda, J., Klicnarová, K., Frýdová, B., Mergl, M., 2010. Variability in the crystallographic texture of bivalve nacre. Bull. Geosci 85, 645–662.
Furuhashi, T., Beran, A., Blazso, M., Czegeny, Z., Schwarzinger, C., Steiner, G., 2009a. Pyrolysis GC/MS and IR spectroscopy in chitin analysis of molluscan shells. Biosci Biotechnol Biochem 73, 93–103.
Furuhashi, T., Schwarzinger, C., Miksik, I., Smrz, M., Beran, A., 2009b. Molluscan shell evolution with review of shell calcification hypothesis. Comp Biochem Physiol B Biochem Mol Biol 154, 351–371.
Gao, G., Zhao, X., Jiang, M., Gao, L., 2021. Impacts of marine heatwaves on algal structure and carbon sequestration in conjunction with ocean warming and acidification. Front Mar Sci 8, 758651.
Gasch, A.P., Spellman, P.T., Kao, C.M., Carmel-Harel, O., Eisen, M.B., Storz, G., Botstein, D., Brown, P.O., 2000. Genomic expression programs in the response of yeast cells to environmental changes. Mol Biol Cell 11, 4241–4257.
Gaston, K.J., 2000. Global patterns in biodiversity. Nature 405, 220–227.
Gattuso, J.-P., Bijma, J., Gehlen, M., Riebesell, U., Turley, C., 2011. Ocean acidification: knowns, unknowns, and perspectives. Ocean acidification 291–311.
Gazeau, F., Alliouane, S., Bock, C., Bramanti, L., López Correa, M., Gentile, M., Hirse, T., Pörtner, H.-O., Ziveri, P., 2014. Impact of ocean acidification and warming on the Mediterranean mussel (Mytilus galloprovincialis). Front Mar Sci 1, 62.
Gazeau, F., Gattuso, J.-P., Dawber, C., Pronker, A.E., Peene, F., Peene, J., Heip, C.H.R., Middelburg, J.J., 2010. Effect of ocean acidification on the early life stages of the blue mussel Mytilus edulis. Biogeosciences 7, 2051–2060.
Gazeau, F., Gattuso, J.-P., Greaves, M., Elderfield, H., Peene, J., Heip, C.H.R., Middelburg, J.J., 2011. Effect of carbonate chemistry alteration on the early embryonic development of the Pacific oyster (Crassostrea gigas). PLoS One 6, e23010.
Gazeau, F., Parker, L.M., Comeau, S., Gattuso, J.-P., O'Connor, W.A.,

Martin, S., Pörtner, H.-O., Ross, P.M., 2013. Impacts of ocean acidification on marine shelled molluscs. Mar Biol 160, 2207–2245.
Gazeau, F., Quiblier, C., Jansen, J.M., Gattuso, J., Middelburg, J.J., Heip, C.H.R., 2007. Impact of elevated CO2 on shellfish calcification. Geophys Res Lett 34.
Gebauer, D., Verch, A., Borner, H.G., Cölfen, H., 2009. Influence of selected artificial peptides on calcium carbonate precipitation-a quantitative study. Cryst Growth Des 9, 2398–2403.
Gerdol, M., Moreira, R., Cruz, F., Gómez-Garrido, J., Vlasova, A., Rosani, U., Venier, P., Naranjo-Ortiz, M.A., Murgarella, M., Greco, S., 2020. Massive gene presence-absence variation shapes an open pan-genome in the Mediterranean mussel. Genome Biol 21, 1–21.
Gillikin, D.P., Lorrain, A., Paulet, Y.-M., André, L., Dehairs, F., 2008. Synchronous barium peaks in high-resolution profiles of calcite and aragonite marine bivalve shells. Geo-Marine Letters 28, 351–358.
Gobler, C.J., DePasquale, E.L., Griffith, A.W., Baumann, H., 2014. Hypoxia and acidification have additive and synergistic negative effects on the growth, survival, and metamorphosis of early life stage bivalves. PLoS One 9, e83648.
Gomes-dos-Santos, A., Lopes-Lima, M., Castro, L.F.C., Froufe, E., 2020. Molluscan genomics: the road so far and the way forward. Hydrobiologia 847, 1705–1726.
Gooday, G.W., 1999. Aggressive and defensive roles for chitinases. EXS 87, 157–169.
Gosling, E., 2008. Bivalve molluscs: biology, ecology and culture. John Wiley & Sons.
Goulletquer, P., Wolowicz, M., 1989. The shell of Cardium edule, Cardium glaucum and Ruditapes philippinarum: organic content, composition and energy value, as determined by different methods. Journal of the Marine Biological Association of the United Kingdom 69, 563–572.
Grenier, C., Román, R., Duarte, C., Navarro, J.M., Rodriguez-Navarro, A.B., Ramajo, L., 2020. The combined effects of salinity and pH on shell biomineralization of the edible mussel Mytilus chilensis. Environmental Pollution 263, 114555.
Gricourt, L., Bonnec, G., Boujard, D., Mathieu, M., Kellner, K., 2003. Insulin-like system and growth regulation in the Pacific oyster Crassostrea gigas: hrIGF-1 effect on protein synthesis of mantle edge cells and expression of an homologous insulin receptor-related receptor. Gen Comp Endocrinol 134, 44–56.

Grienke, U., Silke, J., Tasdemir, D., 2014. Bioactive compounds from marine mussels and their effects on human health. Food Chem 142, 48–60.

Gu, H., Shang, Y., Clements, J., Dupont, S., Wang, T., Wei, S., Wang, X., Chen, J., Huang, W., Hu, M., 2019. Hypoxia aggravates the effects of ocean acidification on the physiological energetics of the blue mussel Mytilus edulis. Mar Pollut Bull 149, 110538.

Guerriero, G., Avino, M., Zhou, Q., Fugelstad, J., Clergeot, P.-H., Bulone, V., 2010. Chitin synthases from Saprolegnia are involved in tip growth and represent a potential target for anti-oomycete drugs. PLoS Pathog 6, e1001070.

Guo, X., 2009. Use and exchange of genetic resources in molluscan aquaculture. Rev Aquac 1, 251–259.

Guo, X., Li, X., Zhao, F., Liu, D., Yang, Z., Li, M., Li, Y., Wei, H., Wang, H., Qin, Z., 2023. Full-length transcriptome analysis provides insights into larval shell formation in Mulinia lateralis. Front Mar Sci 9, 1111241.

Gutierrez, A.P., Matika, O., Bean, T.P., Houston, R.D., 2018. Genomic selection for growth traits in Pacific oyster (Crassostrea gigas): potential of low-density marker panels for breeding value prediction. Front Genet 9, 391.

Gutiérrez, J.L., Jones, C.G., Strayer, D.L., Iribarne, O.O., 2003. Mollusks as ecosystem engineers: the role of shell production in aquatic habitats. Oikos 101, 79–90.

Hamester, M.R.R., Balzer, P.S., Becker, D., 2012. Characterization of calcium carbonate obtained from oyster and mussel shells and incorporation in polypropylene. Materials Research 15, 204–208.

Han, Y., Shi, W., Guo, C., Zhao, X., Liu, S., Wang, Y., Su, W., Zha, S., Wu, H., Chai, X., 2016. Characteristics of chitin synthase (CHS) gene and its function in polyspermy blocking in the blood clam Tegillarca granosa. Journal of Molluscan Studies 82, 550–557.

Harayashiki, C.A.Y., Márquez, F., Cariou, E., Castro, Í.B., 2020. Mollusk shell alterations resulting from coastal contamination and other environmental factors. Environmental Pollution 265, 114881.

Harper, E.M., 2000. Are calcitic layers an effective adaptation against shell dissolution in the Bivalvia? J Zool 251, 179–186.

Harper, E.M., Checa, A.G., 2020. Tightly shut: flexible valve margins and microstructural asymmetry in pterioid bivalves. Mar Biol 167, 1–12.

Haszprunar, G., Wanninger, A., 2012. Molluscs. Current Biology 22, R510–R514.

Helmkampf, M., Bruchhaus, I., Hausdorf, B., 2008. Phylogenomic analyses of lophophorates (brachiopods, phoronids and bryozoans) confirm the Lophotrochozoa concept. Proceedings of the Royal Society B: Biological Sciences 275, 1927–1933.

Heredia, A., Aguilar-Franco, M., Magaña, C., Flores, C., Piña, C., Velázquez, R., Schäffer, T.E., Bucio, L., Basiuk, V.A., 2007. Structure and interactions of calcite spherulites with α-chitin in the brown shrimp (Penaeus aztecus) shell. Materials Science and Engineering: C 27, 8–13.

Hiebenthal, C., Philipp, E.E.R., Eisenhauer, A., Wahl, M., 2013. Effects of seawater p CO 2 and temperature on shell growth, shell stability, condition and cellular stress of Western Baltic Sea Mytilus edulis (L.) and Arctica islandica (L.). Mar Biol 160, 2073–2087.

Hockey, P.A.R., Schurink, C. van E., 1992. The invasive biology of the mussel Mytilus galloprovincialis on the southern African coast. Transactions of the Royal Society of South Africa 48, 123–139.

Hoegh-Guldberg, O., Mumby, P.J., Hooten, A.J., Steneck, R.S., Greenfield, P., Gomez, E., Harvell, C.D., Sale, P.F., Edwards, A.J., Caldeira, K., 2007. Coral reefs under rapid climate change and ocean acidification. Science (1979) 318, 1737–1742.

Hofmann, G.E., Barry, J.P., Edmunds, P.J., Gates, R.D., Hutchins, D.A., Klinger, T., Sewell, M.A., 2010. The effect of ocean acidification on calcifying organisms in marine ecosystems: an organism-to-ecosystem perspective. Annu Rev Ecol Evol Syst 41, 127–147.

Hongkuan, Z., Karsoon, T., Shengkang, L., Hongyu, M., Huaiping, Z., 2021. The functional roles of the non-coding RNAs in molluscs. Gene 768, 145300.

Hönisch, B., Ridgwell, A., Schmidt, D.N., Thomas, E., Gibbs, S.J., Sluijs, A., Zeebe, R., Kump, L., Martindale, R.C., Greene, S.E., 2012. The geological record of ocean acidification. Science (1979) 335, 1058–1063.

Horan, R.C., 1983. Shell matrix and extrapallial fluid proteins of mercenaria mercenaria: a comparative electrophoretic and immunoelectrophoretic analysis. St. John's University (New York).

Hosseini, S.F., Rezaei, M., McClements, D.J., 2022. Bioactive functional ingredients from aquatic origin: A review of recent progress in marine-derived nutraceuticals. Crit Rev Food Sci Nutr 62, 1242–1269.

Huang, X. De, Dai, J. ge, Lin, K. tao, Liu, M., Ruan, H. ting, Zhang, H., Liu, W. guang, He, M.X., Zhao, M., 2018. Regulation of IL-17 by

lncRNA of IRF-2 in the pearl oyster. Fish Shellfish Immunol. https://doi.org/10.1016/j.fsi.2018.07.020

Huang, J., Liu, Y., Liu, C., Xie, L., Zhang, R., 2021. Heterogeneous distribution of shell matrix proteins in the pearl oyster prismatic layer. Int J Biol Macromol 189, 641–648.

Huang, L.J., Li, H.D., 1991. Observation of the phase transition in the growth of a biomineralized calcium carbonate. Biochem Biophys Res Commun 176, 654–659.

Ip, Y.K., Hiong, K.C., Lim, L.J.Y., Choo, C.Y.L., Boo, M. V, Wong, W.P., Neo, M.L., Chew, S.F., 2018. Molecular characterization, light-dependent expression, and cellular localization of a host vacuolar-type H+-ATPase (VHA) subunit A in the giant clam, Tridacna squamosa, indicate the involvement of the host VHA in the uptake of inorganic carbon and its supply to the symbiotic zooxanthellae. Gene 659, 137–148.

IPCC, Ip., 2018. Summary for Policymakers" in Global warming of 1.5° C. An IPCC Special Report on the impacts of global warming of 1.5° C above pre-industrial levels and related global greenhouse gas emission pathways, in the context of strengthening the global response to the threat of climate change, sustainable development, and efforts to eradicate poverty. Sustainable Development, and Efforts to Eradicate Poverty. Geneva, Switzerland: World Meteorological Organization 32.

Ishikawa, A., Shimizu, K., Isowa, Y., Takeuchi, T., Zhao, R., Kito, K., Fujie, M., Satoh, N., Endo, K., 2020. Functional shell matrix proteins tentatively identified by asymmetric snail shell morphology. Sci Rep. https://doi.org/10.1038/s41598-020-66021-w

Islam, M.S., Wang, H., Admassu, H., Sulieman, A.A., Wei, F.A., 2022. Health benefits of bioactive peptides produced from muscle proteins: Antioxidant, anti-cancer, and anti-diabetic activities. Process Biochemistry 116, 116–125.

Ivanina, A. V, Borah, B., Rimkevicius, T., Macrander, J., Piontkivska, H., Sokolova, I.M., Beniash, E., 2018. The role of the vascular endothelial growth factor (VEGF) signaling in biomineralization of the oyster Crassostrea gigas. Front Mar Sci 5, 309.

Ivanina, A. V, Falfushynska, H.I., Beniash, E., Piontkivska, H., Sokolova, I.M., 2017. Biomineralization-related specialization of hemocytes and mantle tissues of the Pacific oyster Crassostrea gigas. Journal of Experimental Biology 220, 3209–3221.

Jackson, D.J., Degnan, B.M., 2016. The importance of evo-devo to an

integrated understanding of molluscan biomineralisation. J Struct Biol 196, 67–74.
Jackson, D.J., McDougall, C., Green, K., Simpson, F., Wörheide, G., Degnan, B.M., 2006. A rapidly evolving secretome builds and patterns a sea shell. BMC Biol. https://doi.org/10.1186/1741-7007-4-40
Jacob, D.E., Soldati, A.L., Wirth, R., Huth, J., Wehrmeister, U., Hofmeister, W., 2008. Nanostructure, composition and mechanisms of bivalve shell growth. Geochim Cosmochim Acta 72, 5401–5415.
Jing, G., Yan, Z., Li, Y., Xie, L., Zhang, R., 2007. Immunolocalization of an acid phosphatase from pearl oyster (Pinctada fucata) and its in vitro effects on calcium carbonate crystal formation. Marine biotechnology 9, 650–659.
Johnson, A.B., Fogel, N.S., Lambert, J.D., 2019. Growth and morphogenesis of the gastropod shell. Proceedings of the National Academy of Sciences 116, 6878–6883.
Johnson, K.M., Hofmann, G.E., 2017. Transcriptomic response of the Antarctic pteropod Limacina helicina antarctica to ocean acidification. BMC Genomics 18, 1–16.
Jović, M., Mandić, M., Šljivić-Ivanović, M., Smičiklas, I., 2019. Recent trends in application of shell waste from mariculture. Studia Marina 32, 47–62.
Kaplan, D.L., 1998. Mollusc shell structures: novel design strategies for synthetic materials. Curr Opin Solid State Mater Sci 3, 232–236.
Kassambara, A., 2017. Practical guide to principal component methods in R: PCA, M (CA), FAMD, MFA, HCPC, factoextra. Sthda.
Keihan, R., Ghorbani, A.R., Salahinejad, E., Sharifi, E., Tayebi, L., 2020. Biomineralization, strength and cytocompatibility improvement of bredigite scaffolds through doping/coating. Ceram Int 46, 21056–21063.
Ken, C., Wickett, M.E., 2003. Oceanography: anthropogenic carbon and ocean pH. Nature 425, 365.
Kennedy, W.J., Taylor, J.D., Hall, A., 1969. Environmental and biological controls on bivalve shell mineralogy. Biol Rev Camb Philos Soc 44, 499–530. https://doi.org/10.1111/j.1469-185x.1969.tb00610.x
Khan, B.M., Liu, Y., 2019. Marine mollusks: Food with benefits. Compr Rev Food Sci Food Saf 18, 548–564.
Kim, D., Paggi, J.M., Park, C., Bennett, C., Salzberg, S.L., 2019. Graph-based genome alignment and genotyping with HISAT2 and HISAT-genotype. Nat Biotechnol 37, 907–915.

Kniprath, E., 1981. Ontogeny of the molluscan shell field: a review. Zool Scr 10, 61–79.
Kobayashi, I., 1969. Internal microstructure of the shell of bivalve molluscs. Am Zool 9, 663–672.
Kobayashi, I., Samata, T., 2006. Bivalve shell structure and organic matrix. Materials Science and Engineering: C 26, 692–698.
Kocot, K.M., Aguilera, F., McDougall, C., Jackson, D.J., Degnan, B.M., 2016. Sea shell diversity and rapidly evolving secretomes: Insights into the evolution of biomineralization. Front Zool. https://doi.org/10.1186/s12983-016-0155-z
Kolde, R., Kolde, M.R., 2015. Package 'pheatmap.' R package 1, 790.
Kong, H., Jiang, X., Clements, J.C., Wang, T., Huang, X., Shang, Y., Chen, J., Hu, M., Wang, Y., 2019. Transgenerational effects of short-term exposure to acidification and hypoxia on early developmental traits of the mussel Mytilus edulis. Mar Environ Res 145, 73–80.
Kramer, K.J., Koga, D., 1986. Insect chitin: physical state, synthesis, degradation and metabolic regulation. Insect Biochem 16, 851–877.
Krebs, H.A., 1975. The August Krogh principle:"For many problems there is an animal on which it can be most conveniently studied." Journal of Experimental Zoology 194, 221–226.
Kroeker, K.J., Kordas, R.L., Crim, R., Hendriks, I.E., Ramajo, L., Singh, G.S., Duarte, C.M., Gattuso, J., 2013. Impacts of ocean acidification on marine organisms: quantifying sensitivities and interaction with warming. Glob Chang Biol 19, 1884–1896.
Kroeker, K.J., Kordas, R.L., Crim, R.N., Singh, G.G., 2010. Meta-analysis reveals negative yet variable effects of ocean acidification on marine organisms. Ecol Lett 13, 1419–1434.
Kroeker, K.J., Sanford, E., Jellison, B.M., Gaylord, B., 2014. Predicting the effects of ocean acidification on predator-prey interactions: a conceptual framework based on coastal molluscs. Biol Bull 226, 211–222.
Krylova, E.M., Sahling, H., 2010. Vesicomyidae (Bivalvia): current taxonomy and distribution. PLoS One 5, e9957.
Kubota, K., Kintsu, H., Matsuura, A., Tsuchihashi, Y., Takeuchi, T., Satoh, N., Suzuki, M., 2018. Functional analyses of MMPs for aragonite crystal formation in the ligament of Pinctada fucata. Front Mar Sci 5, 373.
Kubota, K., Tsuchihashi, Y., Kogure, T., Maeyama, K., Hattori, F., Kinoshita, S., Sakuda, S., Nagasawa, H., Yoshimura, E., Suzuki, M., 2017. Structural and functional analyses of a TIMP and MMP in the

ligament of Pinctada fucata. J Struct Biol 199, 216–224.
Kurihara, H., Kato, S., Ishimatsu, A., 2007. Effects of increased seawater pCO2 on early development of the oyster Crassostrea gigas. Aquat Biol 1, 91–98.
Lannig, G., Eilers, S., Pörtner, H.O., Sokolova, I.M., Bock, C., 2010. Impact of ocean acidification on energy metabolism of oyster, Crassostrea gigas—changes in metabolic pathways and thermal response. Mar Drugs 8, 2318–2339.
Lassoued, J., Babarro, J.M.F., Padín, X.A., Comeau, L.A., Bejaoui, N., Pérez, F.F., 2019. Behavioural and eco-physiological responses of the mussel Mytilus galloprovincialis to acidification and distinct feeding regimes. Mar Ecol Prog Ser 626, 97–108.
Lazo, C.S., Pita, I.M., 2012. Effect of temperature on survival, growth and development of Mytilus galloprovincialis larvae. Aquac Res 43, 1127–1133.
Le Franc, L., Petton, B., Favrel, P., Rivière, G., 2022. N6-Methyladenosine Profile Dynamics Indicates Regulation of Oyster Development by m6A-RNA Epitranscriptomes. Genomics Proteomics Bioinformatics.
Le Roy, N., Jackson, D.J., Marie, B., Ramos-Silva, P., Marin, F., 2014. The evolution of metazoan α-carbonic anhydrases and their roles in calcium carbonate biomineralization. Front Zool 11, 1–16.
Levine, T.D., Hansen, H.B., Gerald, G.W., 2014. Effects of shell shape, size, and sculpture in burrowing and anchoring abilities in the freshwater mussel Potamilus alatus (Unionidae). Biological Journal of the Linnean Society 111, 136–144.
Li, J., Wu, X., Bai, Z., 2018. Freshwater pearl culture. Aquaculture in China: Success Stories and Modern Trends 185–196.
Li, S., Chen, W., Zhan, A., Liang, J., 2018. Identification and characterization of microRNAs involved in scale biomineralization in the naked carp Gymnocypris przewalskii. Comp Biochem Physiol Part D Genomics Proteomics 28, 196–203.
Li, S., Liu, Y., Liu, C., Huang, J., Zheng, G., Xie, L., Zhang, R., 2016. Hemocytes participate in calcium carbonate crystal formation, transportation and shell regeneration in the pearl oyster Pinctada fucata. Fish Shellfish Immunol 51, 263–270.
Li, Z., Cardoso, J.C.R., Peng, M., Inácio, J.P.S., Power, D.M., 2021. Evolution and potential function in molluscs of neuropeptide and receptor homologues of the insect allatostatins. Front Endocrinol (Lausanne) 12, 725022.

Liang, Y., Martín-Zamora, F.M., Guynes, K., Carrillo-Baltodano, A.M., Tan, Y., Moggioli, G., Seudre, O., Tran, M., Mortimer, K., Luscombe, N.M., 2022. Annelid functional genomics reveal the origins of bilaterian life cycles. bioRxiv.

Liao, Q., Qin, Y., Zhou, Y., Shi, G., Li, X., Li, J., Mo, R., Zhang, Y., Yu, Z., 2021. Characterization and functional analysis of a chitinase gene: Evidence of Ch-chit participates in the regulation of biomineralization in Crassostrea hongkongensis. Aquac Rep 21, 100852.

Lindskog, S., Coleman, J.E., 1973. The catalytic mechanism of carbonic anhydrase. Proceedings of the National Academy of Sciences 70, 2505–2508.

Liu, C., Li, S., Kong, J., Liu, Y., Wang, T., Xie, L., Zhang, R., 2015. In-depth proteomic analysis of shell matrix proteins of Pinctada fucata. Sci Rep 5, 17269.

Liu, S., Shi, W., Guo, C., Zhao, X., Han, Y., Peng, C., Chai, X., Liu, G., 2016. Ocean acidification weakens the immune response of blood clam through hampering the NF-kappa β and toll-like receptor pathways. Fish Shellfish Immunol 54, 322–327.

Lopes-Lima, M., Teixeira, A., Froufe, E., Lopes, A., Varandas, S., Sousa, R., 2014. Biology and conservation of freshwater bivalves: past, present and future perspectives. Hydrobiologia 735, 1–13.

Love, M.I., Huber, W., Anders, S., 2014. Moderated estimation of fold change and dispersion for RNA-seq data with DESeq2. Genome Biol 15, 1–21. https://doi.org/10.1186/s13059-014-0550-8

Lu, Y., Wang, Li, Wang, Lianshun, Cong, Y., Yang, G., Zhao, L., 2018. Deciphering carbon sources of mussel shell carbonate under experimental ocean acidification and warming. Mar Environ Res 142, 141–146.

Lutier, M., Di Poi, C., Gazeau, F., Appolis, A., Le Luyer, J., Pernet, F., 2022. Revisiting tolerance to ocean acidification: insights from a new framework combining physiological and molecular tipping points of Pacific oyster. Glob Chang Biol 28, 3333–3348.

Mackenzie, C.L., Ormondroyd, G.A., Curling, S.F., Ball, R.J., Whiteley, N.M., Malham, S.K., 2014. Ocean warming, more than acidification, reduces shell strength in a commercial shellfish species during food limitation. PLoS One 9, e86764.

Peng, M., Liu, X., Niu, D., Ye, B., Lan, T., Dong, Z., Li, J., 2019. Survival, growth and physiology of marine bivalve (Sinonovacula constricta) in long-term low-salt culture. Sci Rep 9, 2819.

Marek, L., Yochelson, E.L., 1976. Aspects of the biology of Hyolitha (Mollusca). Lethaia 9, 65–82.
Mariani, S., Piccari, F., De Matthaeis, E., 2002. Shell morphology in Cerastoderma spp.(Bivalvia: Cardiidae) and its significance for adaptation to tidal and non-tidal coastal habitats. Journal of the Marine Biological Association of the United Kingdom 82, 483–490.
Marie, B., Arivalagan, J., Mathéron, L., Bolbach, G., Berland, S., Marie, A., Marin, F., 2017. Deep conservation of bivalve nacre proteins highlighted by shell matrix proteomics of the Unionoida Elliptio complanata and Villosa lienosa. J R Soc Interface 14, 20160846.
Marie, B., Jackson, D.J., Ramos-Silva, P., Zanella-Cléon, I., Guichard, N., Marin, F., 2013. The shell-forming proteome of L ottia gigantea reveals both deep conservations and lineage-specific novelties. FEBS J 280, 214–232.
Marie, B., Joubert, C., Tayalé, A., Zanella-Cléon, I., Belliard, C., Piquemal, D., Cochennec-Laureau, N., Marin, F., Gueguen, Y., Montagnani, C., 2012. Different secretory repertoires control the biomineralization processes of prism and nacre deposition of the pearl oyster shell. Proceedings of the National Academy of Sciences 109, 20986–20991.
Marie, B., Le Roy, N., Zanella-Cléon, I., Becchi, M., Marin, F., 2011. Molecular evolution of mollusc shell proteins: insights from proteomic analysis of the edible mussel Mytilus. J Mol Evol 72, 531–546.
Marie, B., Zanella-Cléon, I., Le Roy, N., Becchi, M., Luquet, G., Marin, F., 2010. Proteomic analysis of the acid-soluble nacre matrix of the bivalve unio pictorum: detection of novel carbonic anhydrase and putative protease inhibitor proteins. ChemBioChem 11, 2138–2147.
Marin, F., 2020. Mollusc shellomes: past, present and future. J Struct Biol 212, 107583.
Marin, F., Le Roy, N., Marie, B., 2012. The formation and mineralization of mollusk shell. Frontiers in Bioscience-Scholar 4, 1099–1125.
Marin, F., Luquet, G., 2004. Molluscan shell proteins. C R Palevol 3, 469–492.
Marin, F., Luquet, G., Marie, B., Medakovic, D., 2007. Molluscan shell proteins: primary structure, origin, and evolution. Curr Top Dev Biol 80, 209–276.
Martynov, A., Schroedl, M., 2011. Phylogeny and evolution of corambid nudibranchs (Mollusca: Gastropoda). Zool J Linn Soc 163, 585–604.
McClintock, J.B., Angus, R.A., Mcdonald, M.R., Amsler, C.D., Catledge,

S.A., Vohra, Y.K., 2009. Rapid dissolution of shells of weakly calcified Antarctic benthic macroorganisms indicates high vulnerability to ocean acidification. Antarct Sci 21, 449–456.
McDougall, C., Degnan, B.M., 2018. The evolution of mollusc shells. Wiley Interdiscip Rev Dev Biol 7, e313.
Mehrbach, C., Culberson, C.H., Hawley, J.E., Pytkowicx, R.M., 1973. Measurement of the apparent dissociation constants of carbonic acid in seawater at atmospheric pressure 1. Limnol Oceanogr 18, 897–907.
Melzner, F., Stange, P., Trübenbach, K., Thomsen, J., Casties, I., Panknin, U., Gorb, S.N., Gutowska, M.A., 2011. Food supply and seawater p CO2 impact calcification and internal shell dissolution in the blue mussel Mytilus edulis. PLoS One 6, e24223.
Meng, J., Song, K., Li, C., Liu, S., Shi, R., Li, B., Wang, T., Li, A., Que, H., Li, L., 2019. Genome-wide association analysis of nutrient traits in the oyster Crassostrea gigas: genetic effect and interaction network. BMC Genomics 20, 1–14.
Merzendorfer, H., 2011. The cellular basis of chitin synthesis in fungi and insects: common principles and differences. Eur J Cell Biol 90, 759–769.
Merzendorfer, H., 2006. Insect chitin synthases: a review. Journal of Comparative Physiology B 176, 1–15.
Meyers, M.A., Chen, P.-Y., Lin, A.Y.-M., Seki, Y., 2008. Biological materials: Structure and mechanical properties. Prog Mater Sci 53, 1–206.
Michaelidis, B., Ouzounis, C., Paleras, A., Pörtner, H.O., 2005. Effects of long-term moderate hypercapnia on acid–base balance and growth rate in marine mussels Mytilus galloprovincialis. Mar Ecol Prog Ser 293, 109–118.
Miossec, L., Deuff, R.-M. Le, Goulletquer, P., 2009. Alien species alert: Crassostrea gigas (Pacific oyster). ICES Cooperative Research Reports (CRR).
Mizi, A., Zouros, E., Moschonas, N., Rodakis, G.C., 2005. The complete maternal and paternal mitochondrial genomes of the Mediterranean mussel Mytilus galloprovincialis: implications for the doubly uniparental inheritance mode of mtDNA. Mol Biol Evol 22, 952–967.
Moon, B., Lim, S., Choi, J., Suh, Y., 2000. Effects of pre-or post-harvest application of liquid calcium fertilizer manufactured from oyster shell on the calcium concentration and quality in stored'Niitaka'pear fruits. Journal of the Korean Society for Horticultural Science 41, 61–64.

Morozov, A.A., Likhoshway, Y. V, 2016. Evolutionary history of the chitin synthases of eukaryotes. Glycobiology 26, 635–639.
Morris, J.P., Backeljau, T., Chapelle, G., 2019. Shells from aquaculture: a valuable biomaterial, not a nuisance waste product. Rev Aquac 11, 42–57.
Morton, B., 1983. Feeding and digestion in Bivalvia. The Mollusca. Physiology Part 2, 65–147.
Morton, B., Peharda, M., 2008. The biology and functional morphology of Arca noae (Bivalvia: Arcidae) from the Adriatic Sea, Croatia, with a discussion on the evolution of the bivalve mantle margin. Acta Zoologica 89, 19–28.
Mount, A.S., Wheeler, A.P., Paradkar, R.P., Snider, D., 2004. Hemocyte-mediated shell mineralization in the eastern oyster. Science (1979) 304, 297–300.
Mu, C., Wang, R., Li, T., Li, Y., Tian, M., Jiao, W., Huang, X., Zhang, L., Hu, X., Wang, S., 2016. Long non-coding RNAs (lncRNAs) of sea cucumber: large-scale prediction, expression profiling, non-coding network construction, and lncRNA-microRNA-gene interaction analysis of lncRNAs in Apostichopus japonicus and Holothuria glaberrima during LPS challenge and radial organ complex regeneration. Marine Biotechnology 18, 485–499.
Munday, P.L., Dixson, D.L., Donelson, J.M., Jones, G.P., Pratchett, M.S., Devitsina, G. V, Døving, K.B., 2009. Ocean acidification impairs olfactory discrimination and homing ability of a marine fish. Proceedings of the National Academy of Sciences 106, 1848–1852.
Muzzarelli, R.A.A., 2013. Chitin. Elsevier.
Muzzarelli, R.A.A., 2011. Potential of chitin/chitosan-bearing materials for uranium recovery: An interdisciplinary review. Carbohydr Polym 84, 54–63.
Nagai, K., 2013. A history of the cultured pearl industry. Zoolog Sci 30, 783–793.
Nam, J.-W., Bartel, D.P., 2012. Long noncoding RNAs in C. elegans. Genome Res 22, 2529–2540.
Neves, R.A.F., Nascimento, S.M., Santos, L.N., 2021. Harmful algal blooms and shellfish in the marine environment: An overview of the main molluscan responses, toxin dynamics, and risks for human health. Environmental Science and Pollution Research 28, 55846–55868.
Niu, Y.-Q., Liu, J.-H., Aymonier, C., Fermani, S., Kralj, D., Falini, G., Zhou, C.-H., 2022. Calcium carbonate: Controlled synthesis, surface

functionalization, and nanostructured materials. Chem Soc Rev 51, 7883–7943.
Nudelman, F., 2015. Nacre biomineralisation: A review on the mechanisms of crystal nucleation, in: Seminars in Cell & Developmental Biology. Elsevier, pp. 2–10.
Nudelman, F., Shimoni, E., Klein, E., Rousseau, M., Bourrat, X., Lopez, E., Addadi, L., Weiner, S., 2008. Forming nacreous layer of the shells of the bivalves Atrina rigida and Pinctada margaritifera: an environmental-and cryo-scanning electron microscopy study. J Struct Biol 162, 290–300.
Núñez-Acuña, G., Fernandez, C., Sanhueza-Guevara, S., Gallardo-Escárate, C., 2022. Transcriptome profiling of the early developmental stages in the giant mussel Choromytilus chorus exposed to delousing drugs. Mar Genomics 65, 100970.
Odeleye, T., White, W.L., Lu, J., 2019. Extraction techniques and potential health benefits of bioactive compounds from marine molluscs: A review. Food Funct 10, 2278–2289.
O'Donnell, M.J., George, M.N., Carrington, E., 2013. Mussel byssus attachment weakened by ocean acidification. Nat Clim Chang 3, 587–590.
Oliveira, D. V, Silva, T.S., Cordeiro, O.D., Cavaco, S.I., Simes, D.C., 2012. Identification of proteins with potential osteogenic activity present in the water-soluble matrix proteins from Crassostrea gigas nacre using a proteomic approach. The Scientific World Journal 2012.
Osterauer, R., Marschner, L., Betz, O., Gerberding, M., Sawasdee, B., Cloetens, P., Haus, N., Sures, B., Triebskorn, R., Köhler, H.R., 2010. Turning snails into slugs: Induced body plan changes and formation of an internal shell. Evol Dev. https://doi.org/10.1111/j.1525-142X.2010.00433.x
Padilla, D.K., 2010. Context-dependent impacts of a non-native ecosystem engineer, the Pacific oyster Crassostrea gigas. Integr Comp Biol 50, 213–225.
Page, L.R., 2006. Modern insights on gastropod development: Reevaluation of the evolution of a novel body plan. Integr Comp Biol. https://doi.org/10.1093/icb/icj018
Page, L.R., 2003. Gastropod Ontogenetic Torsion: Developmental Remnants of an Ancient Evolutionary Change in Body Plan. J Exp Zool B Mol Dev Evol. https://doi.org/10.1002/jez.b.12
Pallela, R., 2014. Nutraceutical and pharmacological implications of marine carbohydrates. Adv Food Nutr Res 73, 183–195.

Peck, L.S., Clark, M.S., Power, D., Reis, J., Batista, F.M., Harper, E.M., 2015. Acidification effects on biofouling communities: winners and losers. Glob Chang Biol 21, 1907–1913.

Peijnenburg, K.T.C.A., Janssen, A.W., Wall-Palmer, D., Goetze, E., Maas, A.E., Todd, J.A., Marlétaz, F., 2020. The origin and diversification of pteropods precede past perturbations in the Earth's carbon cycle. Proceedings of the National Academy of Sciences 117, 25609–25617.

Penaloza, C., Gutierrez, A.P., Eöry, L., Wang, S., Guo, X., Archibald, A.L., Bean, T.P., Houston, R.D., 2021. A chromosome-level genome assembly for the Pacific oyster Crassostrea gigas. Gigascience 10, giab020.

Peng, C., Zhao, X., Liu, S., Shi, W., Han, Y., Guo, C., Peng, X., Chai, X., Liu, G., 2017. Ocean acidification alters the burrowing behaviour, Ca2+/Mg2+-ATPase activity, metabolism, and gene expression of a bivalve species, Sinonovacula constricta. Mar Ecol Prog Ser 575, 107–117.

Peng, Maoxiao, Cardoso, C.R. João, Pearson, Gareth, Canário, V.M. Adelino, Power, M.D., 2023. Core genes of biomineralization and cis-regulatory long non-coding RNA regulate shell growth in bivalves. Journal of Advanced Research （under review）.

Peng, Maoxiao, Cardoso, C.R.J., Sorigué, P., Power, M.D., 2023. Species-specific responses of bivalves to ocean acidification. Science of the Total Environment (submitted).

Peng, M., Li, Z., Cardoso, J.C.R., Niu, D., Liu, X., Dong, Z., Li, J., Power, D.M., 2022. Domain-dependent evolution explains functional homology of protostome and deuterostome complement C3-like proteins. Front Immunol 13, 840861.

Peng, M., Liu, Z., Li, Z., Qian, S., Liu, X., Li, J., 2021. The temptin gene of the clade Lophotrochozoa is involved in formation of the prismatic layer during biomineralization in molluscs. Int J Biol Macromol 188, 800–810.

Perfetto, R., Del Prete, S., Vullo, D., Sansone, G., Barone, C., Rossi, M., Supuran, C.T., Capasso, C., 2017. Biochemical characterization of the native α-carbonic anhydrase purified from the mantle of the Mediterranean mussel, Mytilus galloprovincialis. J Enzyme Inhib Med Chem 32, 632–639.

Pertea, M., Pertea, G.M., Antonescu, C.M., Chang, T.-C., Mendell, J.T., Salzberg, S.L., 2015. StringTie enables improved reconstruction of a transcriptome from RNA-seq reads. Nat Biotechnol 33, 290–295.

Peters, W., 1972. Occurrence of chitin in Mollusca. Comparative

Biochemistry and Physiology Part B: Comparative Biochemistry 41, 541–550.
Pickett, T., David, A.A., 2018. Global connectivity patterns of the notoriously invasive mussel, Mytilus galloprovincialis Lmk using archived CO1 sequence data. BMC Res Notes 11, 1–7.
Pierrot, D.E., Wallace, D.W.R., Lewis, E., 2011. MS Excel program developed for CO2 system calculations. Carbon dioxide information analysis center.
Pilkey, O.H., Goodell, H.G., 1964. Comparison of the composition of fossil and recent mollusk shells. Geol Soc Am Bull 75, 217–228.
Pinsky, M.L., Selden, R.L., Kitchel, Z.J., 2020. Climate-driven shifts in marine species ranges: Scaling from organisms to communities. Ann Rev Mar Sci 12, 153–179.
Poloczanska, E.S., Brown, C.J., Sydeman, W.J., Kiessling, W., Schoeman, D.S., Moore, P.J., Brander, K., Bruno, J.F., Buckley, L.B., Burrows, M.T., 2013. Global imprint of climate change on marine life. Nat Clim Chang 3, 919–925.
Pompa, S., Ehrlich, P.R., Ceballos, G., 2011. Global distribution and conservation of marine mammals. Proceedings of the National Academy of Sciences 108, 13600–13605.
Ponder, W., Lindberg, D.R., 2008. Phylogeny and Evolution of the Mollusca. Univ of California Press.
Ponder, W.F., Lindberg, D.R., Ponder, J.M., 2019. Biology and Evolution of the Mollusca, Volume 1. CRC Press.
Pörtner, H.O., Langenbuch, M., Reipschläger, A., 2004. Biological impact of elevated ocean CO 2 concentrations: lessons from animal physiology and earth history. J Oceanogr 60, 705–718.
Pörtner, H.O., Peck, M.A., 2010. Climate change effects on fishes and fisheries: towards a cause-and-effect understanding. J Fish Biol 77, 1745–1779.
Pourmozaffar, S., Tamadoni Jahromi, S., Rameshi, H., Sadeghi, A., Bagheri, T., Behzadi, S., Gozari, M., Zahedi, M.R., Abrari Lazarjani, S., 2020. The role of salinity in physiological responses of bivalves. Rev Aquac 12, 1548–1566.
Powell, D., Subramanian, S., Suwansa-Ard, S., Zhao, M., O'Connor, W., Raftos, D., Elizur, A., 2018. The genome of the oyster Saccostrea offers insight into the environmental resilience of bivalves. DNA Research 25, 655–665.
Qi, H., Li, L., Zhang, G., 2021. Construction of a chromosome-level genome and variation map for the Pacific oyster Crassostrea gigas.

Mol Ecol Resour 21, 1670–1685.
Rajan, K.C., Vengatesen, T., 2020. Molecular adaptation of molluscan biomineralisation to high-CO2 oceans–The known and the unknown. Mar Environ Res 155, 104883.
Ramakrishna, C., Thenepalli, T., Nam, S.Y., Kim, C., Ahn, J.W., 2018. Extraction of precipitated calcium carbonate from oyster shell waste and its applications. 에너지공학 27, 51–58.
Ramesh, K., Yarra, T., Clark, M.S., John, U., Melzner, F., 2019. Expression of calcification-related ion transporters during blue mussel larval development. Ecol Evol 9, 7157–7172.
Remy, M., Hillebrand, H., Flöder, S., 2017. Stability of marine phytoplankton communities facing stress related to global change: Interactive effects of heat waves and turbidity. J Exp Mar Biol Ecol 497, 219–229.
Ren, F., Wan, X., Ma, Z., Su, J., 2009. Study on microstructure and thermodynamics of nacre in mussel shell. Mater Chem Phys 114, 367–370.
Ren, J.S., Ragg, N.L.C., Cummings, V.J., Zhang, J., 2020. Ocean acidification and dynamic energy budget models: parameterisation and simulations for the green-lipped mussel. Ecol Modell 426, 109069.
Revelle, W., 2011. An overview of the psych package.
Rey-Campos, M., Novoa, B., Pallavicini, A., Gerdol, M., Figueras, A., 2021. Comparative genomics reveals 13 different isoforms of mytimycins (AM) in mytilus galloprovincialis. Int J Mol Sci 22, 3235.
Rice, M.A., 2001. Environmental impacts of shellfish aquaculture: filter feeding to control eutrophication, in: Marine Aquaculture and the Environment: A Meeting for Stakeholders in the Northeast. Cape Cod Press, Falmouth, MA, USA. pp. 77–86.
Richardson, C.A., Runham, N.W., Crisp, D.J., 1981. A histological and ultrastructural study of the cells of the mantle edge of a marine bivalve, Cerastoderma edule. Tissue Cell 13, 715–730.
Ries, J.B., Cohen, A.L., McCorkle, D.C., 2009. Marine calcifiers exhibit mixed responses to CO2-induced ocean acidification. Geology 37, 1131–1134.
Roberts, S.D., Van Ruth, P.D., Wilkinson, C., Bastianello, S.S., Bansemer, M.S., 2019. Marine heatwave, harmful algae blooms and an extensive fish kill event during 2013 in South Australia. Front Mar Sci 6, 610.
Robledo, J.A.F., Santarem, M.M., Gonzalez, P., Figueras, A., 1995.

Seasonal variations in the biochemical composition of the serum of Mytilus galloprovincialis Lmk. and its relationship to the reproductive cycle and parasitic load. Aquaculture 133, 311–322.
Roncero, C., 2002. The genetic complexity of chitin synthesis in fungi. Curr Genet 41, 367–378.
Rousseau, M., Bédouet, L., Lati, E., Gasser, P., Le Ny, K., Lopez, E., 2006. Restoration of stratum corneum with nacre lipids. Comp Biochem Physiol B Biochem Mol Biol 145, 1–9.
Roy, E.D., 2017. Phosphorus recovery and recycling with ecological engineering: A review. Ecol Eng 98, 213–227.
Ruiz-Herrera, J., Ruiz-Medrano, R., 2004. Chitin biosynthesis in fungi, in: Arora, D.K., Bridge, P.D., Bhatnagar, D. (Eds.), Handbook of Fungal Biotechnology. Marcel Dekker Inc., New York, pp. 315–330.
Runnegar, B., Pojeta Jr, J., 1974. Molluscan Phylogeny: The Paleontological Viewpoint: The early Paleozoic fossil record shows how living and extinct molluscan classes originated and diversified. Science (1979) 186, 311–317.
Sabine, C.L., Feely, R.A., Gruber, N., Key, R.M., Lee, K., Bullister, J.L., Wanninkhof, R., Wong, C.S.L., Wallace, D.W.R., Tilbrook, B., 2004. The oceanic sink for anthropogenic CO2. Science (1979) 305, 367–371.
Saleuddin, A.S.M., 1974. An electron microscopic study of the formation and structure of the periostracum in Astarte (Bivalvia). Can J Zool 52, 1463–1471.
Saleuddin, A., Petit, H.P., 1983. The mode of formation and the structure of the periostracum, in: The Mollusca. Elsevier, pp. 199–234.
Saleuddin, A.S.M., Sevala, V.M., Sevala, V.L., Mukai, S.T., Khan, H.R., 1992. Involvement of mammalian insulin and insulin-like peptides in shell growth and shell regeneration in molluscs. Hard tissue mineralization and demineralization 149–169.
Santini, O., Chahbane, N., Vasseur, P., Frank, H., 2011. Effects of low-level copper exposure on Ca2+-ATPase and carbonic anhydrase in the freshwater bivalve Anodonta anatina. Toxicol Environ Chem 93, 1826–1837.
Santos, R.M., Gerven, T. Van, 2011. Process intensification routes for mineral carbonation. Greenhouse Gases: Science and Technology 1, 287–293.
Savazzi, E., 2005. The function and evolution of lateral asymmetry in boring endolithic bivalves. Paleontological Research. https://doi.org/10.2517/prpsj.9.169

Scarratt, K., Moses, T.M., Akamatsu, S., 2000. Characteristics of nuclei in Chinese freshwater cultured pearls. Gems & Gemology 36, 98–109.
Schneider, J.A., Carter, J.G., 2001. Evolution and phylogenetic significance of cardioidean shell microstructure (Mollusca, Bivalvia). J Paleontol 75, 607–643.
Schönitzer, V., Weiss, I.M., 2007. The structure of mollusc larval shells formed in the presence of the chitin synthase inhibitor Nikkomycin Z. BMC Struct Biol 7, 1–24.
Schwaner, C., Farhat, S., Barbosa, M., Boutet, I., Tanguy, A., Pales Espinosa, E., Allam, B., 2023. Molecular Features Associated with Resilience to Ocean Acidification in the Northern Quahog, Mercenaria mercenaria. Marine Biotechnology 25, 83–99.
Scialla, S., Carella, F., Dapporto, M., Sprio, S., Piancastelli, A., Palazzo, B., Adamiano, A., Degli Esposti, L., Iafisco, M., Piccirillo, C., 2020. Mussel shell-derived macroporous 3D scaffold: characterization and optimization study of a bioceramic from the circular economy. Mar Drugs 18, 309.
Ghatak, A.S., Koch, M., Guth, C., Weiss, I.M., 2013. Peptide induced crystallization of calcium carbonate on wrinkle patterned substrate: implications for chitin formation in molluscs. Int J Mol Sci 14, 11842–11860.
Sharma, V., Srinivasan, A., Nikolajeff, F., Kumar, S., 2021. Biomineralization process in hard tissues: The interaction complexity within protein and inorganic counterparts. Acta Biomater 120, 20–37.
Shi, J., Wu, X., Sun, R., Ban, B., Li, J., Chen, J., 2019. Synthesis and performance evaluation of paraffin microcapsules with calcium carbonate shell modulated by different anionic surfactants for thermal energy storage. Colloids Surf A Physicochem Eng Asp 571, 36–43.
Shi, Y., Fan, Z., Li, G., Zhang, L., Yue, Z., Yan, X., Xu, A., Huang, S., 2020. The family of amphioxus chitin synthases offers insight into the evolution of chitin formation in chordates. Mol Phylogenet Evol 143, 106691.
Silva, C., Yáñez, E., Martín-Díaz, M.L., DelValls, T.A., 2012. Assessing a bioremediation strategy in a shallow coastal system affected by a fish farm culture–application of GIS and shellfish dynamic models in the Rio San Pedro, SW Spain. Mar Pollut Bull 64, 751–765.
Skeffington, A.W., Donath, A., 2020. ProminTools: shedding light on proteins of unknown function in biomineralization with user friendly tools illustrated using mollusc shell matrix protein sequences. PeerJ 8, e9852.

Sleight, V.A., Antczak, P., Falciani, F., Clark, M.S., 2020. Computationally predicted gene regulatory networks in molluscan biomineralization identify extracellular matrix production and ion transportation pathways. Bioinformatics 36, 1326–1332.

Smith, J.A., Auerbach, D.A., Flessa, K.W., Flecker, A.S., Dietl, G.P., 2016. Fossil clam shells reveal unintended carbon cycling consequences of Colorado River management. R Soc Open Sci 3, 160170.

Song, J., Zhou, S., 2020. Post-transcriptional regulation of insect metamorphosis and oogenesis. Cellular and Molecular Life Sciences 77, 1893–1909.

Song, X., Liu, Z., Wang, L., Song, L., 2019. Recent advances of shell matrix proteins and cellular orchestration in marine molluscan shell biomineralization. Front Mar Sci. https://doi.org/10.3389/fmars.2019.00041

Stanton, S.A., 2012. Structure and function of the external ciliation of larval bivalves with different life history strategies.

Stenzel, H.B., 1963. Aragonite and calcite as constituents of adult oyster shells. Science (1979) 142, 232–233.

Stöger, I., Sigwart, J.D., Kano, Y., Knebelsberger, T., Marshall, B.A., Schwabe, E., Schrödl, M., 2013. The continuing debate on deep molluscan phylogeny: evidence for Serialia (Mollusca, Monoplacophora+ Polyplacophora). Biomed Res Int 2013.

Su, W., Zha, S., Wang, Y., Shi, W., Xiao, G., Chai, X., Wu, H., Liu, G., 2017. Benzo [a] pyrene exposure under future ocean acidification scenarios weakens the immune responses of blood clam, Tegillarca granosa. Fish Shellfish Immunol 63, 465–470.

Suchanek, T.H., Geller, J.B., Kreiser, B.R., Mitton, J.B., 1997. Zoogeographic distributions of the sibling species Mytilus galloprovincialis and M. trossulus (Bivalvia: Mytilidae) and their hybrids in the North Pacific. Biol Bull 193, 187–194.

Summa, D., Lanzoni, M., Castaldelli, G., Fano, E.A., Tamburini, E., 2022. Trends and opportunities of bivalve shells' waste valorization in a prospect of circular blue bioeconomy. Resources 11, 48.

Sun, J., Bhushan, B., 2012. Hierarchical structure and mechanical properties of nacre: a review. RSC Adv 2, 7617–7632.

Sun, W., Feng, J., 2018. Differential lncRNA expression profiles reveal the potential roles of lncRNAs in antiviral immune response of Crassostrea gigas. Fish Shellfish Immunol 81, 233–241.

Suzuki, M., Nagasawa, H., 2013. Mollusk shell structures and their

formation mechanism. Can J Zool 91, 349–366.
Suzuki, M., Sakuda, S., Nagasawa, H., 2007. Identification of chitin in the prismatic layer of the shell and a chitin synthase gene from the Japanese pearl oyster, Pinctada fucata. Biosci Biotechnol Biochem 71, 1735–1744.
Suzuki, M., Saruwatari, K., Kogure, T., Yamamoto, Y., Nishimura, T., Kato, T., Nagasawa, H., 2009. An acidic matrix protein, Pif, is a key macromolecule for nacre formation. Science (1979) 325, 1388–1390.
Takeuchi, T., 2017. Molluscan genomics: implications for biology and aquaculture. Curr Mol Biol Rep 3, 297–305.
Takeuchi, T., Suzuki, Y., Watabe, S., Nagai, K., Masaoka, T., Fujie, M., Kawamitsu, M., Satoh, N., Myers, E.W., 2022. A high-quality, haplotype-phased genome reconstruction reveals unexpected haplotype diversity in a pearl oyster. DNA Research 29, dsac035.
Talmage, S.C., Gobler, C.J., 2011. Effects of elevated temperature and carbon dioxide on the growth and survival of larvae and juveniles of three species of northwest Atlantic bivalves. PLoS One 6, e26941.
Talmage, S.C., Gobler, C.J., 2009. The effects of elevated carbon dioxide concentrations on the metamorphosis, size, and survival of larval hard clams (Mercenaria mercenaria), bay scallops (Argopecten irradians), and Eastern oysters (Crassostrea virginica). Limnol Oceanogr 54, 2072–2080.
Tan, K., Zhang, H., Zheng, H., 2020. Selective breeding of edible bivalves and its implication of global climate change. Rev Aquac 12, 2559–2572.
Tan, K., Zheng, H., 2020. Ocean acidification and adaptive bivalve farming. Science of the Total Environment 701, 134794.
Tang, W.J., Fernandez, J.G., Sohn, J.J., Amemiya, C.T., 2015. Chitin is endogenously produced in vertebrates. Current Biology 25, 897–900.
Taylor, J., Strack, E., 2008. Pearl production. The pearl oyster 273–302.
Taylor, J.D., Kennedy, W.J., Hall, A., 1969. The Shell Structure and Mineralogy of the Bivalvia Introduction. Nuculacea—Trigonacea. Bulletin of the British Museum (Natural History). Zoology. Supplement 1–125.
Thanos, C.D., Goodwill, K.E., Bowie, J.U., 1999. Oligomeric structure of the human EphB2 receptor SAM domain. Science (1979) 283, 833–836.
Thomsen, J., Casties, I., Pansch, C., Körtzinger, A., Melzner, F., 2013. Food availability outweighs ocean acidification effects in juvenile M ytilus edulis: laboratory and field experiments. Glob Chang Biol 19,

1017–1027.
Thomsen, J., Haynert, K., Wegner, K.M., Melzner, F., 2015. Impact of seawater carbonate chemistry on the calcification of marine bivalves. Biogeosciences 12, 4209–4220.
Thomsen, J., Melzner, F., 2010. Moderate seawater acidification does not elicit long-term metabolic depression in the blue mussel Mytilus edulis. Mar Biol 157, 2667–2676.
Timmins-Schiffman, E., Coffey, W.D., Hua, W., Nunn, B.L., Dickinson, G.H., Roberts, S.B., 2014. Shotgun proteomics reveals physiological response to ocean acidification in Crassostrea gigas. BMC Genomics 15, 1–18.
Topić Popović, N., Lorencin, V., Strunjak-Perović, I., Čož-Rakovac, R., 2023. Shell waste management and utilization: Mitigating organic pollution and enhancing sustainability. Applied Sciences 13, 623.
Treccani, L., Mann, K., Heinemann, F., Fritz, M., 2006. Perlwapin, an abalone nacre protein with three four-disulfide core (whey acidic protein) domains, inhibits the growth of calcium carbonate crystals. Biophys J 91, 2601–2608.
Tripp, B.C., Smith, K., Ferry, J.G., 2001. Carbonic Anhydrase: New Insights for an Ancient Enzyme* 210. Journal of biological chemistry 276, 48615–48618.
Trueman, E.R., 1966. Bivalve mollusks: fluid dynamics of burrowing. Science (1979) 152, 523–525.
Umayaparvathi, S., Arumugam, M., Meenakshi, S., Dräger, G., Kirschning, A., Balasubramanian, T., 2014. Purification and characterization of antioxidant peptides from oyster (Saccostrea cucullata) hydrolysate and the anticancer activity of hydrolysate on human colon cancer cell lines. Int J Pept Res Ther 20, 231–243.
Andrew van der Schatte, O., Jones, L., Vay, L. Le, Christie, M., Wilson, J., Malham, S.K., 2020. A global review of the ecosystem services provided by bivalve aquaculture. Rev Aquac 12, 3–25.
Vandepas, L.E., Tassia, M.G., Halanych, K.M., Amemiya, C.T., 2023. Unexpected Distribution of Chitin and Chitin Synthase across Soft-Bodied Cnidarians. Biomolecules 13, 777.
Vaughn, C.C., Hoellein, T.J., 2018. Bivalve impacts in freshwater and marine ecosystems. Annu Rev Ecol Evol Syst 49, 183–208.
Vecchio, K.S., 2005. Synthetic multifunctional metallic-intermetallic laminate composites. Jom 57, 25–31.
Venugopal, V., Gopakumar, K., 2017. Shellfish: nutritive value, health benefits, and consumer safety. Compr Rev Food Sci Food Saf 16,

1219–1242.
Vermeij, G.J., 1995. A natural history of shells. Princeton University Press.
Vinther, J., 2015. The origins of molluscs. Palaeontology 58, 19–34.
Vinther, J., Parry, L., Briggs, D.E.G., Van Roy, P., 2017. Ancestral morphology of crown-group molluscs revealed by a new Ordovician stem aculiferan. Nature 542, 471–474.
Waite, J.H., 2017. Mussel adhesion–essential footwork. Journal of Experimental Biology 220, 517–530.
Waldbusser, G.G., Brunner, E.L., Haley, B.A., Hales, B., Langdon, C.J., Prahl, F.G., 2013. A developmental and energetic basis linking larval oyster shell formation to acidification sensitivity. Geophys Res Lett 40, 2171–2176.
Waldbusser, G.G., Gray, M.W., Hales, B., Langdon, C.J., Haley, B.A., Gimenez, I., Smith, S.R., Brunner, E.L., Hutchinson, G., 2016. Slow shell building, a possible trait for resistance to the effects of acute ocean acidification. Limnol Oceanogr 61, 1969–1983.
Waldbusser, G.G., Hales, B., Langdon, C.J., Haley, B.A., Schrader, P., Brunner, E.L., Gray, M.W., Miller, C.A., Gimenez, I., 2015. Saturation-state sensitivity of marine bivalve larvae to ocean acidification. Nat Clim Chang 5, 273–280.
Waldbusser, G.G., Salisbury, J.E., 2014. Ocean acidification in the coastal zone from an organism's perspective: multiple system parameters, frequency domains, and habitats. Ann Rev Mar Sci 6, 221–247.
Waller, T.R., 1978. Morphology, morphoclines and a new classification of the Pteriomorphia (Mollusca: Bivalvia). Philosophical Transactions of the Royal Society of London. B, Biological Sciences 284, 345–365.
Walton, K., 2015. New Zealand living Solemyidae (Bivalvia: Protobranchia). Molluscan Res 35, 246–261.
Wanamaker Jr, A.D., Gillikin, D.P., 2019. Strontium, magnesium, and barium incorporation in aragonitic shells of juvenile Arctica islandica: Insights from temperature controlled experiments. Chem Geol 526, 117–129.
Wang, S., Zhang, J., Jiao, W., Li, J.I., Xun, X., Sun, Y., Guo, X., Huan, P., Dong, B., Zhang, L., 2017. Scallop genome provides insights into evolution of bilaterian karyotype and development. Nat Ecol Evol 1, 1–12.
Wang, X., Li, P., Cao, X., Liu, B., He, S., Cao, Z., Xing, S., Liu, L., Li, Z.-H., 2022. Effects of ocean acidification and tralopyril on bivalve

biomineralization and carbon cycling: A study of the Pacific Oyster (Crassostrea gigas). Environmental Pollution 313, 120161.
Wang, Y., Tang, H., DeBarry, J.D., Tan, X., Li, J., Wang, X., Lee, T., Jin, H., Marler, B., Guo, H., 2012. MCScanX: a toolkit for detection and evolutionary analysis of gene synteny and collinearity. Nucleic Acids Res 40, e49–e49.
Wanninger, A., Ruthensteiner, B., Dictus, W.J.A.G., Haszprunar, G., 1999. The development of the musculature in the limpet patella with implications on its role in the process of ontogenetic torsion. Invertebr Reprod Dev. https://doi.org/10.1080/07924259.1999.9652702
Wanninger, A., Wollesen, T., 2019. The evolution of molluscs. Biological Reviews 94, 102–115.
Watabe, N., Wilbur, K.M., 1976. Mechanisms of mineralization in the invertebrates and plants, in: International Symposium on the Mechanisms of Mineralization in the Invertebrates and Plants, Georgetown, SC, 1974. Published for the Belle W. Baruch Institute for Marine Biology and Coastal ….
Webb, J., St. Pierre, T.G., Macey, D.J., 1991. Iron biomineralization in invertebrates. Iron biominerals 193–220.
Wei, L., Wang, Q., Wu, H., Ji, C., Zhao, J., 2015. Proteomic and metabolomic responses of Pacific oyster Crassostrea gigas to elevated pCO2 exposure. J Proteomics 112, 83–94.
Wei, L., Xu, F., Wang, Y., Cai, Z., Yu, W., He, C., Jiang, Q., Xu, X., Guo, W., Wang, X., 2018. The Molecular Differentiation of Anatomically Paired Left and Right Mantles of the Pacific Oyster Crassostrea gigas. Marine Biotechnology. https://doi.org/10.1007/s10126-018-9806-8
Weiner, S., Addadi, L., 1997. Design strategies in mineralized biological materials. J Mater Chem 7, 689–702.
Weiner, S., Talmon, Y., Traub, W., 1983. Electron diffraction of mollusc shell organic matrices and their relationship to the mineral phase. Int J Biol Macromol 5, 325–328.
Weiner, S., Traub, W., 1984. Macromolecules in mollusc shells and their functions in biomineralization. Philosophical Transactions of the Royal Society of London. B, Biological Sciences 304, 425–434.
Weiner, S., Traub, W., 1980. X-ray diffraction study of the insoluble organic matrix of mollusk shells. FEBS Lett 111, 311–316.
Weiss, I., 2012. Species-specific shells: chitin synthases and cell mechanics in molluscs. Zeitschrift für Kristallographie-Crystalline Materials 227, 723–738.

Weiss, I.M., Lüke, F., Eichner, N., Guth, C., Clausen-Schaumann, H., 2013. On the function of chitin synthase extracellular domains in biomineralization. J Struct Biol 183, 216–225.
Weiss, I.M., Schönitzer, V., Eichner, N., Sumper, M., 2006. The chitin synthase involved in marine bivalve mollusk shell formation contains a myosin domain. FEBS Lett 580, 1846–1852.
Weiss, I.M., Tuross, N., Addadi, L.I.A., Weiner, S., 2002. Mollusc larval shell formation: amorphous calcium carbonate is a precursor phase for aragonite. Journal of Experimental Zoology 293, 478–491.
Welsh, D.T., 2003. It's a dirty job but someone has to do it: the role of marine benthic macrofauna in organic matter turnover and nutrient recycling to the water column. Chemistry and Ecology 19, 321–342.
Wen, K., Yang, L., Xiong, T., Di, C., Ma, D., Wu, M., Xue, Z., Zhang, X., Long, L., Zhang, W., 2016. Critical roles of long noncoding RNAs in Drosophila spermatogenesis. Genome Res 26, 1233–1244.
Wernberg, T., Russell, B.D., Moore, P.J., Ling, S.D., Smale, D.A., Campbell, A., Coleman, M.A., Steinberg, P.D., Kendrick, G.A., Connell, S.D., 2011. Impacts of climate change in a global hotspot for temperate marine biodiversity and ocean warming. J Exp Mar Biol Ecol 400, 7–16.
Wickham, H., 2016. ggplot2: elegant graphics for data analysis. springer, Verlag New York.
Wickham, H., 2009. Elegant graphics for data analysis (ggplot2). Applied Spatial Data Analysis R 784, 785.
Widdicombe, S., Spicer, J.I., 2008. Predicting the impact of ocean acidification on benthic biodiversity: what can animal physiology tell us? J Exp Mar Biol Ecol 366, 187–197.
Wilbur, K.M., Saleuddin, A.S.M., 1983. Shell formation, in: The Mollusca. Elsevier, pp. 235–287.
Wilkins, D., 2019. gggenes: draw gene arrow maps in 'ggplot2'. R package version 0.4. 0.
Wilkins, N.P., Fujino, K., Gosling, E.M., 1983. The mediterranean mussel Mytilus galloprovincialis Lmk. in Japan. Biological Journal of the Linnean Society 20, 365–374.
Windoffer, R., Jahn, A., Meyberg, F., Krieger, J., Giere, O., 1999. Sulphide-induced metal precipitation in the mantle edge of Macoma balthica (Bivalvia, Tellinidae)--a means of detoxification. Mar Ecol Prog Ser 187, 159–170.
Wittmann, A.C., Pörtner, H.-O., 2013. Sensitivities of extant animal taxa to ocean acidification. Nat Clim Chang 3, 995–1001.

Wonham, M.J., 2004. Mini-review: distribution of the Mediterranean mussel, Mytilus galloprovincialis (Bivalvia: Mytilidae), and hybrids in the northeast Pacific. J Shellfish Res 23, 535–544.

WoRMS Editorial Board, 2023. World Register of Marine Species [WWW Document]. Available from httpswww.marinespecies.org at VLIZ.

Wu, F., Lu, W., Shang, Y., Kong, H., Li, L., Sui, Y., Hu, M., Wang, Y., 2016. Combined effects of seawater acidification and high temperature on hemocyte parameters in the thick shell mussel Mytilus coruscus. Fish Shellfish Immunol 56, 554–562.

Yabe, T., Yamada-Okabe, T., Nakajima, T., Sudoh, M., Arisawa, M., Yamada-Okabe, H., 1998. Mutational analysis of chitin synthase 2 of Saccharomyces cerevisiae: identification of additional amino acid residues involved in its catalytic activity. Eur J Biochem 258, 941–7.

Yamaguchi, K., 1994. Shell structure and behaviour related to cementation in oysters. Mar Biol 118, 89–100. https://doi.org/10.1007/BF00699222

Yang, B., Zhai, S., Zhang, F., Wang, H., Ren, L., Li, Y., Li, Q., Liu, S., 2022. Genome-wide association study toward efficient selection breeding of resistance to Vibrio alginolyticus in Pacific oyster, Crassostrea gigas. Aquaculture 548, 737592.

Yao, Z., Xia, M., Li, H., Chen, T., Ye, Y., Zheng, H., 2014. Bivalve shell: not an abundant useless waste but a functional and versatile biomaterial. Crit Rev Environ Sci Technol 44, 2502–2530.

Yap, C.K., Sharifinia, M., Cheng, W.H., Al-Shami, S.A., Wong, K.W., Al-Mutairi, K.A., 2021. A commentary on the use of bivalve mollusks in monitoring metal pollution levels. Int J Environ Res Public Health 18, 3386.

Yarra, T., Blaxter, M., Clark, M.S., 2021. A bivalve biomineralization toolbox. Mol Biol Evol 38, 4043–4055.

Yonge, M., 1977. Form and evolution in the anomiacea (mollusca: bivalvia)-pododesmus, anomia, patro, enigmonia (anomiidae): placunanomia, Placuna (placunidae fam. nov.). Philosophical Transactions of the Royal Society of London. B, Biological Sciences 276, 453–523.

Yoshiba, S., Hamada, H., 2014. Roles of cilia, fluid flow, and Ca2+ signaling in breaking of left–right symmetry. Trends in genetics 30, 10–17.

Young, C.S., Gobler, C.J., 2018. The ability of macroalgae to mitigate the negative effects of ocean acidification on four species of North

Atlantic bivalve. Biogeosciences 15, 6167–6183.
Yu, H., Zhao, X., Li, Q., 2016. Genome-wide identification and characterization of long intergenic noncoding RNAs and their potential association with larval development in the Pacific oyster. Sci Rep. https://doi.org/10.1038/srep20796
Zakrzewski, A.-C., Weigert, A., Helm, C., Adamski, M., Adamska, M., Bleidorn, C., Raible, F., Hausen, H., 2014. Early divergence, broad distribution, and high diversity of animal chitin synthases. Genome Biol Evol 6, 316–325.
Zamarreño, I., De Porta, J., Vázquez, A., 1996. The shell microstructure, mineralogy and isotopic composition of Amussiopecten baranensis (Pectinidae, Bivalvia) from the Miocene of Spain: a valuable paleoenvironmental tool. Geobios 29, 707–724.
Zenger, K.R., Khatkar, M.S., Jones, D.B., Khalilisamani, N., Jerry, D.R., Raadsma, H.W., 2019. Genomic selection in aquaculture: application, limitations and opportunities with special reference to marine shrimp and pearl oysters. Front Genet 9, 411091.
Zhang, G., Fang, X., Guo, X., Li, L.I., Luo, R., Xu, F., Yang, P., Zhang, L., Wang, X., Qi, H., 2012. The oyster genome reveals stress adaptation and complexity of shell formation. Nature 490, 49–54.
Zhang, R., Xie, L., Yan, Z., Zhang, R., Xie, L., Yan, Z., 2019. The Study on Enzymes Related to Biomineralization of Pinctada fucata. Biomineralization Mechanism of the Pearl Oyster, Pinctada fucata 445–507.
Zhang, Y., Liu, Z., Song, X., Huang, S., Wang, L., Song, L., 2019. The Inhibition of Ocean Acidification on the Formation of Oyster Calcified Shell by Regulating the Expression of Cg chs1 and Cg chit4. Front Physiol 10, 1034.
Zhang, Y., Mao, F., Xiao, S., Yu, H., Xiang, Z., Xu, F., Li, J., Wang, L., Xiong, Y., Chen, M., 2022. Comparative genomics reveals evolutionary drivers of sessile life and left-right shell asymmetry in bivalves. Genomics Proteomics Bioinformatics.
Zhang, Y., Xie, L., Meng, Q., Jiang, T., Pu, R., Chen, L., Zhang, R., 2003. A novel matrix protein participating in the nacre framework formation of pearl oyster, Pinctada fucata. Comp Biochem Physiol B Biochem Mol Biol 135, 565–573.
Zhang, Z.-Q., 2011. Animal biodiversity: An outline of higher-level classification and survey of taxonomic richness. Magnolia press.
Zhao, L., Shirai, K., Tanaka, K., Milano, S., Higuchi, T., Murakami-Sugihara, N., Walliser, E.O., Yang, F., Deng, Y., Schöne, B.R., 2020.

A review of transgenerational effects of ocean acidification on marine bivalves and their implications for sclerochronology. Estuar Coast Shelf Sci 235, 106620.

Zhao, R., Takeuchi, T., Luo, Y.-J., Ishikawa, A., Kobayashi, T., Koyanagi, R., Villar-Briones, A., Yamada, L., Sawada, H., Iwanaga, S., 2018. Dual gene repertoires for larval and adult shells reveal molecules essential for molluscan shell formation. Mol Biol Evol 35, 2751–2761.

Zhao, X., Guo, C., Han, Y., Che, Z., Wang, Y., Wang, X., Chai, X., Wu, H., Liu, G., 2017. Ocean acidification decreases mussel byssal attachment strength and induces molecular byssal responses. Mar Ecol Prog Ser 565, 67–77.

Zhao, X., Han, Y., Chen, B., Xia, B., Qu, K., Liu, G., 2020. CO2-driven ocean acidification weakens mussel shell defense capacity and induces global molecular compensatory responses. Chemosphere 243, 125415.

Zhao, X., Yu, H., Kong, L., Li, Q., 2012. Transcriptomic responses to salinity stress in the Pacific oyster Crassostrea gigas.

Zheng, Z., Li, W., Xu, J., Xie, B., Yang, M., Huang, H., Li, H., Wang, Q., 2020a. LncMSEN1, a mantle-specific LncRNA participating in nacre formation and response to polyI: C stimulation in pearl oyster Pinctada fucata martensii. Fish Shellfish Immunol 96, 330–335.

Zheng, Z., Xie, B., Cai, W., Yang, C., Du, X., 2020b. Identification of a long non-coding RNA (LncMSEN2) from pearl oyster and its potential roles in exoskeleton formation and LPS stimulation. Fish Shellfish Immunol 103, 403–408.

Zheng, Z., Xiong, X., Zhang, J., Lv, S., Jiao, Y., Deng, Y., 2019. The global effects of PmRunt co-located and co-expressed with a lincRNA lncRunt in pearl oyster Pinctada fucata martensii. Fish Shellfish Immunol. https://doi.org/10.1016/j.fsi.2019.05.037

Zhu, C., Southgate, P.C., Li, T., 2019. Production of pearls. Goods and services of marine bivalves 73–93.

Zhukova, N. V, 2014. Lipids and fatty acids of nudibranch mollusks: potential sources of bioactive compounds. Mar Drugs 12, 4578–4592.

Zieritz, A., Sousa, R., Aldridge, D.C., Douda, K., Esteves, E., Ferreira-Rodríguez, N., Mageroy, J.H., Nizzoli, D., Osterling, M., Reis, J., 2022. A global synthesis of ecosystem services provided and disrupted by freshwater bivalve molluscs. Biological Reviews 97, 1967–1998.